The University Of Sheffield.

Automated indentation analysis technique for the investigation of plant and fungal cell nano-mechanics using Atomic Force Microscopy

By:

Sovatzoglou Spyridon

A thesis submitted in partial fulfilment of the requirements for the degree of Doctor of Philosophy

The University of Sheffield

Faculty of Science

School of Physics and Astronomy

September 2019

Declaration

The work presented and described in this thesis was undertaken at the University of Sheffield between October 2015 and September 2019 under the supervision of Professor Jamie K. Hobbs and Professor Andrew J. Fleming. Unless stated otherwise it is the work of the author and has not been submitted, in whole or in part, for any other degree at this or any other institute.

Signed

Spyridon Sovatzoglou

September 2019

Acknowledgements

There are many people I would like to thank for their invaluable help towards the completion of this research work. Top of this list is my primary supervisor, Jamie K. Hobbs, who supervised my project along the way, providing me with solid advice and encouragement to implement my ideas and -most importantly- enjoy the project. He also suggested and shared many of his original ideas, a result of his long experience and expertise on the field.

I would also like to thank my second supervisor, Andrew J. Fleming for his scientific advice, and his help on all other academic issues as well. Thank you to both for the opportunity they gave me to conduct my PhD research under their supervision in the University of Sheffield.

I would also like to thank all the other members of the Jamie Hobbs' group in the University of Sheffield, past and present: Johnny Burns, David Owen, Raveen K. Tank, Nick Jenkins, Laid Pasquina Lemonche, Vinny Verma, Sandip Kumar, Xinyue Chen, Anaam Alomari and of course Nic Mullin for his clear and omnipresent scientific (both experimental and theoretical) advice.

I'd like to thank Harriet Knopfler, Professor Kathryn Ayscough, and Dr Christian Voigt for their collaboration. Thanks to the administrative staff in the Department of Physics and Astronomy for their help towards secondary, but still important matters. Thanks also to members of the Andrew Fleming's lab of the Animal and Plant Science department who let me use their facilities.

Finally, I'd like to thank my parents George and Anastasia, my big brother Anestis, all my friends in Athens and Sheffield, and of course my wife Evi. Nothing would have been possible without your support.

Abstract

In this project, we investigated the mechanics of different types of cells with the help of an Atomic force microscope (AFM) in force mapping mode. We investigated the stomatal mechanics of *Arabidopsis Thaliana* and its mutant *pme6*, and we also investigated the cell mechanics of the pathogenic yeast *Candida albicans* and one of its mutants missing the *AP-2* adaptor complex. The *pme6* mutant alters the pectin concentration in the cell wall and has an effect in both plant growth and the stomatal biological function, while the *AP-2* mutation in *C. albicans* is considered to have an effect to cell wall's regulation and its virulence.

We developed a dynamic programming technique for the analysis of AFM force mapping experiments, and we implemented an analytical equation/Contact mechanics model found in literature (*Pharr-Bolshakov's* analytical approach based on *Sneddon*'s work) for the calculation of the elastic modulus. This equation assumes the contact of an elastic half-space (cell surface) with a rigid indenter (AFM silicon tip) of arbitrary axisymmetric shape.

Instead of the use of a single standard model for the whole force map (e.g. *Hertz* or *Sneddon*), we make use of a generalised model for the case when the contact is unknown, by calculating the fitting parameter *beta*, and backed up by the mapping of the fitting residuals for the first time. We also discuss on the different modulus values resulting from the different models, and its relation to *beta*.

We found that the mutant stomata cells exhibited higher (~*x*2) modulus than the wild type, and this could be connected to the mutant's altered wall pectin composition. We also found that under the presence of cell turgor pressure the differences in mechanics were clearer compared to when turgor was removed with the help of a buffer, something we did not expect since turgor is considered an overwhelming factor to cell forces. Then, we noticed that in the case of a

mutant cell, with no buffer and under the new model, the modulus decreased with increase of indentation depth. As for the *Candida albicans* we found significantly higher modulus (~*x*5) in mutants and higher adhesion ratio values, and this may be an explanation for the mutant's changed phenotype.

List of figures

List of tables

List of symbols

β	FI curve power fit exponent, '*beta*'
δ	Indentation
F	Force
E_r	Reduced/effective modulus
E	Elastic modulus (Young's moduli)
Ψ_l	Cell's water potential
H	Hardness
W_{AD}	Work of adhesion
F_{AD}	Force of adhesion
δ_{MAX}	Max indentation reached
F_{MAX}	Max force applied
h_t	Tip's height
φ	Tip's half-angle
R_t	Tip's radius of curvature
t_t	Cantilever's thickness
w_t	Cantilever's width
l_t	Cantilever's length
ν	Poisson's ratio
Z_n	vertical height displacement of the cantilever
Z_d	tip deflection
h	*hyphae* (part of the candida cell)
m	*mother cell* (part of the candida cell)
p	p-value

List of abbreviations

FI	Force-indentation (curve)
ple	power law exponent, '*beta*'
AFM	Atomic force microscopy
SPM	Scanning Probe Microscopy
CM	Contact Mechanics
cp	contact point (of the force-distance curve)
WT	Wild-type
RoI	Region of interest (on the cell's surface)
Mt	Mutant
RMSE	Root-mean-squared error (estimator)
FD	Force-distance (curve)
pdf	Probability density function (of a normal distribution of data)
CV	Coefficient of variance
SEM	Scanning Electron Microscope

Table of Contents

Chapter 1: Introduction

1.1. Research motivation

There are some fundamental problems in biology and plant science which struggle to be understood in the absence of quantitative tools and physical models, and which cannot be explained or further investigated without an interdisciplinary scientific collaboration. Here, physics, biology and (bio)mechanics are linked together, and this project aims to accurately measure cell mechanics via AFM (1) based indentation at the cellular and nano-scale level with the aim to better understand the biological function of plant (and fungus) cells. On this basis, this research project is the product of an interdisciplinary collaboration between physical and plant sciences, with the aim to tackle two distinct but inter-connected problems: 1. A biological -by nature- problem; "How do induced plant (and fungal) cell wall mutations affect the mechanical properties of stomatal (and fungal) cells, and how is this connected to the cell's biological function?", and 2. A technical problem; "How do we accurately analyse, measure, and subsequently interpret AFM nano-indentation experiments?"

We know that the biological function and morphogenesis of plant cells is largely based on forces, mechanical signalling and mechanical stimuli. As such, combined with the fact that there exist many tools to genetically manipulate plant cell properties, targeted mutations are useful to understand, and subsequently control via genetically altering the structure and composition of the cell wall. Through the process of DNA being inserted into the gene of interest (e.g. pme6 in our case), this disrupts the gene's DNA sequence and therefore the expression of the gene alters, subsequently altering the cell wall composition of specific constituents (e.g. pectin in our project).

With that as a starting basis, we aimed to explore the alterations that the mutations induced to our cell samples, with the help of (a) an AFM in force-mapping[1] mode (consisting of up to 16384 individual force-distance (FD) curves[2]) as the experimental technique, (b) a specially developed (for the purposes of this project) automated indentation analysis technique for the analysis and interpretation of the results, (c) a strong knowledge of the contact mechanics (CM) and the elasticity theoretical background and analytical models, (d) a strong background knowledge of the materials and the cell wall, and (e) the novel implementation of a complex analytical model for the calculation of the elastic modulus (based on curve fitting) for our cell samples.

The motivation behind the development of the technique (b) was to be able to implement the novel model of analysis (e), inside an independent environment (Matlab/Python) and out of the commercial one accompanying the instrumentation, so that more parameters could be calculated, and an immediate feedback could be available. The motivation for the implementation of (e) arose from the observation that not a single contact mechanics model was able to fit the analysis of all the FD curves of the same force map, and that different CM models/analytical equations needed to apply for the fitting (and subsequently modulus calculation) of the different FD curves of the force map.

With such information in hand, spanning from curve fitting constants to changes in the surface-indenter contact geometry, it became reasonable to question the standard single-model modulus analysis of force maps of highly heterogeneous cell wall surfaces. Here, based on a detailed fitting algorithm, we present a new way of mechanical analysis of (bio) materials' nano-surfaces, inside the general elastic context; based on the literature in contact mechanics and its

[1] Alternatively named "force-volume"
[2] AFM raster scanning of a surface with either 64*64 or 128*128 pixels, and regions of approximately 20μm (scan pixel resolution of ~200nm)

affiliated analytical equations. The aim is to provide a specialised modulus calculation for each point/FD curve of the same force map. This technique was generated alongside research on the mechanics of plant cells (stomata), albeit it has been successfully applied for the analysis of other types of cells as well, including fungus (presented here).

The field of AFM bio-mechanics (the use of (a) in connection to (d)) is relatively new, and it mostly borrows the experimental and analysis procedures from the relevant AFM mechanics field, even if the same experimental conditions that apply in the investigation of traditional materials and their surfaces do not apply in the case of biological matter, due to the high levels of surface heterogeneity and to their dynamic nature[3]. The AFM force mapping mode works as an elasticity probe of inhomogeneous soft biological matter at the micro- and nano-scale in a raster scan manner, and in this work, we exploit the full capability of this technique for our bio-mechanical analysis project.

Additionally, with the advent of huge processing computing power and the utilisation of statistical tools and dedicated programming language libraries it is easier than ever to properly handle big and complex data coming out of the experimental instrumentation for an insightful analysis into a different programming environment. For all these reasons, an automated and elaborate technique for the analysis of AFM nano-indentation data is crucial for applications in multiple scientific and industrial fields, including bio-physical cell research, cell bio-engineering and polymer science surface applications, and commercial nano-indentation software development.

[3] And the need for the maintenance of an environment of physiologically relevant conditions for the cell

1.2. AFM bio-mechanics in biological cells

There is an increasing interest in the use of the AFM to mechanically investigate surfaces of complex biological matter (cells, tissues, bio-polymers, DNA strands), both for basic biological research and for clinical use. This experimental analysis can be done on single cells, multiple cells, or even cell walls requiring simultaneous acquisition of AFM imaging and nano-indentation data over relatively large regions of interest (RoI's). Although these approaches have provided valuable new insights at the interface of physics and biology, they pose significant problems for the correct interpretation of the generated mechanical data. Interpretation requires knowledge of many aspects of the problem, such as the underlying (bio)-material properties, sample's surface structure and geometry, geometrical and mechanical properties of the cantilever tip interacting with the probed material, and an understanding of the contact between the indenter and the material being probed; especially in the case of complex biological material of essentially variable, non-homogeneous mechanical properties and cell wall structure.

To provide a test bed for our analysis, we examined specialized cells on the outer layer of plant leaf epidermis, termed guard cells (or stomata), which our previous AFM analysis (2) had shown a distinctive pattern of relative stiffness, and also we examined fungal cells from different strains to check altered mechanics between those strains and between different regions of the same cell (different formations of the same cell). With this analysis, we will try to improve our understanding of AFM cell nano-(bio) mechanics, while at the same time we provide a new technique for the analysis of the generated data and also suggest a new way of force map/force-indentation analysis model for the calculation of the elastic modulus (E).

1.3. Dissertation overview

Following the establishment of the research motivation and of the brief background, an overview is required to put things into perspective. Starting from a background to the fields of cell mechanics and AFM, we move to the preparation of the materials under investigation, the techniques used, and the analysis technique developed. Then, we discuss on the theoretical background of contact mechanics, we present our developed technique and implementation, we present and discuss the results, and finally, we conclude the thesis by summarizing the findings and suggesting future research direction.

Specifically, in the first part of this thesis, and in rest of the first chapter, we set the problem to be solved in clear detail and we discuss on how we managed to solve it.

In the second chapter, we will introduce the field of AFM bio-mechanics, a rapidly emerging interdisciplinary field which deals with the imaging and physical/mechanical properties investigation of bio-(nano) surfaces and cells. This means investigating the nano-structure of cell walls or cell cross-section, the surface heterogeneity of whole cells, the presence of bio-polymers inside the cell wall matrix (cell wall constituents) etc., while being capable as well of measuring physical properties of the same cells (in parallel with imaging) like mechanical (and also chemical, electrical and magnetic). Also, a background in AFM bio-mechanical analysis of the involved cells is presented, followed by the state of the art of the analysis methods needed to interpret the AFM experimental data. Initially, we present the role of mechanics in our cells (plant cells and yeast cells), and later we discuss on the contact mechanics, the theoretical field which deals with the mathematical analysis of the experimental nano-indentation curves and with the mechanical quantities that yield from this analysis. Also, we discuss the limitations of the currently used theoretical contact mechanics models used, the

implementation of a model we suggest based on our developed technique and the implications this has in the field of AFM bio-mechanics.

Next, in chapter 3, a full description of both the materials and the methods/techniques used in this project will be presented in detail. More specifically, all the information needed for the sample preparation, cell growth, choice of mutants, sample mounting on the AFM stage, mounting of the sample inside the petri dish, the buffers introduced, and the design of the experiment and the experimental conditions is presented. Also, from the side of the experimental techniques used, we discuss the different modes of AFM implementation, the ones used for this research, the different tips used, the experimental conditions and all the other details needed to recreate accurately the resulting experiments of this project.

In the second part of the thesis, in chapter 4, a deeper look into the theoretical background of contact mechanics is given. An overview of the state-of-the-art models for the calculation of mechanical properties of sample surfaces are presented, together with their analytical equations and how these evolved from the principles firstly presented by contact mechanics pioneers like *Hertz* and *Sneddon*.

In chapter 5, a detailed look into the developed analysis technique and many details are introduced. Starting with the import of the raw experimental data into the programming environment, to the calculation of important critical points like the contact point (cp) and the max point, to the fitting routine which yields the most important features of this analysis, to the plethora of the visualization output figures for the better understanding of the results, we go step by step to the understanding of the developed analysis technique.

In the third part, in chapters 6 and 7, the experiments conducted during this project will be presented for analysis and discussion. We will analyse them under the developed technique and the novel implementation of a model, and we will present the important comparison analytics

and any important findings that occur from it. We will perform statistical significance tests to validate this analysis.

In chapters 6, we present the results of the stomata cell wall indentation experiments. We investigate the effect of cell wall modifications (as a result of DNA mutations to the plant) in the mechanics of the cell wall, and any differences occurred under the new analysis technique presented in chapter 5.1. Additionally, we compare the data resulting from the two different populations (wild type and mutant samples) and we report statistically significant findings. Also, we see how the high surface heterogeneity introduces implications to both the experimentation and the interpretation of the experimental results, by observing a topography effect in the mapping of the fitting residuals.

In chapter 7, we follow a similar path to presenting the results of the *C. albicans* AFM force mapping experiments. We investigate the effect of cell wall modifications (mutant samples) in the mechanics of the cell wall, and any differences occurred under the new way of analysis presented in chapter 5.1. Also, we compare the data resulting from the two different populations (wild type and mutant samples) and we report statistically significant findings.

Finally, in the last chapter 8, the conclusions and findings of this research project are discussed, further improvements are proposed, and future work on the field is suggested. The improvements and suggested future work include suggestions in sample preparation, experimental conditions, experiment design, algorithmic improvement of the developed analysis technique, further AFM bio-mechanical experiments of different cells, etc.

Chapter 2: Cell mechanics - Background

2.1. Introduction

Nano-mechanical indentation experiments and relevant simulations have been conducted in many biological materials (cells, tissues, other biological material surfaces) with different interpretations, following the emerging and rapidly growing field of AFM (nano)-biomechanics. Apart from plant and fungal cells, which we investigated during this research, bacterial (3) (4) (5), cancer (6) (7), brown algae (8), and bone (9) cells, collagen and fibres (10), embryonic and brain tissues (11) (12), and membranes (13) have been investigated using an AFM. This has led to the analysis of their mechanical properties, and the relation of these properties to cell growth, biological function, and morphogenesis (14).

Mechanical forces are generated through all the cell development stages, and the transmission of mechanical stimuli mediates -and sometimes is the onset of- many important biological functions. At the same time, the AFM is the only technique which can successfully measure cell nano-mechanics (with the help of micro- and nano-indentation) while scanning the cell surface for topographical imaging as well. Thus, the investigation of cell mechanics, and the subsequent measurement of cell forces, cell elasticity and other mechanical properties can reveal valuable information about the cell and the connection of mechanics to cell signalling, morphogenesis, growth and its biological function.

2.2. Plant cell mechanics

This complex hierarchical structure (plant), composed by ‘dissimilar structural elements with each element bringing new aspects to the overall properties of the material’ (15) has raised much attention lately from biologists and physicists, due to their desire to explain all the different mechanical properties of plants and plant cells. Studying plant mechanics is important

for the understanding of plant growth (16), growth control (17), morphogenesis (18), etc. AFM has been used for measuring the mechanics of plant cells for decades (2) (19) (20) (21) (22) (23).

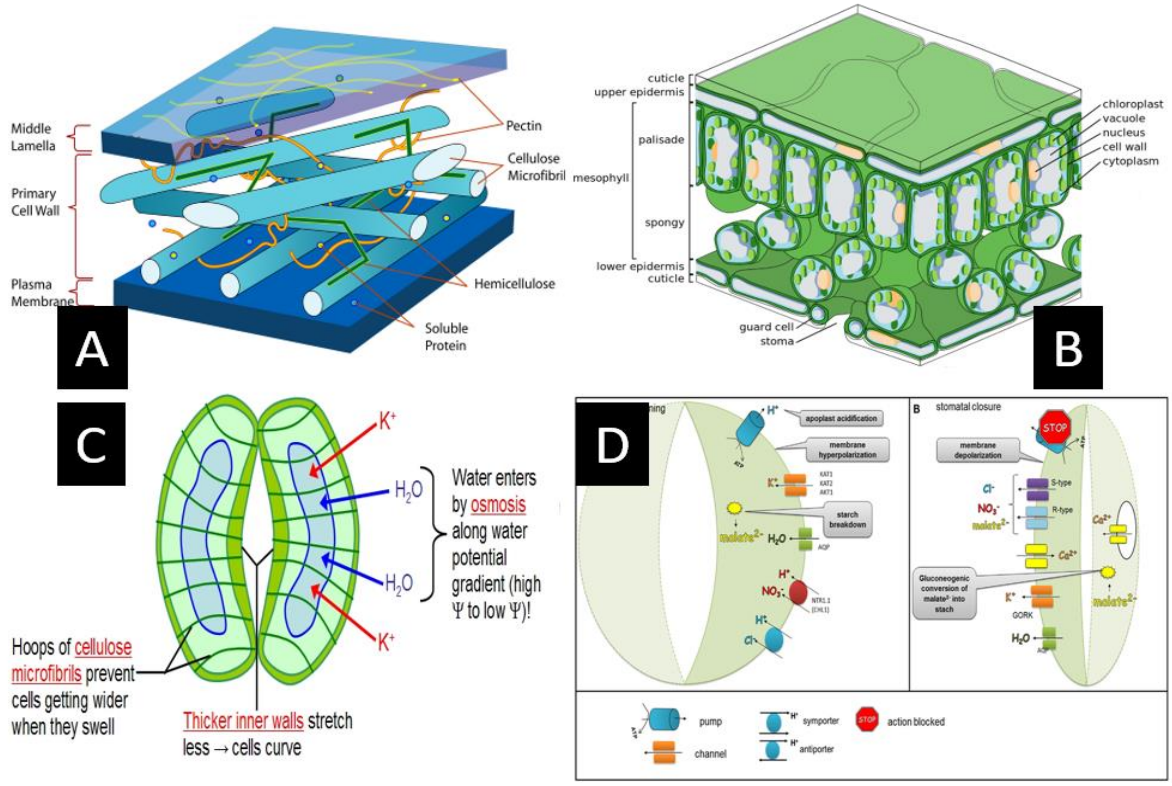

Figure 1: A: A plant cell wall, depicted with its main constituents; Cellulose, hemicellulose & pectin. (24) B: Cross section of a leaf indicating all the different features of it. A stomata appears at the bottom layer (25) C: How guard (stomatal) cell work (26) D: Membrane hyperpolarization and Depolarization; ion pumps on the cell membrane. (27)

Stomatal cells provide an excellent model for basic research studies on how a cell integrates numerous kinds of input signals[4] (Figure 1-C, D) to produce a response/biological function, such as stomatal aperture 'opening' and 'closing'. They comprise a pair of highly specialized 'guard' cells that are encompassed by larger and thinner subsidiary (pavement) cells (Figure 2). Though it is obvious that the stomata differ a lot from species to species, they exhibit some

[4] Chemical (ion channels, ion transport), mechanical (turgor pressure, forces, elasticity), electrochemical (plasma membrane polarization, membrane potential, action potentials), etc.

universal features, presented here. They form pores of a few μm and are in the leaf epidermis of plants (Figure 1-B), covered by a waxy cuticle with a very low permeability to CO_2 (28). They differ from other epidermis cells by their biological function and in having chloroplasts, and are responsible for gas and water exchange between plants and their environment, thereby controlling water supply and the rate of CO_2 uptake. Flux depends on the pore size, and on the dynamic processes of the cells.

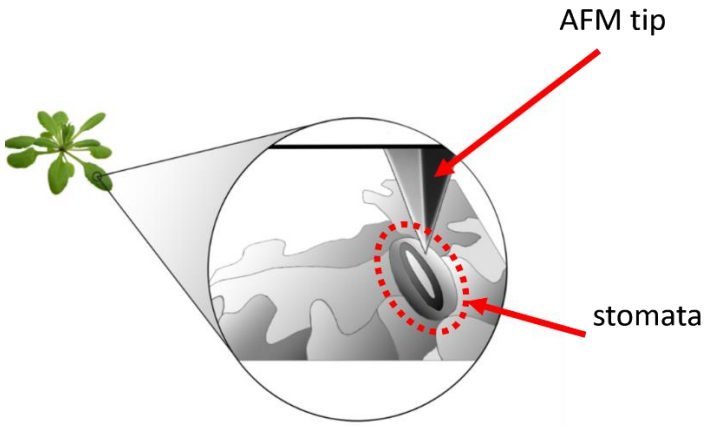

Figure 2: Schematic representation -at the micron-scale- of the AFM indenter-probing of the stomata cells on the plant leaf epidermis; the cylindrical shape being probed consists of the stomata cells, while it is surrounded by the so-called pavement cells. The tip is a cone-shaped tip attached at the AFM to scan the cell and tissue surface.

The biological function of stomata is based in a simple principle, outlined as following; the introduction of active ions into the cell wall vacuole causes the osmotic flow of water from an area of low solute concentration outside the cell into the cell's vacuole, an area of high solute concentration (Figure 1-C). Then, turgor pressure increases, pushing the plasma membrane against the cell wall and affecting its properties (26). This results to an increase of volume and changing of the guard cell's shape.

Furthermore, the deformation in guard cells is controlled by geometrical constraints and cell wall polymer composition, where the radial orientation of the cellulose micro-fibrils is thought

to induce anisotropy to the system (Figure 1-C). Guard cells regulate the stomatal aperture through a signalling pattern and triggering mechanisms in order to let CO_2 enter the plant, but at the same time the open pore facilitates the loss of water through transpiration. Thus, it is important the "decision" that the stomata must take, trying to compromise between CO_2 uptake and water loss, based upon the size of the aperture, the speed of the stomatal movement and the possible stimuli from environmental signals.

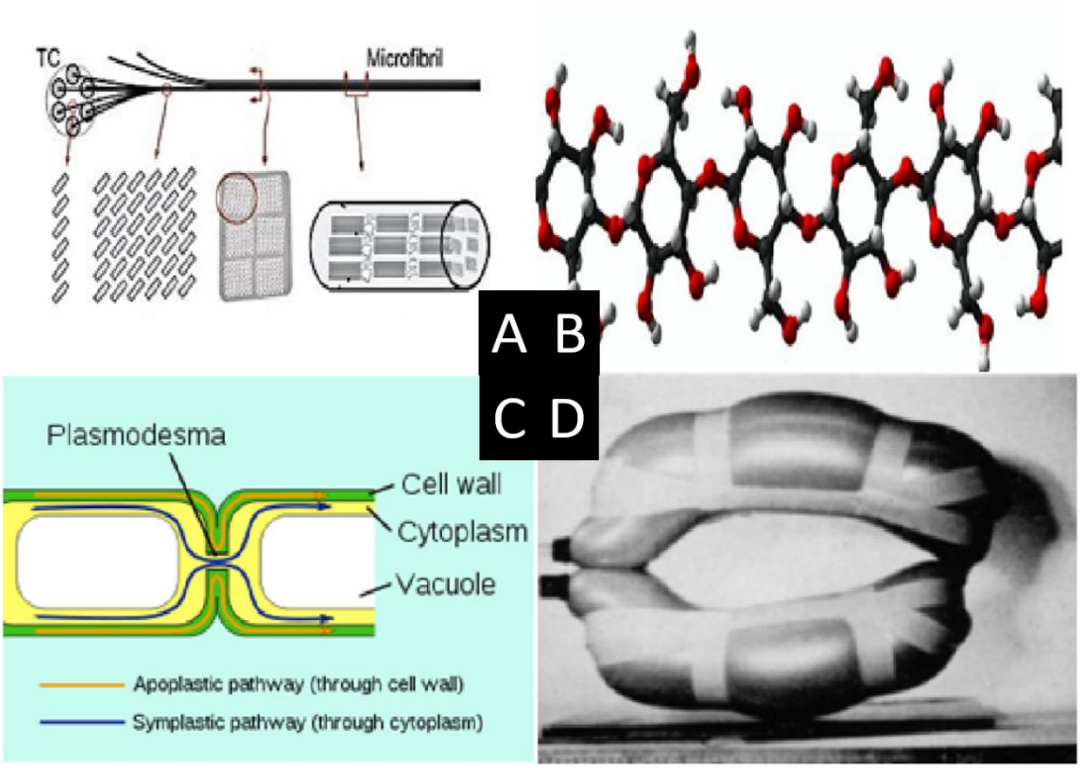

Figure 3: A: From the structure of a microfibril down to an individual Cellulose chain. B: 3-D intramolecular hydrogen-bonding network in a representative cellulose structure. C: Symplastic & apoplastic pathways inside a plant cell. D: Simulation of the swelling activity of the guard cells

The investigation of plant mechanics/elasticity with the help of AFM nano-indentation aims to enhance our understanding on how specialized plant cells/stomata biological function works and give feedback to the plant scientists for the optimization of the cellular structure and cell biological function through DNA manipulation and gene mutation.

In this project we collaborated with Professor Andrew Fleming for the investigation of the mechanics of stomata, and how this -assumed- alteration in mutant cell's mechanics can be linked to the stomatal biological function. The stomatal cells exhibit a set of mechanical features, which can be probed immediately or in a successive manner with the use of indentation techniques. At different depths of indentations one can measure cell wall elasticity and the internal turgor pressure of the cell, and the adhesion of the surface.

2.2.1. State of the art – stomatal mechanics

From the side of biomechanics, this complex hierarchical structure has been investigated in a number of studies (2) (29) (30) (31) (18) (32) (33) (34) (16) (35) (36) (37). Turgor pressure and the cell wall mechanics are the main mechanical factors affecting the biological function of stomata, due to an internal biochemical process and to the cell wall's constituents and their relationship, respectively. Turgor pressure actively pushes towards the cell surface while growth and morphogenesis is thought to be due to the yielding of the cell walls under the generated tension (20). Thus, the plant cell wall must be 'strong enough to withstand turgor pressure, and at the same time flexible enough to allow controlled cell expansion and contraction' (30). The mechanical term "strong" refers to the cell wall polymeric matrix and the cross-linking that enables it to create a strong elastic net, while the term "flexible" refers to resistance to dynamic mechanical response. More specifically, the stomatal cell undergoes a large number of opening and closing cycles through its lifetime and, in mechanical terms, this can induce "yield" to the (biological) material after a specific point. There is also a well-established theory, according to which the plasma membrane swells isotropically due to increasing turgor pressure until the moment when the radially oriented micellation of cross-linked cellulosic micro-fibrils sets limiting factors to the movement of plasma membrane, forcing it now to deform anisotropically (Figure 3-D). This anisotropic deformation is the basis

of the hypothesis that there is variation in the mechanical properties of guard cell walls. This project aims to investigate the nature of those mechanical properties.

For the case of our project, we mainly discuss on bio-mechanical phenomena like the turgor pressure, cell wall elasticity and adhesion, and we also address the effect that the guard cell wall structure and constituents (which are expected to alter with the induced mutations) have on these. In order to put things into perspective, it would be helpful to introduce some of the aforementioned mechanical terms. As stated before, turgor pressure is the pressure that pushes the cell membrane towards the cell wall, resulting from an internal biochemical process involving the movement of ions and subsequently the osmotic flow of water. Following, crosslinking is the phenomenon where different (bio)-polymers bind with each other with covalent or ionic bonds with or without the help of "agents". Continuing, the investigation of elasticity through indentation techniques refers to the analysis of the relation between deformation and load resulting in the Young's modulus (E) value, which is an intrinsic property of a linear elastic material and is independent of shape. Stiffness is force divided by displacement and, in indentation experiments, it is related to the linear part of the FD curve (in the contact area). Yield point in a mechanical deformation of a material is the transition point from elastic to plastic (permanent) deformation. As aforementioned, the stomatal cell undergoes a cycle of expansion and contraction as an effect of its biological function, and this behaviour may lead, after many cycles, to a yield in the material properties of the cell. Finally, a strong cell wall means that it is resistant to its deformation (and yield).

Turgor pressure pushes the plasma membrane against the cell wall, affecting its properties. It is caused by the osmotic flow of water from an area of low solute concentration outside the cell into the cell's vacuole (an organelle existing only in plant cells), an area of high solute concentration. It is mostly triggered by the introduction of active ions into the vacuole and the

action of the ion pumps and the cell signalling patterns channels (see chapter 2.2.2.1). Turgor pressure is connected to the cell's water potential (Ψ_I), in the way that the guard cells pump in ions, lowering Ψ_I and thus provoking the influx of water via osmotic flow. This results in the swelling of guard cells, opening the stomatal aperture. Then, guard cells pump out ions, increasing the Ψ_I causing water efflux due to osmosis and stomatal aperture closing.

Following, the cell wall's structure and composition is of crucial importance for the understanding of the mechanical properties of the guard cells. The cell wall of guard cells exhibits two distinctive features: an uneven thickening of walls forming the pore in either case & a radial micellation of micro-fibrils (38). A key feature of the guard cell wall structure is the radial orientation of cellulose micro-fibrils. Cellulose $(C_6H_{10}O_5)_n$ is a mostly crystalline (Figure 2-A) fibrous organic biopolymer which plays an important role, maintaining the structure of plant cell walls and has known mechanical, electrical and dielectric properties (39) (40). Cortical microtubules control the orientation of the micro-fibrils and thus the anisotropy of the cell wall (2). It has been experimentally demonstrated (31) that without this exact orientation, the stomatal pore wouldn't open.

Another feature of the guard cells is the asymmetrical thickening of guard cell walls. Back in 1881, Schwendener (41) had already identified this feature of the guard cells as a potential basis for stomatal opening and closing. The guard cells apply tension against each other at the regions of their ends, resulting in the formation of a pore. Continuing, in 1941, Vaihinger noted that the thick ridges observed at the edge of the guard cells (31) (also observed by (2)) act protectively upon the mechanical properties of guard cells, preventing them from an extensive opening of the pore and other less important contributions. The guard cell wall is not a homogenous material, also complicating the interpretation of indentation data.

Moreover, plant cells' wall loosening together with the increased water uptake leads to plant growth and morphogenesis. The case of stomatal cells is different because they switch between the states of swollen and shrunken (expansion and contraction), denoting a more complex mechanical behaviour taking place in this case. Here, the thicker-thinner opposite walls together with anisotropic distribution of the cellulosic micro-fibrils leads to the bending of the guard cells, and thus the opening of the stomatal aperture. There are a lot of suggested complementary substances that can interfere to the cell wall structure and change the mechanical properties of the stomatal cell by crosslinking the biopolymers (e.g. arabinan (42)), and a lot of genetic mutations that can affect the cell wall's structure and subsequently the cell's mechanical properties, as in the case of this project's scope.

In cell wall's elasticity, it has been shown in a number of studies that the mechanics of the wall (and subsequently to its biological function) is mediated by the cell wall's biopolymers (cellulose, hemi-cellulose, pectin, etc.) and their interaction with each other, e.g. cross-linking (2) (37). Cellulose micro-fibrils form the major structural component of the primary cell wall and are thought to be cross-linked with hemi-cellulose in order to form a load-bearing network which is embedded within a pectin matrix (43). Also, the anisotropy with which these biopolymers are oriented inside the cell wall is considered to play a role in the distribution of the mechanics of the cell wall, the control of the expansion and contraction of the cell during its biological function, and this concept has been the centre of research for a few studies (44) (45) (36) (46). Regarding the internal turgor pressure, it is considered that after a couple of 10s of nanometres of indentation inside the cell, this is the dominant factor of the measurements, and it can be recognised in the FD curve as the part of the curve which follows a linear (almost "Hookean") trend (see chapter 4.1).

Complementary to the investigation of cell wall's elasticity is the measurement of viscoelasticity, which plays a very important role to the cell's biological function as well. In order to fully research the mechanics of the cell and its contribution to the cell's function and growth, viscoelasticity is of crucial importance (although not a part of a specialised analysis like in this project), and this is shown in relative studies (47), (35), (48). It was shown that finite element method (FEM) analysis and indentation experiments (AFM, nano-DMA) can be combined to investigate dynamic, time-dependent viscoelastic properties of the cell at the nano-scale and that differences in these properties were observed between wild type plant cells and modified ones. Finally, advanced AFM methods for the investigation of the mechanical properties of living cells examine the dissipation of the mechanical energy and its role in morpho-mechanics (49).

Another very interesting concept found in literature is mechanosensitivity. This term refers to the ability of biological systems to recognize and to react to mechanical stimuli (50) (51) (stress, strain, pressure, shear forces, acceleration, vibration, etc.), and the responses to the mechanical stimuli are thought to be mediated by mechanosensitive ion channels in the plasma membrane. Thus, it is important to present all these electrochemical features exhibited in the guard cells and have a more than obvious direct connection to the mechanical ones.

Finally, expansins are proteins located inside the cell wall and they are expressed after the acidification of the cell wall (after environmental stimuli), guard cell plasma membrane H^+-ATPase pumps out towards the cell wall H^+, acidifying the cell wall). They break the non-covalent bonds between cellulose micro-fibrils, allowing the cell to yield, and as a result, the bulk elastic modulus decreases (52).

Other works (53), (47) have reported Young's moduli values in the past, and these values are in the range of [1e+6 1e+8] Pa. In this work, we present measured modulus values from our force mapping experiments inside the same range.

2.2.2. Further physical properties of the cell

2.2.2.1. Electrochemical analysis of stomata

It is well known in the literature how the K^+, NO_3^-, Ca_2^+, etc. ion pumps and channels (54) (55) (Figure 1-C) function by triggering the water flow and turgor pressure, and their role on the plasma membrane polarization is something to be further investigated. Over the last decade, it has been clear that ionic transport and conductivity are fundamental in plant physiology.

As of the membrane (de- or hyper-) polarization, this is a positive or negative shift to the membrane potential, which is responsible for the transmission of electrical impulses (Figure 1-D). A membrane potential is the difference in electric potential between the interior and the exterior of a biological cell, with typical values ranging from -40 mV to -80 mV. It is responsible for a lot of cell functions and for the transmission of short and long-distance signals.

Sufficiently large de-polarizations induce action potentials (*AP*) (56) (57), which are rapid and significant membrane potential changes, often reversing the membrane's polarity. Changes in membrane potential operate in close relationship to the activation of voltage-gated ion channels, which are transmembrane ion channels. Membrane features several cellular processes such as ion conductivity and cell signalling, and membrane hyper-polarization and de-polarization take place during stomatal opening and closing.

Moreover, there is the concept of the electrical long-distance signalling in plants (Action Potentials (*AP*), and slow-wave potentials (*SWP*) or Variation Potentials (*VP*)). They appear as temporary de-polarizations in the membrane potential of affected cell, and they exhibit a time

interval before another signal can be induced or propagated (58) (59) (40). Electrical signalling in plants lets us understand the structure and the processes of the information network within plants.

2.2.2.2. Mechanobiology of stomatal cells

Stress phytormone Abscisic acid (*ABA*), pH, hydraulic signal, CO_2 and microbe (or pathogen)-associated molecular patterns (*MAMP*s or *PAMP*s) are some of the triggers of metabolism or growth provoking mechanisms of guard cells. Stomatal movements in response to drought stress may be the best characterized example considering the long-distance signalling under environmental stresses (60). During times of severe drought (environmental stress), *ABA* acts as an important chemical signal to close the stomatal aperture with the aim of preventing important water loss (28) (60). It has also been shown that the mesophyll (Figure 1-B) generates a signal in response to light and CO_2 that regulates the stomatal aperture (61) and this signal has also a dependence on the process of photosynthesis (62). So, it is thought that the signal needed for stomatal movement cannot be processed before passing through the mesophyll.

Finally, transpiration causes loss of water from the stomatal pores, but it also acts proactively triggering the uptake of nutrients from soil, while the response of guard cells to environmental signals can be directly connected to the width of the stomatal aperture & to electrical excitability and signalling (60). For example, functioning under a range of temperatures, in a liquid environment, in an environment with varying air humidity and/or light intensity, environmental gas fluxes regulation, water stress, can affect the biological response of plants and of guard cells.

2.2.2.3. The role of electromechanical coupling in plants

Electromechanical interactions at different structural levels play an important role in the functionality of biological samples and in the distribution of the signalling network within

biological entities. Since the discovery of electrically-induced mechanical response in muscle tissues (Galvani's experiment, late 18th century) the ubiquitous presence of the electromechanical coupling in biological systems, either in the form of piezoelectricity5 or flexoelectricity (spontaneous electrical polarization induced by strain gradients) has been revealed. Piezoelectricity stems from the non-centrosymmetric crystal structure of most biopolymers including cellulose[6], collagen, keratin, etc. (15); And the most characteristic experiments are the ones of piezoelectricity in bones (63), wood (64) (65) and other biological materials (66). Most recently, the research has gone even further with the introduction of the concept of flexoelectricity into the biological measurements (67), where now the electromechanical coupling can be in theory applied in all crystal structures, centrosymmetric or not. Bio membrane flexoelectricity (68) (69) introduces the concept of the relationship between electricity and mechanics in biological membranes and enables membrane structures to function like soft micro- and nano-machines. The work of (70) goes even further attempting to make a correlation of the electromechanical coupling and especially of flexoelectricity with the concept of ion channels discussed before.

2.3. Fungal cell mechanics

Many principles from the realm of cell mechanics can -and have been- transferred to the investigation of fungal cell mechanics as well. AFM nano-indentation experiments have been conducted in the past (63-67) in fungal cells, and –as in the case of other biological cells- the authors take advantage of the important feature of AFM force mapping being able to probe cell wall elasticity, cell adhesion and cell dynamics while acquiring surface topography at the same time.

[5] linear electromechanical interaction between electrical mechanical state in crystalline materials, as cell wall's cellulose

[6] a biopolymer found in the stomatal cell wall

One characteristic example of fungal cell mechanical investigation with the AFM is the paper of (71), where viscoelasticity and compliance are measured via AFM force spectroscopy at the hyphae of fungal cells with their main finding being that the hyphae from their fungal specimen have significant structure and viscoelastic differences between growing tip, and mature walls. In our project, we will try something similar, to look for altered mechanics between wild-type and mutant cells, and between the mother cell (yeast) and the growing tip (hyphae).

In the paper of (72), the authors look for mechanical differences on the candida cell wall induced by anti-fungal drug treatment. This drug acts to prevent *candida* cell wall synthesis but resistance to it from *candida* mutants is increasing, and thus, a physical and mechanical investigation of such mechanisms is imperative[7]. The best way to address this physical and mechanical investigation has proven to be via implementing AFM nano-indentation techniques, and this is what the authors do in this paper; by investigating two different strains, one susceptible and one resistant to the drug, they found out that resistance affects significantly the cell wall structure and that the act of the drug is due to cell wall stiffening through chitin synthesis. This chitin substance will be the case of investigation for our project as well, since we investigate its effect on the cell wall for altered mechanics.

In the paper of (73) the authors are investigating the role of cell adhesion in a variety of cell processes. This approach is beyond the scope of this project, but nevertheless shows the significant importance of mechanical investigation to the overall cell research.

In this project, we conducted two different sets of experiments, resulting from two different collaborations, aiming to answer two discrete biological questions; in the first case, we collaborated with Harriet Knafler and Professor Kathryn Ayscough from the Department of Biomedical Sciences, and we conducted AFM force mapping experiments of wild type and

[7] As in the case of bacteria and bacterial cell walls

mutant *Candida Albicans* cells, with the aim to investigate the role of cell wall mechanics in its biological function (and subsequently virulence), by understanding the effect of the mutation on the cell wall's elasticity. We tested two different sets of wild-type and mutant *C. albicans* cell strains, in which the mutant relates to cell wall compositional differences. Like in the case of the stomatal mutant, the induced mutation (*apm4* deletion in *AP-2* complex protein) causes a change in a specific cell wall constituent's composition (*Chs3*, chitin synthase), and this is expected to have an effect on the cell wall composition and cell morphology. We will probe the mechanics by AFM nano-indentation experimentation in order to support this relation. In the second case, we wanted to investigate the altered mechanics of two different fungal cell samples of different mutant strains, as well, but we do not present these data in this project.

As for the first case, *Candida albicans* is a fungal human pathogen, which can cause infections to immuno-compromised patients. We are working on *C. albicans* firstly because finding out information about its virulence may help develop new anti-fungal drugs in the future, but also, because it is a good model organism to study polarised growth (74); *C. albicans* can switch between 2 different morphologies. One is yeast (round cells) and the other is '*hyphae*' (long filamentous cells). We know that this ability to switch between the two morphologies is crucial to its virulence. Our mutant has the gene *apm4* deleted. *Apm4* is a member of the *AP-2* complex, and this complex is involved in a process called endocytosis, which is how the cell internalises proteins which are at its surface. Endocytosis is how the cell brings these proteins back inside to the cell, if it no longer needs them (e.g. if the environment changes). So, a mutant missing the *AP-2* complex is unable to internalise certain proteins (74).

The mutant with which we worked on this project, and which can't do endocytosis, has lots of defects in hyphal growth (the *hyphae* are much shorter and wider than WT / normal cells[8]) and

[8] This can be seen later in our results, but we do not discuss on it in this project because it is a preliminary result.

it has an altered cell wall. We know the mutant has a thicker cell wall, with more chitin (this is a structural component of the cell wall). Thus, we probed the cell's mechanics to check whether the mutant wall has altered mechanical properties. We wanted to test this because, the mechanical properties of *hyphae* are probably important in disease and in its virulence. This is where the AFM can be utilised to investigate the mechanical properties of the mutant cell, compared to wild-type.

2.4. Cell mechanics experimental techniques

The most suitable research technique for the case of this project, of cell mechanical investigation, is AFM in force mapping/force spectroscopy mode with help of indentation technique. It serves both as a nano-indenter with the aim to get surface mechanical data (FD curves and force interactions, and mechanical properties) at the vicinity of stomata, and as a tool to acquire high resolution images of the cell walls. A technical downside of AFM is that the surface of the epidermal plant cells (like stomatal cells) is highly heterogeneous (a few microns of height), and the features on it either extend over the limited z-range of most AFM instruments, or make it difficult for the AFM's feedback mechanism to adjust to them. Thus, we plan on taking measurements at only small local areas (RoI) at the vicinity of stomata. We will discuss extensively on AFM and indentation in the next chapters.

The available techniques for the purposes of imaging and/or mechanical investigation of plant cell walls, as reviewed by the literature (2) (75) (76) are presented in the following table:

Table 1: Experimental techniques for imaging and/or mechanical characterization at the single-cell level.

Experimental technique / Method	Imaging	Mechanical Investigation
Single cell compression **(77)**		Yes
Ball tonometry **(78)**		Yes
Micro indentation		Yes
Cellular Force Microscopy (CFM) **(29)**	Yes	Yes
Nano-scale Dynamic Mechanical Analysis (Nano DMA)		Yes
Scanning Ion Conductance Microscopy (SICM)	Yes	Yes
Atomic Force Microscopy (AFM)	Yes	Yes

These techniques differ -apart from other- at the size of the probe with which they try to measure the mechanical properties of the cell walls; in Tonometry, the ball has a diameter of 300 to 5000 μm, a probe used for Micro indentation and Cellular force microscopy has a tip radius of 2 to 11 μm, and a probe used for Nano-DMA and AFM has a nominal tip radius of about 10 nm to several 10's of nm.

2.5. Atomic Force Microscopy

The most suitable research experimental technique for the investigation of plant cell mechanics and nano-indentation experiments is the AFM (Figure 4). AFM is a highly sophisticated surface analysis technique, which performs an approach-retract indentation cycle on the scanned area of the surface in a vertical manner. It is a system of tip-sample interaction, coupled to a feedback-regulated controller for the investigation of interactions between the probe and the sample surface (Figure 4).

Before the contact, these interactions include *Van-der-Waals* forces, electrostatic repulsion and hydration forces[9] (between hydrophilic surfaces) (79). The forces depend on the properties of the tip and the sample and on the ionic strength of the medium, and can give us information about the nano-scale surface topography of the sample and the forces generated between the tip and the sample. DLVO theory includes this concept of attractive and repulsive forces depending on the salt concentration of the medium (80) (81) (82). After the contact, forces arise from the indentation of the tip into the surface and this can be interpreted via the appropriate use of contact mechanics theory.

Specifically for the case of AFM plant cell mechanics investigation, as discussed before in 2.2, the interaction of a rigid indenter and an area on the cell surface area inside an appropriate medium can be conducted by a clear understanding of the forces involved in the interaction, and can be interpreted through the use of a contact mechanics model.

Depending on other the adhesion forces act inside or outside of the tip-sample contact area, different contact mechanics theory is needed to interpret the mechanics of the contact, and this is mentioned later in 4.3.

[9] dipole-dipole or H-bonding interactions

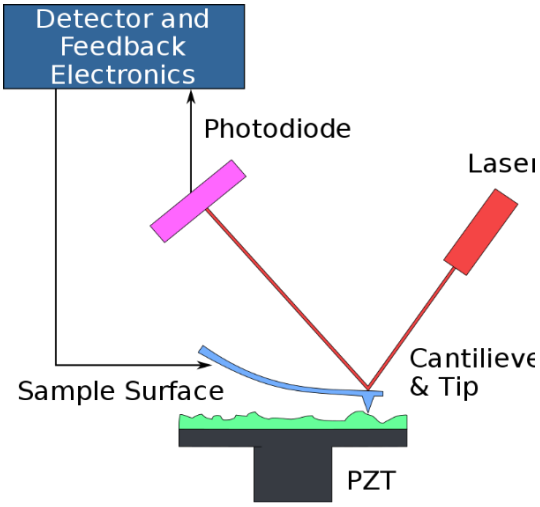

Figure 4: AFM working principle (83). A tip approaches the sample surface under investigation while a photodiode records its relative motion via a laser beam reflected from the rear side of its head, as this interacts with the surface in contact. Then this information is inserted into the feedback loop in order to adjust the height of the tip.

The application domains of the AFM have increased dramatically in recent years, together with the increase in the rate of publications devoted to Nano-biomechanics of cells (15) (84) and plants (84) (20) (2) (80) (76). AFM is a relatively new powerful technique and for probing complex biomechanical structures. After it became clear that the understanding of the role of the physical forces and the mechanical interactions at the cellular and at the sub-cellular level is crucial for the understanding of cellular biological function and plant growth and morphogenesis, AFM has served for a series of experiments. In (85) and (86), the authors investigated the interaction of an AFM and plant leaves of wild type "*Arabidopsis thaliana*", trying to mechanically interpret and analyse the experimental data. They did so, either calculating mechanical quantities like the elastic modulus from the analysis of the AFM force curves or trying to fit their data into mechanical models. Apart from *A. thaliana*, with which we'll be mostly working on, brown algae (8), onion (87) and even pear (88) epidermal cells were investigated under the AFM for the analysis of their mechanical properties and their contribution to growth and morphogenesis. Moreover, according to a paper from (22), nano-

indentation experiments in plant cells have to be interpreted carefully in order to retrieve the right information for the mechanical properties of plant cells, because it is challenging to distinguish between the different mechanical contributions of the plant cells. Turgor pressure, cell wall stiffness, cell and indenter geometry, all bear different parameters for the analysis of the indentation data. This analysis is possible with both a mathematical mechanical model (*Hertz* model, Oliver-Pharr, etc. (19)) and a finite element analysis of the cell wall, where the cell wall is considered as a membrane, a shell, or even as a 3-D solid object. Additionally, the guard cell wall is a dynamic structure, with it controlling differentiation and growth through controlling the cell wall expansion (30).

2.5.1. AFM force mapping mode / nano-indentation

AFM is a powerful technique, able to probe the mechanical properties of materials' surfaces down to the nanometre scale through force mapping and nano-indentation experiments, and the subsequent measuring of the intermolecular forces (attractive and repulsive) that arise at the proximity of the two surfaces while in contact (89) (90) (91) (80). The instrument controls the vertical movement of a cantilever of known dimensions (length l_t, width w_t, thickness t_t), material properties (modulus E, Poisson's ratio ν) and geometry with a tip of known height h_t, half-angle φ and radius of curvature R_t attached at its front end, as this approaches and indents the surface of interest (Figure 6, Figure 5).

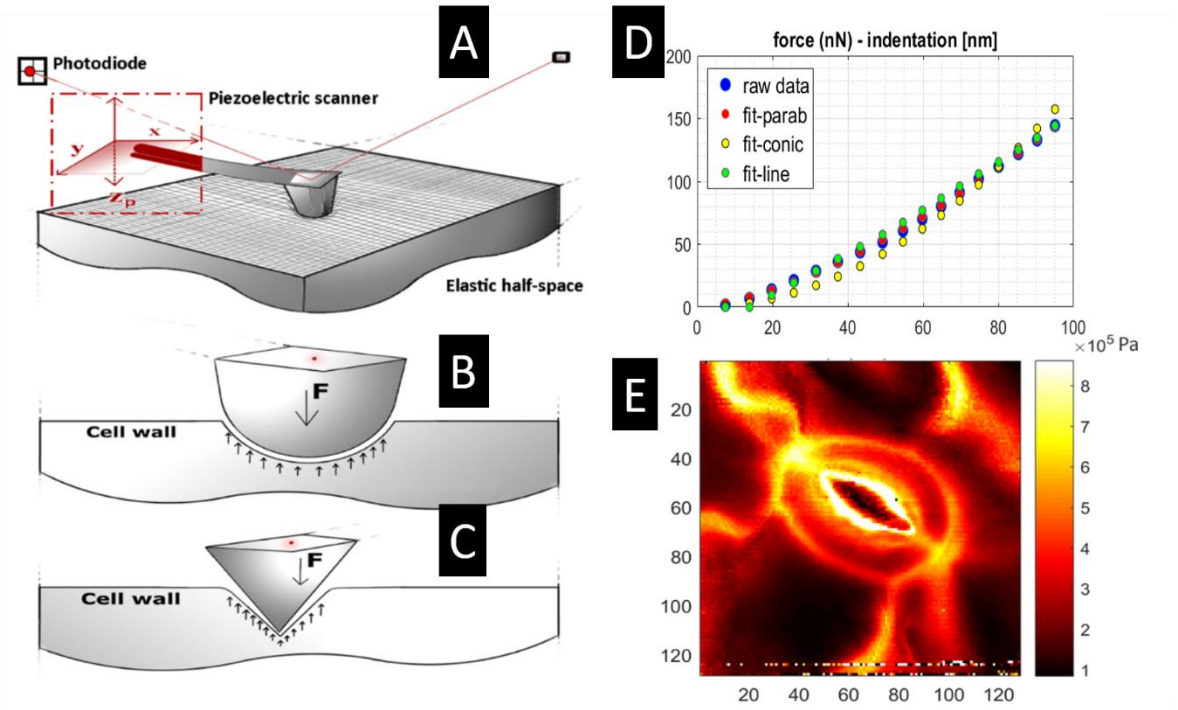

Figure 5: A: Indenter-surface contact B: Spherical indenter C: Conical indenter D: Force-Indentation curve (blue: raw data, red/yellow/green: fitted lines according to different *beta*) E: Example of a modulus map depicting variation of modulus (E) value (measured in Pa) for the different points of the force map.

With the help of a laser beam, reflected from the rear side of the tip and travelling towards a split photodiode (generating a voltage difference ΔV), and a sensitive nano-positioning piezoelectric sensor, the AFM nano-indenter records the vertical height displacement Z_n of the cantilever against the tip deflection Z_d resulting from the contact of the two mechanical bodies. This set of data -after its transformation into force F and indentation δ with the help of cp and the cantilever's spring constant k_C represent the "force-indentation" Force-indentation (FI) curve for a specific point of the force map, and an m *x* n set of relevant arrays constitutes a force map (Figure 17).

The analysis of a force map produces the desired modulus map (Figure 5-E), from which we can see the variation of the modulus values across the selected surface. This analysis can take place either inside the instrument's accompanying and dedicated software, or in a different scientific analysis environment, as in the case of this project (see chapter 5.1). The data of

interest comes in the form of a big dataset consisting of arrays of height (piezoelectric displacement) (Z_n in m) and vertical tip deflection10 (Z_d in m) (Figure 6). Each pair of these is inserted into a 4-D matrix [(*m x n*) *x* (*l x* 2)] (Figure 17), where *l* is the size (number of curve data points) of each FI curve of the force map.

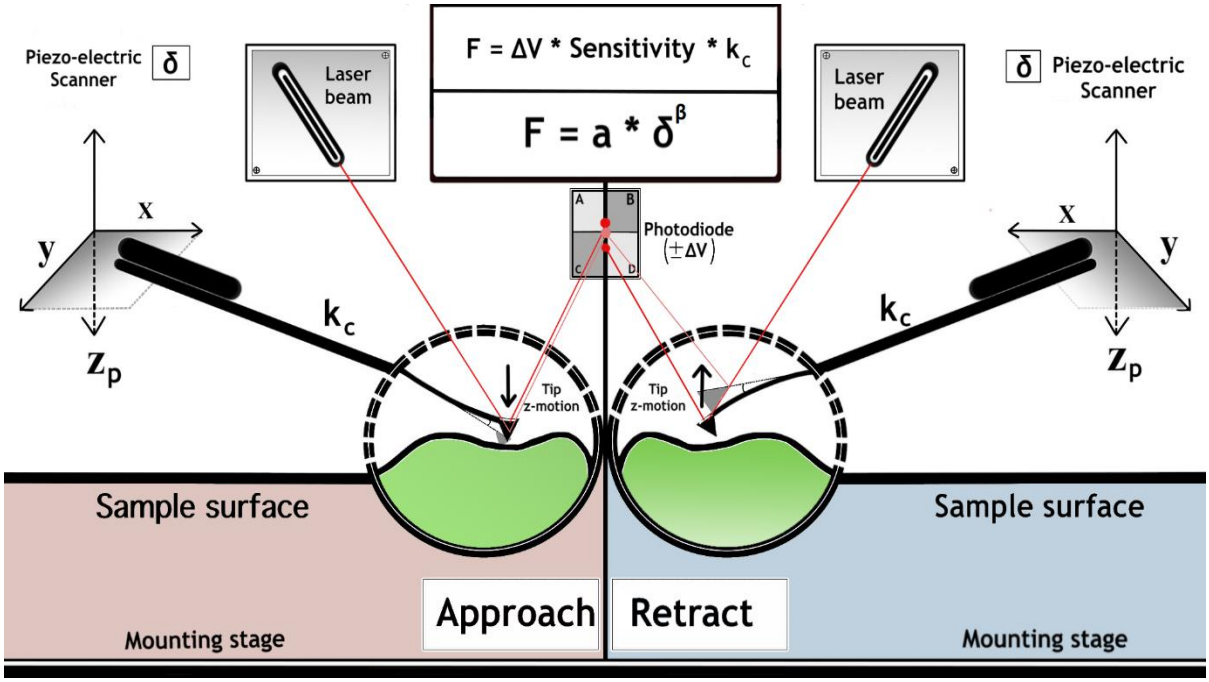

Figure 6: A cartoon depicting the principles of cell AFM nano-indentation experimentation. The figure is split into two parts; the left represents the approach of the indenter towards the surface, while the right one represents the retract off of the surface. In a whole cycle of indentation, two vectors of data are generated, one with piezo-sensor data and the other with deflection. This set represents the force-distance curve to be analysed for the measurement of cell elasticity. Deflection and piezo data are translated into force-indentation with respect to the indenter's spring constant and the cp determination.

The mechanical characterization of a material is not only about the modulus but a lot of other mechanical information and properties as well like stiffness, adhesion, maximum indentation, maximum force, hysteresis, etc. In order to extract this information from each FD curve, we

[10] The optical lever sensitivity has already been applied to our data

follow a specific (and developed for the purposes of this project) analysis technique, which will be described in detail in chapter 5.1.

2.5.2. AFM contact mode

Contact mode AFM is the simplest mode of AFM. It is based on the interplay between a tip attached on a cantilever, and a sample surface. This interaction is monitored by the deflection of a beam on the back of the cantilever (Figure 4), towards the direction of a split photodetector. The deflection signal is used to determine how much the z-piezo must move to maintain a constant cantilever deflection, called set point. Then, this movement of the piezo forms the "topography image".

2.5.3. AFM tapping mode

The surface of our sample is relatively soft and so, we do not desire strong interplay between the tip and the sample surface for the topographical analysis of the cell surface. Tapping mode is a dynamic mode of operation in which a cantilever oscillates near its resonant frequency and it is in position so, during a small portion of its oscillation, it is in contact with the sample (92). While in contact, height is adjusted by the feedback loop in order to keep the amplitude of the oscillation constant. Similar to contact mode, the amplitude signal can be used to reconstruct the shape of the sample surface. This mode of operation has as a bonus the ability to detect the phase difference between the drive and selected signals. From this phase signal, it is possible to infer adhesive and viscoelastic properties.

2.5.4. AFM in liquid

With the advent of AFM nano-indentation mediated cell mechanical investigation, it became reasonable to find a way to test cell samples inside a liquid environment. This is to secure an environment of physiologically relevant conditions (pH, ionic strength, temperature, etc.) for

the cell, to conduct in-situ imaging, and also to minimize surface contamination. Recent research has shown that AFM is able to investigate the molecular structure and the mechanical properties of hydrated cell wall samples. There are some difficulties that the researcher faces when trying to get AFM images of cell walls, and some of them are removed when working under a liquid environment, either with the aid of the droplet technique, a closed fluid cell (93), or the use of a petri dish (Figure 7).

When imaging in air, a water layer is ubiquitous on any surface of a given material and this results to a meniscus force, which dominates the force interaction between the sample and the cantilever and introduces a distortion in the data collected. When imaging in air, there will also be adhesive forces affecting the interaction between the sample and the cantilever, due to capillary condensation effects. To negate this contribution, it is possible to image in a liquid environment.

When working in liquid, there are lots of technical differences as well, from working in air. The most important is that when we introduce the tip-sample system into the liquid environment, we have to let it rest for some time, re-align the laser and correct the deflection since it travels through a different medium now. Finally, we have to discard every time the cantilever with which we had been working for the reason of possible contamination from the working environment.

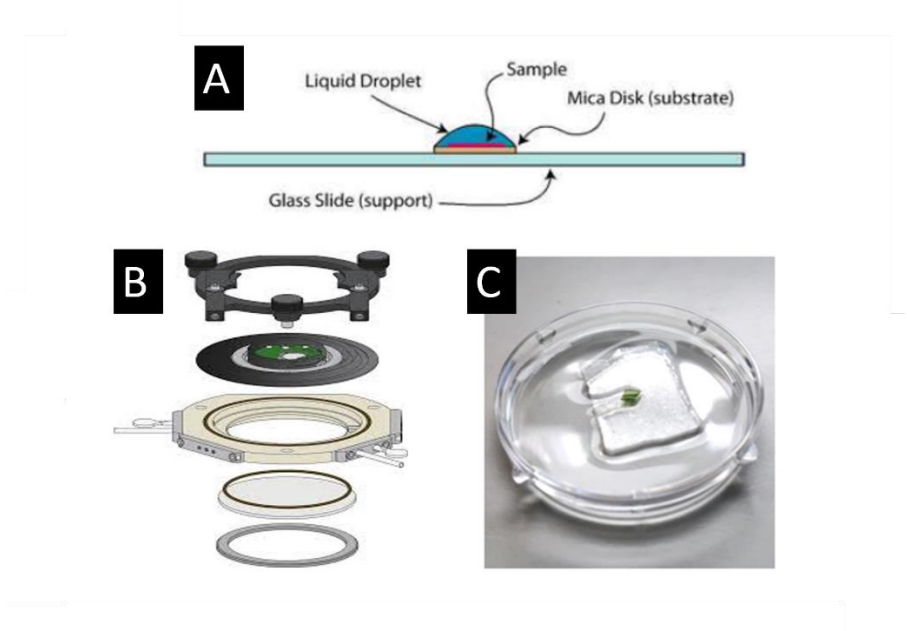

Figure 7: A: Liquid droplet technique B: Schematic of Closed fluid cell assembly; from top to bottom, we see the fluid cell clamp, the membrane, the cantilever holder, the closed fluid cell dish, inlet/outlet tube, glass disk, etc. (93) C: plant leaf piece, mounted on double-sticky tape, inside a petri dish, with a drop of buffer on top of its surface

2.6. Measuring cell mechanics

During experimental conduct, we noticed that –and based on the fact that it has been mentioned solidly in literature (20)- the analysis and interpretation of such results is both challenging and important. It is challenging due to the biological surface's high heterogeneity (as we will see in a later chapter), to the cell's dynamic nature and to the unknown underlying cell wall mechanisms that take place during indentation[11]. It is important because it has been generally noted in different articles (94) that there is a lack of reproducibility when it comes to the measuring of soft biomaterials, in the range of lower than a few MPa of elastic modulus ($E < 5\ MPa$) (Figure 8). This is mainly due to the challenges that researchers face when dealing with such specimens to experiment with and analyse.

[11] Long-range forces prior to contact, Hertzian-like elastic contact during initial part of indentation, and Hookean-like linear stress-strain relationship

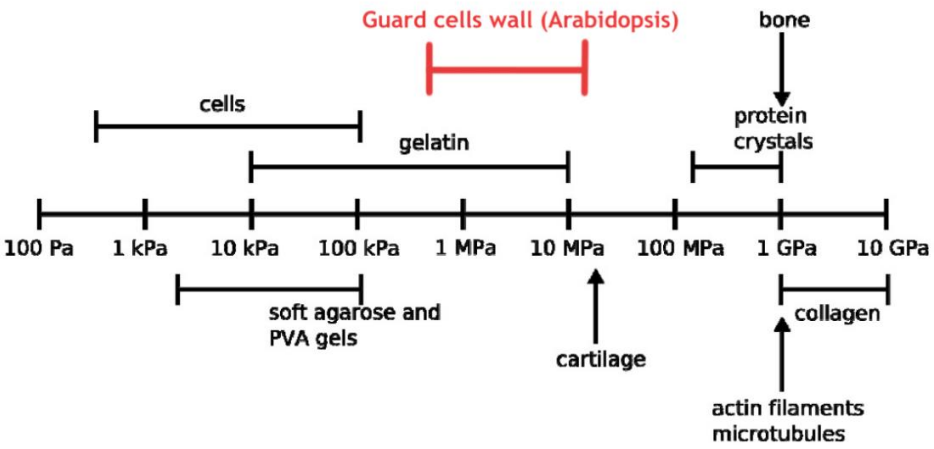

Figure 8: Relative cell elasticity modulus values of different biological material (95). Stomata (guard) cells of *Arabidopsis Thaliana* plants are highlighted with red.

For these reasons, the measurement of the cell mechanics requires good experimental experience of bio-AFM nano-indentation, strong knowledge of cell mechanics and contact mechanics literature, thorough analysis of the surface topographical variation, and a rigorous curve fitting routine. These will be considered in detail in the rest of this thesis.

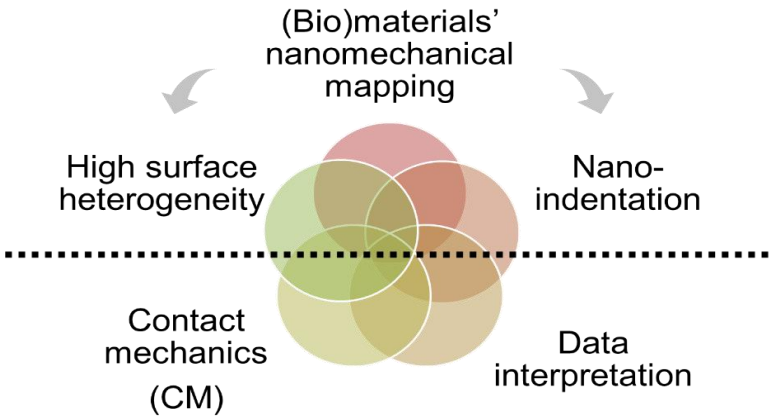

Figure 9: Schematic representation of the workflow and the challenges of AFM nano-mechanical mapping in cells. The most important part is the interpretation of the experiments. The workflow is split in two main parts; on top of the dotted line we have the experiment (indentation) and the challenge it bears (high surface heterogeneity), and at the bottom of it we have the analysis background field (Contact mechanics) and the data interpretation.

Chapter 3: Materials & methods

3.1. Cells

In this project, we worked with two different families of samples; *Arabidopsis Thaliana* plant cells called stomata, and *Candida Albicans* cells.

3.1.1. Stomata - *Arabidopsis Thaliana*

In this work, we investigate the mechanics of plant cells by examining the relationship between biological function, cell structure and cell mechanics. Since the biological function of stomata largely depends on turgor pressure and the mechanics of the cell wall, we were motivated to examine the relationship between the structure of the wall and the modulus on top of it. Thus, the plant leaves used for this work, come from the wild type & transgenic *Arabidopsis Thaliana* and mutants (Wild-type *Col-0*, mutants *pme6*[12] and *LE*) (96).

Plant seeds were cultivated, and after that, small flat parts were cut from the leaves in order to investigate them. A big effort was given to the maintenance of physiologically relevant conditions (buffer) for our samples and the preservation of a constant set of environmental conditions such as room temperature, humidity, etc. The liquid environment consists of bioassay buffers, such as the 'opening' buffer (50 mM KCL & 10 mM MES in a 500 ml water solution) and the 'resting' buffer (10 mM MES in a 500 ml water solution). We investigated Arabidopsis leaves from plants that grew both in a soil environment (Figure 10-A) and an MS medium (Figure 10-B).

3.1.1.1. Microbiology methods

[12] Its function is to modify cell walls via de-methyl-esterification of cell wall pectin constituent

For the MS media germination and growth technique, firstly, the seeds were sterilized, then they were placed in the fridge (4 ^{o}C) for 3-4 days to stratify, then the ½ MS-media was prepared, then poured into plates in laminar flow, and finally seeds were placed into the plates. For the preparation of plants in soil, we had to pour 1 part of Perlite with 3½ parts of M3 composte inside a small plastic pot, water them, then place the seeds onto the surface, and finally let them germinate and grow inside the growth chamber. Transgenic plant leaves have altered cell wall structure, something that is expected to induce different mechanical measurements over the surface of the guard cell walls.

Figure 10: A: Plants (wild type *Arabidopsis Thaliana, Col-0*) grown in a soil environment inside a controlled growth chamber. B: Wild type & transgenic plants of *Arabidopsis Thaliana*, grown in an MS medium.

3.1.1.2. Plant growth & germination

The samples belong to plants of the species *Arabidopsis thaliana* (both wild type and mutants), cultivated in soil inside a controlled environment chamber. Plants were grown at 21 ^{o}C with a 16/8 hr photoperiod (c.200 µEinstein m-2 s-1), relative humidity 60%. After letting plants grow for about 3 to 4 weeks, we finely cut small leaf pieces and mounted them with green glue inside a 5 cm diameter petri-dish with the adaxial (upper) surface facing upwards. Samples were then

immediately immersed in a resting buffer of approximately 15 mL (MES/KCL buffer, pH 6.15 - 1.86 g 50 mM KCL and 5.549 mg 0.1 mM $CaCL_2$ and 1.066 g 10 mM MES-KOH (pH 6.15)) and D-*Mannitol*. After successfully mounting the sample surface, trichomes were gently removed using fine forceps.

3.1.2. *Candida albicans* cells

AFM experiment was performed on *Candida albicans* cells. *C. albicans* cells samples were prepared for AFM experiment by Harriet Knafler from the Department of Biomedical Sciences and the author. Cell cultures were induced to form *hyphae,* and then hyphal cells were harvested by centrifugation at 3000 x g and washed three times with acetate buffer which had been passed through an 0.2 μm filter. The hyphal cell pellet was re-suspended 1:10 in acetate buffer, and 2 μL of this pipetted onto a glass slide. A glass coverslip was placed on top of the cells and left for two minutes for the cells to adhere on the surface. Then the coverslip was removed with forceps and washed three times with acetate buffer to remove most of the cells. The coverslip was introduced on the AFM stage, and AFM force mapping experiments were performed in a liquid environment (acetate buffer, pH: 5.2).

3.1.3. Cell replica

In order to test the validity of our technique (chapter 5.1) and of the several contact mechanics models' implementation on our cell experimental data of high surface heterogeneity, we created a replica of the plant cell's surface, and subsequently we performed AFM nano-indentation experiments on it, in the same way we did for normal stomatal cells. We did that by following the routine, we:

1. mixed Flexbar's "reprorubber" Thin Pour Kit (mix of base and catalyst) on a glass slide
2. used a pipette tip to apply the mix to the cell surface (creating a cast)

3. let the mix harden on top of the surface (making sure sample is not wet, since it stops the hardening of the mix)
4. removed the mix from the sample
5. mixed a small bit more of silicon on the slide and placed the inverse sample cast face up on it and allowed to set
6. Applied a newly mixed silicon into the surface mould that we just made using a new pipet tip
7. Let it set a bit but not the whole way (or they bond together). When it was mostly set but still a bit stretchy, we pulled it out of the mould
8. Mounted the replica inside the same petri dish we used for the cell experiment.

By conducting this experiment, we expect the modulus value to be homogeneous (practically in a small range of modulus values) along the surface of the replica, since the material's surface now is expected to be homogeneous. We present our results in chapter 6.1.

3.2. AFM experiments

In this project we conducted mechanical nano-indentation measurements (force mapping – force distance curves) on stomatal and fungal cells samples using an Asylum Research's (Santa Barbara, CA, USA) MFP3D-BIO AFM in force mapping and nano-indentation mode, and a set of cantilevers (see chapter 3.2.2), aiming to obtain the variation of mechanics over the cell wall's surface, and identify altered mechanical features between different cell strains and different RoI on the same cell.

This working mode is so-called AFM Force-mapping mode and is employed when we conduct a series of nano-indentation experiments around a selected area on the sample's surface. We

conducted a series of force mapping experiments of both wild-type and mutant stomata. We used buffers for the experiments, as explained in chapter 3.1.

We used the closed fluid cell clamp (as seen in Figure 7-B) to mount the petri dish containing the leaf piece and the liquid environment. We also used 50 mm petri dish and we mounted it at the centre of the stage with the clamp, in order to insure the immobility of the petri dish during experimentation.

The stomata have an -approximate- length of 15-25 μm, so most of our experiments had a square scan size of 20-40μm in order to include the whole stomata in the scan. With this scan area, and in order to have a distinguishable resolution on top of the stomatal surface, it was reasonable to have pixel resolution (force map points in total) 64 by 64 or more (128 by 128). Later, the high resolution proved to be important in the advanced analysis of the tip-sample contact interaction that we conducted, and especially the contact-angle effect.

A big challenge of the experiment is the high topography of our sample's surface (both in the case of the stomata and the fungal cells). The height differences that arise along the area of the whole cell can reach up to a few micrometres and the MFP-3D has a vertical piezo range of 15μm. For the case of some experiments it was difficult sometimes to conduct the whole scan, and on top of that we had to ensure a small height difference along the scan, since the results are more accurate when the maximum of the piezo is not reached. Finally, we experimented with other parameters like the tip velocity and force distance in order to standardize our experimental process.

Some experimental factors which would affect the mechanical experimentation -and analysis- are the use of buffers (*Mannitol*, as described in chapter 3.1), the speed with which the tip reaches the surface every time the feedback loop records a full FD curve of the force map, and the heterogeneity of the surface being scanned; this is ever-present in soft, biological,

inhomogeneous matter, it affects and at the same time sets limits to the scanning of the RoI, and finally it is transferred as an artefact in the analysis as well[13] sometimes.

The design of the series of experiments included the following stages:

1. Collection of WT and mutant seeds, and cultivation of them inside a controlled environment
2. Cut of a small piece of the leaf and removal of the trichomes of the surface
3. Mounting of the sample, introduction of buffer and placed under the stage of the AFM
4. Set experimental parameters to the optimal level[14] for the case of biological material experimentation
5. Export all data after experiment, import them with a numerical computing programming language (Matlab / python) and define some analysis parameters.
6. Run the experiment under developed algorithmic technique
7. Interpret the data in the best possible way

3.2.1. Locating stomata

The most challenging part was to locate the stomata in order to start conducting the force map experiment on and around the stomatal area on the leaf surface. One way to do it is with the two optical microscopes provided; the one attached on the head which is responsible for the optical laser alignment, and the one at the bottom of z-stage (comes with the -BIO version of the MFP-3D) which unfortunately cannot be used in our case due to the non-transparency of our samples. This top view has a relatively low resolution and is not helpful when it comes to recognize micro-meter features on the surface of the sample. Another way to locate the stomata is to use do some consecutive topographic scans all over the surface until you locate the

[13] One of our main goals for this project is to emphasize on this artifact of biological experiments and subsequently to try and minimize it
[14] Based on the author's experience

stomata. Then, because of the big wear on the tip, you have to change the tip and conduct the force map experiment, hoping that the new tip will land on the same surface as the previous discarded one. In our case, we built up on experience, where we could locate approximately the stomata on the surface with the top-view optical microscope.

3.2.2. AFM cantilever selection

It is common practice to use rectangular cantilevers for force measurements, whereas V-shaped cantilevers are often used for contact and tapping mode imaging in liquid. As the tip is prone to noise and drift, a 'medium' spring constant cantilever is appropriate to increase the deflection signal for our experiments. MLCT cantilevers are suitable for contact, tapping and force measurements, and PPP-CONT cantilevers are suitable for high- to medium-k mechanical experiments.

The stiffness of the cantilever to be selected for the prevailing experiment has to match approximately the stiffness of the sample's surface in order to achieve a high signal to noise ratio. Also, the level of indentation of the indenter into the sample defines what is going to be measured. For example, in the case of cells, it is common that an indentation of a few 10's of nanometres is purposed to reveal cell wall elasticity, while an indentation of a few 100's of nanometres investigates the internal turgor pressure and how stiff is the cell.

Cantilever selection for our mechanical measurements (force maps) on the stomatal cell walls plays an important role in the type of information to be collected. Because, according to the cantilever's stiffness and the depth of indentation, we can extract information either for the stiffness of the cellulosic microfibril matrix of the guard cell wall or for the interaction between guard cells and their subsidiary neighbouring pavement surface cells. Here, we mainly used two different cantilevers for our experiments; the 'Nanosensors PPP-CONTSC' tips, and the 'Bruker MLCT-F'.

Since we follow a rigorous numerical analysis in this project via our developed analysis technique, we wanted to be as accurate as possible to the quantities inserted in our equations. In order to calculate the elasticity of an indentation experiment, one needs to have correct values for the radius of the tip in use to probe the material's elasticity.

Thus, we conducted SEM experiments of the tips (before and after experimentation) used in this project and we report our findings in the following table (Table 2). We found big differences from the manufacturer's tip specification details, especially in the diameter of the spherical indenters. One way to interpret this could be that these tips undergo a long scanning session in a highly inhomogeneous surface with a lot of abrupt surface change encounters during the raster scanning of the selected RoI. Nevertheless, and for any reason involved in this matter, the important thing is to have as accurate values as possible to introduce into the mathematical models during experimental analysis.

Table 2: Images and details (SEM experimental and manufacturer's) of the cantilevers in use for this project M: measured, N: nominal. The cantilever highlighted in red is the one mainly used for this project's experiments.

Tip specs/Cantilever	k_c N/m N	f Hz N	k_c N/m M	f Hz M	R_t nm N	R_t nm M	SEM image (our experiment)	Manufacturer's image
Bruker MLCT F	0.6	125	0.8	115	20	-	-	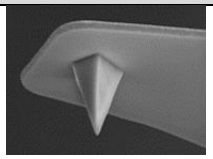
Nanosensors PPP-CONT	0.2	13	0.2	21	<10	~30	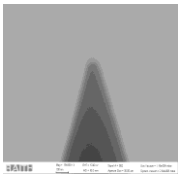	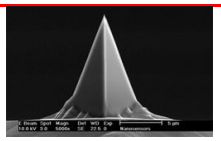 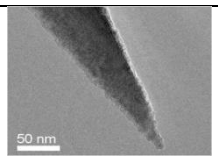
Budget AFM sensors All-in-one	2.7	80	3.5	77	<10	~35	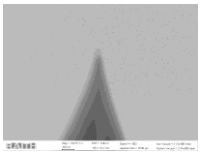	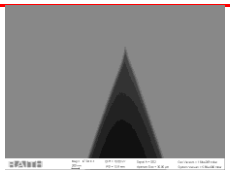

3.3. Analysis of experiments

Of the same importance as the experimental part of this work is the analysis part for the successful completion of this project. This includes initially the analysis of the experiments for the calculation of the mechanical quantities of the samples, and subsequently the application of analytics (inferential statistics) with the aim of inferring important biological results (statistically significant altered mechanics between modified and not modified cells or between different regions on the same cell).

The first part, of analysing the experiments, evolved to a side-project on its own as we developed an automated analysis technique for the analysis of force mapping/nano-indentation

data. This is why it cannot fit into the limits of this chapter, and as a result, it will be described in detail in chapter 5.1, after we introduce the concept of Contact mechanics in chapter 4.1.

In the second part, where now we have a dataset of different populations of mechanical data (modulus and adhesion ratio), we now have to compare the different distributions and check potential mechanical differences. For these reasons, we make use of some hypothesis-testing functions from the "Statistics and Machine Learning Toolbox" from Matlab. Firstly, we use the function *lillietest* which implements the Kolmogorov–Smirnov test in order to test a distribution's normality. This is to validate our later use of the median of each experiment in order to compare modulus. Later, we make use of the Wilcoxon rank sum test (*ranksum* from Matlab) in order to test the equality of the different population medians upon comparison in each case. We will check the data at the 95% significance level. If a given p-value is very small, we will report it as: '$p < 0.001$'. Finally, we will make use of histograms and boxplots showing the distributions and a visual representation of the results and their statistics.

Chapter 4: Theoretical study of Contact Mechanics

4.1. Introduction

Contact mechanics (CM) is a branch of mechanics dealing with the mechanical contact of two bodies. It is an analytical method for the investigation of the elastic-plastic behaviour of material and bio-material surfaces, and especially for measuring a material's elastic modulus, when this gets indented by an indenter of known stiffness and geometry (Figure 5-A-C). From a materials science point of view (in contrast to mechanical engineering), it is common practice to conduct experiments of depth-sensing nano-indentation and analyse the FD curve resulting from the indenter-surface contact. From this analysis it is possible to extract mechanical quantities like modulus (E), hardness (H), adhesion, hysteresis, etc. (in contrast to a priori knowing the mechanical properties and investigating the contact).

In the current contact mechanics literature, the most used CM models are the original work of *Hertz* (97) (based on the elastic contact between two cylindrical-shaped bodies) and its following *Sneddon* variation (equations 5,6), the *JKR* model (98), the *DMT* model (99), and the Oliver-Pharr model (100) (101), with each one of the models taking into account different mechanical quantities like the force of adhesion F_{AD}, the maximum force applied F_{MAX}, maximum displacement δ_{MAX}, the work of adhesion W_{AD}, hardness H, plasticity index ψ_P (80), permanent deformation δ_F, different part of the force curve (approach-retract), or behaviour (elasticity, adhesion, plasticity, hysteresis), in order to calculate the sample's modulus.

For this work, we mainly focus on analysis inside the following context:

1. The elastic properties of the samples,
2. Assuming relatively low adhesion,
3. Not considering electrostatic forces (pre-contact forces)

4. Relatively low indentation depths, inside the range of the cell wall measured depth
5. Analysis of the non-linear part of the FD curve, the part in which Hertzian-like theoretical models apply
6. SEM experiments for the measure of the tip's radius in order to introduce this value in our analysis for more accurate numerical results

Also, we did not conduct dynamic measurements (time-dependent), and thus we do not investigate the viscoelasticity of our samples. In practice, the *Hertz* model is applied in the approach curve of the FD curve, the *DMT* and *JKR* consider a shift of the origin point in the force curve plot and are applied in the retract part of the curve, and the Oliver-Pharr is applied to the retract curve and quantities derived from it. We will examine the use of the appropriate contact mechanics (CM) model for the analysis of our experiment, considering the curve fitting, the adhesion and the hysteresis of the force curves. We will do so by firstly calculating the plasticity index ($\uparrow \psi_P \rightarrow$ Oliver-Pharr), then the ratio between the adhesion force and the max force ($\downarrow {}^{F_{AD}}/_{F_{MAX}} \rightarrow$ *Hertz*), and finally the power fitting constants (80) (Figure 11). We will attempt to calculate the modulus considering non-elasticity for comparison purposes, though our theoretical approach and analysis will take place in the elastic regime.

4.2. The elastic regime

According to contact mechanics pioneers *Sneddon* (102), *Hertz* and *Boussinesq*, for any indenter that can be described as a solid of revolution of a smooth function (Figure 5-B, C) and for an elastic half space sample surface (in our case meaning reasonably low indentation so that the underlying material properties don't change with depth), the load vs displacement FI relationship can be expressed in the form:

$$P = a\ x\ h^{\beta} \tag{1}$$

where P[15] is the force applied by the indenter to the surface, h is the indentation, α and β can be calculated from fitting the FD curve, and from this relationship one is able to calculate modulus from the α, β values. This general equation can be applied for indentation problems in all length scales, as long as the aforementioned conditions stand solid.

4.2.1. *Hertz – Sneddon*

In the case of the *Hertz* model, for spheres and paraboloids, *beta* is:

$$\beta = {}^{3}/_{2} \tag{2}$$

The contact radius[16] (80) is:

$$\alpha = \sqrt[3]{\frac{R\ x\ F}{E_{eff}}} \tag{3}$$

Whereas in the case of *Sneddon*'s variation to the *Hertz* model for a conical indenter (103), *beta* is:

$$\beta = 2 \tag{4}$$

And then, we have the following equations for the FI relationship:

Hertz
$$F = \frac{4}{3}\ x\ \left(E_{eff}\ x\ \sqrt{R_t}\right) * \delta^{3}/_{2} \tag{5}$$

Sneddon
$$F = \frac{2}{\pi}\ x\ \frac{E_{eff}\ x\ \tan\varphi}{1 - {\nu_s}^2}\ x\ \delta^2 \tag{6}$$

[15] P and F are going to be used interchangeably during this study, and so are h, D and δ, for they've been used so by different authors in contact mechanics literature
[16] Not to be confused with fitting parameter α

where F is the force applied by the tip, R_t is the tip's radius, ν_s is the sample's Poisson's ratio[17], δ is the surface indentation, φ is the tip's half angle, and E_{eff} is the effective (or reduced) modulus (taking into account the contributions of the indenter's elasticity and Poisson's ratio, and the sample's Poisson's ratio), which is connected to the sample's elastic modulus via the following equation:

$$E = \frac{1 - {\nu_s}^2}{\frac{1}{E_{eff}} - \frac{1 - {\nu_t}^2}{E_t}} \quad (7)$$

Where ν_t is the tip's Poisson's ratio (~0.26 to 0.28 for silicon cantilevers), ν_s is the sample's Poisson's ratio (~0.5 for biological material), and E_t is the tip's elastic modulus (~130 to 185 GPa for a silicon cantilever[18] (80)).

The *Hertz* model can only be applied in the case of a material surface of an elastic half-space (sample infinitely thick, relative to the depth of indentation), and when the adhesion force F_{AD} is much smaller than the maximum load F_{MAX} applied from the indenter to the sample[19], because it does not consider the effect of the surface energy, neither inside nor outside the contact area. The above criteria apply for the *Sneddon* model as well. The *Hertz* and *Sneddon* models are two very frequently used, established, cases of the same problem, as stated in (102).

4.2.2. Function shaped indenters

In the more general case, when the rigid indenter is described by a smooth function f, and has rotational symmetry around its z-axis, *Sneddon* and *Galin* (104) give their general solution to the problem of the relationship between load and penetration, from which the aforementioned special (limit) cases of the original solution emerge, according to different special shapes of a

[17] Typically, 0.5 for biological material (96)
[18] Depending on its crystallographic orientation
[19] $|F_{AD}| \leq 0.05 * |F_{MAX}|$, ideally zero

rigid indenter. These are the straight line and the quadratic function, which -due to the rotational symmetry of the tip- form a cone (*Sneddon*) and a parabola (*Hertz*) in 3-D space, respectively, as shown in Figure 5. The general solution is modelled inside the aforementioned context, the so called "*Hertz*-type contact problem" (104), and the two sets of equations describing indentation and load for this problem are the following:

Sneddon solution $$D = \int_0^1 \frac{f' dx}{\sqrt{1 - x^2}} \quad (8)$$

Sneddon solution $$P = 4\mu\alpha(1 - \eta)^{-1} \int_0^1 \frac{x^2 f_x' dx}{\sqrt{1 - x^2}} \quad (9)$$

where D is the indentation, P is force, $x = \frac{\rho}{a}$, ρ is the variable contact radius ranging from 0 to α, μ is the shear modulus, η is the material's Poisson's ratio, α is the radius of the circle in contact, and the function f is related to the indenter's profile[20]. Also, for the same problem, we have the following set of equations describing indentation and load:

Galin solution $$D = \int_0^1 x \Delta f(x) \sqrt{a^2 - x^2} dx \quad (10)$$

Galin solution $$P = \int_0^1 x \Delta f(x) \tan h^{-1} \sqrt{1 - \frac{x^2}{a^2}} dx \quad (11)$$

Where Δ is the Laplace operator.

[20] $f = ax^2$ for a conical indenter

4.2.3. Power law shaped bodies

For the special case in which the function f is described as a power law (104) (102), we recognize two sub-categories, for both of which, we have to solve the problem, as described by the two sets of solutions; equations (8,9) for the *Sneddon* solution, and equations (10, 11) for the Galin solution.

4.2.3.1. Monomial

In the first (more simple solution), we have the power law (monomial) function described by:

$$f = c_n \, x \, a^n \tag{12}$$

Where α is the radius of contact. Using the side of *Sneddon*'s solution, Pharr and Bolshakov (105) solved the equations 8 and 9[21], and give their own solution based on *Sneddon*'s work:

$$P = \frac{2E_{eff}}{\sqrt{\pi} c^{1/n}} \, x \, \left(\frac{n}{n+1}\right) \, x \, \left[\frac{\Gamma\left(\frac{n}{2}+\frac{1}{2}\right)}{\Gamma\left(\frac{n}{2}+1\right)}\right]^{1/n} \, x \, D^{1+1/n} \tag{13}$$

Where Γ is the factorial function

For the calculation of modulus directly from FI curves, provided that we know the value of c_n from the function of the indenter's shape, and the value of m from the curve fitting, where m is connected to n as such:

$$m = 1 + \frac{1}{n} \tag{14}$$

Considering *Galin's* solution, *Galin* solved the equations, resulting in the equation:

$$P = 2 \, x \, \theta^{-1} \, x \, \left[c^{-1/n} \, x \, 2^{2/n} \, x \, n^{n-1/n} \, x \, \frac{1}{n+1} \, x \, \Gamma\left(\frac{n}{2}\right)^{-2/n} \, x \, \Gamma(n)^{1/n}\right] \, x \, D^{1+1/n} \tag{15}$$

[21] By inserting equation 12 into equations 8 and 9, and then raising equation 8 to the power of $n + 1/n$ and combining this to equation 9.

Where θ is the modulus.

For the calculation of modulus directly from FI curves, provided again that we know the value c_n from the function of the indenter's shape, and the value of m from the curve fitting.

Here it is important to note that we will only use equation 13, and not 14 (Pharr-Bolshakov) for our calculations.

4.2.3.2. Power series

In the second and more complex sub-category, we have a power series, described by the polynomial

$$f = \sum_{n=1}^{k} c_n \, x \, a^n \tag{16}$$

Where α is the radius contact and it is illustrated in Figure 5. Starting from *Sneddon*'s solution, *Segedin* (102) offered his advanced solution to the problem, resulting in the analytical equations:

Segedin solution
$$D = \sqrt{\pi} \, x \sum_{n=1}^{k} \left[\frac{\Gamma\left(\frac{n}{2}+1\right)}{\Gamma\left(\frac{n}{2}+\frac{1}{2}\right)} \, x \, c_n \, x \, a^n \right] \tag{17}$$

Segedin solution
$$P = \frac{2 * \sqrt{\pi} * \mu * \alpha}{1-\eta} * \sum_{n=1}^{k} \left[\frac{n * \Gamma\left(\frac{n}{2}+1\right)}{\Gamma\left(\frac{n}{2}+\frac{1}{2}\right)} * c_n * a^n \right] \tag{18}$$

This set of equations (17, 18) is extremely difficult to be analysed and subsequently derive a simple equation for the calculation of modulus (as in the case of equations 5, 6, 13, 15) using the findings of the curve fitting, due to their analytical nature. Starting from Galin's solution, Borodich (104) offers his advanced solution to the problem:

Borodich solution

$$D = \sum_{n=1}^{k} \left[c_n \, x \, n \, x \, 2^{n-2} \, x \, \frac{\Gamma(\frac{n}{2})^2}{\Gamma(n)} \, x \, a^n \right] \tag{19}$$

Borodich solution

$$P = 2 \, x \, \theta^{-1} \sum_{n=1}^{k} \left[c_n \, x \, 2^{n-1} \, x \, \frac{n^2}{n+1} \, x \, \frac{\Gamma(\frac{n}{2})^2}{\Gamma(n)} \, x \, a^{n+1} \right] \tag{20}$$

Where θ is the modulus. Again, this set of equations (19, 20) is extremely difficult to analyse and derive a simple equation for the calculation of modulus, but this time, Borodich gives another solution in the form of an axiom:

Axiom 1. (Solution for polynomial indenters):

If we consider an indenter whose shape is defined by equation 16 and pressed into an elastic half-space by a force:

$$P_{\Sigma} = \sum_{n} P_n \tag{21}$$

As in equation 20 or 18, then its contact radius is also α, and the solution to the problem is a superposition of solutions to linear Hertz-type contact problems with identical contact regions.

So now, instead of the case of a monomial function, which would be an improvement to the standard models only if during the contact the function of the indenter shape didn't change (equation 13, Figure 5), we have the improved case of Figure 5, meaning that it is better to assume a combination of two shapes (say of a sphere -at the apex of the tip- and one of a cone -rest of contact). This combination is better described by a superposition of shapes defined by a polynomial fit of the tip shape (as calculated by the tip half-angle). By applying a polynomial fit to the linear function of the tip, we get the coefficients to superimpose the different solutions and can obtain the final modulus value.

In conclusion, based on *Borodich's* statement, and the equations ($m = 1 + \frac{1}{n}$ and 13, 14), we now have two additional ways of calculating modulus inside the same force map, according to the fitting, the tip's shape, and inside the general elastic context. The "*Pharr-Bolshakov*" analytical equation/model, which lets us better understand the indenter's shape (with the condition that this does not change along indentation), and the "*Sneddon-Borodich*" model, which offers a better solution to the contact problem for the case where a two-sectioned tip indents the surface (e.g. the tip apex as a sphere, and the rest of the tip as a cone). We will discuss the application of these two approaches later in a more practical detail. In Figure 11 all the different models discussed here (not only of the elastic regime) are presented.

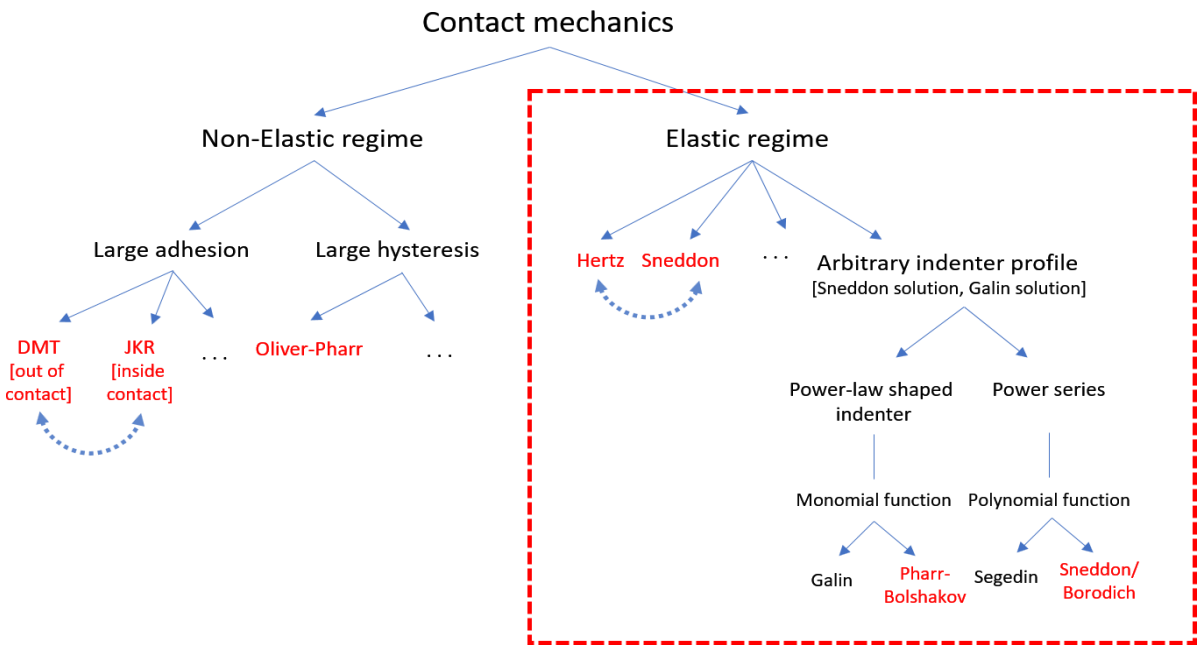

Figure 11: Contact mechanics models tree. In this project we calculate modulus value only inside the elastic regime (red-dotted box).

4.2.4. The effect of the contact angle

Ideally, we should aim to ensure a vertical position of the cantilever relative to the surface as the former approaches the latter -for we aim to calculate the vertical to the surface elastic tensor component E_{33}- but for cases such as plant cells with high surface heterogeneity, it is not always

possible. It is reasonable to think, and it is accurately illustrated in Figure 12, the effect that the contact angle between the indenter and the sample's surface may have in the contact area, in the indentation depth, and ultimately in the calculation of Young's modulus. With our analysis technique we are able to extract the surface normal out of every point of the force map and calculate the contact angle as follows:

$$\cos\theta = \frac{|N_z|}{\sqrt{|N_x|^2 + |N_y|^2 + |N_z|^2}} \tag{22}$$

The modulus calculation may be affected only in the case where the tip is not defined by a smooth function (e.g. the depth of indentation exceeds the tip's radius R_t).

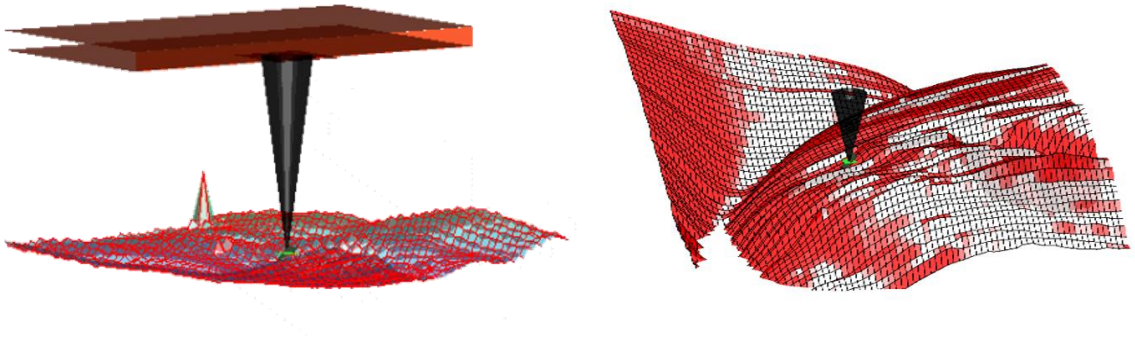

Figure 12: Simulation of the contact between the indenter and the sample surface (real experimental topographical data, both for the shape of the indenter and for the morphology of the surface). Tip's details are from manufacturer's details, and topography (height) data come from an *Arabidopsis thaliana* sample.

4.3. The non-elastic regime

The *JKR*[22] and *DMT*[23] models are essentially modifications to the *Hertz* model taking in consideration the adhesion force F_{AD} and the work of adhesion W_{AD} in their equations (80), with the one -*JKR*- accounting for short range forces generated between the two contact bodies

[22] Large tip, soft sample, large adhesion
[23] Small tip, stiff sample, small adhesion

and inside the contact region, while the other -*DMT*- accounting for long range forces outside the contact region. It has been found by (106) that there is a continuous transition between the *DMT* and the *JKR* models, and that a highly accurate modulus calculation from these two is not possible. We have the following equations:

$$F + F_{AD} = a\ x\ \delta^{\beta} \tag{23}$$

or

$$F + 2\ x\ \pi\ x\ R_t\ x\ W_{AD} = a\ x\ \delta^{\beta} \tag{24}$$

For the case of *DMT*, and

$$F + \frac{3\ x\ \pi\ x\ R_t\ x\ W_{AD}}{2} = a * \delta^{\beta} \tag{25}$$

For the case of JKR.

The Oliver-Pharr model is employed when the so-called loading-unloading hysteresis in the force distance curve is sufficiently big and a 'plastic'[24] deformation occurs[25]. For the case of the Oliver-Pharr model, regarding the modulus' calculation in materials with plastic behaviour, the authors came up with an analytical equation for its calculation from the unloading (retract) curve, and from the sample's stiffness S, the contact area A, the maximum force applied F_{MAX}, the maximum indentation depth δ_{MAX}, and the contact depth δ_C:

$$E_{eff} = \frac{\sqrt{\pi}}{2\ x\ \beta} x \frac{S}{\sqrt{A_C}} \tag{26}$$

Where

[24] A purely elastic sample exhibits no hysteresis and no permanent deformation during its loading-unloading cycle

[25] Applies both in the case of conic and of spherical axisymmetric indenters

$$S = \frac{dF_{MAX}}{d\delta_{MAX}}\,^{26} \tag{27}$$

Is the stiffness of the sample measured at the initial part of the unloading curve, $\beta = 1.05$ for an ideal Berkovich indenter, and:

$$\delta_C = \delta_{MAX} - \varepsilon\, x\, \frac{F_{MAX}}{S}\,^{27} \tag{28}$$

is the contact depth at peak load. The projected contact area A_C is calculated either by the equation

$$A_C = 24.5\, x\, \delta_C^2 \tag{29}$$

for a perfect Berkovich indenter[28], or from the equation

$$A_C = f(\delta_C) = C_0\, x\, \delta_C^2 + C_1\, x\, \delta_C + C_2\, x\, \sqrt{\delta_C} \tag{30}$$

When the parameters C_0, C_1, C_2 are experimentally calculated and introduced into the analysis.

In the following chapter we consider the implementation of the analytical approaches outlined here to AFM nano-indentation and through our developed technique.

[26] Alternatively, stiffness S can be calculated from the fitting parameters A and m, as: $S = A * m * \left(\delta_{MAX} - \delta_f\right)^{m-1}$

[27] $\varepsilon = 0.72, 0.75, 1$ for the cases of a conical, a spherical, and a flat punch indenter respectively

[28] General solution for contact area, more details can be found in (83)

Chapter 5: Automated indentation analysis technique using Optimization & dynamic programming

5.1. Introduction

The motivation behind the development of this analysis technique was that currently available commercial software for the analysis of AFM nano-indentation data (force mapping, FD curve analysis) didn't provide a lot of insight into the cell's mechanical behaviour, and at the same time we wanted to implement advanced Contact Mechanics (CM) models for the calculation of our samples' elastic properties and modulus. Thus, we started extracting the experimental data out of the instrumentation and subsequently processing them with a dedicated developed algorithm, inside a different programming environment (*Matlab, python, see Appendix* - Developed technique algorithm [*Matlab code*]). That gave us the opportunity to understand better the physics/mechanics underlying the problem, to interpret carefully the results, and to create a novel technique for the analysis of relevant experiments of bio-materials' surfaces.

The analysis technique consists of three main parts: import, analysis, and visualization. The first step of analyzing a single force map (of m *x* n scan points/pixels) (Figure 13) is to import into Matlab the whole dataset of the AFM force curves (each force curve consists of raw experimental data of deflection and piezoelectric sensor data (Figure 6), depending on the instrument used). In different commercial instruments (rather than the Asylum's MFP-3D used in this project), this dataset is stored in a different manner and file format. After importing the data and reading the experiment's details, it is time to set/initiate the values of some preliminary

variables. Here, the user can make some decisions for the type of analysis[29], and these are discussed later in detail.

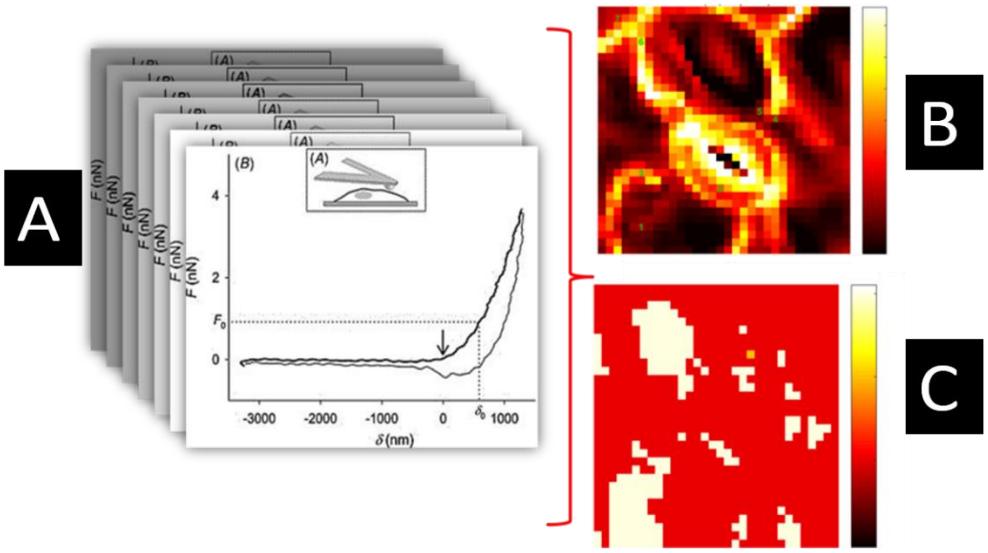

Figure 13: An m *x* n dataset of FD curves is imported into the algorithm, analysed one-by-one and the mechanical results are presented in a heatmap manner. A: A collection of FD curves (107), whose analysis generates the B: Modulus map, where each pixel represents a value obtained by the analysis of the relevant FD curve. C: CM model map; every pixel represents the optimal CM model (80) with which to calculate modulus for the relevant FD curve (different colours represent different suggested CM model).

Now, the algorithm is ready to perform its automated analysis routine which involves a collection of actions, until it is finished and ready to be displayed through a series of figures. The first step of the analysis routine is to store the data into large data arrays so that they can be accessible throughout the runtime. Then we initiate a loop[30], within which -for each point of the same force map- a series of calculations takes place, working out the physical/mechanical quantities of the material's surface (Figure 14). These include the local Young's modulus (E), the suggested contact mechanics (CM) model, the adhesion work (W_{ad}) of the curve, the 'yield-like' point, the max force applied (F_{MAX}), the total indentation (I_{tot}), the plasticity index, etc.

[29] Which CM model to analyse the data under, if 'indentation' analysis will be conducted, etc.
[30] In series or in parallel computing

For the final step of the analysis, a graphical representation of all these findings with both spatial maps and universal charts is essential for a full insight on the mechanical problem. This technique has been proven to be fully automated (producing the best result for diverse set of experimental data, with minimum user intervention), universal (effective for the surface of stomatal, fungal, and other tissue and cell surfaces), straightforward (full insight into the problem), and innovative (new ways of analysis and new way of implementing contact mechanics models).

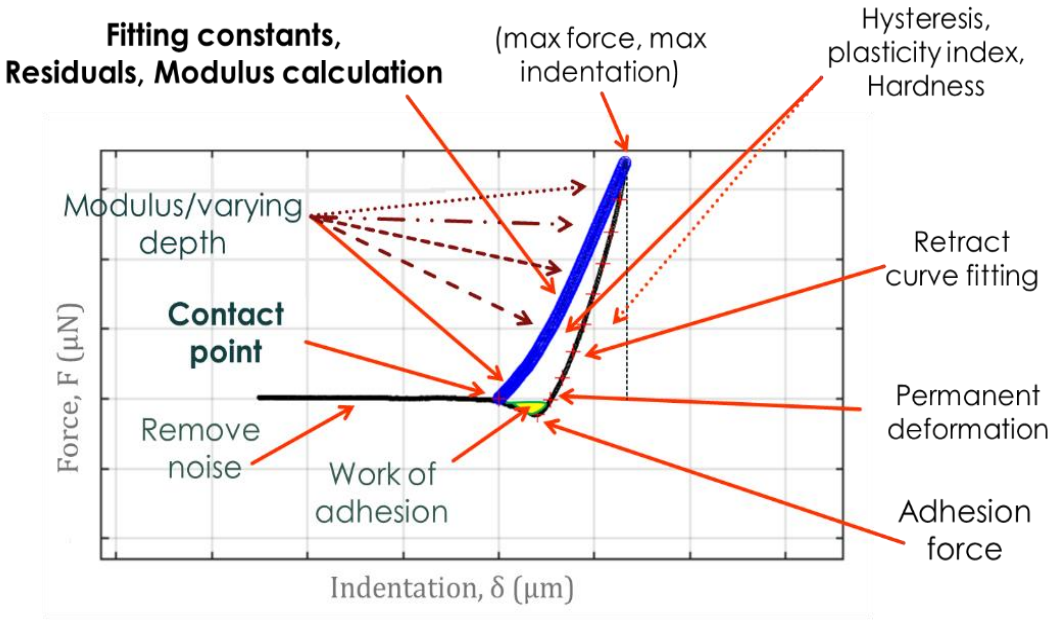

Figure 14: Mechanical quantities worked out during technique's FD analysis (80). Each feature extracted from the individual curve is used later for mechanical analysis of the individual force map, or for comparison analysis between different force mapping experiments.

A few key aspects of AFM indentation data interpretation lie in the curve fitting, in the correct cp [31] calculation, and in the optimal contact mechanics (CM) model used to analyze them (Figure 15). Current commercial packages allow the implementation of different/suitable models across different force maps but do not facilitate the use of different models within the

[31] the initial (critical) point of contact between the indenter tip and the surface

same force map. For cases described as above, we show that this may not always be the appropriate way of approaching the problem. An analytical tool to address this issue would be of potential broad use in biological and materials science AFM research, allowing more confidence to be placed on the data interpretation. Here, a successful implementation of such a tool is presented. A new analysis technique is provided, together with a new method for the calculation of the elastic modulus of biomaterials in a force mapping manner using different analytical equations for each individual point of a force map, providing a continuum transition between different contact mechanics models, according to the fitting of the relevant curve and to the indentation depth. Later, we will break down each part of the analysis in detail.

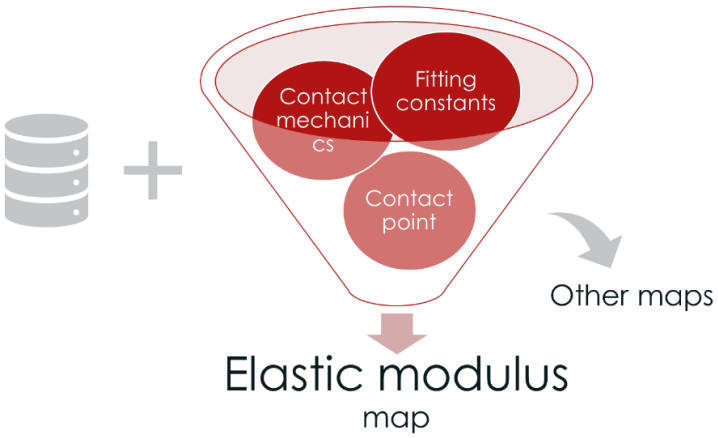

Figure 15: Key aspects of AFM indentation data interpretation: curve fitting, cp calculation, and optimal contact mechanics (CM) model.

5.2. State of the art

Before getting into the details of the technique, let's start by presenting the state of the art in the field of automated FD curve and force-volume image[32] analysis. The automation of the acquisition of nano-mechanical properties of samples and surfaces, and of the mechanical investigation of materials from the analysis of AFM indentation experiments has been a challenging project during the last years. This makes sense, since on the one hand AFM nano-

[32] A collection of force-distance curves

indentation is important for both clinical applications and basic biological research, but on the other hand the analysis of such experiments can only be conducted by experienced personnel on topics like force spectroscopy, mathematical optimization and contact mechanics, and thus an automated technique is of importance if it is to be used by a broader personnel. Furthermore, after experimentation and analysis, a third step is important, and this is the reading and interpretation of the results. In this sub-chapter we focus on previous related work, both for the automation of the analysis and of the reading of the analysis results.

There have been several attempts in the past towards an automated AFM FD curve analysis, like the works of (108) (109) (32) (110) (111) (112) (113) (114) (115) (116) and the various commercial software accompanying the instruments (or stand-alone applications), and in this work we aim to contribute to the development of field.

In the paper of (108) the authors make a review, and focus on strategies found in literature for calculating cp and analyzing the material's elasticity from the FD curve, while at the same time they offer their customized approach on the problem (based on the reviewed ones). They present a set of pre-processing evaluation steps to check which objective strategy is best to be followed for the *cp* calculation, and then they implement this via their own customized technique. Some strategies found in literature are based on the calculation of 1^{st} and 2^{nd}-order derivatives (of which an abrupt change throughout the curve would indicate a cp) while others rely on the evaluation of the fit with free parameters E, Z_d and Z_P. It is important to mention that, as stated in (108) not a single approach is suitable for all the cases since each dataset comes with its own difficulties. Thus, there is need for a combination of approaches to combat this challenging problem.

In the paper of (109), the authors follow a similar rigorous data processing and analytical routine in order to produce a collection of maps for the prevailing force map experiment[33]. For the calculation of critical points (jumps, change of slope, etc.) they also use a similar technique to ours, employing derivative and polynomial calculations. They investigate the electrostatic forces produced at the non-contact area (pre-*cp*), which is something that we do not, but they examine surface elasticity at the contact area under Hertzian-like theoretical models and stiffness measurements (mainly dominated by internal turgor pressure) under *Hookean* analysis. Moreover, in the case of biological cells, this linear part of the FD curve is used to measure the internal turgor pressure of the cell. Finally, in this paper, the critical points are found using the minimization of the squared error of a set of elements which are following a non-linear trend, specifically to the power of 2 (since in this paper, it is assumed that the indenter has a conical shape and thus $\beta = 2$).

In the paper of (110), a whole different approach to the problem of FD curve analysis is presented. Here, the problem to be solved is a classification problem between malignant and benign tumorous tissue. As it is a classification problem and supervised machine learning techniques have found their way into data-driven problem-solving[34], the authors choose to feed a neural network classification algorithm with all these FD curves that traditional techniques are using as their input, in order to train it. In this way, the goal is that indentation experimentation is expected to yield clinical finding in a small time.

Here, we present our own version of an automated FD curve analysis technique, implementing a novel approach to the problem of calculating *cp* (without the need of minimizing the squared

[33] Force map and force-volume are used interchangeably throughout literature and subsequently throughout this thesis

[34] This is a data-driven problem, since huge datasets are the output of nano-indentation experiments. In the case of our project, a single force mapping experiment consists of 1.2e+5 files worth of 3.89 GB of data

error), and the previously discussed contact mechanics (CM) literature, and in order to test its application in practice we analyze our own experimental data for the investigation of altered mechanics in mutant plant and fungus cells. As aforementioned, the mechanical analysis of the experimental data can take place either inside the instrument's accompanying software, or in a different scientific analysis environment, as in this case.

5.3. Analysis technique

In this section, many technical details will be presented for the understanding of the workflow of the technique. Starting from the import of the raw data files, to some pre-processing routines, to the calculation of the cp between the sample surface and the indenter, to the fitting of the curve, to the calculation of the modulus and other mechanical parameters, to the final presentation of the output of the analysis, we will present in depth the separate parts of the technique.

5.3.1. Import data & set analysis parameters

Initially, we export the force distance data from the prevailing experimental technique with which we are conducting the experiments (in this project, it is mainly the Asylum's MFP3D-BIO). This is usually saved in a .txt file, or in a proprietary file format (like .ARDF in the case of the MFP-3D), and it contains information such as experimental parameters (e.g. tip velocity, map resolution, force distance, etc.), the height map (often acquired by the instrument's feedback loop in parallel, during the force map experiment), and of course the force distance curves. Then, we read this information from the file and save it into our analysis environment (needs caution, since it is a huge file dataset in most of the cases). More specifically, in Asylum Research's MFP-3D, information is stored in a file format called .ARDF and it contains both the experimental data and the FD data in a single entity. The developed algorithm can read the experiment's details directly from the .ARDF file but not the other data, and thus one has to

extract this from the accompanied to the technique software and into a large collection of .txt files. In JPK's Nanowizard, this force map information is saved all at once in a .txt file, together with the experiment's details, making it easier and quicker to import into Matlab.

After the import, the user can decide about the type of analysis, the visualization output, and if they want to interact with the output; selecting data from specific regions of the cell rather than the whole force map. As for the type of analysis, it can be decided from the user whether only the approach part of the curve is analyzed (or the retract part, or both), or how much of the total indentation is analyzed, or how modulus values are calculated (*Hertz* model, Oliver-Pharr model, *Pharr-Bolshakov*, etc.), power law (β) analysis, indentation vs β analysis, etc. Also, some materials may prove to be challenging to analyse and thus, the user might have to intervene. Experimentally, it may happen that the curve points are not enough for the analysis to be conducted properly, or the changes in the curve are too abrupt for the algorithm to follow, or there is too much noise in the zero line, and it confuses the search for the cp. Even though the algorithm is developed so that it can adjust to such limit cases, it may be necessary for the user to either lower the criteria due to lack of points, or to lower the threshold for evaluating a cp (chapter 5.3.2.1), or to smoothen the curve. As of the visualization part, when the analysis is finished, a collection of figures is available for the user to get an immediate insight to the results of the experiment. Here, one can see how the mechanical properties compare to their neighbouring pixel's ones in a mapping manner (Figure 16) (modulus map, *beta* map, adhesion map, "yield-like" point map, etc.). At the same time, other figures are available, with the most important ones being the visualization of selected FD curves of the map, gif's (for the visualization of the progression of mechanical quantities like modulus, *beta* and RMSE along different levels of indentation), and histograms for the distribution of values. Finally, as of the way someone wants to interact with the figures, there is the option of manually selecting a

collection of points from the map and subsequently perform a specialized and comparative analysis with these selected data from the force map (chapter 5.3.3.1.5).

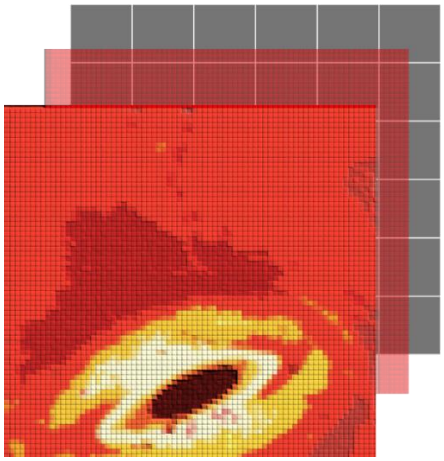

Figure 16: Matrix data to a colormap (modulus map). All modulus values of an AFM force map experiment are calculated and turned into a heatmap.

5.3.2. Analysis

After the data having been saved in our working space as a 3-D matrix (`Figure 17`), we start by storing the FD curve data in large arrays, in order to be accessible throughout the analysis, and then we begin analyzing each force distance curve one-by-one successively (serial or in a parallel computing manner, if dataset is huge and runtime is important). Firstly, we calculate the cp (`Figure 14`, chapter 5.3.2.1), then we choose the level of indentation[35], we transform the Z_P-Z_d set data into FI data (force and cantilever motion are related via the equation: $F = k_C\, x\, (\Delta Z_d)$ (80) and indentation is calculated via the equation: $\delta = \Delta Z_P - \Delta Z_d$), fit our data to the optimal power law (multivariate, unconstrained, non-linear optimization, *beta* in equation 1), and finally use the appropriate contact mechanics model (80) (108) to calculate modulus E from equations `5`,`6`, `13`. Additionally, we can extract information about the mechanical behavior of our sample, and particularly mechanical quantities such as the max

[35] analyse only a part of the force curve, for the case when δ is big relative to the cell wall's thickness, and thus the sample is not considered still as a half-space

force applied F_{MAX}, max indentation δ_{MAX}, hysteresis, adhesion force F_{AD}, work of adhesion W_{AD}, hardness H, etc.

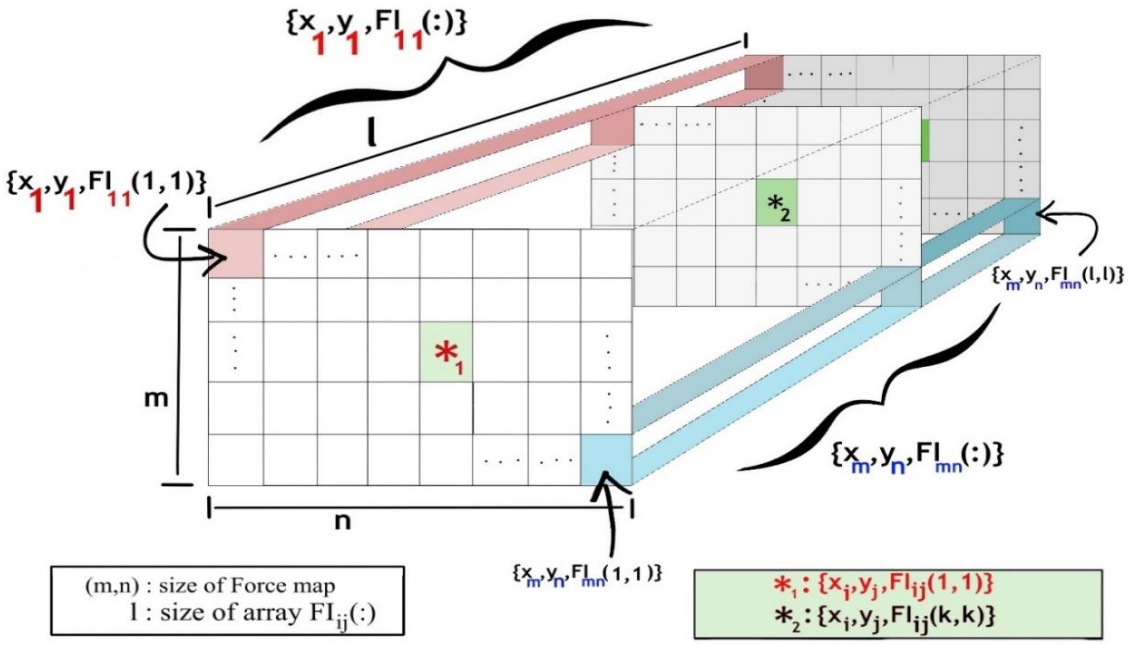

Figure 17: A big 3-D matrix containing m * n force-distance curves. Here, l is the size of each FD curve/array of the map, m*n are the scan points of the map, FIij is a full force distance curve for the scan point (i,j), and the red and the blue arrays represent random full force distance curves of the map.

5.3.2.1. Calculate contact point (*cp*)

One of the most challenging problems is the calculation of the cp in biological AFM indentation. Since –as described in the start of chapter 5.3.2- the transformation of sensor and deflection data into Force-indentation data relies on the correct calculation of cp, it is clear that we need to focus our strategies on this primarily. And there are many ways of approaching this problem, one of which is through the expert's visual recognition; analyzing one FI curve at a time, visually choosing the optimal data point on the curve, and finally assigning it to *cp*.

Another common approach on the calculation of *cp*[36] is through non-linear regression, trying to fit the FI curve under a non-linear model, and this approach has problems for the following

[36] Different strategies reported before in chapter 5.2.

reasons; the algorithm works as such: starting from a data point close to the starting one, common algorithms successively search to optimize the fit of the curve under a given *beta* (1.5 for spherical/round tips and 2 for conical tips). Here, there are two problems:

1. If, and in this project, we show that it is happening, the FI curve should not be analysed under the given *beta*, then this affects the "correct" calculation of *cp*.
2. It happens, especially in very soft biological materials, that the zero line is very noisy. And even if we decide to remove the noise, we still may lose valuable information. In such case, the search for an optimal fit of the FI curve is not possible, since the optimization process will most probably never converge.

If the experiment design part (best choice of tip, optimal choice of parameters like tip velocity, surface resolution, buffer selection, scan rate, etc.) is optimal and the sample is more compliant to the standards of non-biological matter, then these two problems can be ignored. If not, then a different approach is needed. With our solution to this problem, we successively look through all the data points, searching for one which will satisfy a set of score values (numerical computations involving gradient calculation). In this work, two new ways of calculating *cp* are presented, based on this approach.

5.3.2.1.1. Calculate cp via gradient testing

The first one is based on the simulation of the way an experienced scientist would follow to visually identify the *cp* by examining one-by-one all the FI curves. So, trying to simulate this visual examination, a technique was developed to tackle this problem and it works as follows:

1. Starting from the first curve data point of the raw data (the algorithm can be optimized to start at a later data point in order to reduce the run time), we search successively along the curve data points to find a data point which satisfies a set of requirements.

2. For the prevailing test data point *cp_t*, the algorithm implements a set of six "tests", and subsequently collects a set of 'scores' (*c1*-*c6*) for those tests, for this data point:
    a. **c1:** *percentage of 'pass' points to k (k to be selected from the algorithm according to how many data points the curve has in total and to the relevant position of cp_t to c_max[37]), depending on whether the ratio of the height difference between this data point and the max point of the curve c_max (*Figure 14-max indentation/max force*), and of the height difference between this data point and the next k points is higher than 1.*
    b. **c2:** *percentage of 'pass' points to k, depending on whether the ratio of the gradient between this data point and the max point of the curve c_max, and of the gradient between this data point and the next k points is higher than 1.*
    c. **c3:** *percentage of 'pass' points to k, depending on whether there is an abrupt change of gradient in the next k data points (as this would possibly be a case of discontinuous contact between the indenter and the surface)*
    d. **c4:** *percentage of 'pass' points to k, depending on whether the gradient between this data point and the next k points has the same sign as the gradient between c_max and the first point of the curve.*
    e. **c5:** *percentage of 'pass' points to k, depending on whether the height difference between this data point and the next k points has the same sign as the height difference between c_max and the first point of the curve.*
    f. $\boldsymbol{c6} = {}^{cp\_t}/_{c\_max}$
3. When these scores have been calculated, this set of scores $c\_t = [c1, c2, c3, c4, c5, c6]$ is compared to a set of 'optimal' scores $c = [c01, c02, c03, c04, c05, c06]$[38].

[37] Curve data point with the maximum value, endpoint of the approach curve.
[38] *c* is set by the author according to their experience

4. If $c\_t(i) \geq c(i)$, for $i \in [1,6]$, then *cp_t* is now the cp of the curve, so: $cp = cp\_t$.

5.3.2.1.2. Calculate cp via logistic regression (binary classification)

The second one is an improvement to the first approach. As we said before, for the *cp* calculation, a set of 'score values' *cp_t* is applied successively on the curve points and once an optimal score set is found, this data point is assigned to *cp*. But later in the project, and with the aim to choose a better set of *c*, we implemented a binary classification algorithm (*see Appendix* - Contact point calculation method (logistic regression) [*python code*], multivariate logistic regression[39] (117)) to better solve the problem, and to do that, we manually selected the *cp* (positive result, $y = 1$) and random points (negative result, $y = 0$) from ~1600 different curves. So, we manually collected a large dataset with the tests *c_t* as features, y as the predict variable, and observations all the 'test scores' we collected. Then, and after some pre-processing (removing nulls) and feature-scaling, we split the data into a train (70%) and a test (30%) set, we implemented the Logistic Regression classifier from 'scikit-learn' python library (118), and finally we generated a Logistic Regression model, with 94% accuracy, 94% precision and 94% recall.

[39] Logistic regression (100) is a commonly used Machine Learning algorithm to estimate the probability that a new instance belongs to a certain class or not (in our case, cp or not).

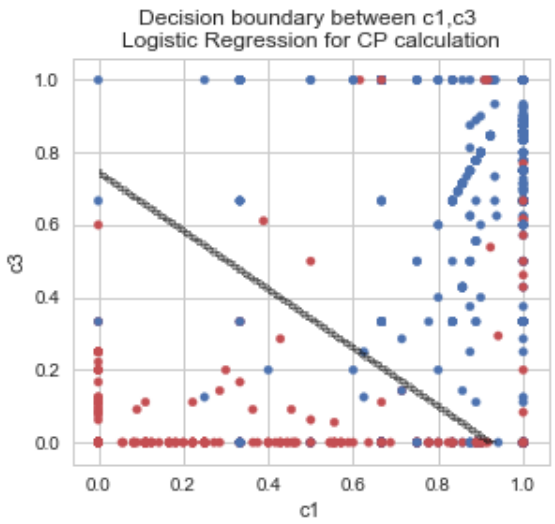

Figure 18: Multi-variate logistic regression – linear decision boundary between two -selected- features of the classification, c1 and c3. The full decision boundary can't be shown since it is a 6-dimension feature space (c1-c6).

This model (its attributes) was then extracted and later implemented into the developed technique to enhance *cp* calculation. This approach increased the accuracy by ~20% and it was promoted to default. The classification report is presented in the following table:

Table 3: Classification report for the *cp* calculation training; this report acts as a validation of the classification statistical analysis

	Precision	**Recall**	**F1-score**	**support**
0 (non-*cp*)	0.94	0.93	0.93	242
1 (*cp*)	0.93	0.94	0.93	242
Average / total	0.93	0.93	0.93	484

5.3.2.2. Regression

When the cp has been optimally calculated, then it is the time to fit the curve with the aim to extract the preferred mechanical properties of the sample surface under the contact mechanics

model of choice. The algorithm tries to minimize the RMSE -which is a measure of the deviation of the observed values y_i to the ones calculated by the equation/model $\widehat{y_i}$ (equation 1):

$$RMSE = \sqrt{\frac{\sum_{i=1}^{N}(\widehat{y_i} - y_i)^2}{N}} \tag{31}$$

Where N is the total number of data points, and:

$$\widehat{y_i} = a * {x_i}^{\beta} \tag{32}$$

Where α, β are the fitting parameters.

The minimization technique that we use here is Matlab's implementation of the simplex search method of (119), called "fminsearch" from the Optimization package of the programming language suite for finding the "minimum of unconstrained multivariable function using derivative-free method".

The result of this fitting is an optimal value for the parameter α from equation 2, and can be used to calculate the modulus E according to the contact mechanical models discussed in chapter 4.1. For example, for the case of the *Hertz* model:

$$a = {}^{4}/_{3} * \left(E_{eff} * R_t\right) \tag{33}$$

<=>

$$E_{eff} = \frac{3 * a}{4 * R_t} \tag{34}$$

for the case of the *Sneddon* model:

$$a = {}^{2}/_{\pi} * \frac{E_{eff} * \tan\varphi}{1 - {\nu_s}^2} \tag{35}$$

<=>

$$E_{eff} = \frac{\pi * (1 - {\nu_s}^2)}{2 * \tan\varphi} \tag{36}$$

And for the case of *Pharr-Bolshakov*:

$$a = \frac{2E_{eff}}{\sqrt{\pi} * c^{1/n}} * \frac{n}{n+1} * \left[\frac{\Gamma\left(\frac{n}{2} + \frac{1}{2}\right)}{\Gamma\left(\frac{n}{2} + 1\right)}\right]^{1/n} \tag{37}$$

<=>

$$E_{eff} = \frac{a * \sqrt{\pi} * c^{1/n}}{2} * \frac{n+1}{n} * \left[\frac{\Gamma\left(\frac{n}{2} + \frac{1}{2}\right)}{\Gamma\left(\frac{n}{2} + 1\right)}\right]^{n} \tag{38}$$

In the case of our project, not only the α value is optimized, but the value of β as well, which means that we do not take for a fact that a single model/equation/power-law is able to describe all the force curves of a force map, and thus, we look for the optimal β value for each curve fit individually.

5.3.2.3. Control of indentation depth, “Tomography” & “yield” point

Initially, the developed technique provides the ability to control the level of indentation for fitting analysis. If the user selects to fit only a part of the curve, then the algorithm selects a part of the approach force distance curve (either a percentage or an absolute value, e.g. either 50% of max indentation, or just 50 nm after the cp). After the RoI is selected, we fit this part of the curve as it was our normal approach curve and we calculate the modulus value.

This leads us to the second feature called “modulus tomography” (23) (120) (121). In this analysis scheme, one can divide the indentation depth in equally distanced parts (e.g. divide the approach curve in 10 equally spaced sections) and successively fit and calculate the modulus (or stiffness) value for the different sections (all of them starting from the cp and

ranging until the division points). In this way, the progress of the mechanics of the sample can be viewed and assessed in a successive manner (Figure 19), and this can also be stored in a gif file or a video format. Very important findings can be gathered via this technique, including the underlying material and mechanical properties, and the point (or points), as translated in indentation depth, in which changes in the curve are observed, and which can have a bio-physical explanation.

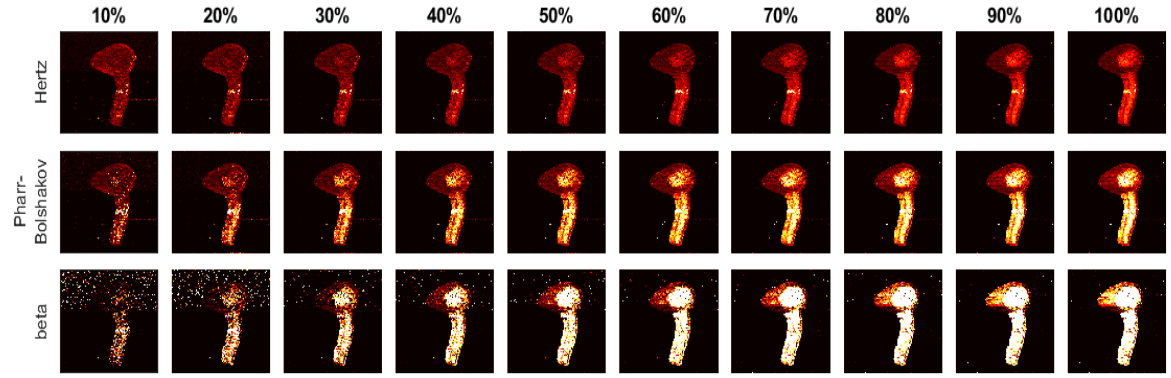

Figure 19: The succession of modulus (1st row: *Hertz* model, 2nd row: *Pharr-Bolshakov* model) and *beta* values (3rd row) of an example experiment along the 100% of selected indentation (scale: [1.1 2]), for an example experiment.

The third feature is the critical point ("yield"[40] point); after the calculation of the cp, we can select the option of further investigating the contact area, successively searching from the *cp* and onwards to the F_{MAX} for a data point on the curve after which, a set of criteria are met (like a consistent change in the gradient of the curve followed by another trend thereafter). This data point is a key indicator of the underlying material properties of the sample. And furthermore, it informs us for the indentation depth in which this "yielding" occurs.

[40] It is not actually a yielding point, as referenced in the Engineering literature, but rather the curve exhibits a yielding-like behavior

5.3.2.4. Calculate optimal power-law-exponent (*beta*)

This part is at the core of this analysis tchnique. At the start of the experiments' analysis, we noticed that not a single contact mechanics model/analytical equation could fit all the force distance curves of the same force map. At the same time, not enough informaton was available at the time, for further analysis. Here, as explained before in chapter 5.3.2.2, we conduct a multivariate optimization search for the RMSE values of the curve with the aim to find the optimal power law *beta* that describes theforce distance curve, and then choose for the prevailing curve the optimal version of equation13 to calculate modulus. From a range of 1.1 to 2 with increasing steps of 0.1 for the value of β, we calculate the optimum and we apply this to the equation 8, having already calculated the c_n values at the beginning of the process, based on the tip characteristics given from the manufacturer and/or the SEM analysis of the tip before and after the experiment. Here, we calculate the c_n values of the tip via simulating the indenter shape (Figure 20-A,B). We perform a polynomial fit of the tip profile (assuming a rotational symmetry and constrains for the diameter from manufacturer's tip details), and for the different degrees of the polynomial we calculate the relevant c_n values of the indenter's shape for the different *n* (*beta*) values.

$$f = c_n * a^n \tag{39}$$

where α is the radius of the tip, and *n* the degree of the polynomial fit.

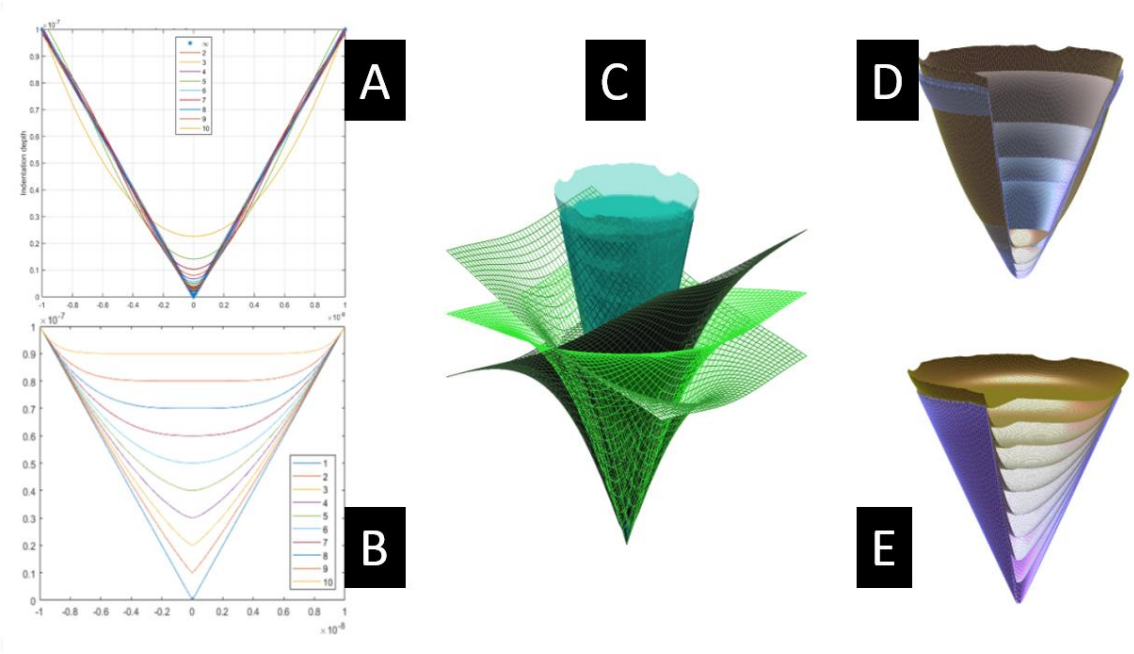

Figure 20: A: Simulation of the tip's shape for the calculation of c_n values according to tip's details and chapter 4.2.3.1. B: Simulation of the tip's shape for the calculation of c_n values according to tip's details and chapter 4.2.3.2. C: 3-D simulation of the indenter-surface contact for different interaction contact angles. This simulation helps us calculate c_n values for modulus calculation, and also give a sense of the contact between the indenter (blue tip indenting the green surface) and the sample surface (green mesh, in different topographical angles). D: 3-D representation of case (A) for an axis-symmetric tip. E: 3-D representation of case (B) for an axis-symmetric tip.

5.3.2.5. Calculate Elastic modulus through various CM models

After the fitting of the curve and having calculated the fitting parameters, we use the following models/equations to calculate modulus.

Hertz

$$E_{eff} = \frac{3 * a}{4 * R_t} \tag{40}$$

Sneddon

$$E_{eff} = \frac{\pi * (1 - {\nu_s}^2)}{2 * \tan\varphi} \tag{41}$$

Pharr-Bolshakov

$$E_{eff} = \frac{a * \sqrt{\pi} * c^{1/n}}{2} * \frac{n+1}{n} * \left[\frac{\Gamma\left(\frac{n}{2}+\frac{1}{2}\right)}{\Gamma\left(\frac{n}{2}+1\right)}\right]^n \tag{42}$$

5.3.3. Output

The resulting output of this analysis is split in two parts; figures and metadata.

5.3.3.1. Figures

The figures that this technique can produce are divided in five parts; Maps, gifs, force distance curves, histograms, profile analysis, and RoI analysis. A description of each one follows.

5.3.3.1.1. Maps

Since the experiment is a force map, meaning a collective acquisition of force distance curves of the selected sample's area in a raster scan manner, then it is obvious that the mechanical properties of the sample under investigation will come as well as a heat map. The output maps of the analysis are the following:

1. Modulus, as calculated by the different models (Figure 21:) listed below:
    a. "*Hertz*"; it is a standard CM model used in literature and it assumes a spherical indenter. It is based on the original calculations for the contact between the indenter and the surface and on the double integrals used, and the relation between force and indentation is in the form of: $F = a * \delta^{3/2}$. Modulus E is calculated from the fitting constant α which contains details about the tip's radius and other geometry and mechanical details of the indenter.
    b. "*Sneddon*" model; it is a standard CM model used in literature, and it assumes a conical indenter. It is based on the original calculations for the contact between the indenter and the surface and on the double integrals used, and the relation between force and indentation is in the form of: $F = a * \delta^2$. Modulus E is calculated from the fitting constant α which contains details about the tip's half-angle and other geometry and mechanical details of the indenter.

c. '*Pharr-Bolshakov*'; here, we calculate modulus, based on *Pharr-Bolshakov*'s equation and on the optimal *beta* as this is found by the multivariate fitting routine.

d. *DMT*: Derjaguin-Muller-Toporov model of elastic contact, which assumes additional interaction forces outside the contact area.

e. Oliver-Pharr (2 approaches; the first measures modulus based on the slope at the start of the retract curve, and the second one relies on experimentally acquired geometrical values of the tip-surface contact).

2. Modulus error: this is the error, calculated by the following equation:

$$\Delta E = E * \sqrt{Er_1 + {Er_2}^{-1} * \sqrt{\left|Er_3 * \sqrt{{Er_4}^2 + {Er_5}^2 + {Er_6}^2}\right|^2 + \left(|Er_7| * \sqrt{{Er_8}^2 + {Er_9}^2}\right)^2}} \quad (43)$$

$$where$$

$$Er_1 = 4 * \nu_s^2 * {\delta\nu_s}^2 * (1 - \nu_s^2)^2$$

$$Er_2 = {}^4/_3 * \sqrt{R_t} * (1 - \nu_s^2)^{-1} * a^{-1} - E_t^{-1} * (1 - \nu_t^2)$$

$$Er_3 = {}^4/_3 * \sqrt{R_t} * (1 - \nu_s^2)^{-1} * a^{-1}$$

$$Er_4 = {}^1/_2 * \delta R_t * {R_t}^{-1}$$

$$Er_5 = 2 * \delta(\nu_s) * \nu_s * (1 - \nu_s^2)^{-1}$$

$$Er_6 = \delta a * a^{-1}$$

$$Er_7 = E_t^{-1} * (1 - \nu_t^2)$$

$$Er_8 = 2 * \delta\nu_t * \nu_t * (1 - \nu_t^2)$$

$$Er_9 = \delta E_t * E_t^{-1}$$

Where ν_s is the sample's poison's ratio, R_t is the tip's radius, a is the fitting parameter from the fitting routine described in chapter 5.3.2.2, E_t is the tip's modulus, and ν_t is the tip's poison's ratio. This equation for the calculation of the error takes in account

any source of error that could enter the equation for the calculation of modulus; from uncertainties in indenter and surface geometry, to measured confidence intervals for the mechanical details of the indenter, to confidence intervals for the value of a biological material's Poisson's ratio.

3. Optimal fitting power law (*beta*): mapping the fitting parameter *beta* from the fitting routine.
4. Fitting residuals: for the validity of the results we present three maps, RMSE | *beta*, RMSE | *p*, and RMSE | *c*:
    a. RMSE | *p*: the residuals of the FI curves, resulting from a universal fitting under *beta* equal to 1.5 (the standard "*Hertz*" fit).
    b. RMSE | *c*: the residuals of the FI curves, resulting from a universal fitting under *beta* equal to 2 (the standard "*Sneddon*" fit).
    c. RMSE | *beta*: the residuals of the FI curves, resulting from a specialized fitting, where optimal *beta* is selected according to the minimum RMSE values.
5. Adhesion: this map displays for each curve the value $F_{AD}/F_{MAX}\ x\ 100$. A big value of adhesion indicates the need to use CM models such as *JKR* and *DMT*
6. Hysteresis: this map displays for each curve the value of

$$\psi_P = \frac{area\ between\ approach\ and\ retract\ curve}{area\ below\ retract\ curve}$$

    A relatively big value of ψ_P indicates the need of analysing the retract curve through CM models like the *Oliver-Pharr*.
7. Indentation: this is the indentation depth reached at the prevailing pixel of the force map. In some instruments, the trigger of the feedback loop is set by the force, while in others this is set by the indentation depth reached. In any case, it is worth reporting (together with its variation inside a force map via this indentation map) since we do specialized indentation

analysis and it is important to see how the underlying surface behaves in different points of the selected RoI.

8. Contact point: this is the variation of cp of each curve, as calculated from the routine described in previous sub-chapter. Sometimes, it is important to check the variation of the index of cp as well, and this is the case when we have abrupt changes in the surface of the investigated material, and thus the feedback loop doesn't adjust immediately to these changes.
9. Contact mechanics (CM) model: according to (80) and briefly described in chapter 4.1, there is a standard method to decide whether to fit the data with a specific model, and this relies on the calculation of quantities like adhesion, plasticity index, etc. Here, based on this method we present the variation of the "suggested" CM model across the force map, even if we decide to work in the *elastic regime* only.
10. Height map.

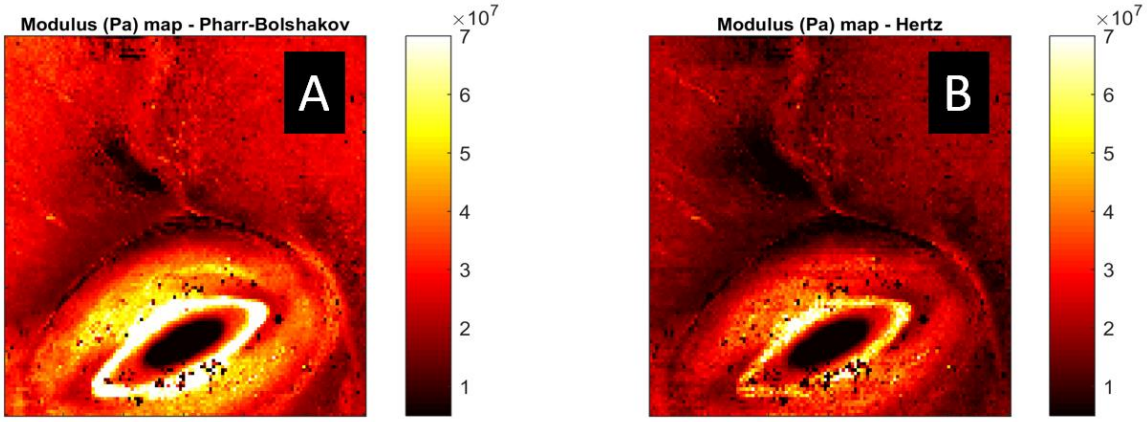

Figure 21: Modulus map, according to chapter 5.3.3.1.1 [1.a] (A), and chapter 5.3.3.1.1 [1.c] (B).

5.3.3.1.2. Gifs

A very good way to visually demonstrate the progression of modulus and *beta* values along different levels of indentation depth is a Gif. It is essentially a collection of consecutive

modulus maps (or *beta* maps, or RMSE maps), calculated for the different steps, and collated together in a successive manner to show the change of the properties along the way indenting into the surface. This is a very important and informative feature of this algorithm as it can give us information about underlying material changes, and underlying tip-surface contact. Figure 19 depicts this succession of mechanical values of modulus and *beta* for an example force map.

One way to read this experiment is that as we investigate larger parts of the indentation contact area, the fitting routine results into higher *beta* values denoting a more cone-like contact between the indenter and the surface. This makes sense due to the high indentation compared to the indenter's shape (spherical at the initial ~20nm and conical thereafter). Later, in chapters 6 and 7 we will see a practical application of this feature and how we can interpret it.

5.3.3.1.3. Force distance curves

A way to evaluate the cp, and the curve fitting is by visualizing them in a single figure with subplots. After the initial collection of the mechanical maps, a couple of selected FI curve data of the force map experiment is presented in Figure 22. This figure shows in 2 columns, 2 different curves, with each one of them being a random force map point/FI curve. In the first curve, which lies on top of a *C. albicans mother cell* region, the *beta* resulting from the curve fitting is ~2, and the adhesion is low, while in the second curve, which is at the edge of the *hyphae*, *beta* is ~1.8, and the adhesion is low. In the first row of each curve/column, one can observe the fitting of the raw data (blue) with different power law exponents (*beta*). The red line is a data fitting with a *beta* of 1.5 (*Hertz* model), the green line is a fitting with a *beta* of 1 (punch), and the yellow line is a fitting of the curve with a *beta* of 2 (*Sneddon* model).

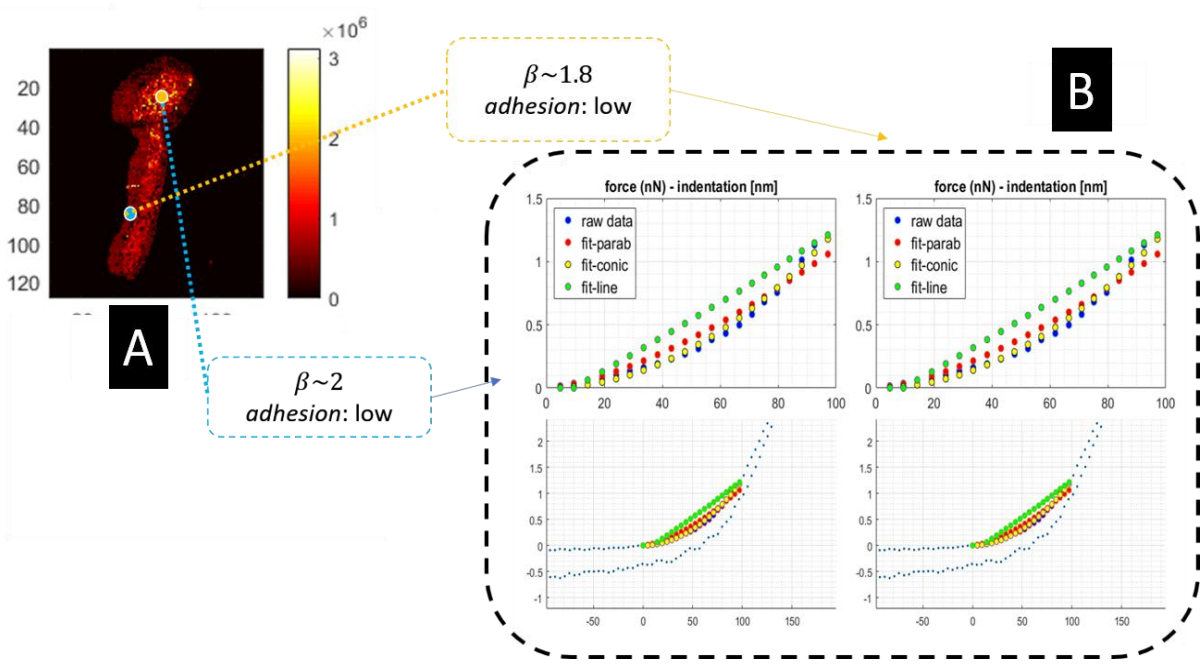

Figure 22: Example experiment; A: modulus map with 2 selected spots for Force-Indentation (FI) further analysis; Each one of the 2 spots (green, orange, blue) is represented by 2 force plots in B (each of the force plot shows a different analysis of the same data of the prevailing map spot).

5.3.3.1.4. Histograms and other plots

A histogram is used in this case when the distribution of modulus values is of use. One can compare between the statistical distributions of modulus values, as calculated from different ways and depicted in a single histogram of different colored sets. Later, in the results, we elaborate on this statistical analysis and on its potential use for sample's mechanical investigation. The main idea behind this routine is to fit a probability density function in order to model the distribution and subsequently compare the model parameters between different sets of modulus values (resulting from different experiments or from different implementations of the same experiment).

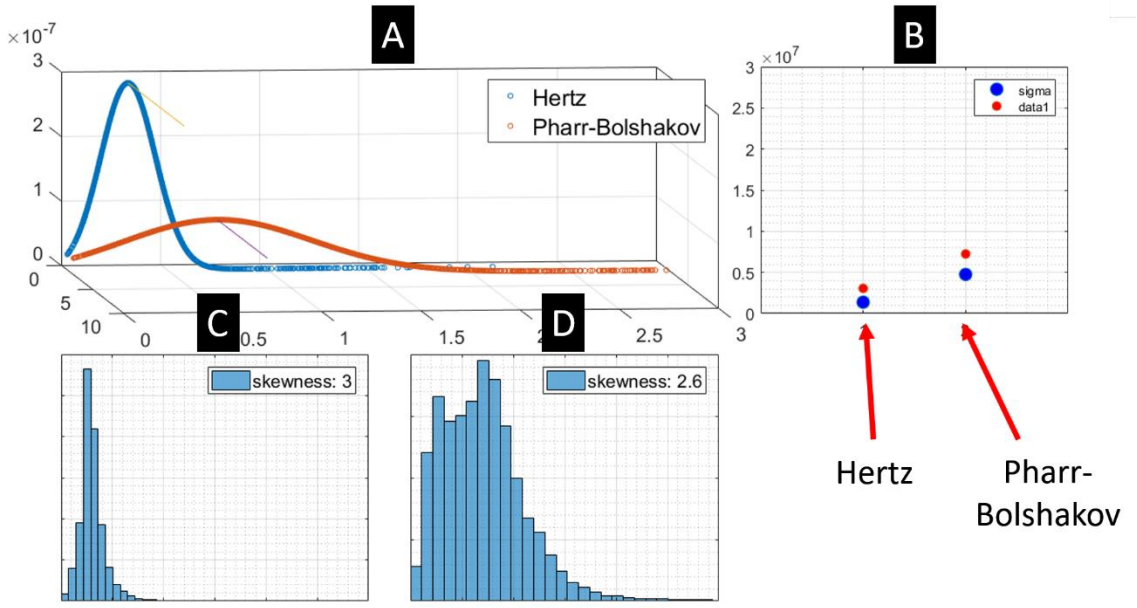

Figure 23: A: Statistical analysis of the different modulus maps (chapter 5.3.2.5, Figure 26). A: Fitted probability distributions on the different sets of calculated modulus. B: Median and sigma plot for the different sets. C-D: Distribution of modulus values for the different implementations of modulus calculation [D: *Pharr-Bolshakov* model, A: *Hertz* model]. The x-limits in A,C-D are: [0 3e+7].

5.3.3.1.5. Pick spots, line and/or region of the map and analyse

In some cases, like the one of this work, we need to pick some spots (Figure 24), lines, or whole regions from a map, and get some metrics out of these selections, as we are only interested in parts of the cell, and the distribution of all the values of the map could include other areas as well. For these situations, this developed technique offers this feature, and as it will be shown later in the thesis, it is important since we will try to compare the mechanical properties of different samples, both in the case of the stomatal cells and in the case of the fungal cells. So, there is a choice of picking some points (randomly or selected by the user), a line (profile analysis), or a region (as defined by the selection of multiple points on the map, in a polygon manner). This is valuable, since we can compare different areas (edges vs mid-wall areas for the stomata, and *hyphae* vs *mother cell* for the candida and fungal cells) of the cell.

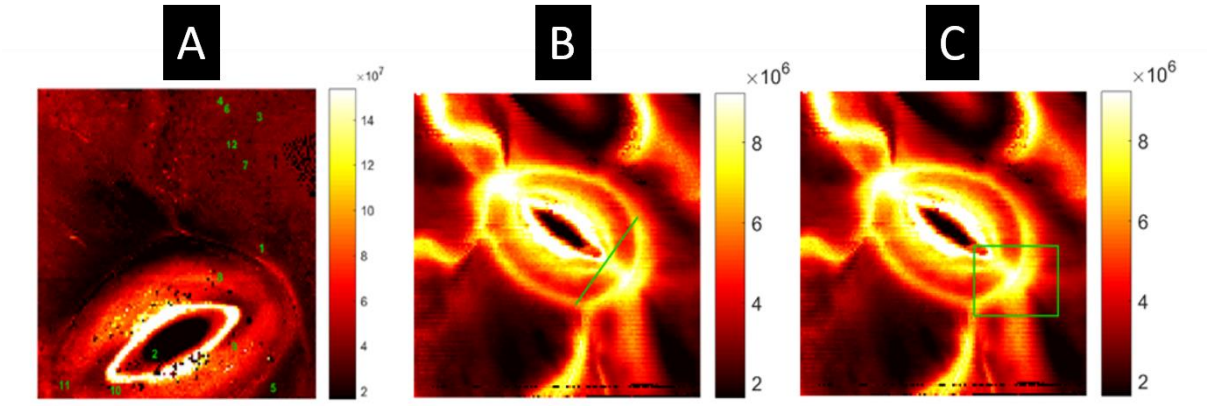

Figure 24: Green spots on the heat map are selected to investigate the mechanics of a selected RoI; A: User-selected points for dedicated analysis. B: User-selected line (profile analysis) for dedicated analysis. C: User-selected rectangle (RoI) for dedicated analysis.

5.3.3.2. Metadata

When the analysis is finished, all the resulting analysis variables (matrices, arrays, etc.) are stored in a single Matlab file, and all the figures are stored in a different file. The user can later import it into their programming environment in order to do further analysis.

5.4. Flowchart describing the data analysis technique

The routine that the algorithm follows to analyse a given experiment is outlined in the following flowchart:

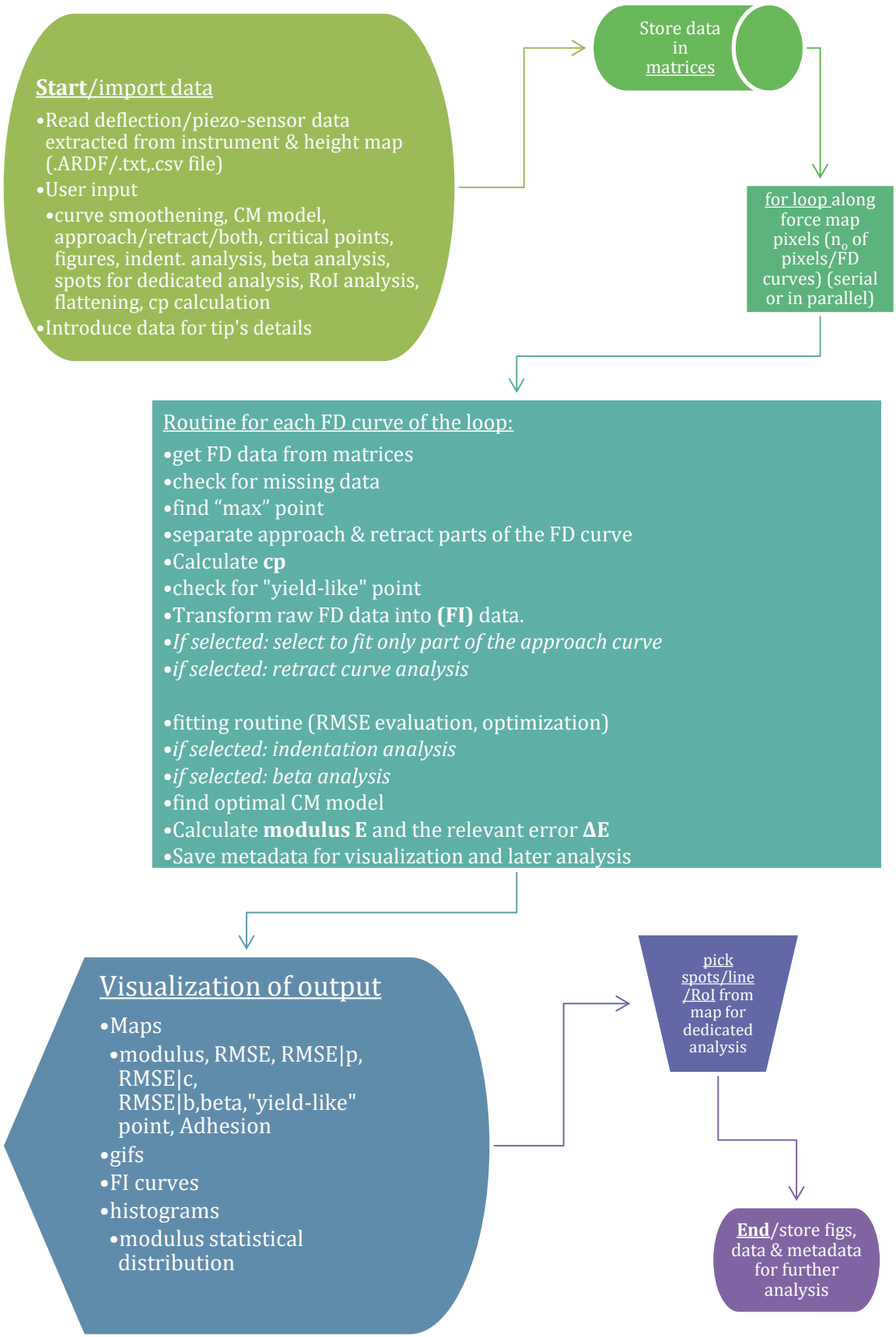
Start/import data
•Read deflection/piezo-sensor data extracted from instrument & height map (.ARDF/.txt,.csv file)
•User input
•curve smoothening, CM model, approach/retract/both, critical points, figures, indent. analysis, beta analysis, spots for dedicated analysis, RoI analysis, flattening, cp calculation
•Introduce data for tip's details
Store data in matrices
for loop along force map pixels (n0 of pixels/FD curves) (serial or in parallel)
Routine for each FD curve of the loop:
•get FD data from matrices
•check for missing data
•find "max" point
•separate approach & retract parts of the FD curve
•Calculate cp
•check for "yield-like" point
•Transform raw FD data into (FI) data.
•If selected: select to fit only part of the approach curve
•if selected: retract curve analysis
•fitting routine (RMSE evaluation, optimization)
•if selected: indentation analysis
•if selected: beta analysis
•find optimal CM model
•Calculate modulus E and the relevant error ΔE
•Save metadata for visualization and later analysis
Visualization of output
•Maps
•modulus, RMSE, RMSE|p, RMSE|c, RMSE|b,beta,"yield-like" point, Adhesion
•gifs
•FI curves
•histograms
•modulus statistical distribution
pick spots/line /RoI from map for dedicated analysis
End/store figs, data & metadata for further analysis

Figure 25: Algorithm flowchart - a cylindrical shape denotes internal storage, an inverse trapezoid shape indicates user intervention, a round shape indicates start/end, and a box represents a process/routine.

5.5. Application field

This project aimed initially to investigate the cell wall mechanics of *A. thaliana* stomata and *C. albicans* cells, but since the developed analysis technique proved to be helpful in acquiring mechanical insight into the data, we decided to test it with other cell samples and with their own specific biological questions, and it also produced new insights in the case of *beta* and indentation analysis, some of which will be discussed later in chapters 6 and 7. Apart from the investigation of cell nano-mechanics in this project, we aim is to deliver a new technique for relevant bio-mechanical and bio-elasticity analysis of AFM force mapping and nano-indentation experiments. We hope that this study will contribute to the field of AFM bio-mechanics by letting scientists and clinicians test their experimental and clinical data with a fully automated technique, and with -hopefully- more accurate findings.

5.6. Runtime

It is important to mention how much time it takes to process a single experiment under this newly developed technique. The laptop we used is a DELL Inspiron 5521, with a CPU i7/2-core/2.4 GHz (8 workers in parallel computing), 16 GB RAM (required due to big datasets during analysis). A single experiment takes approximately 4 hours to be analyzed, and 1 hour in the case of parallel processing (Matlab has a parallel computing library). Runtime depends a lot on the type of analysis preferred, with the ‘tomography’ analysis being the most time consuming.

Chapter 6: Stomata: altered mechanics induced by mutations

6.1. Introduction

The goal of this project was to investigate the relationship between cell wall modification through DNA mutations and altered cell wall mechanics, in order to better understand the biological function of stomata on top of other factors affecting it like environmental signaling, ion transportation and chemical signaling. As we noted before, there is an extensive literature in the way that turgor pressure, ion fluxes and molecular signaling affect biological function, but little has been told for its relation to cell wall composition/structure and wall mechanics. Here, we investigate this relation, with the aim to connect this to the overall biological function.

In order to do that, we had to measure the -altered- mechanics of the stomatal cell wall, as a direct effect of the underlying material properties change, induced by mutations in the plant's DNA. Force-indentation curves acquired with the use of AFM mediated indentation give a sense of the contact between the cantilever tip and the sample's surface, and the forces generated on the tip while it indents into the cell wall. Subsequently, force maps give us a sense of the variation of the elastic modulus E over the scanned micro-surface of the plant leaf.

The primary cell wall of guard cells has been measured to have a thickness of approximately 100 nm, while the thickness of the secondary (inner) wall can often be much thicker (122) (123). Thus, the level of indentation is considered to play a crucial role in the interpretation of cell nano-mechanical data. Finally, yet importantly, the developed algorithm will choose the appropriate Contact Mechanics model (from a variety of standard and not-so-standard CM models like *Hertz, Sneddon, Pharr-Bolshakov,* etc.), depending on the contact area, the shape of the tip, the shape of the surface in contact and the optimal fitting *beta* calculated.

As it has been stated in previous chapter, the mutant under analysis has been the so-called *pme6* mutant guard cell, which is known to enhance the concentration of methyl-esterified pectin biopolymers inside the cell wall matrix (124). Pectin's role is to induce the cross-linking between cellulose and hemi-cellulose, presumably "stiffening" the cell wall matrix . Thus, by introducing this cell wall modification to the stomata, one expects a plethora of mechanical phenomena taking place in the cell wall, but most importantly, a higher modulus E value on the altered cell wall stomata. This is what we investigate here (whether there are noticeable[41] differences in the mechanics of the cell wall between wild-type and mutant samples), while at the same time we record a series of other experimental and analysis parameters which would potentially be of biological interest, and AFM nano-indentation experimentation is able to probe those cell wall mechanics.

Some experimental factors which would affect the mechanical experimentation -and analysis- are the use of liquid buffers (so-called "stomatal buffer", or *Mannitol*, as described in chapter 3.1, which reduces the turgor pressure inside the cell, making it easier to investigate the stiffness of the wall -but not the modulus- since it removes the overwhelming effect of turgor pressure from the mechanical measurements), and the AFM cantilever selection. We will investigate the effect of both of these factors.

Some analysis factors which make the interpretation of the experiments difficult are the challenging calculation of the cp and the combination of the modulus map to the *beta* and RMSE map. Also, one of the most challenging parts of the analysis is to define whether there are real modulus differences between the different populations of data, or just statistical and/or sampling error.

[41] Statistically significant

The resulting data in this chapter will be presented in the following manner: firstly, we will present and discuss on the full output of our analysis technique for a single experiment, and then we will briefly present and discuss on a few other conducted experiments, but with less detail. Then, we will present our findings on the comparison between wild-type and mutant (modified cell wall) populations of experiments with their resulting findings. Finally, we will discuss the effect of contact angle in our measurements, with the help of an experiment on a homogeneous material with similar topography.

6.2. Experiments

We will start by presenting our analysis technique results of a single experiment (mutant *pme6* stomata experiment) in its full output, and then we will present all the other experiments' results, but with less detail. This is due to this technique's high load of output and the fact that not all of it can be presented in the context of this thesis. Nevertheless, in the next sub-chapter, we draw comparison tests between different sample populations, and the mechanical differences between wild-type and mutants are presented, and in the following next sub-chapter, other noticeable findings are presented.

What we aim to acquire from this analysis is mainly the modulus E map, meaning a heat map showing the distribution of modulus across the selected surface RoI for indentation/nano-mechanical investigation. This research project was designed around obtaining -and comparing- modulus (and other mechanical) values between wild-type and mutant stomatal samples. This analysis technique (presented in chapter 5.1) was developed around our goal to put confidence in the numerical results, citing on the side of these results a set of force-indentation mechanical analysis output as well.

It is also important to note that all the experiments were analyzed under the same indentation depth of 100 nm. This is to create a common ground for the comparative analysis that will

follow after the citing of the experiment results, and a good indentation depth to analyze the curve fitting behavior along.

6.2.1. Single experiment

Here, we present the results of a single selected stomatal experiment and more specifically of a mutant experiment which is a model experiment for the presentation of our analysis technique output. We will start by showing the modulus map, as it was calculated through the different contact mechanics models (described with detail in chapter 5.3.2.5) implemented in this technique.

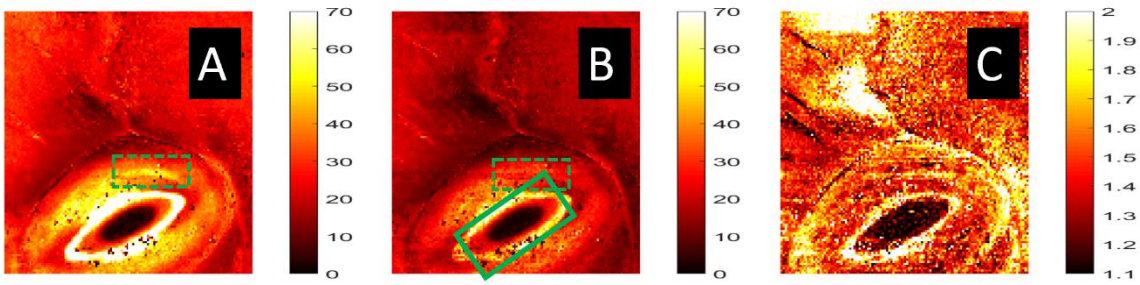

Figure 26: A-C: Modulus maps, each one representing a different implementation [A: *Pharr-Bolshakov* model, B: *Hertz* model], C: *beta* values (from fitting). The green rectangles show the areas of interest, in which the modulus calculation varies from model to model. The stomatal cell is at the bottom of the figure (cylindrical shape, with a hole at the middle). The colormap limits for A-B are in MPa, while C is unitless.

In sub-figure A of Figure 26, we use equation 13 to calculate modulus from the fitting of the force indentation curves of the scanned map. In B, we use the standard *Hertz* model (equation 5). Finally, C is a *beta* map, showing not the modulus but the result of the fitting analysis of the FI curves of the map, and the optimal power law describing the fitting of the curve.

We can see that –in general- the qualitative characteristics do not vary much from map to map, except cases A and B, where there are some differences between those two cases. This can be traced in the area on top of the stomata (A/green square), and around the aperture (B/ green

area). The difference (A vs B) is –mathematically- due to better curve fitting and –biologically- probably a material difference around this very top of the stomatal wall.

Quantitatively, this can be seen in the following figure, where on the first row we have four different maps (modulus, as calculated by *Pharr-Bolshakov* model, modulus *Hertz*, height map, and *beta* values map), and on the 2nd and 3rd row, we have the resulting map values from the white and the yellow line, respectively.

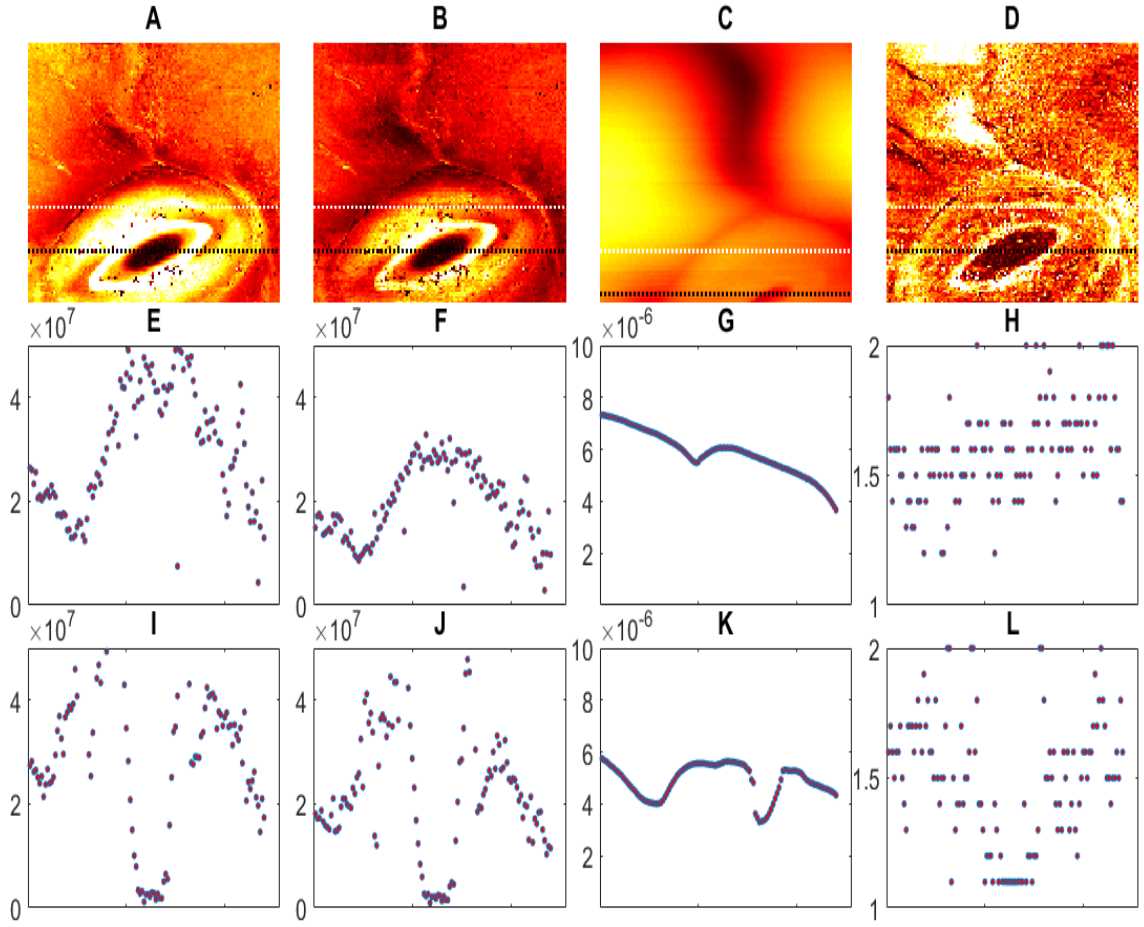

Figure 27: Profile analysis of the modulus values on top of the stomata cell. Maps A,B,D point to the relevant ones in Figure 25. C: Height map. E-H: Values obtained from the white profile in the relevant A-D heatmap. I-L: Values obtained from the black profile in the relevant A-D heatmap. The colormap limits are (map A,B: [0 5e+7] [Pa], map C: [1e-9 1e-5] [m], map D: [1.1 2]).

We see in the pairs of plots E-F and I-J, that on top of the RoI, the modulus values are different calculated by the different models. Especially, in the pair of E and F, we see that in the middle of the line there is a variation in E, whereas in F, it seems to be smoother. Also, we see in G and K, the height difference along the 2 lines, and in H and L, we see the *beta* values of these selected lines. In K, one can see the abrupt change in height, which is due to the pore formed in the middle of the stomatal cell. In H, we see that the modulus values on top of the cell wall are around 1.4 to 1.6.

We continue our analysis of this experiment by citing some other maps, whose ability of contrasting a selected mechanical property via a heat map, can reveal interesting findings. We start with the so-called "CM model selection" map (Figure 28-A), which displays the "optimal" CM model that each curve of the map should be analyzed under, if:

1. We pre-considered non-elasticity in our measurements (which we don't), and
2. We only had to select between the *Hertz* and the *Sneddon* model to analyze our curve data under (again, we don't; the purpose of this project is to not assume a certain tip-surface contact shape and subsequently use the *Hertz* or the *Sneddon* model, but rather follow each curve's fitting specially and use equation 13 instead of the relevant equations to *Hertz* and *Sneddon*).

The reasoning developed in the 2nd aforementioned condition led us to generate a map of "*beta* values", as seen in B. Here, the colored range is from 1.1 to 2, and it shows what *beta* each curve of the map gives under non-linear fitting of the raw FI data. Following, we have maps D and E, which map respectively the relevant curve's hysteresis and adhesion (as pointed in Figure 14), and as we see in this experimental force map, we have very low adhesion (essentially adhesion ration, F_{AD} / F_{MAX}) across the map and some regions with high plasticity index/hysteresis compared to others. The main information obtained from maps B,D and E can

be seen collectively in A as well. We see that the white areas of A (high hysteresis) coincide with the relevant whites of D (high hysteresis), there is almost no sign of a yellow pixel in A (very low adhesion, as seen in E), and also the white areas of B (high $beta \sim 2$) are similar to the dark red ones of the A (*Sneddon*, $beta = 2$) and the red areas of B ($beta \sim 1.5$) are similar to the red ones of the A (*Hertz*, $beta = 1.5$).

Following this, we also cite the "yield-like" point map and the "height" map. The former is a heat map displaying the percentage of the total indentation for each curve of the map, in which there is a change in the curve's gradient. This is an important information since after this point, it is not theoretically correct to fit the curve for the modulus calculation. There may be a situation where this "change of gradient" could be just noise, but this is a very low possibility since we have set strong criteria for the identification of such critical point. Here, we see that the majority of such "faulty" map points lies in the aperture of the stomata, a region which is not of big interest. Also, there are some other scattered map points in which the curve exhibits an early critical point but there is not a clear pattern to discuss upon.

The latter map ("height map", F) displays the calculated cp, the data point at which the indenter meets the surface. What we see here is that the range of the colormap is around ~8 μm. This is a high surface topography for an AFM force map experiment, but the RoI (surface on top of the stomata/green box in F) has a relatively low height difference and this is where we will collect our mechanical data later for comparison.

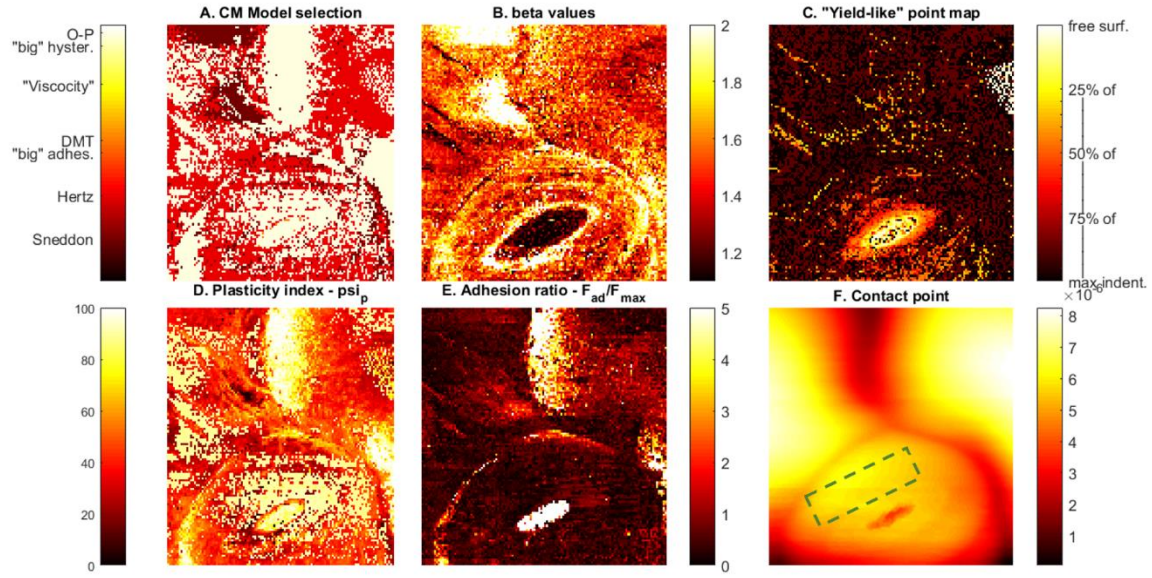

Figure 28: Support figures for the experiment of A. thaliana stomata. A: "CM model" selection map. B: beta values map (range: [1.1 2]). C: "Yield-like" point map (range 0-100) [unitless]. D: Hysteresis (plasticity) map (range 0-100) [unitless]. E: Adhesion ratio map (range 0-100) [unitless]. F: Contact point map (range: [0 4.]).

After the initial collection of the mechanical maps, it is important to offer an insight to the curve fitting, the heart of this analysis which yields all the aforementioned results in a heat map manner. The raw curve data of the selected (52) experiment is presented in Figure 29. This figure shows in 3 columns 3 different curves (displayed in 2 different ways in 2 different rows), with each one of them being a random force map point/FI curve. Each column represents a different curve and each row, a different presentation of the same curve. We can see 2 different force distance curves from different areas of the force map, with each one being connected to a different spot on the top-left force map. In the first curve, which lies on top of the stomatal region, the *beta* resulting from the curve fitting is ~1.5, and the adhesion is relatively low. In the second curve, which is on top of the stomata, *beta* is ~1.5, and the adhesion is low. In the first row of each curve/column, one can observe the fitting of the raw data (blue) with different power law exponent (*beta*). The red line is a data fitting with a *beta* of 1.5 (*Hertz* model), the

green line is a fitting with a *beta* of 1, and the yellow line is a fitting of the curve with a *beta* of 2 (*Sneddon* model).

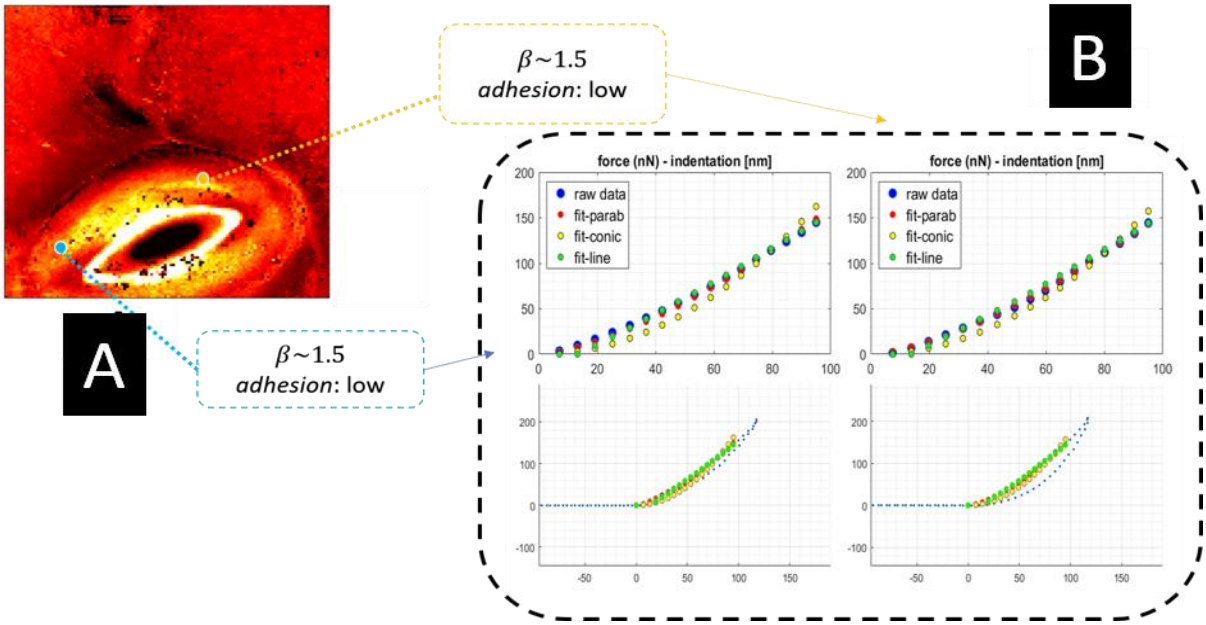

Figure 29: Modulus map (A) with 3 selected spots for Force-Indentation (FI) further analysis; Each one of the 3 spots (green, orange, blue) is represented by two variable values and two force plots (each of the force plot shows a different analysis of the same data of the prevailing map spot). We see that FI curves of the stomata experiment have miniscule adhesion ratio and medium hysteresis (as shown in Figure 28).

Further on the analysis, and while staying on the fitting part of the algorithm, we present the residuals of the fitting (RMSE values) of each curve of the map, for three different cases; for the case of fitting all the curves with a *beta* of 1.5, with a *beta* of 2, and with the optimal *beta* for the different curves (as this is calculated via the optimization of the RMSE value of each curve separately). In this sense, let's see how these 3 maps compare, and what information can bear for the better understanding of the modulus calculation. The three sub-figures at the bottom of Figure 30 show the RMSE values for the whole map, as calculated for the three different strategies of fit optimization. Specifically, C displays the RMSE fitting values of all the force curves of the map, calculated for a *beta* value of 1.5. D displays the RMSE fitting values of all the force curves of the map, calculated for a *beta* value of 2, and E displays the

RMSE fitting values of all the force curves of the map, calculated for the optimal *beta* value resulting from our optimization routine. In addition, plot A shows a histogram with all three different sets of RMSE values from C,D and E, and plot B shows 3 boxplots for the relevant cases of C,D and E. As we see in B, the median value decreases with the following order:

$$median_{\beta=opt.} < median_{\beta=1.5} < median_{\beta=2}$$

Also, the boxplot limit values (here, they represent the 25th and 75th quantiles of the distribution) follow the same order, and the red crosses show the –considered by the boxplot- outliers. Thus, we see that not only the overall values are smaller (meaning a better fit take place), but also the distribution is narrower, giving us a strong reasoning to validate our analysis and our implementation of modulus calculation.

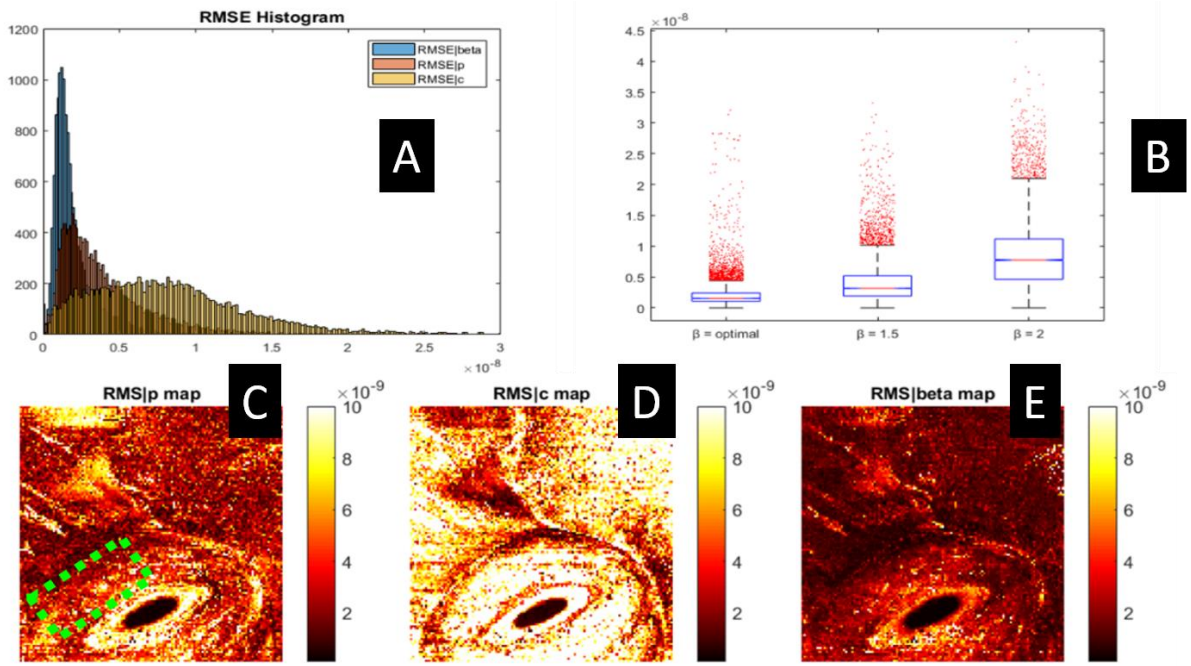

Figure 30: Fitting residual analysis after the FI analysis of the map's curves; A: Histogram showing 3 different distributions (blue: RMSE | b, red: RMSE | p, yellow: RMSE | c). B: 3 boxplots representing the median (red horizontal line), 25th & 75th quantiles (upper & lower limits of blue box), and outliers (red dots, outside the thinner horizontal black lines) for each one of the distributions. C-E: 3 different maps, showing the RMSE values for the 3 different cases.

But this figure does not give us the detailed stomata statistics that we look for, since A and B contain the modulus values of the whole force map, including both the stomata and the neighboring pavement cells. Even though for this case (compared to chapter 7 where we have a cell on top of a glass substrate) we were interested -at the beginning- in the surroundings of the cell itself, and how the mapping of the fitting residuals looked like, we were ultimately interested in the stomata area (green-dotted box in C). This is the reason why we generated the following figure where the histogram data and their statistical values come specifically from the aforementioned area on the cell wall.

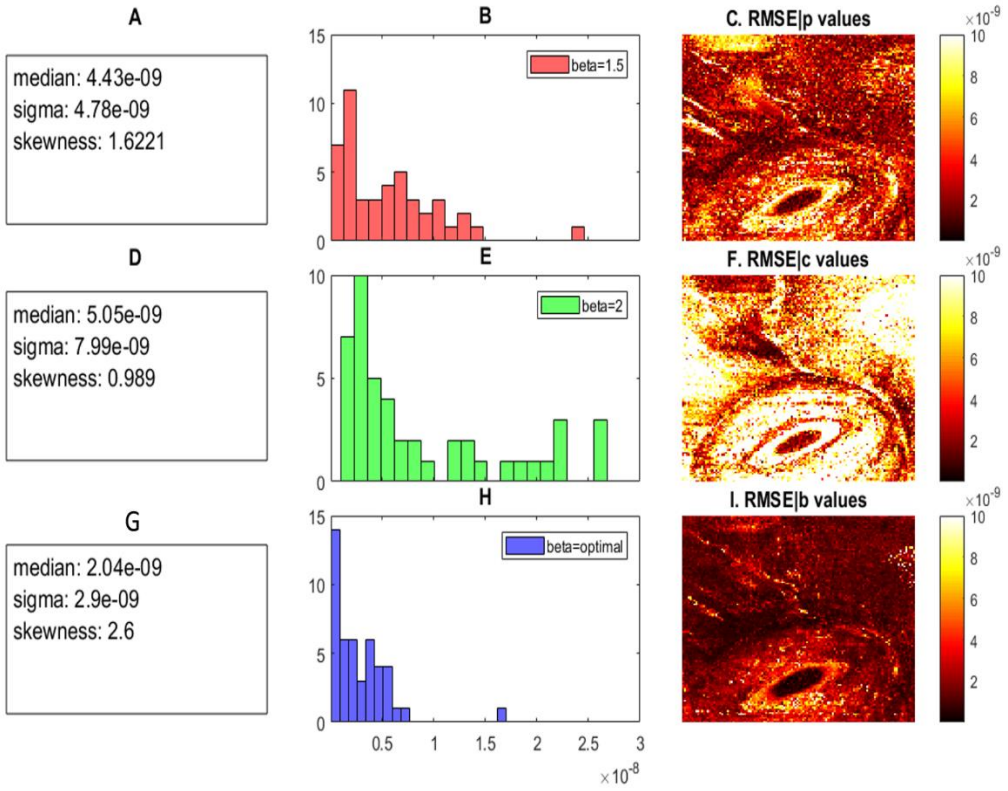

Figure 31: Fitting residual analysis for the stomatal wall area after the FI analysis of the map's curves; A,D,G: Statistical values for the relevant distributions of B, E, and H. B,E,H: Histogram showing 3 different distributions (blue: RMSE | b, red: RMSE | p, green: RMSE | c). C,F,I: 3 different fitting residuals maps, showing the RMSE values for the 3 different cases.

As we see in this figure, the trend is the same as before,

$$median_{\beta=opt.} < median_{\beta=1.5} < median_{\beta=2}$$

But now this stands only for the region on top of the cell wall. We see than the median value of RMSE | *beta* is the smallest, and all the distributions have a light skewness to the right.

One other routine of the developed analysis examines the relationship between the fitting and the indentation depth. With this analysis, as aforementioned in chapter 5.3.2.3, we have the option of analyzing different portions of the same curve simultaneously, and we do this in a "tomography" manner to observe different mechanical behavior as we examine further into the sample's surface. In this context, we present how the investigation of *beta* (Figure 28-B) and of the different RMSE values (Figure 30-C,D,E) changes as we indent further into the surface, starting from 10 nm and finishing to an indentation of 100 nm. This is seen in the next figure (Figure 32), where each different row represents respectively the *beta*, RMSE | *beta*, RMSE | *p* and RMSE | *c* in relevant order, and the succeeding columns point to a different portion of the indentation being fitted.

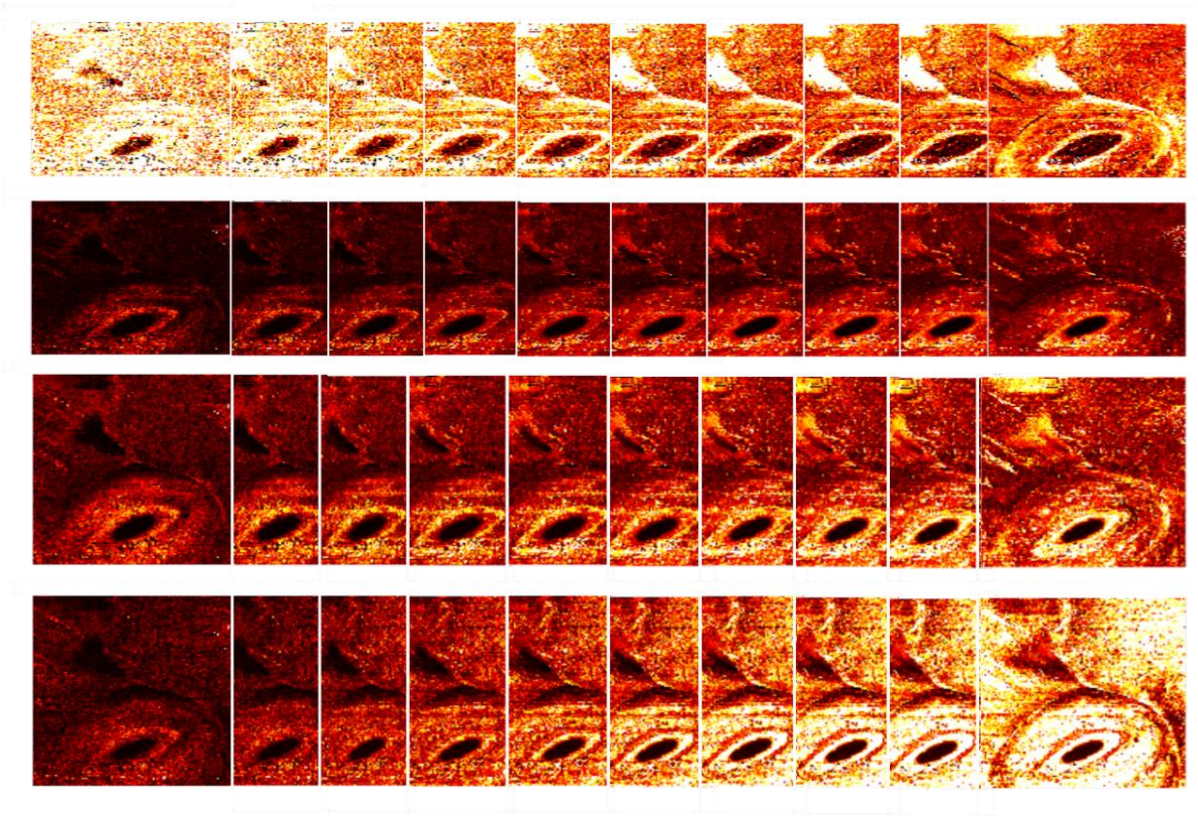

Figure 32: Progression of 4 different maps along different levels of indentation; Different rows represent different analysis depth, while different columns represent different map for indentation analysis; 1st row: *beta* values map (range: [1.1 2]). 2nd row: RMS | *beta* (range: [1e-14 1e-10]). 3rd row: RMSE | p (range: [1e-14 1e-10]). 4th row: RMSE | c (range: [1e-14 1e-10]).

As we see from the progression of the *beta* values along different indentation depths (row 1st), we observe a general trend of *beta* decrease along. This trend is something that we did not expect initially; we expected –according to the theory and the mathematical formulation of the elastic context between a rigid axisymmetric indenter and a surface of elastic half-space- a *beta* value of 2, since the indentation depth in this case is 100nm, way more than the 10 nm of nominal tip's diameter at the tip's apex (and more than the –approximately- 30 nm of SEM-experimented tip's diameter at the apex). Then, looking at the following rows of the figure, we see how the different RMSE values (row 2: Optimal *beta*, row 3: 1.5, row 4: 2 respectively for rows 2, 3 and 4) change as we fit bigger portions of the contact area. What we see is something expected, since rows 2-4 are mathematically connected to the 1st row's outcome. Firstly, we

see that on top of the stomatal cell wall, the RMSE | b (3nd row) is smaller than RMSE | c (4th row), and of course they are both lower than RMSE | b (2nd row) since the latter represents the optimal fitting for each curve of the map collectively. Also, there are some areas in RMSE | c which have lower values than RMSE | p and this can be seen in the first row; white areas show a fitting of close to 2, thus the fitting with a *beta* value of 2 is better than a fitting with a *beta* value of 1.5, and subsequently, the RMSE | *c* values are lower than the RMSE | *p* values.

Furthermore, on the analysis of the modulus calculations for the same experiment, we show a collective way to display modulus. In Figure 33, we show how the different modulus calculation methods compare with each other for the same problem. In Figure 33-C-D, we see histogram charts with the modulus data of the force map, as calculated with different models (see 4.1), in A we see a fitted probability distribution on the same data, and in B, we see how *sigma* and *mu* values (*sigma* and *mu*, as a result of the probability distribution fitting on the aforementioned modulus data) compare with each other. Specifically, we see in A, C-D that – overall- the distributions of the modulus from the new *Pharr-Bolshakov* model lie on the right side of the *Hertz* distribution, we see in A that the distribution of modulus values as calculated by a varying *beta* method are wider than the relevant to *Hertz* (mainly due to outliers), and finally, in B, we see a plot with how the mean and standard deviation values of the different distributions compare.

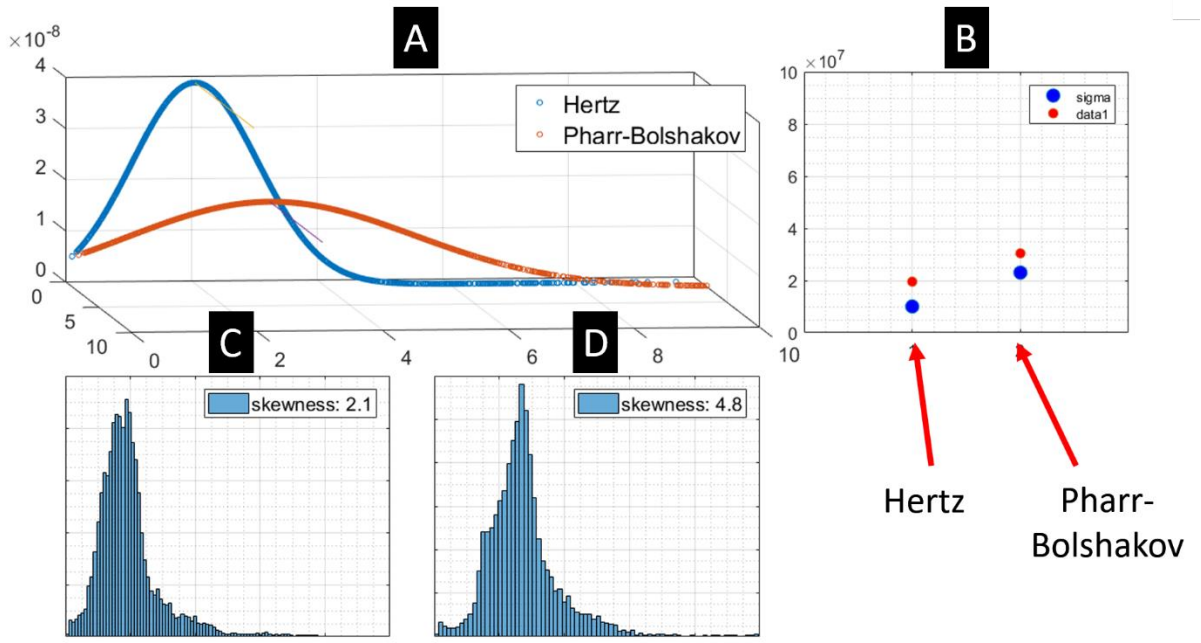

Figure 33: Statistical analysis of the different modulus maps (chapter 5.3.2.5, Figure 26). A: Fitted probability distributions on the different sets of calculated modulus. B: Median and sigma plot for the different sets. C-D: Distribution of modulus values for the different implementations of modulus calculation [D: *Pharr-Bolshakov* model, A: *Hertz* model]. The x-limits in A,C-D are: [0 10e+7].

6.2.2. All experiments

Here, we present a selection of the conducted experiments for the stomata-altered mechanics project. We present the details of 33 experiments (Figure 34), 14 of which were mutant samples of the type *pme6* (labelled '*pme6*' in column *type* in Table 4, labelled as "Mt(xx)" in Figure 34), and 19 of which were wild type samples (labelled 'WT' in column *type* in Table 4, and "WT(xx)" in Figure 34). In this project we conducted AFM nanoindentation experiments with a different *A. thaliana* mutant other than the *pme6* as well, the so-called *LE* mutants, but we only present their details in the following table (labelled 'LE' in column *type* in the table, not in Figure 34) and not their results since we do not have a sufficient amount of data to compare with the other samples.

The full output of all the force map experiments is not needed and will not be presented here. The most important goals of this project were to compare the mechanics of the different cell populations -which we do in the following sub-chapter- and to present the information that we get from the experiments, from our developed technique.

We tried to maintain relevant experimental conditions so we could be able to compare the mechanical measurements between wild-type and mutant samples. An important factor for the measurement of modulus was the use of *Mannitol* as a buffer during experimentation (as we'll see it plays an important role), and a less important factor was the use of a completely different cantilever (MLCT-F) for a set of experiments and we will discuss its effect as well.

Table 4: Experimental details for the stomata experiments (In column "type", light red for mutant, light blue for wild type). Each columned is color-scaled by its own. Black outline is the experiment presented before, red outline is for the experiments presented later, and the dotted lines are the mutant experiments not considered for analysis here.

Expt. No	Type	Scan area (µm)	Force map pixels	Sensitivity (nm/V)	Force distance (µm)	Mannitol
3	pme-6	40	64	250.4	10	Yes
4	pme-6	40	64	260	10	Yes
5	pme-6	40	64	260	10	Yes
6	pme-6	90	64	260	10	Yes
7	pme-6	44	64	260	10	Yes
8	pme-6	44	64	260	10	Yes
9	pme-6	33.8	64	260	10	Yes
10	WT	40	64	327.2	5	Yes
11	WT	40	64	327.2	10	Yes
13	WT	40	32	355.4	5	Yes
14	WT	30	128	355.4	3.53	Yes
15	WT	20	128	355.4	1	Yes
19	LE	40	32	310.8	2	Yes
20	LE	30	128	310.8	1	Yes
21	LE	20	64	310.8	2	Yes
27	*pme-6*	*40*	*64*	*245.3*	*5*	*Yes*
28	pme-6	40	64	245.3	5	Yes
29	WT	40	64	264.8	-	Yes
33	WT	40	64	383.1	5	No
34	WT	14.6	64	383.1	5	No
35	WT	7.7	64	383.1	5	No
36	pme-6	40	64	296.6	6	No
37	pme-6	18	64	296.6	6	No
40	pme-6	40	64	476.4	7	Yes
41	pme-6	40	64	250.4	10	Yes
45	WT	40	64	356.3	6.2	No
46	WT	40	128	356.3	6.2	No
47	WT	40	64	487.3	8	No
52	**pme-6**	**40**	**128**	**266**	**8**	**No**
76	WT	25.5	128	104.3	3.5	No
87	WT	30	64	63.9	3.5	Yes
88	WT	30	64	63.9	3.5	Yes
89	WT	30	64	63.9	3.5	Yes
90	WT	30	64	63.9	3.5	Yes
91	WT	30	64	63.9	3.5	Yes
92	WT	30	64	63.9	3.5	Yes

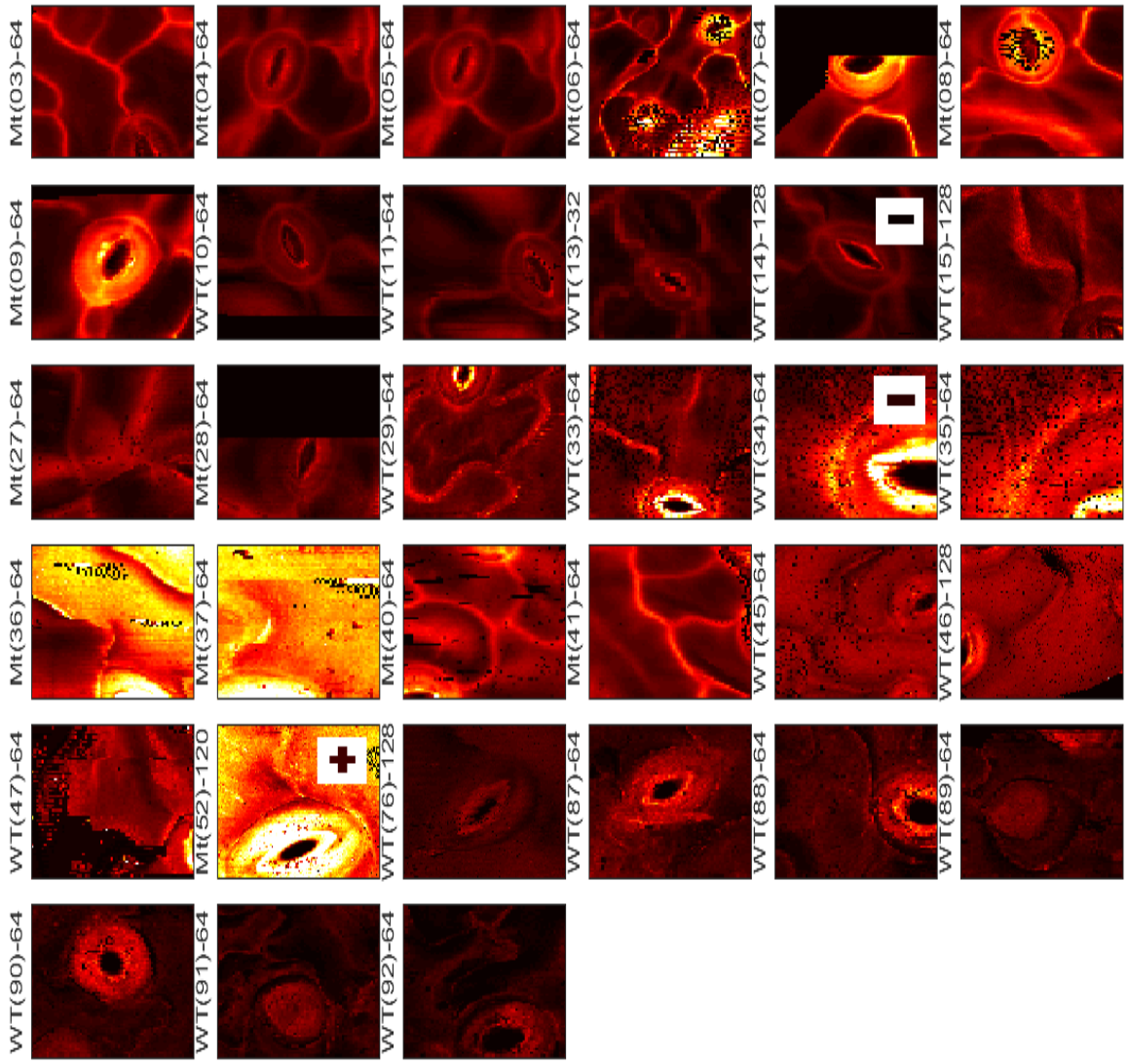

Figure 34: All the AFM force map (modulus) maps collected in a single figure. All maps are in the same colour scale (8e+5 to 5e+7). The title of each map (xx(yy)-z) points to the cell type (xx), number of experiment (yy), and number of force map pixels (z). The map with the symbol ' + ' has been analysed extensively before. The maps with the symbol ' - ' are analysed briefly here.

Two representative experiments of the ones presented in Figure 34 (14 and 34, shown with the symbol '-') and in Table 4(lines with a red outline) are the following:

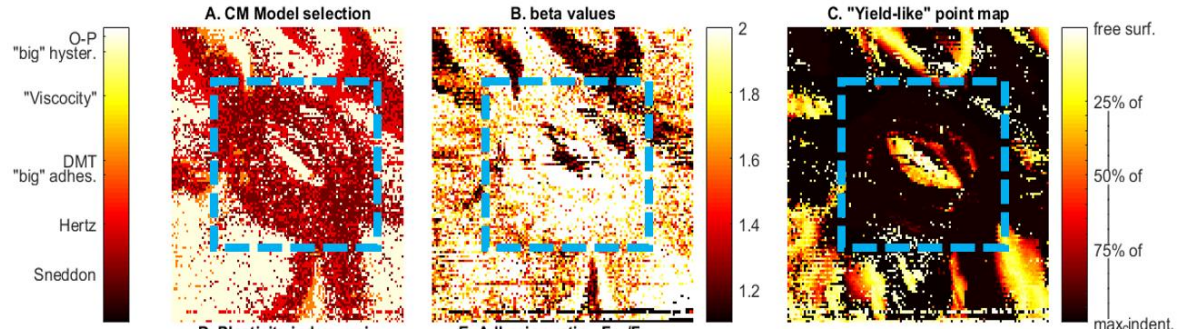

Figure 35: Support figures for the experiment 14. A: "CM model" selection map. B: *beta* values map. C: "Yield-like" point map. The blue-dotted box annotates the area of the stomata cell.

Here we see that the dominant CM models under which one should analyze this map is the *Sneddon* and the *Hertz* models. We see in A that on top of the cell region (blue-dotted box), the dominant color is dark red, as we would expect by looking at the same region of B. In B, we see that on top of the stomata, *beta* is ~1.9. Finally, we see in C that on top of the stomata there is almost no data point with a non-smooth curve, while on the surrounding area there are a lot of FI curves which exhibit a 'yield-like' behavior.

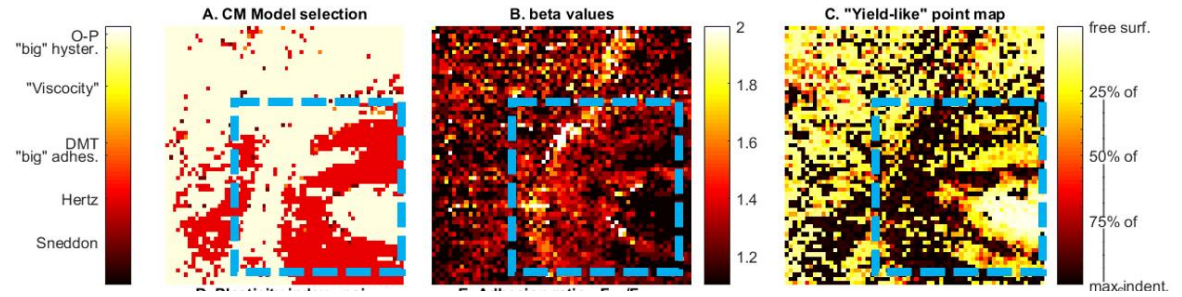

Figure 36: figures for the experiment 34. A: "CM model" selection map. B: *beta* values map. C: "Yield-like" point map. The blue-dotted box annotates the area of the stomata cell.

In this experiment (n^{o} 34) we can see that the dominant CM models under which one should analyze this map is the *Hertz* model. We see in A that on top of the cell region (blue-dotted box), the dominant color is light red, as we would expect by looking at the same region of B. In B, we see that on top of the stomata, *beta* is ~1.4, which is connected to the use of the *Hertz*

model for the calculation of modulus. Finally, we see in C that on top of the stomata there are a few data points with a light-yellow color, meaning that in these points the FI curve has a change in gradient at the beginning of the curve.

6.3. Altered mechanics – Wild type (WT) vs mutants

One of the reasons we developed this analysis technique was to have more insight in the experimental data through comparative analysis of the experiments under investigation. The differences between Wild-type and mutants is expected to be the aftermath of the modified cell wall constituents. Here, we present the finding that, in general, the elastic modulus in *pme6* is higher than the relevant value in wild type stomata. This agrees with our expectation, based on the fact that a cell wall enriched with the pectin biopolymer would exhibit higher E on the stomatal wall. We are looking for altered mechanics between the two groups of cell samples, as described before. We investigated mechanical differences (modulus, adhesion) between wild-type and mutant samples.

6.3.1. Comparison of modulus

In order to compare the modulus between wild type and mutant cells, we extracted the modulus values from all 33 experiments (19 of Wild-Type and 14 of mutant *pme6*) and this resulted into the following collective chart, where each boxplot represents the distribution of modulus values for each experiment (as seen in the x-axis).

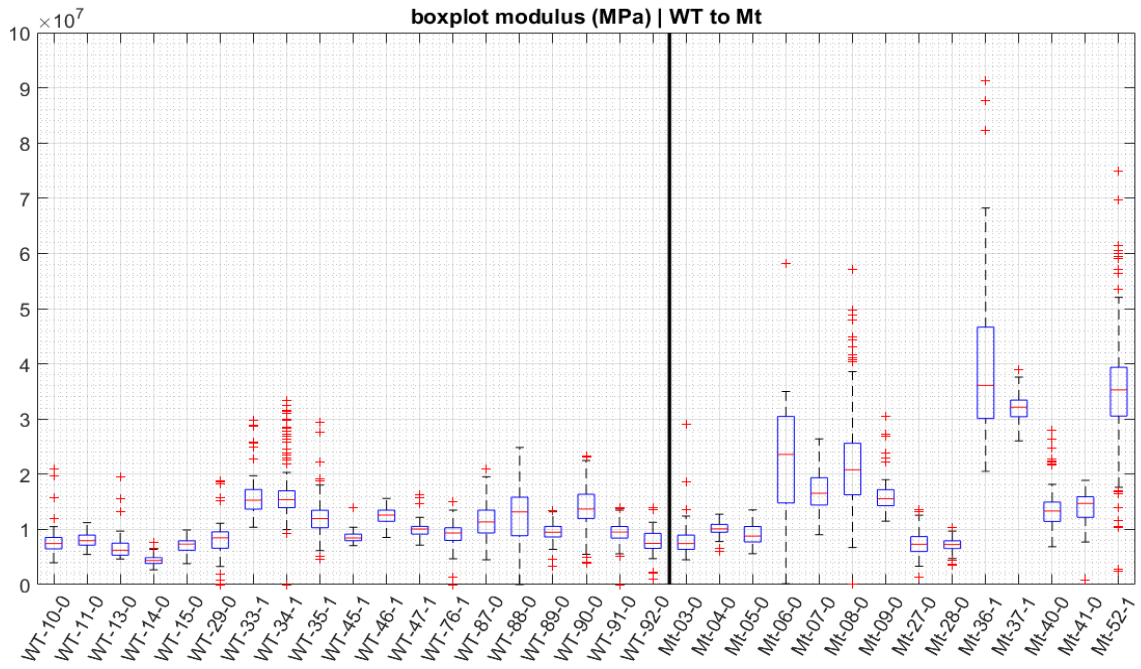

Figure 37: Modulus comparison between wild type (*WT*) and mutant (*Mt*) cells. The black vertical line separates the different populations of data. Each experiment is represented here by a boxplot with its median and 25th and 75th quantiles. The value in the y-axis is in Pa. The label for each experiment (xx-yy-z) denotes the type (xx), the nº (yy) of experiment, and the use (z) of *Mannitol* or not as a buffer in the experiments.

In this plot, we check the differences in modulus, where each one of two sides of the plot (as this is divided by the vertical blue line) representing a different group of data; on the left side, one can check the wild-type experiments, while on the right side of it there are the mutant experiments. The plot consists of different boxplots[42] with each one representing statistically each experiment's relevant mechanical property. In each boxplot: the red line represents the median value of experiment's results, the limits of the blue box represent the 25th and 75th quantiles of the statistical distribution, the whiskers extend to the distribution's limit values (of those not considered outliers), and the red dots represent outliers. Finally, the horizontal axis shows the different experiments to be compared upon, and the vertical axis shows the range of values (in MPa) for the relevant mechanical property being investigated and compared.

[42] As obtained by the Matlab's toolbox (109)

Here, it is important to note that when referring to “experiments’ results”, we mean the collected values of modulus from the experiment’s map, using the user-selected RoI method, described in chapter 5.3.3.1.5. For example, in order to compare modulus between wild-type stomata of experiment “10”, and mutant of experiment “03”, we run the individual experiments under our analysis technique, we used the user-interaction routine described in chapter 5.3.3.1.5, we manually selected two areas (one on top of the “10” stomatal cell and one on top of the “03” stomatal cell), and the algorithm returned a table with all the mechanical properties calculated for each one of the pixels of the user-selected area, modulus included.

As it is immediately obvious, the right-hand side group of experiments exhibit higher modulus values than the left-hand ones. In order to expand this finding, we calculate the mean value of each experiment and subsequently compare the mean of means values. In order to do that, we firstly need to check into each single experiment’s distribution of values in order to put confidence on our results. In the following figure (Figure 38) we see that not all the distributions follow a normal-like distribution at the significance level of 5%.

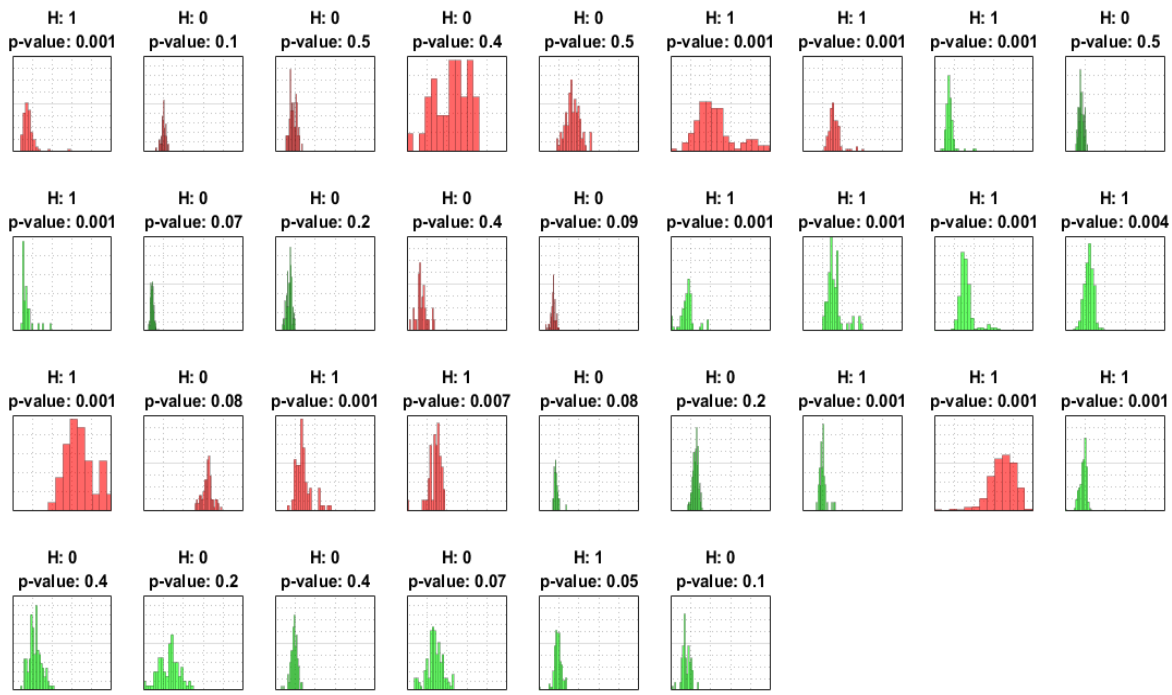

Figure 38: Distribution of modulus value for every experiment (red histogram: mutant, green: wild type) of this work; as it seems, not all of the experiments have a normal distribution. In each title, we have the result for the null hypothesis test for normality of the distribution (H:1 -> rejection, H:0 -> failure of rejection). The x-axis limits are [0 5e+7].

To support that, we conducted a separate test (Matlab's *lillietest*, as described earlier in the methods chapter) for each one of the aforementioned distributions with the aim to check the distributions' normality, and the result was not positive for all the experiments. For this reason, that we cannot assume normality for all the samples (there are also some outliers in the data that cannot be ignored), and since the sample size is relatively small (we compare modulus values from a specified RoI on top of the stomata and not all the values of the force map), the selection of hypothesis testing between the different groups of data (wild type and mutant) is the Matlab's *Wilcoxon ranksum test.*

This test rejects the hypothesis that the wild type distribution and the mutant come from equal distributions with equal medians. The p-value of this test is $p_{WT|Mt} < 0.001$.

So, now we have a plot with two boxplots, each one containing all the experiments/samples for the relevant category.

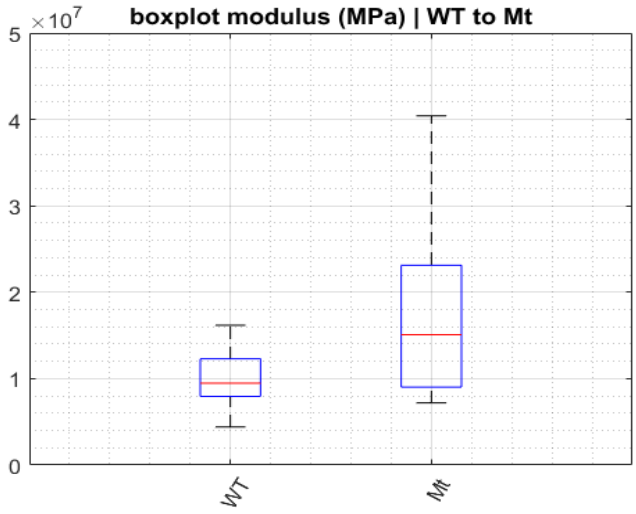

Figure 39: Boxplots representing the wild type and mutant populations for modulus. Mutant experiments have a higher median value, but also a higher variance. The vertical axis is in Pa and shows the modulus value.

As we see from this figure, and backed up by the statistical test performed, median modulus value in mutant is higher than in wild type stomata ($\widetilde{E_{Mt}} > \widetilde{E_{WT}}$). By calculating the statistics, we get the following:

$$WT: \mu_{WT} = 1.0 \times 10^7 \ \& \ \boldsymbol{median_{WT}} = \mathbf{0.99 \times 10^7} \ \& \ \sigma_{WT} = 0.4 \times 10^7$$

$$Mt: \mu_{Mt} = 2.2 \times 10^7 \ \& \ \boldsymbol{median_{Mt}} = \mathbf{1.79 \times 10^7} \ \& \ \sigma_{Mt} = 1.3 \times 10^7$$

But except from higher modulus value, we see that mutant experiments have a higher standard deviation ($\sigma_{Mt} = 1.3 \times 10^7$ vs $\sigma_{WT} = 0.4 \times 10^7$). Thus, the next step is to visualize the histogram of each population in a single plot, in order to dive into the distribution and identify possible bimodality of our results.

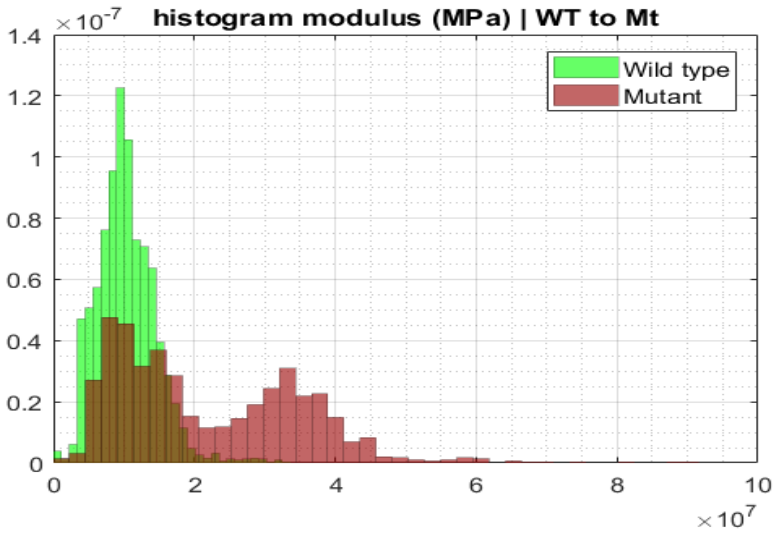

Figure 40: Histogram (normalized) for the two different populations of experimental modulus data; wild type (green) and mutant (red). X-axis is in Pa.

If we dive into this histogram, we see that while the population of wild type results (green) follows a unimodal-like distribution, the relevant one for the mutant results (red) appears to be a bimodal-like distribution. This implies that there are two different groups of data inside the same distribution, possibly due to an experimental feature the different experiments share. Here, we need to say that while conducting experiments on wild type and mutant stomata, we tried to maintain relevant experimental conditions in order to later analyze different populations of data that shared the same conditions. Nevertheless, we altered the experiment design for a set of experiments with the aim to find the best set of conditions, and this search for optimal conditions resulted in some important findings as well. Especially because there is not an established protocol in literature for the case of AFM nano-indentation in stomata.

By looking at the experiments and their properties, we see that the highest mode ($median \sim 3.5 \times 10^7$, on the figure) refers to experiments where *Mannitol* had not been used as a buffer in the experiments, while the lower peak ($median \sim 1.2 \times 10^7$, on the figure) refers to the experiments where *Mannitol* had been introduced in the petri dish. To support this, we split the mutant data into two groups, *Mannitol*- (purple) & *non-Mannitol*-treated (red), and we

generated two histograms from these groups instead of one of all the mutant ones. As we see, it is clear that the bimodality of the mutant population is an aftermath of the *Mannitol* presence.

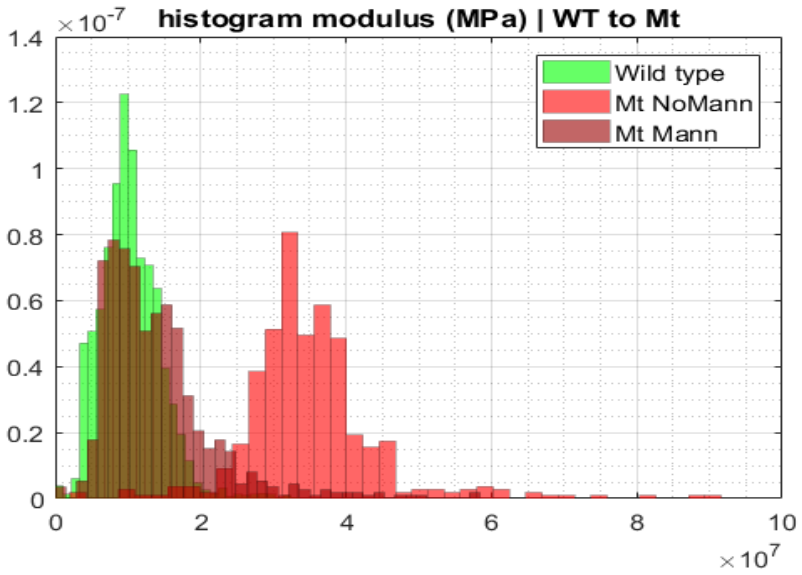

Figure 41: Histogram for the three different populations of experimental modulus data; wild type (green), mutant/No *Mannitol* treated (red), and mutant/*Mannitol* treated (purple). X-axis is in Pa.

For the purposes of how significantly different the two groups of *Mannitol* and *non-Mannitol* treated mutant experiments are, this hypothesis testing rejected the null hypothesis and returned a p-value of:

$$p_{Mt_{Mannitol}|Mt_{non-Mannitol}} < 0.001.$$

Mannitol is used in similar cell experiments with the aim to reduce the internal turgor pressure of the cell. In this sense, the aim is to reduce the internal turgor pressure so one can examine the cell wall mechanics without the overwhelming presence of the internal (turgor) forces.

Also, we tested how different are the distributions between the use or not of *Mannitol* in wild type samples, and the output was the same with a p-value:

$$p_{WT_{Mannitol}|WT_{non-Mannitol}} < 0.001.$$

Collectively, we have the following figure, where we plot the individual (split) distributions of wild type/no *Mannitol* in A, wild type/*Mannitol* in B, mutant/no *Mannitol* in C, mutant/*Mannitol* in D, and all of them together in a single plot in E:

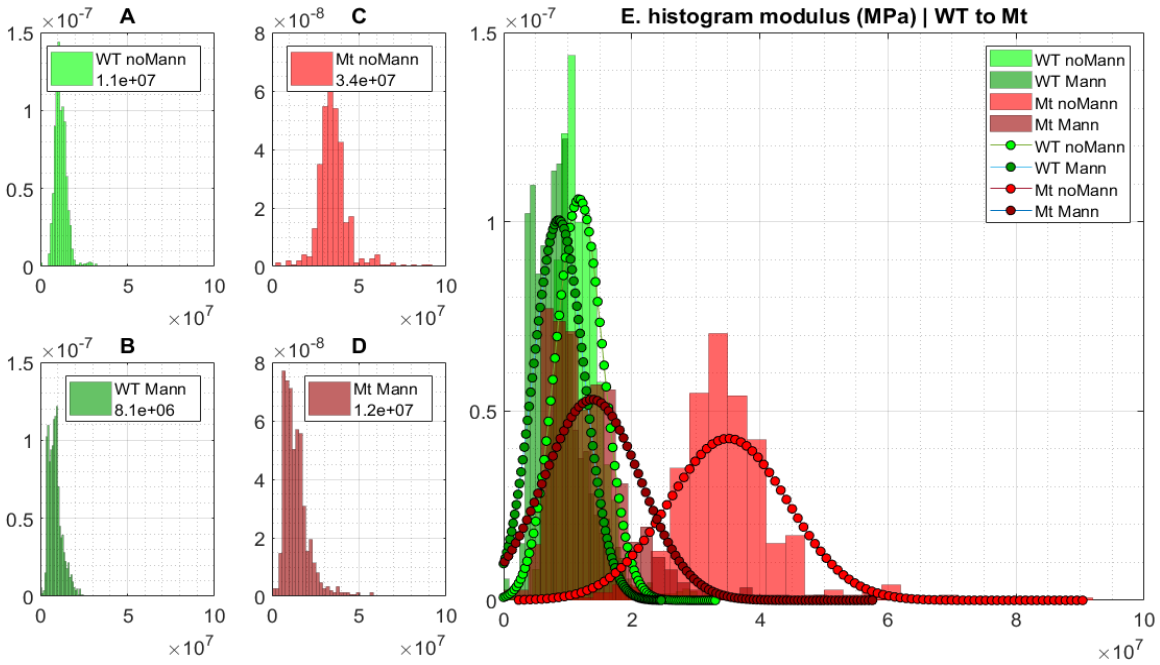

Figure 42: A-D: Histograms of the distributions of the four different groups of data, as these are labelled in the legend of each plot. E. Histogram for the four different populations of experimental modulus data, together with the relevant distributions' probability density functions. Each pdf is represented by a colored dotted line (according to plot legend) with each pdf line sharing the same color with its relevant distribution. The x-axis shows the modulus value (in Pa), while y-axis shows the probability of the relevant x-value.

Where the dotted lines represent the probability density function (pdf) for each one of the aforementioned group's distribution. The dark-green dotted line represents the probability density function of the wild type/*Mannitol* experiments' distribution, the light-green dotted line represents the probability density function of the wild type/no-*Mannitol* experiments' distribution, the purple dotted line represents the pdf of the *Mannitol* treated mutant experiments' distribution, and the red dotted line represents the pdf of the no-*Mannitol* treated mutant experiments' distribution.

For these four distributions, we now have the values:

$$WT|_{Mannitol}: \mu_{WT_M} = 0.89 \times 10^7\ [Pa]\ \&\ median_{WT_M} = 0.81 \times 10^7\ [Pa]\ \&\ \sigma_{WT_M} = 0.40 \times 10^7\ [Pa]$$

$$WT|_{no\ Mannitol}: \mu_{WT_{n-M}} = 1.20 \times 10^7\ [Pa]\ \&\ median_{WT_{n-M}} = 1.10 \times 10^7\ [Pa]\ \&\ \sigma_{WT_{n-M}} = 0.38 \times 10^7\ [Pa]$$

$$Mt|_{Mannitol}: \mu_{Mt_M} = 1.38 \times 10^7\ [Pa]\ \&\ median_{Mt_M} = 1.20 \times 10^7\ [Pa]\ \&\ \sigma_{Mt_M} = 0.75 \times 10^7\ [Pa]$$

$$Mt|_{no\ Mannitol}: \mu_{Mt_{n-M}} = 3.51 \times 10^7\ [Pa]\ \&\ median_{Mt_{n-M}} = 3.40 \times 10^7\ [Pa]\ \&\ \sigma_{Mt_{n-M}} = 0.93 \times 10^7\ [Pa]$$

As it is found from these experiments, the use of *Mannitol* reduces the modulus in the cell wall by eliminating the turgor pressure factor off the wall mechanics, and the absence of it has a bigger effect in the modified cell wall mechanics.

Finally, in order to back it up, we can say that the mutation is affecting only the constituents of the cell wall and not the internal turgor pressure. Thus, if turgor pressure was truly an overwhelming force stopping us from "reading" the wall's surface with the help of nano-indentation, then both populations should have similar modulus value because this would mainly be an effect of the turgor pressure. But even with no *Mannitol* presence, the wild type's modulus is relatively low compared to its counterpart.

We conducted a hypothesis testing to compare the wild type and the mutant samples in two different cases (presence or not of *Mannitol*). We found that in both cases, the mutant and the wild type samples come from different distributions with unequal medians, at the 5% significance level.

6.3.2. Other findings

6.3.2.1. Modulus vs indentation

If we explore a bit more the mechanics of the cell wall, using our own method of calculating modulus, we will test how this set of median values (as seen in Figure 42-E) compares with the relevant set for: 1. different method of calculating modulus (*Hertz* and *Pharr-Bolshakov*, implementing specialized calculation according to *beta* values), and 2. Different level of indentation (50nm and 100nm)[43]. For this case, we create four sets of comparisons, and we see this in the following figures:

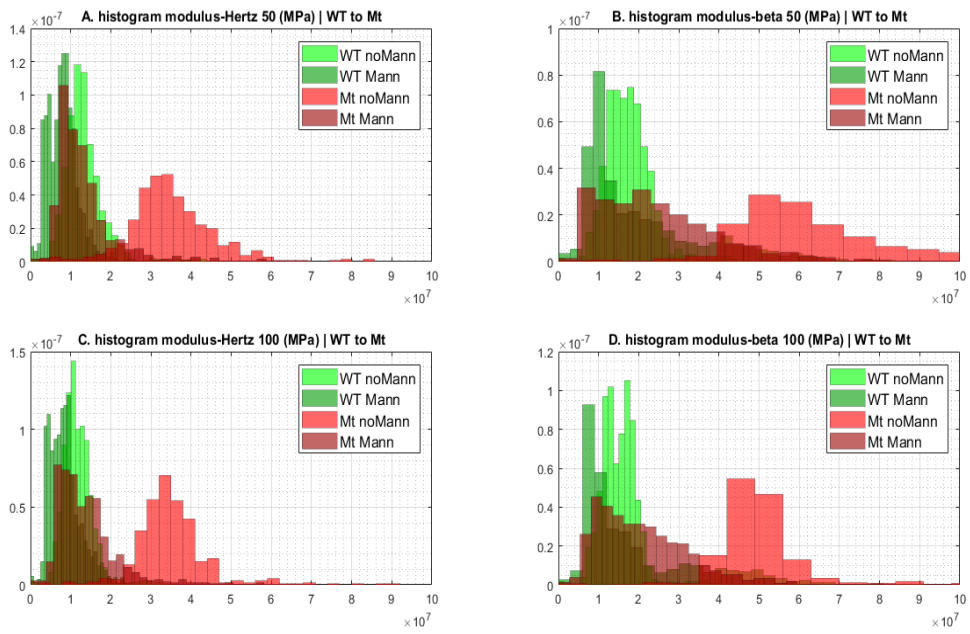

Figure 43: Histograms for the four different populations of experimental modulus data, for 4 different cases; A: *Hertz* model/50 nm. B: *Hertz* model/100 nm. C: *Pharr-Bolshakov* model/50 nm. D: *Pharr-Bolshakov* model/100 nm. The x-axis shows the modulus value (in Pa), while y-axis shows the probability of the relevant x-value.

[43] We saw previously in sub-chapters 5.3.2.3 and in 6.2.1 how we analyze different depths of indentation in order to compare how the fitting *beta* values and the modulus change along indentation

In this figure we see how the set of the four labelled distributions appears in the 4 different aforementioned cases. And in the following plot, we see how the median values of the distributions of Figure 43 compare with each other.

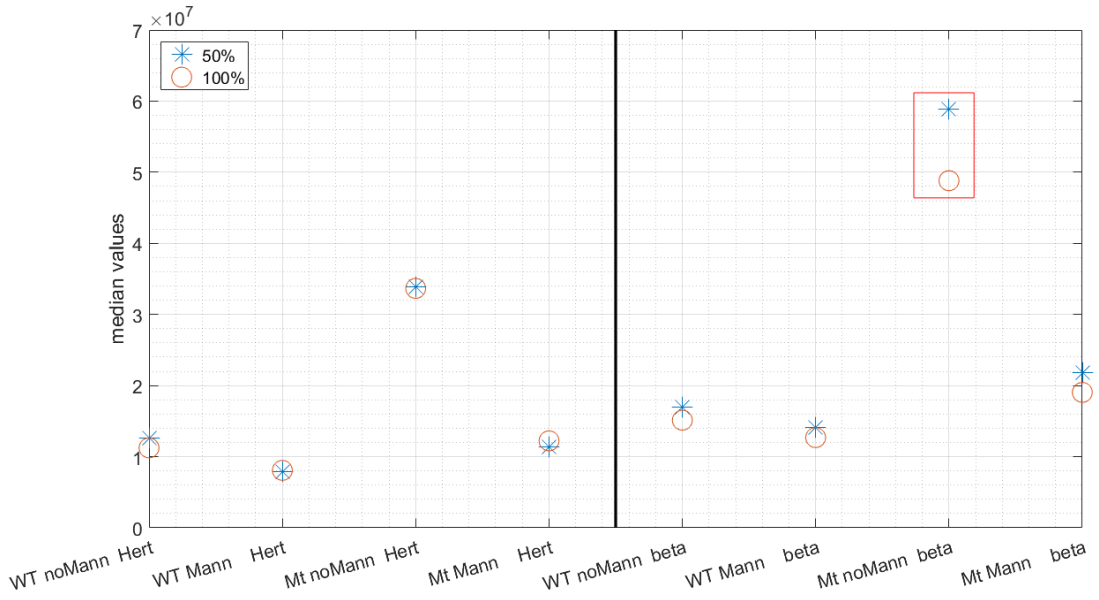

Figure 44: Plot showing how median values for the different cases listed in x-axis labels differ for the case of 50 nm and 100 nm. The case of mutant, no-*Mannitol*, *beta* case is outlined with a red box. The y-axis in in [Pa].

We see that only in the case of AFM force map experiments of mutant cells, coupled with the no-use of *Mannitol* as a buffer and the use of the *beta* values for the modulus calculation, modulus changes as we investigate larger part of the force distance curve. And this is probably a feature of the cell wall that exists in mutant *pme6* cells but can only be seen under the no-use of *Mannitol* and our specialized analysis technique. This feature may be due to a material differentiation in different depths of the exterior (primary) cell wall of the stomata, or due to the cell wall's anisotropy[44] which affects the tip-surface contact.

[44] As discussed in the background chapter

6.3.2.2. Different cantilever

Also, it is important to note that for the case of "modulus comparison", we performed comparative analysis using the prevailing experiment's selected-region modulus values using modulus as calculated with both methods cited in 5.3.2.2. In the second case, (for the modulus calculation using 'Pharr-Bolshakov'), we have the following pdf distributions instead:

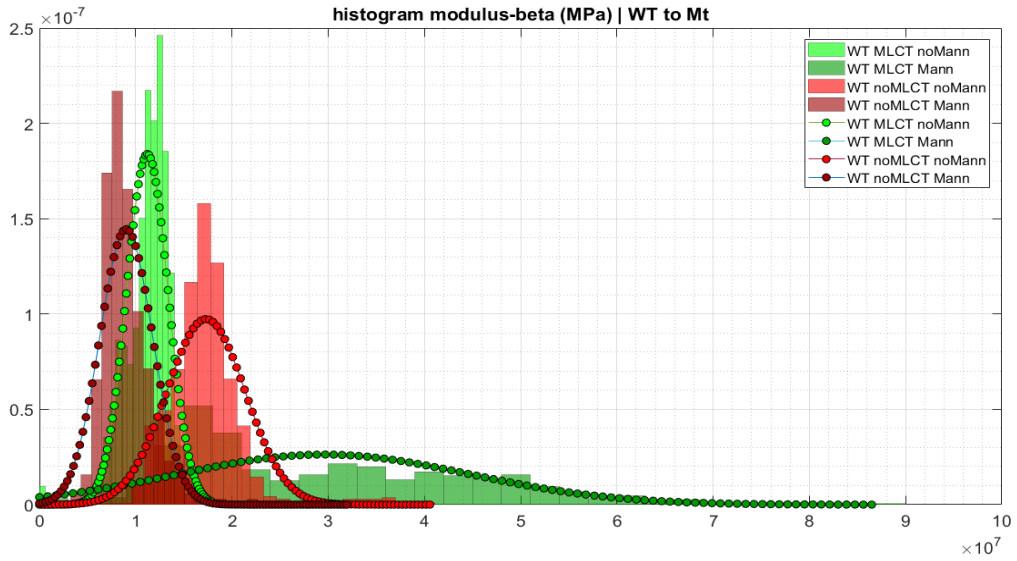

Figure 45: Probability density functions for the different distributions. The x-axis shows the modulus value (in Pa), while y-axis shows the probability of the relevant x-value. Each pdf is represented by a colored dotted line (according to plot legend) with each pdf line sharing the same color with its relevant distribution.

$$WT|_{Mannitol,MLCT}: \boldsymbol{\mu_{WT_{M,MLCT}}} = 2.96 \times 10^7\ [Pa]\ \&\ \boldsymbol{\sigma_{WT_{M,MLCT}}} = 1.52 \times 10^7\ [Pa]$$

$$WT|_{no\ Mannitol,MLCT}: \boldsymbol{\mu_{WT_{n-M,MLCT}}} = 1.12 \times 10^7\ [Pa]\ \&\ \boldsymbol{\sigma_{WT_{n-M,MLCT}}} = 0.22 \times 10^7\ [Pa]$$

$$WT|_{Mannitol,no\ MLCT}: \boldsymbol{\mu_{WT_{M,n-MLCT}}} = 0.90 \times 10^7\ [Pa]\ \&\ \boldsymbol{\sigma_{WT_{M,n-MLCT}}} = 0.28 \times 10^7\ [Pa]$$

$$WT|_{no\ Mannitol,no\ MLCT}: \boldsymbol{\mu_{WT_{n-M,n-MLCT}}} = 1.73 \times 10^7\ [Pa]\ \&\ \boldsymbol{\sigma_{WT_{n-M,n-MLCT}}} = 0.41 \times 10^7\ [Pa]$$

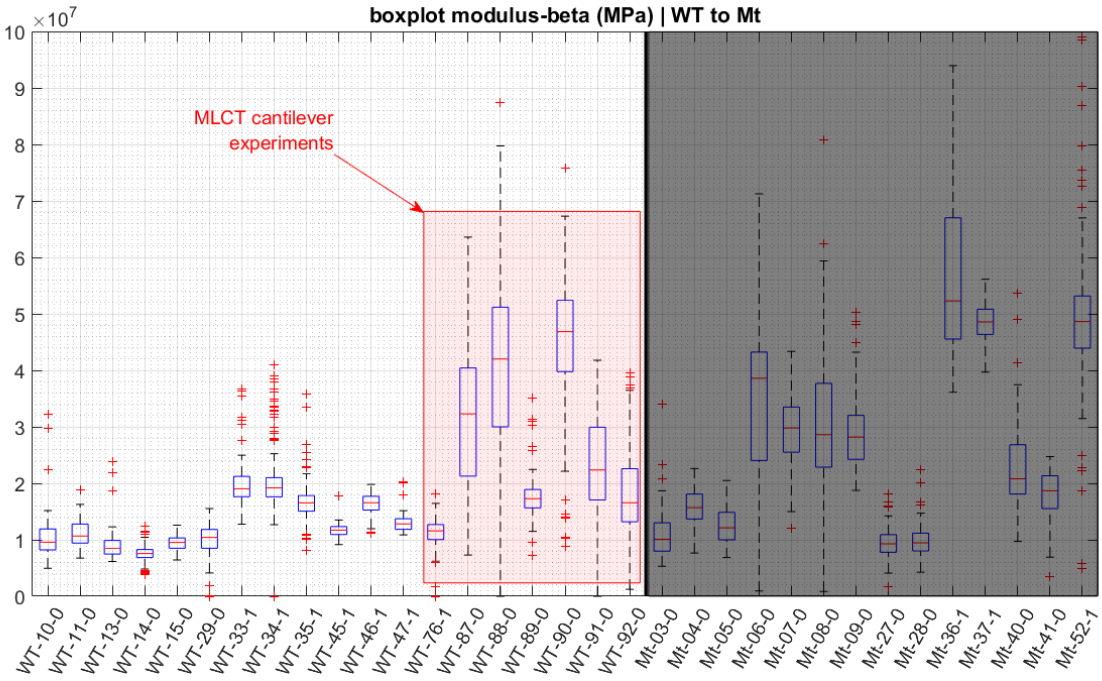

Figure 46: Modulus comparison between WT and *pme6*. The black vertical line separates the different populations of data. The mutant experiments' area has been shaded as it is not considered in this part of the analysis. Each experiment is represented here by a boxplot with its median and 25th and 75th quantiles. The value in the y-axis is in Pa. The MLCT experiments are shaded in light red.

Now, the pdf of the wild type population has split in two distinctive groups; and the defining factor now is the use of different cantilever (MLCT cantilevers with wider angle and bigger diameter) in connection to the use of *Mannitol*. What these data tell us, is that with our technique, differences arise between the different cantilever experiments, but not with the standard *Hertz* model. Thus, it could be the case that when the turgor pressure is reduced from the cell, it makes it difficult for our model to work, since this changes the cell wall surface dramatically.

6.3.3. Comparison of adhesion

In order to compare the adhesion between wild type and mutant cells, we extracted the adhesion values from all 33 experiments (19 WT and 14 *pme6*) in the same way we did with modulus in the previous sub-section, and this resulted into the following collective chart, where each

boxplot represents the distribution of the adhesion values of each experiment (as seen in the x-axis).

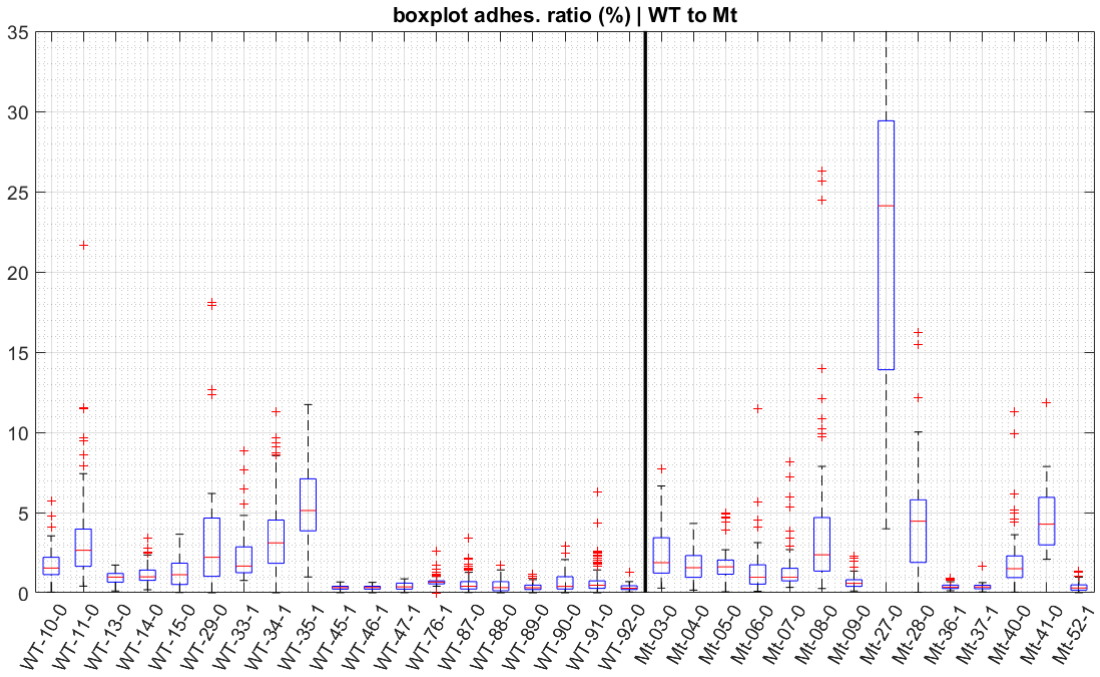

Figure 47: Boxplots representing adhesion values for teach one of the aforementioned experiments of this work. The y-axis shows adhesion value, while the x-axis shows the different experiments. The vertical black line separates the wild type from the mutant experiments. The y-axis is adhesion ratio (dimensionless).

In this plot, we check the differences in adhesion, where each one of two sides of the plot (as this is divided by the vertical black line) represents different population; on the left side, one can check the wild-type experiments, while on the right side of it there are the mutant experiments. Here, it is important to note again that when referring to "experiments' results", we mean the collected values of adhesion from the experiment's map, using the RoI method, as described in chapter 5.3.3.1.5.

If we draw the distributions for the different cases, we have the following figure with 4 different plots. Sub-plot A is for the case of wild type and the absence of *Mannitol*, B is for wild type and *Mannitol*, C is for mutant and no-*Mannitol*, and D is for mutant with *Mannitol*.

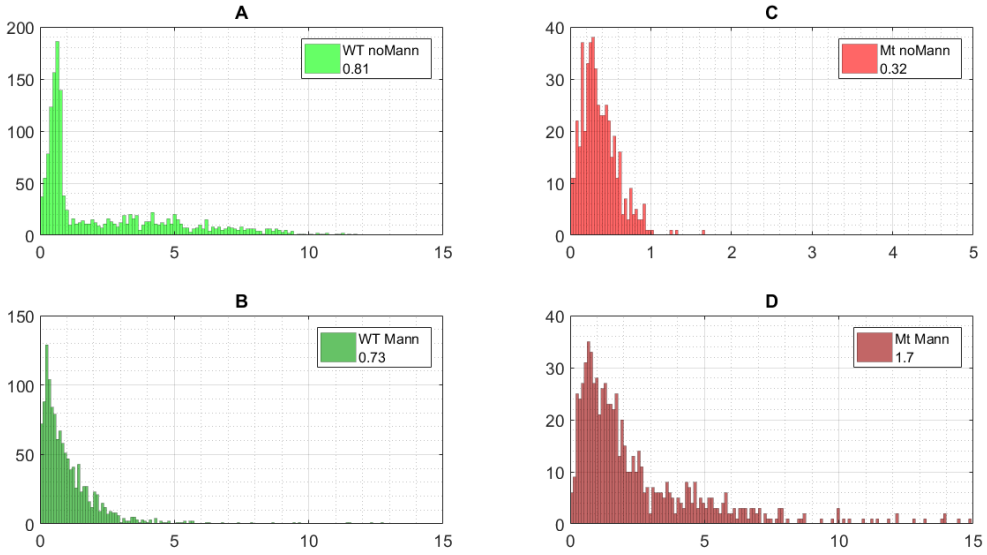

Figure 48: A-D: Histograms of the distributions of the four different groups of data, as these are labelled in the legend of each plot. Each label also contains the median value (in [Pa]) of the relevant plot.

As it is immediately obvious, there is a big variance (and skewness) in the results, and there is not a clear view as to whether one population has a higher adhesion over the other one overall. Also, by checking at the experimental details there is not a defining factor that would classify the different modes/groups according to.

6.4. Plant cell surface vs imprint

From the moment we started noticing that surface inhomogeneity (Figure 49) plays a crucial role in our measurements, we started investigating this phenomenon. Our assumption was that since our method for calculating modulus took account the fitting of the curve into the calculation, then this feature would counterbalance the phenomenon of surface heterogeneity in the modulus calculation.

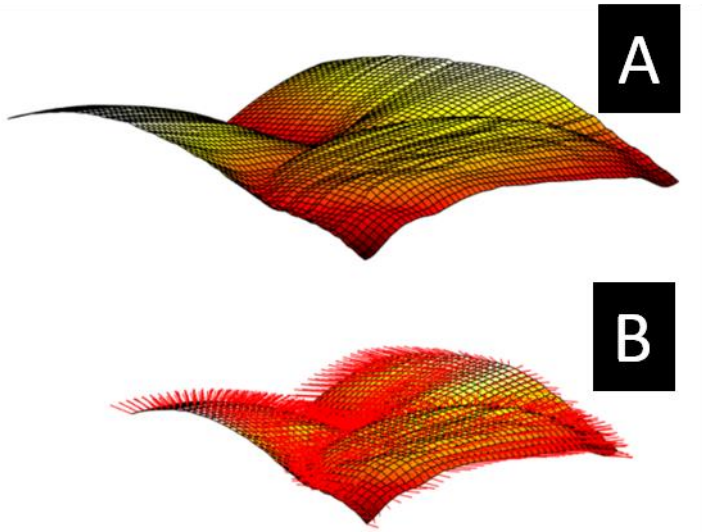

Figure 49: A: 3-D surface representation of the selected area for AFM scanning (dimensions: 40 x 40 x 10µm). The height range of this AFM force map is [0 8e-6] [m]. B: The same surface with the calculated surface normal vectors on top, which makes the surface anisotropy clearer.

For this we designed a series of experiments to test our assumption. In these experiments, we kept the surface inhomogeneity, but removed the material one. And the best way to do this is by creating an imprint/replica of the plant cell (made by casting dental paste[45] onto the plant leaf to recreate plant leaf surface's micrometer features including pavement cells and stomatal cells) and subsequently testing it under the same AFM conditions and conducting a force mapping experiment. The imprint of course would have the same modulus all over its surface. In this way, one would expect that if the effect of surface inhomogeneity was successfully removed with our new way of analysis, then the modulus of the imprint's force map would be -in the range of error- homogeneous.

[45] Details in methods chapter

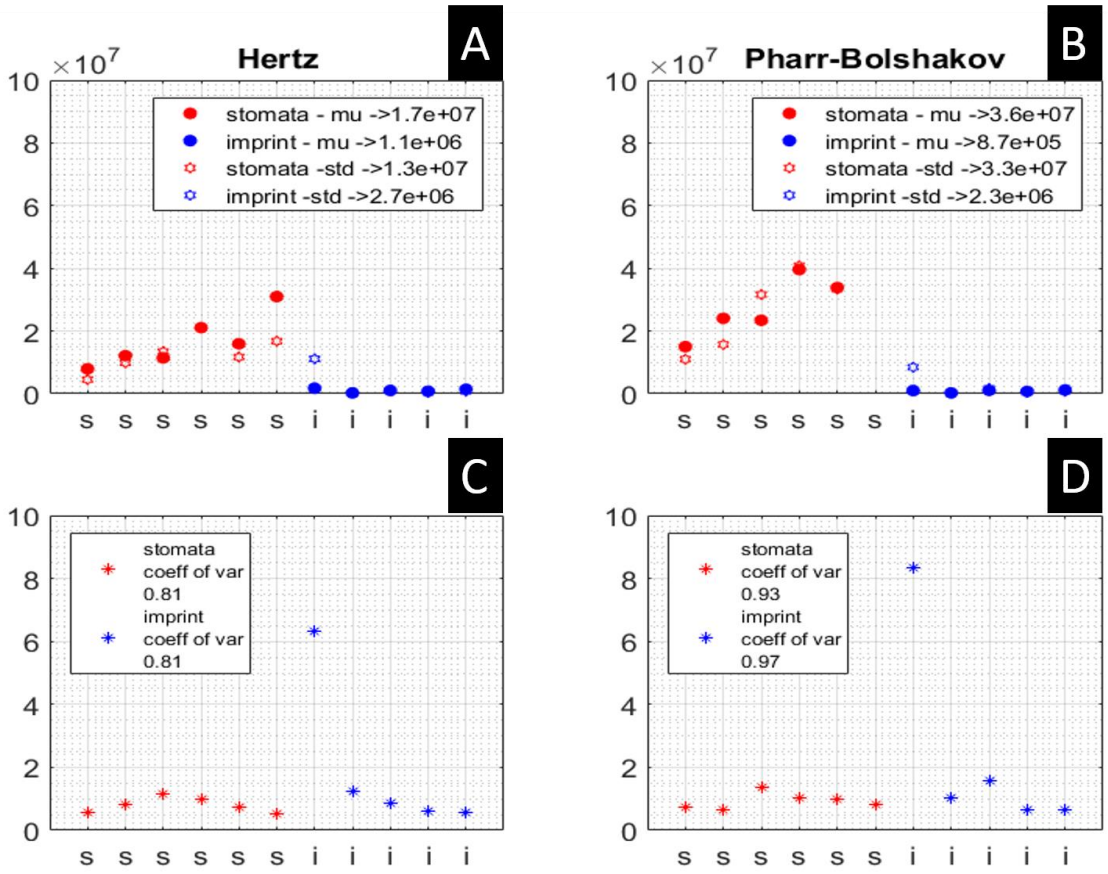

Figure 50: Difference between modulus calculation in stomata (s, red marks) and imprint (I, blue marks) experiments. A-B: mean and standard deviation of modulus comparison between stomata (s-red) and imprint (i-blue) experiments with different CM models (A: *Hertz*, B: *Pharr-Bolshakov*). C-D: coefficient of variance of modulus comparison between stomata (s-red) and imprint (i-blue) experiments with different CM models (C: *Hertz*, D: *Pharr-Bolshakov*).

What we expected from this analysis was to see a homogeneous modulus value on the imprint samples. What we found was a lower modulus value overall and a lower standard deviation (denoting a slight "correction" of the topographical factor in the calculation of modulus) as well. Here, we present the results under the *Pharr-Bolshakov* model, but the relevant ones for the other models exhibit the same behavior

$$stomata: \mu_{stom} = 36.0 \times 10^6\ [Pa]\ \&\ \sigma_{stom} = 33.0 \times 10^6\ [Pa]$$

$$imprint: \mu_{impr} = 0.9 \times 10^6\ [Pa]\ \&\ \sigma_{stom} = 2.3 \times 10^6\ [Pa]$$

Although the lower modulus value was expected (since it is a different material), the low standard deviation was a good indicator of our expectation. This is because the values of modulus across the area of the scan had a much sharper distribution and similar values.

But we also calculated the *coefficient of variation* [46]*(CV)* on our imprints experiments' distributions and what we found was that this was similar to the stomata experiments, meaning that this did not prove helpful for our approach validation.

$$stomata: CV_{stom} = 0.93 \;\&\; imprint: CV_{impr} = 0.97$$

Because the standard deviation may had been lower, but 'relatively' lower. And this is a sign of similar behavior, just shifted in a higher range.

6.5. Conclusions

Initially, we demonstrated the implementation of our developed technique in a single AFM force mapping stomata experiment with the aim to both calculate the modulus value according to the specialized curve fitting analysis routine, and secondly to show how we can analyze each experiment in order to get more mechanical insight in the data. We showed that with our technique the cell's modulus exhibited variation across its cell wall (especially in the middle of the wall), compared to the *Hertz* modulus calculation output. We did a profile analysis to show this finding in more detail, and we found an interesting profile across the middle of the cell wall, compared to the relevant *Hertz* profile analysis. Also, we demonstrated the relation of cell's morphology to its mechanical properties (higher adhesion and hysteresis at some parts of the cell and the surrounding pavement cells), and we presented the reasoning behind our analysis method (lower RMSE | *beta* values due to specialized fitting) for the calculation of

[46] Also known as 'relative standard deviation' takes in account in its calculation both the mean and the standard deviation - sigma normalized by mu

modulus. Finally, we showed through the 'tomography' analysis of features like modulus, *beta* values, and RMSE values that there is a *beta* decrease in some parts of the cell, and this could affect modulus measurements.

Then, we conducted comparison tests between the different populations of modulus and adhesion data. At the beginning of the chapter, when introducing the stomata cells and the *pme6* mutants, we speculated on the altered mechanics and on what can this reveal for the cell's biological function. We performed normality checks on the individual samples, and we did statistical significance analysis tests in order to compare the values that we got for the separate experiments, and we observed higher modulus values (median ~*x*2) in the mutant experiments versus the wild type ones overall:

$$median_{WT} = 0.99 \times 10^7 \ \& \ median_{Mt} = 1.79 \times 10^7.$$

This is an important finding (higher modulus in mutant) and it could be linked to a multitude of cell properties, of both physical/mechanical and biological nature. Mechanical features of the wall, like the wall strengthening due to the altering in cell wall bio-polymer/cross-link agents' composition resulting from the mutation, is the most possible explanation for the higher modulus found in mutant cells. At the biological level, this finding is important since it is both a step towards the regulation of the cell's biological function for optimal growth under stress conditions (selection of mutant according to its phenotype), and also for an enhanced understanding of the relation between stomatal structure and biological function.

Then we observed a bimodality in the two populations of data, and we split each one in two categories, depending on the buffer used for experimentation.

$$WT|_{Mannitol}: median_{WT_M} = 0.81 \times 10^7 \ [Pa]$$

$$WT|_{no\ Mannitol}: \&\ median_{WT_{n-M}} = 1.10 \times 10^7\ [Pa]$$

$$Mt|_{Mannitol}: median_{Mt_M} = 1.20 \times 10^7\ [Pa]$$

$$Mt|_{no\ Mannitol}: median_{Mt_{n-M}} = 3.40 \times 10^7\ [Pa]$$

If we break the two groups and analyze their distribution, we see that whenever we used *Mannitol* as a liquid buffer, modulus values between the two groups was close but in the absence of it differences increase. We did a hypothesis testing that the two groups of data (wild type and mutant) come from different distributions with unequal medians and we got values of $p < 0.001$ for both the cases of *Mannitol* and no-*Mannitol.* The reason for the difference in the modulus values is believed to be due to actual underlying cell wall composition difference (as expected from the cell wall modification due to the mutation), which is translated into the mechanical measurements here (modulus higher in *pme6*). The reason behind the different values in wild type with the use of a different cantilever may be because the contact area in *Mannitol* treated cells is different and this can only be tracked by our method where it takes in account the fitting curve for the calculation of modulus, and as such, the calculation is expected to vary under different contact.

Another thing to note is that when the indentation is higher (technically, we analyze a bigger portion of the force indentation curve), in the case of mutant samples with no use of Mannitol, the modulus (as calculated by the 'Pharr-Bolshakov' model) is smaller. This may be attributed to the fact that with higher indentations, the assumption for "homogeneity" of the biological material under investigation is no longer valid, and the indentation distance reaches underlying layers inside the primary cell wall of the stomata.

Also, we compared the adhesion results between the different populations, we performed statistical analysis as well, but we did not observe clear differences in adhesion between the two different populations of data.

Finally, we conducted some experiments with a replica of the cell's surface in order to check the effect of the surface's anisotropy in our results and whether our method accounted for it, but it was difficult to find a clear answer to this. This is because, we observed that by comparing the two different groups' data, the distributions' standard deviation on the imprint experiments was significant lower, but the 'relative standard deviation' was very similar in the cases of stomata and imprint experiments.

$$stomata: CV_{stom} = 0.93 \;\&\; imprint: CV_{impr} = 0.97$$

Chapter 7: *C. Albicans*: altered mechanics induced by mutations

7.1. Introduction

Following the successful AFM nano-indentation mechanical analysis of the stomatal cells under the developed technique and backed up by the group's expertise on the experimentation with living biological material (bacterial, plant and cancer cells), we were motivated to collaborate with other research groups from different departments and especially from the field of Bio-medical and Animal & Plant Sciences (BMS, APS). Throughout these collaborations we mechanically investigated fungal cells and the altered mechanics between mutant and wild-type cells (as in the case of stomatal cells), and also between different parts of the same cell. The aim of this investigation was to check how these mutations affected the cell's mechanics, and whether this change in mechanics can be linked to the mutation's effect on the cell. We conducted two projects, one of which is for the investigation of altered mechanics in *Candida albicans* cells in collaboration to Harriet Knafler and Professor Kathryn Ayscough from the Department of Biomedical Sciences. For the purposes of not including too much data in thesis we will present only the findings of the first project here.

Specifically, the first project was about mechanical testing of different yeast (*C. albicans*/human pathogen) sample cells, both wild-type (WT) and mutant (Mt). The C. albicans cell wall consists mainly of polysaccharides (glycan and chitin) and proteins. Glycan polymeric chains are linked to chitin microfibrils by covalent bonds (125) and those two form the basic *C. albicans* cell wall scaffold. The mutant samples are expected to have altered mechanics due to different cell wall composition (see chapter 2.3) and with this work we aim to expand our understanding of *C. albicans* biological function and its link to its cell wall structure. The mutants lack *apm4* part of the functional *AP-2* protein, which is responsible for cell wall

regulation and endocytosis in *candida* cells, and it has a big role in *C. albicans'* wall regulation, morphology and virulence. This dysregulation induced by the absence of *AP-2* in the mutant causes an excess of chitin synthase (Chs3) and, subsequently, a defective cell wall composition.

As in the case of stomatal mechanical differences, we investigate the mechanics of the cell wall and its connection to cell wall structure and composition. In both cases we compare between mutant and wild-type cells, where the mutant has been genetically modified to alter its composition of a main biopolymer of the cell matrix. Also, in both cases, this affected biopolymer is a main building block of the cell wall load-bearing network which acts opposite to the cell internal turgor pressure. Finally, this alteration is expected to be expressed in the mechanics of the wall, as measured by AFM indentation experiments, and subsequently, to be a factor affecting the cell's biological function.

We conducted AFM force mapping experiments across individual *C. albicans* cells in an acetate buffer (pH: 5.2) environment, and we examined 16 different samples, 7 of them being wild-type and 9 of them being mutant samples. We used the same cantilever (Nanosensors PPP-CONTSC) and the same buffer (Acetate 5.2) for these experiments, and we indented only the cell wall (tens of nanometers), because we wanted to investigate the elasticity of the cell wall and not the internal turgor pressure of the cell.

In more detail, the design of the experimentation included a series of AFM force mapping experiments on *C. albicans* cells, and subsequently we compared these data for altered mechanics investigation. This comparison included four series of experiments according to two defining factors: the cell type (wild-type or mutant) and the cell region (Figure 51-A/yellow-dotted areas, *mother cell* and *hyphae*):

1. WT | m vs WT | h
2. Mt | m *vs* Mt | h

3. WT | m *vs* Mt | m
4. WT | h *vs* Mt | h

Where WT stands for wild-type, Mt for mutant, m for *mother cell*, and h for *hyphae*. Morphologically, in *C. albicans* the *mother cell* is the main, round-shaped cell from which the *hyphae* (tail) evolves from.

7.2. Experiments

7.2.1. Single experiment

We will start by presenting our analysis technique results in a single experiment, a mutant *C. albicans* experiment. We will start by showing the modulus map, as it was calculated with the different CM models (described in chapter 5.3.2.5).

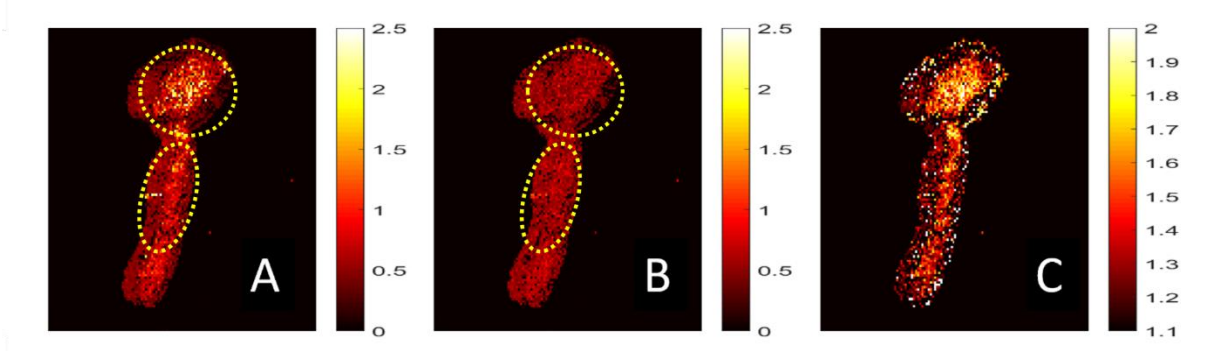

Figure 51: A-C: Modulus maps, each one representing calculation with a different contact mechanics model (A: *Pharr-Bolshakov* model, B: *Hertz* model), C: *beta* values map (from fitting). The colorbar limits for A and B are in MPa, C is unitless.

In sub-figure A of Figure 51, we use equation 13 to calculate modulus from the fitting of the FI curves of the force map. In B, we use the standard *Hertz* model (equation 5). Finally, C is a *beta* map, showing not the modulus but the result of the fitting analysis of the FI curves of the map, and the optimal *beta* describing the fitting of the curve.

We can see that A varies a lot from map B, especially on top of the regions of interest (yellow-dotted areas in A and B), thus this new approach offers a different view on these experiments. This has to do with our specialized analysis of the force curves of the map, where for the calculation of the modulus we take account the fitting of the curve under different *beta* values.

Quantitatively, this can be seen in the following figure, where on the first row we have four different maps (modulus, as calculated by *Pharr-Bolshakov* model, modulus *Hertz*, height map, and *beta* values map), and on the 2nd and 3rd row, we have the resulting map values from the white and the yellow line, respectively.

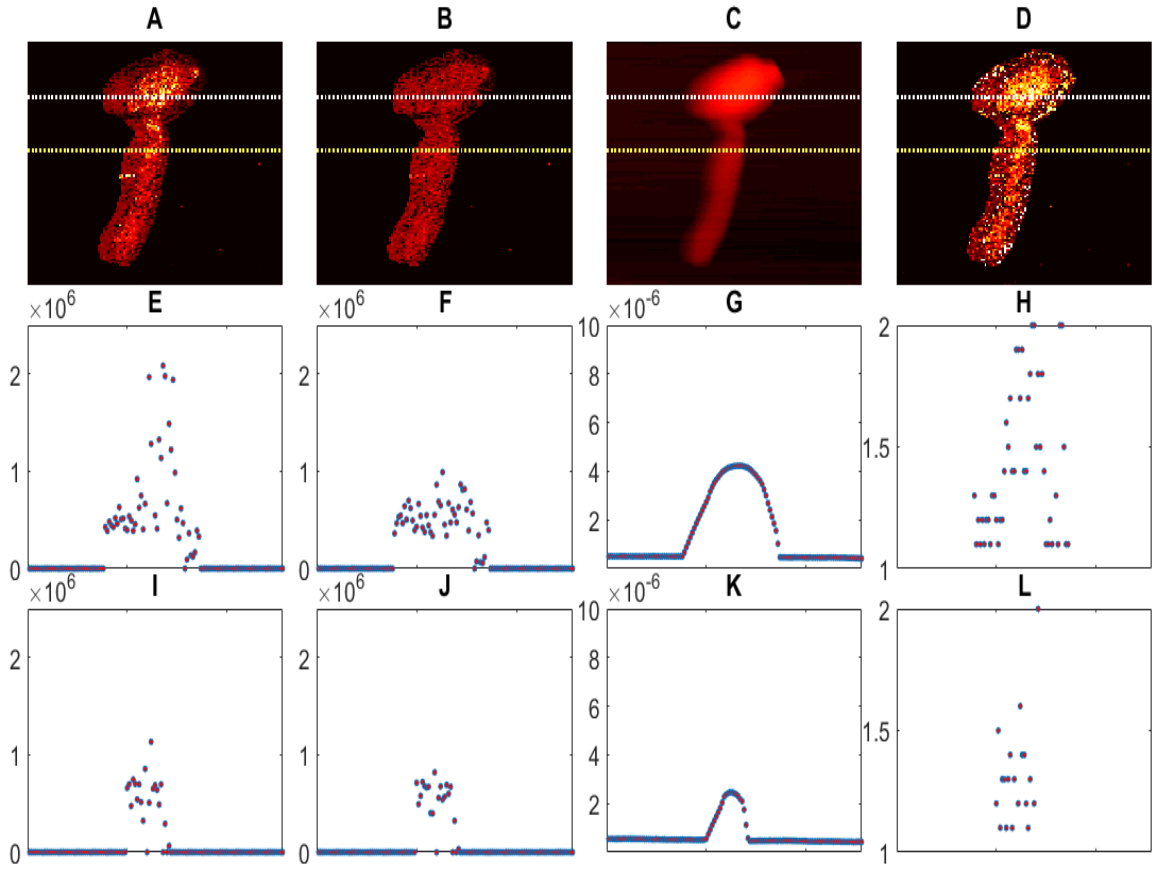

Figure 52: Profile analysis of the modulus values on top of the C. *albicans hyphae* (yellow line) and *mother cell* (white line) cell. Maps A,B,D point to the relevant ones in Figure 51 (A: *Pharr-Bolshakov* model, B: *Hertz* model, D: *beta* values map (from fitting)). C: Height map. E-H: Modulus values obtained from the white profile

in A-D. I-L: Modulus values obtained from the yellow profile in A-D. The colormap limits are (maps A, B: [0 2e+6] [Pa], map C: [1e-9 1e-5] [m], map D: [1.1 2]).

We see in the pairs of plots E-F and I-J, that on top of the RoI, the modulus values are different calculated by the different models. Also, we see in G and K, the height difference along the 2 lines, and in H and L, we see the *beta* values of these selected lines. In G and K, we see that the height of the *mother cell* is approximately 5 μm and the height of the *hyphae* is approximately 3 μm. In H and L, we see that the *beta* values at the middle of the cell are significantly higher than the values on the edges.

We continue our analysis of this experiment by presenting some other mechanical maps (Figure 53), whose ability of contrasting a selected mechanical property via a heat map, can reveal interesting findings. We start with the so-called "CM model selection" map (Figure 28A), which displays the "optimal" CM model that each curve of the map should be analyzed under. As we see, the CM model map (A) indicates that the FI curves of the map exhibit high hysteresis in some parts of the cell (edges) and also in some other parts adhesion is dominant. Following, we have maps D and E, which map respectively the relevant curve's hysteresis and adhesion, and as we see in this experimental force map, we have very low adhesion (essentially adhesion force, F_{AD}) across the middle of the cell and the same stands for the plasticity index/hysteresis.

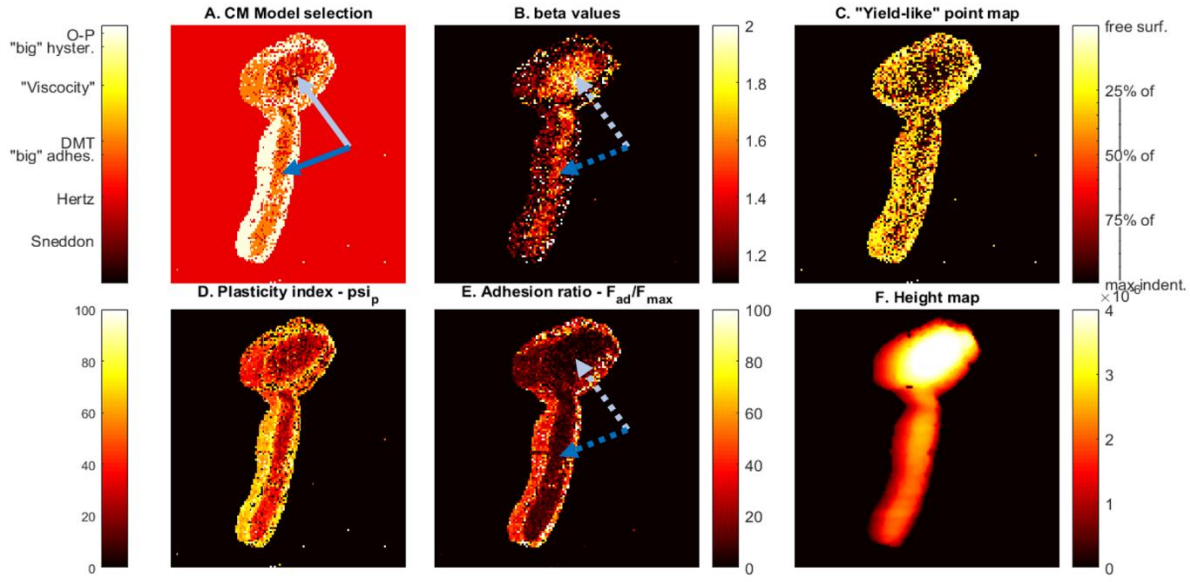

Figure 53: Support figures for the experiment of *C. albicans*. A: "CM model" selection map. B: *beta* values map (range: [1.1 2]). C: "Yield-like" point map (range 0-100) [unitless]. D: Hysteresis (plasticity) map (range 0-100) [unitless]. E: Adhesion ratio map (range 0-100) [unitless]. F: Contact point map (range: [0 4.]).

In B, the colored range is from 1.1 to 2, and it shows what *beta*/power law exponent each curve of the map results under non-linear fitting of the raw FI data. We see that in the middle of the cell, the values are higher, and this can be translated in variation of modulus under the *Pharr-Bolshakov* model.

We see that in the regions on top of the *mother cell* (spherical-shaped) and *hyphae* part (tube-shaped) in map C, most pixels show a black value which means that the relevant curve is smooth and so this is where we will collect data to analyze later for our comparison. Map C is a heat map displaying the percentage of the total indentation for each curve of the map, in which there is a change in the curve. The areas in C that are white make us think that this non-smoothness of the curve is due to the high surface topography of the cell at the edge of the cell. The last map ("height map", F) displays the height map of the force map, as calculated from the cp, the data point at which the indenter meets the surface. This map shows that indeed the

experiment exhibits a high topography (as can be seen in Figure 52-C, G, K), though in the limits of the z-scanner of the instrument.

Further on the analysis, and while staying on the fitting part of the algorithm, we cite the residuals of the fitting (RMSE values) of each curve of the map, in a relevant to the modulus heat map manner, for three different cases; for the fitting of all the curves with a *beta* of 1.5, with a *beta* of 2, and with the optimal *beta* for the prevailing curve (as this is calculated via the optimization of the RMSE value of each curve separately). In this sense, let's see how these 3 maps compare, and what information can bear for the better understanding of the modulus calculation. The three sub-figures at the right of Figure 54 (C, F, and I) show the RMSE values for the whole map. Specifically, C displays the RMSE fitting values of all the force curves of the RoI (as seen in C with blue-dotted annotation), calculated for a *beta* value of 1.5 (as in *Hertz* model), F displays the RMSE fitting values of all the force curves of the RoI (as seen in C with blue-dotted annotation), calculated for a *beta* value of 2 (as in *Sneddon* model), and I displays the RMSE fitting values of all the force curves of the RoI (as seen in C with blue-dotted annotation), calculated for the optimal *beta* value resulting from our optimization routine. In addition, plots B, E, and H show a histogram with all three different sets of RMSE values as obtained from the regions of interest of plots C, F, and I respectively. Finally, A, D, and G show statistics that result from the analysis of B, E, and H respectively. From this, we have the following (as expected):

$$median_{\beta=opt.} < median_{\beta=1.5} < median_{\beta=2}$$

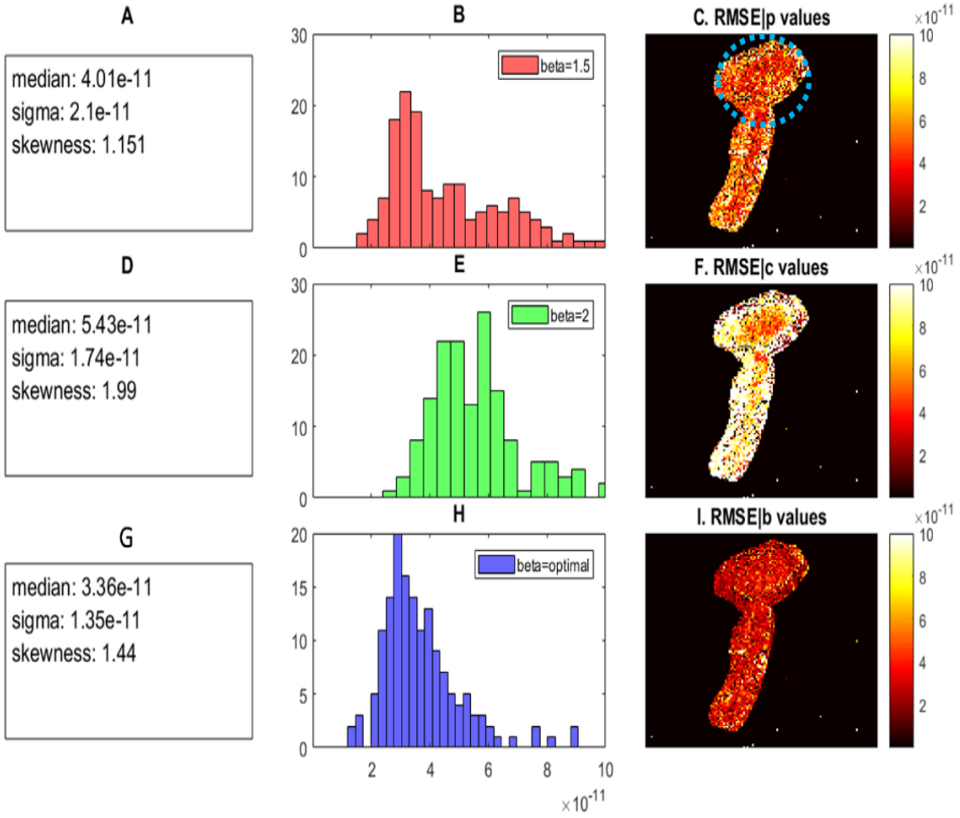

Figure 54: Fitting residuals analysis for the *mother cell* area after the FI analysis of the map's curves; A, D, G: Statistical values for the relevant distributions of B, E, and H. B, E, H: Histogram showing 3 different distributions (blue: RMSE | *beta*, red: RMSE | *p*, green: RMSE | *c*). C, F, I: 3 different fitting residuals maps, showing the RMSE values for the 3 different cases.

The same exact analysis to the one of the previous figure, is the following Figure 55. It shows the same statistics/features exactly, but for the case of *hyphae* now (blue-dotted RoI in C).

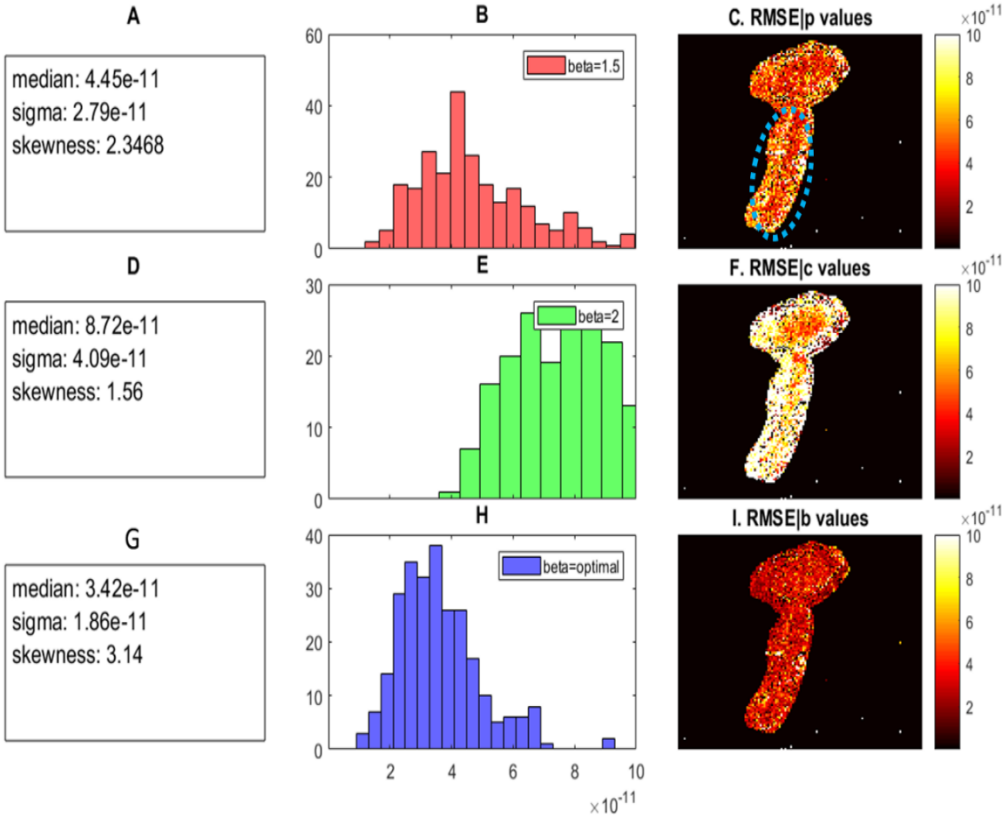

Figure 55: Fitting residuals analysis for the *hyphae* area after the FI analysis of the map's curves; A,D,G: Statistical values for the relevant distributions of B, E, and H. B,E,H: Histogram showing 3 different distributions (blue: RMSE | *beta*, red: RMSE | *p*, green: RMSE | *c*). C,F,I: 3 different fitting residuals maps, showing the RMSE values for the 3 different cases.

Again, we can see that:

$$median_{\beta=opt.} < median_{\beta=1.5} < median_{\beta=2}$$

And this is because we perform specialized fitting on each curve, and thus the fitting is expected to be better in the case of RMSE | *beta.*

Also, on the analysis of the modulus calculations for the same experiment, we show a collective way to display modulus. In Figure 56, we show how the different modulus calculation methods compare with each other for the same problem. Plots A-D refer to the *hyphae* region (blue dotter RoI in Figure 54-C), and E-H refer to the *mother cell* region (blue dotted RoI in Figure

55-C). In C-D and G-H, we see multiple histogram charts with the modulus data of the force map, as calculated with different models (see 4.1), in A and E we see a fitted probability distribution on the same data, and in B and F, we see how *sigma* and *mu* values (*sigma* and *mu*, as a result of the probability distribution fitting on the aforementioned modulus data) compare with each other.

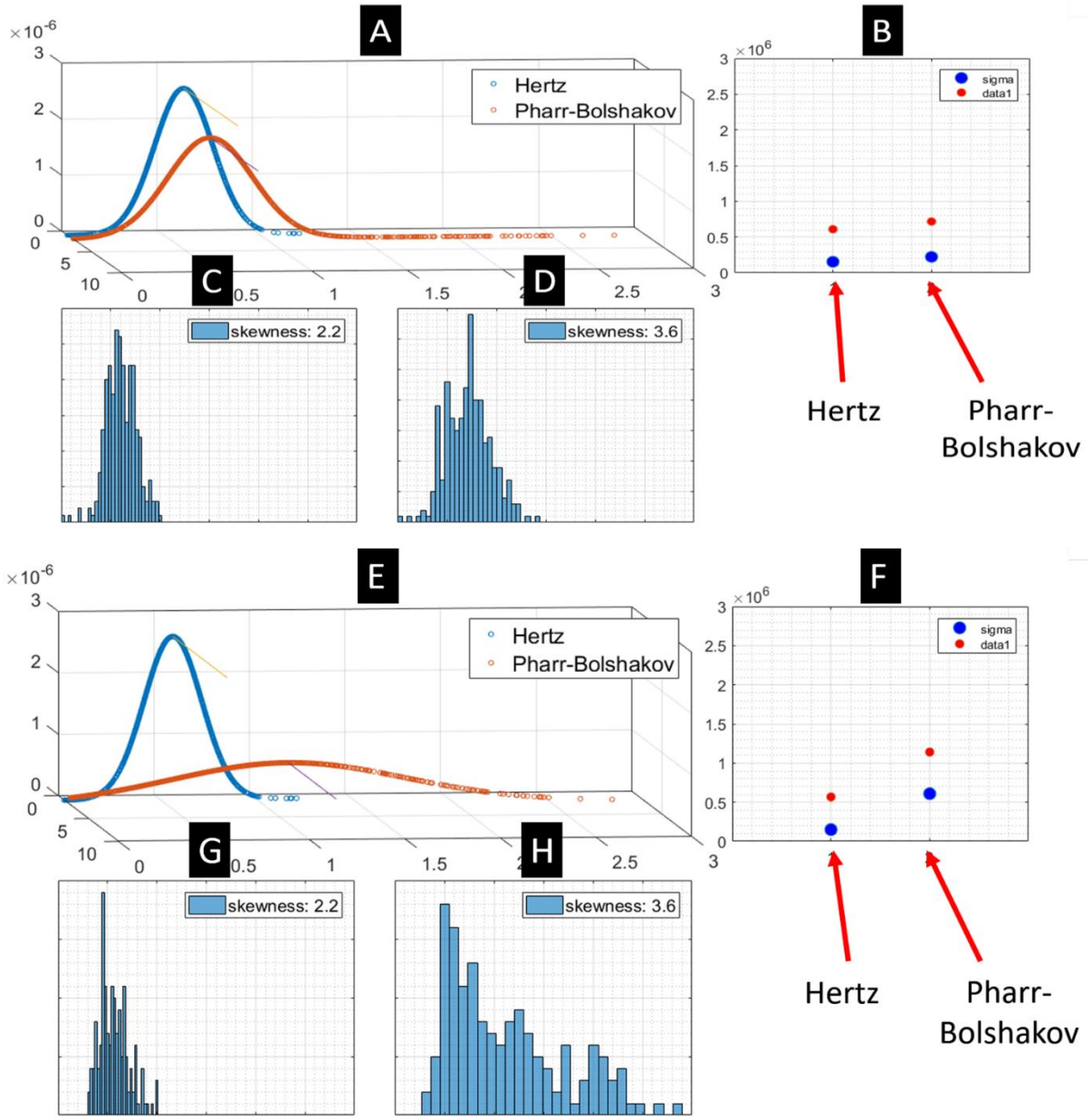

Figure 56: Statistical analysis of the different modulus maps (but only from the RoI now, as shown in Figure 54-C and Figure 55-C (A-D: *hyphae*, E-H: *mother cell*). A,E: Fitted probability distributions on the different sets

of calculated modulus. B,F: Mean and standard deviation values plot for the different sets. C-D,G-H: Histograms of modulus values for the case of *Hertz* and *Pharr-Bolshakov* model, respectively. In A,C-D, E,G-H, x-axis limits are: [0 3e+6].

The information that we get from this graph is similar to the one in Figure 51 that on top of the *mother cell*, there is a big difference in modulus between the different models.

Continuing on citing analysis results, one other routine of the developed analysis examines the relationship between the fitting and the indentation depth. With our analysis technique, as aforementioned in chapter 5.3.2.3, we have the option of analyzing different percentages of the same curve successively, and we do this in a "tomography" manner so to observe different mechanical behavior as we indent further into the sample's surface. In this context, we present how the investigation of *beta* (Figure 53-B) and of the different RMSE values (Figure 54-C,F,I) changes as we indent further into the surface, starting from 10 nm and finishing to an indentation of 100 nm. This is seen in the next figure, where each different row represents respectively the modulus (*Hertz*), modulus (*Pharr-Bolshakov*), *beta*, RMSE | *beta*, RMSE | *p* and RMSE | *c* in respective order, and the succeeding columns point to a different percentage of the indentation being fitted (from 10 nm up to 100 nm).


100%
90%
80%
70%
60%
50%
40%
30%
20%
10%
Hertz
Pharr-
Bolshakov
beta
RMSE|b
RMSE|p
RMSE|c

Figure 57: Progression of 6 different types of mechanical maps (rows) along different levels of indentation (columns, from 10% to 100% of selected indentation-100nm); Different rows represent different mechanical analysis, while different columns represent different percentage of indentation analysis; 1st row: *Hertz* modulus values map (range: [0 1.2e+6] [Pa]). 2nd row: *Pharr-Bolshakov* modulus values map (range: [0 1.2e+6] [Pa]). 3rd row: *beta* values map (range: [1.1 2] [unitless]). 4th row: RMS | *beta* map (range: [1e-14 1e-10]). 5th row: RMSE | p map (range: [1e-14 1e-10]). 6th row: RMSE | p map (range: [1e-14 1e-10]).

As we see from the progression of the *beta* values along different indentation depths (row 3), we observe a general trend of *beta* increasing at the regions of interest. This trend is something different than the relevant in the stomata experiments, and it is something that we did expect initially; we expected -according to the theory and the mathematical formulation of the elastic context between a rigid axisymmetric indenter and a surface of elastic half-space- a *beta* value of <2 (initially) and a *beta* value of 2 thereafter, since the indentation depth in this case is 100nm, way more than the 10 nm of nominal tip's diameter at the tip's apex (and more than the -approximately- 50 nm of SEM'd tip's diameter at the apex). Then, looking at the following rows of the figure, we see how the different RMSE values (row 2: Optimal *beta*, row 3: *beta*=1.5, row 4: *beta*=2 respectively for rows 4, 5 and 6) change as we fit bigger portions of the contact area. What we see is something expected, since these row are mathematically connected to the 3rd row's outcome. We see that the RMSE | *beta* values are lower than the RMSE | *p* and these are lower than the RMSE | *c* values which is shown in Figure 54 as well.

Also, from rows 1 and 2, we can see something interesting, that we did not see in the stomata experiment. We can see that, along indentation, modulus | *Hertz* values decrease, while the modulus | *Pharr-Bolshakov* values decrease -slightly- initially and increase thereafter until the end. This is a very interesting feature, possibly due to material differentiation on the cell wall, and could not have been observed without our implementation for modulus calculation.

7.2.2. All experiments

Now that we cited all the analysis output for a single experiment, we will move on by presenting a few the remaining experiments. Here, we present all the conducted experiments for the candida-altered mechanics project. We conducted 16 experiments (Figure 58,Table 5), 9 of which were mutant samples (column *type* in the table, labelled as “Mt(xx)” in the figure) , and 7 of which were wild type samples (column *type* in the table, labelled as “WT(xx)” in the figure). We tried to maintain relevant experimental conditions so we could be able to compare the mechanical measurements between wild-type and mutant samples.

Table 5: Experimental details for the *C. albicans* experiments; in column "type", light red for mutant, light blue for wild type. Each columned is color-scaled by its own. Black outline is the experiment presented before, red outline is for the experiments presented later, and the dotted lines are the special experiments not considered for comparison.

Expt. No	Type	Scan area (μm)	Force map pixels	Tip velocity (μm/s)	Sensitivity (nm/V)	Resonance frequency (kHz)	K_C (mN/mm)	Trigger point (nN)	Force distance (μm)
53	WT	35	64	4	241.9	22	0.2	11	3
54	WT	5.5	64	10.2	241.9	22	0.2	5.5	4.4
55	WT	4	64	8.6	241.9	22	0.2	5.5	3.5
56	WT	10	64	12.9	241.9	22	0.2	1.8	3.2
58	Mt	8.6	64	7.2	430.2	21.8	0.2	10	3
59	Mt	8.6	64	7.2	430.2	21.8	0.2	10	3
60	Mt	15	64	7.2	430.2	21.8	0.2	10	3
62	Mt	20.5	64	7.5	430.2	21.8	0.2	6.6	3
63	WT	40	128	10	129.6	22.6	0.1	1.9	3
64	Mt	12	64	10	129.6	22.6	0.1	1.9	3
65	Mt	20.5	128	10	129.6	22.6	0.1	1.9	4
66	Mt	20	128	9.87	169.1	23.4	0.2	3	3
67	Mt	19.5	128	9.87	169.1	23.4	0.2	3	3
68	Mt	19	128	9.87	169.1	23.4	0.2	3	3
69	WT	33.5	128	9.15	501.2	23.3	0.2	10.2	3
70	WT	26.3	128	8.93	501.2	23.3	0.2	10.2	3

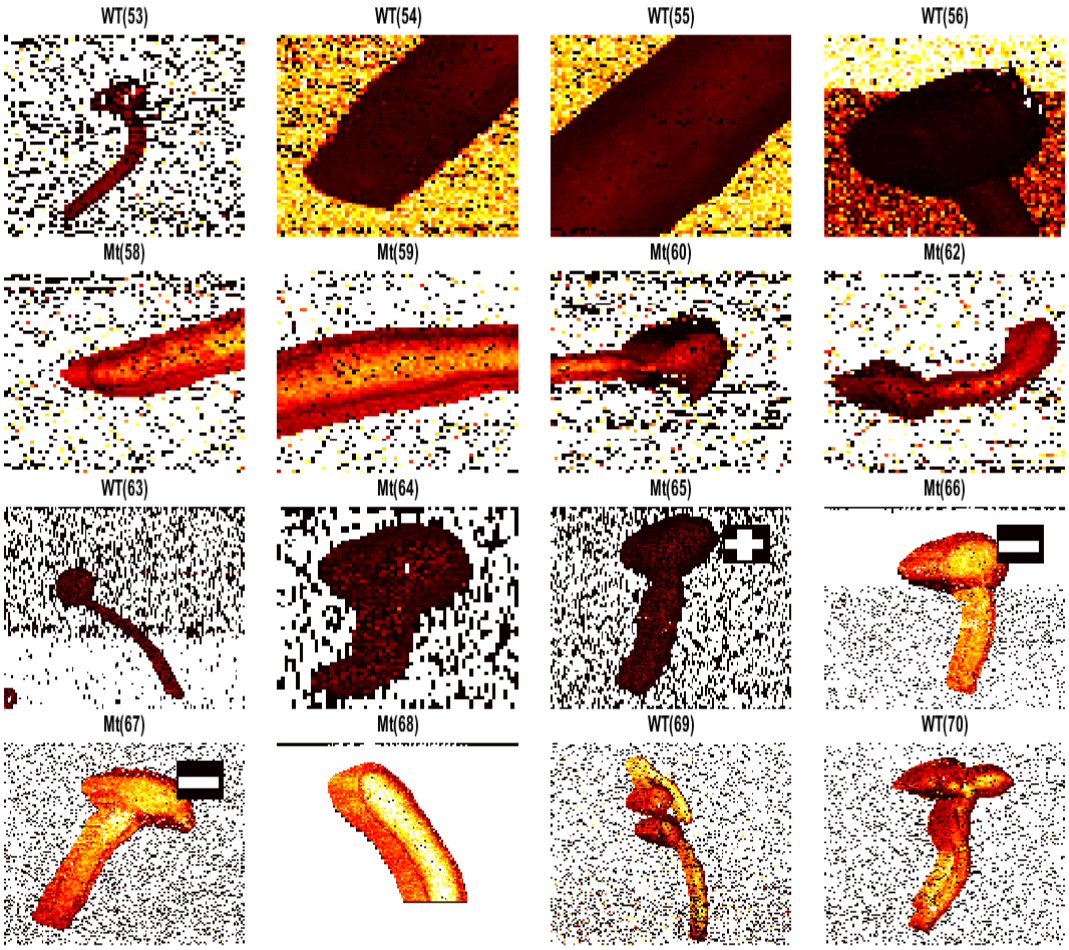

Figure 58: C. *albicans* AFM nano-indentation experiments; WT stands for wild-type, Mt stands for mutant. The numbers are a key for the different experiments. Experiments 69 and 70 (lower right) will not be considered in the calculations for modulus since there are two cells, one on top of the other. The map with the symbol '+' has been analysed extensively before. The maps with the symbol '-' are analysed briefly here.

As we see from this figure, we have some experiments where we have both the *mother cell* and the *hyphae* (as schematically seen in Figure 61), and some others in which only the *hyphae* is in the scan area. Also, we have the experiments WT(69) and WT(70), in which there are two *C. albicans* cells, one on top of the other, and in those two experiments we did not consider their mechanics for comparison between wild type and mutants, as we'll discuss later. The scale of the colormaps depicted in the figure is the same for all the subplots, so one can compare modulus values instantly.

Two representative experiments of the ones presented in Figure 58 (66 and 67, shown with the symbol '-') and in Table 5 (lines with a red outline) are the following:

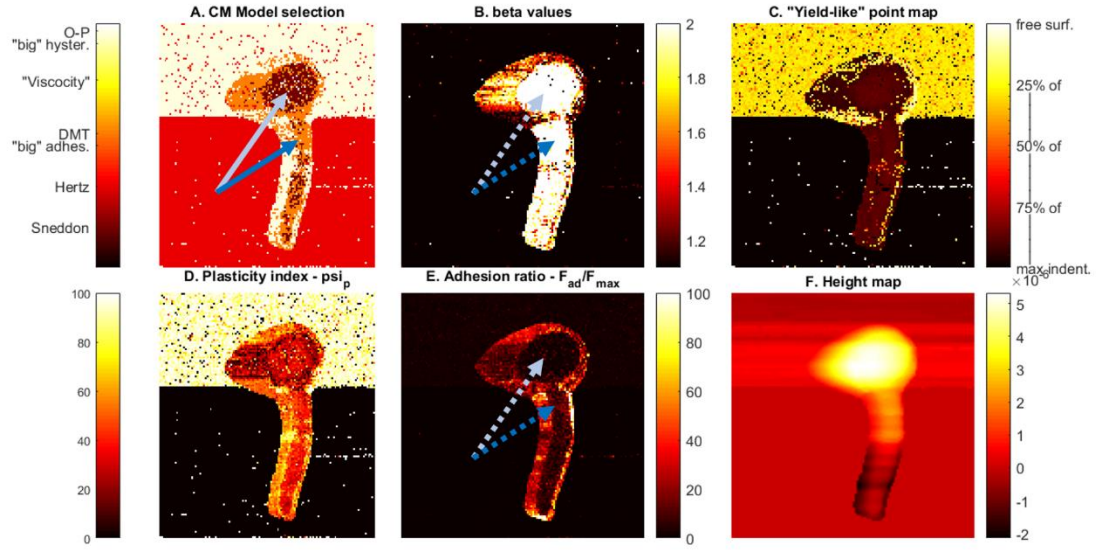

Figure 59: Support figures for the experiment 66. A: "CM model" selection map. B: *beta* values map. C: "Yield-like" point map. D: Hysteresis map. E: Adhesion ratio map. F: Height map. The annotation arrows show the regions of interest for comparative analysis.

Here we see that the dominant CM model under which one should analyze this map is the *Sneddon*, and that the optimal region to analyze data is the one pointed with the two arrows in A (light blue for *mother cell* and blue for *hyphae*). We see in A that on top of the *mother cell* region, the dominant color is dark red, as we would expect by looking at the same region of B (*beta* ~2). In B, we see that on top of the *mother cell* and on the *hyphae*, *beta* is ~2. Finally, we see in C that on the regions of interest there are almost no data points with a non-smooth curve, while on the surrounding area there are a lot of FI curves which exhibit a 'yield-like' behavior (on the edges of the candida cells). In D and E, we see that the adhesion is very low on the regions of interest, and finally we can see in F that the surface topography is high and so data on the edges of the cell are not preferred for analysis.

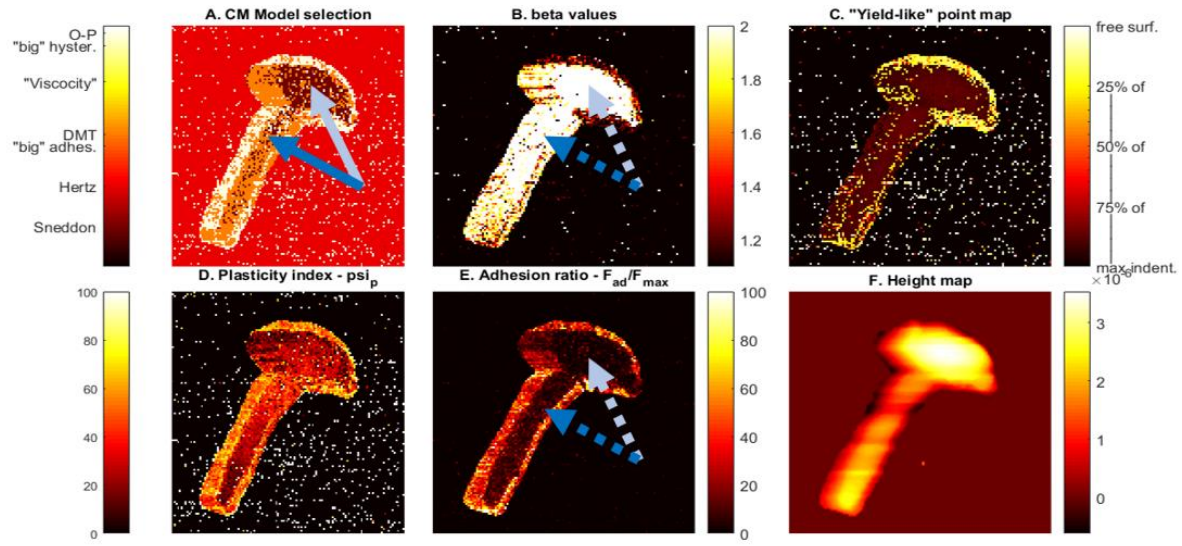

Figure 60: Support figures for the experiment 67. A: "CM model" selection map. B: *beta* values map. C: "Yield-like" point map. D: Hysteresis map. E: Adhesion ratio map. F: Height map. The annotation arrows show the regions of interest for comparative analysis.

Similarly, in this experiment (n^o 67), most of the findings of the previous experiment can be found here as well. We can see in A that the dominant CM model under which one should analyze this map is the *Sneddon*. In B, we see that on top of the *mother cell* and on the *hyphae*, *beta* is ~2, and in C, the regions of interest have almost no data points with a non-smooth curve. Finally, in D and E, we see that the adhesion is very low on the regions of interest, and finally we can see in F that the surface topography is high and so data on the edges of the cell will not be used for comparison analysis.

7.3. Altered mechanics

One of the reasons we developed this analysis technique was to have more insight in the experimental data through comparative analysis of the experiments under investigation. As it was discussed earlier, we are looking for altered mechanics between the four couples of cell samples. Schematically, this is illustrated in Figure 61, where Candida cells (green for Wild-Type, and red for mutant) are composed by a so-called spherical *mother cell* (light green for

Wild-Type, and light red for mutant) and a tip-shaped *hyphae* cell (dark green for Wild-Type, and dark red for mutant). Below the cell cartoons (in the same figure), the comparison table shows the 4 different sets of experimental analysis we conducted; we investigated mechanical differences (modulus and adhesion) between cell types and between cell regions.

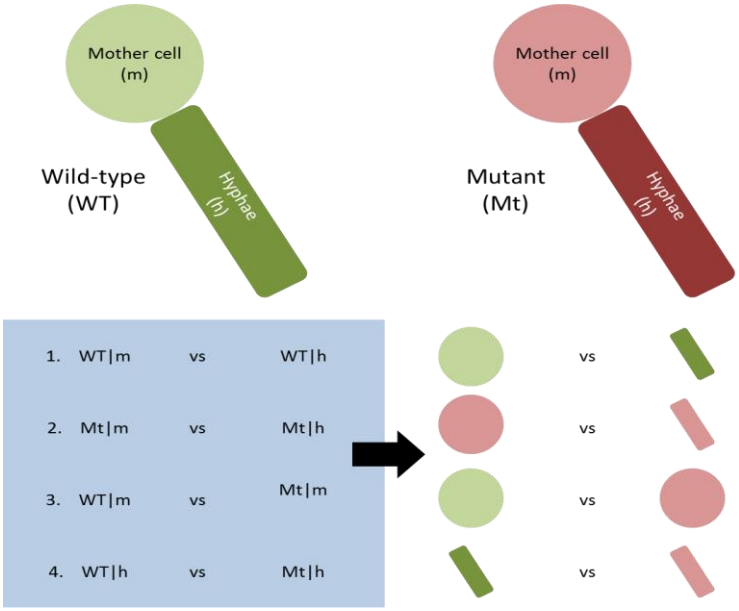

Figure 61: Top: Cell cartoon of a *C. albicans* cell; it consists of a spherical "mother-cell" and of a tip-shaped "*hyphae*"; green is for WT, while red is for mutant Bottom: Comparison table showing the 4 different sets of comparative analysis conducted for this project.

Here, it is important to note that when referring to an experiment's data, we mean the collected values of the relevant mechanical property from the experiment's map, using the user-selected RoI method, described in chapter 5.3.3.1.5. Also, it is important to note that for the case of "modulus comparison", we performed comparative analysis using the prevailing experiment's selected-region modulus values using modulus as calculated with the *Pharr-Bolshakov* model.

7.3.1. Comparison of modulus

7.3.1.1. Comparison of modulus between different cell areas

Here, we are looking for altered modulus for the four cases of the four comparisons, as described before, in Figure 61. We will compare the different populations of data by performing a statistical significance test and comparing the median values of the two groups of each comparison.

Initially, need to check into each single experiment's distribution of values in order to put confidence on our results. In the following figures we have the distributions for the different *hyphae* (Figure 62) and *mother cell* (Figure 63) experiments. We see that not all the distributions follow a normal-like distribution.

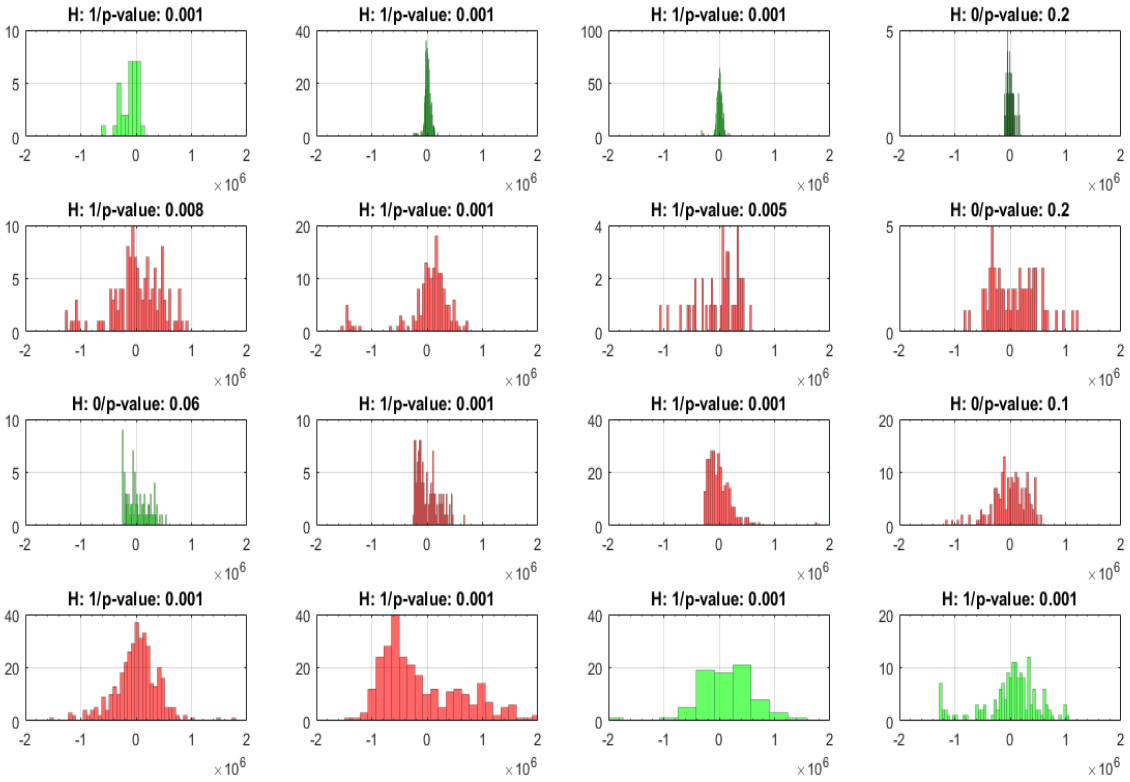

Figure 62: Distribution of modulus values (from RoI) for every experiment of *hyphae* of this work; as it seems, not all of the experiments have a normal distribution. In each title, we have the result for the null

hypothesis test for normality of the distribution (H:1 -> rejection, H:0 -> failure of rejection) together with the relevant p-value. The x-axis limits are [-2e+6 2e+6].

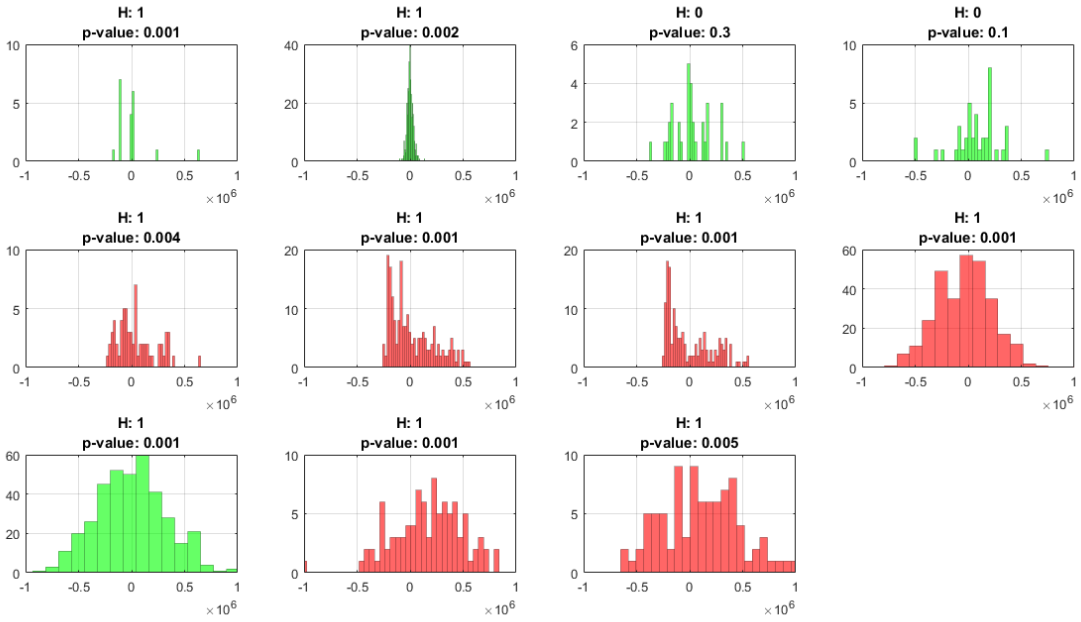

Figure 63: Distribution of modulus values (from RoI) for every experiment of *mother cell* of this work; as it seems, not all of the experiments have a normal distribution. In each title, we have the result for the null hypothesis test for normality of the distribution (H:1 -> rejection, H:0 -> failure of rejection) together with the relevant p-value. The x-axis limits are [-2e+6 2e+6].

In order to check this, we conducted a separate test (Matlab's *lillietest*, as described earlier in the methods chapter) for each one of the aforementioned distributions with the aim to statistically check if they can be represented by a normal distribution, and the result was not positive for all the experiments for a significance level of 0.05. For this reason, that we cannot assume normality for all the samples (there are also some outliers in the data that cannot be ignored), and since the sample size is relatively small (we compare modulus values from a specified RoI on top of the stomata and not all the values of the force map), the selection of hypothesis testing between the different groups of data (wild type and mutant) is the Matlab's *Wilcoxon ranksum test.*

Following, we will separate the analysis in the four comparison tests, in the following sub-sections:

***Note**: In the following sections we compare samples from different populations in the four aforementioned categories. There is the case of two experiments/samples, 69 & 70 (*Figure 58,Figure 62*) where in those two experiments we see two different cells, one on top of the other, which may possibly give "false values" and blur our comparison tests. Those two experiments are annotated with text and red dotted lines-defined in the following figures/tests wherever applied. We will not include them in our comparison analysis tests, but we will include them in the figures.*

7.3.1.1.1. Comparison between wild-type hyphae (WT | h) and wild-type mother cell (WT | m)

In order to compare modulus between *WT | h* and *WT | m* cells, we extracted the modulus value from the relevant experiments, and this resulted to the following boxplot chart:

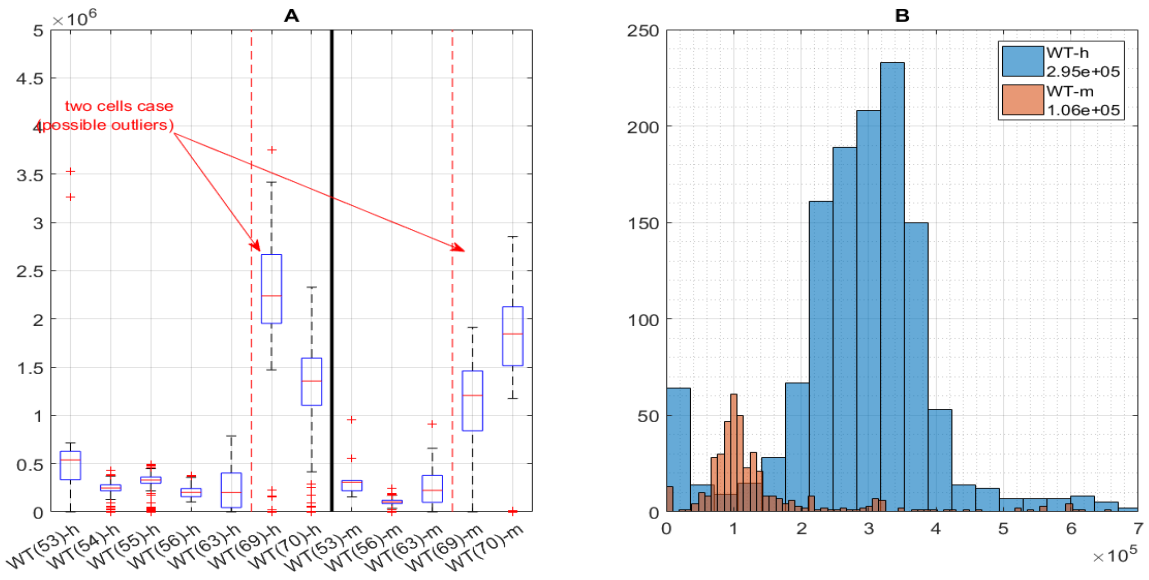

Figure 64: A: Modulus comparison between WT | *h* and WT | *m* with boxplots. The black line separates the plot into the two different areas. The red dotted lines indicate the two experiments (69 and 70), which we choose not to include in the comparison. B: Histogram of the two distributions in A.

In plot A, the plot consists of different boxplots (126) with each one representing statistically each experiment's modulus where in each boxplot the red line represents the median value of experiment's results, the vertical black line separates the two different compared sets of values in each case/sub-figure, the horizontal axis show the different sets of experiments to be compared upon, and the vertical axis is in Pa. The figure is divided in two separate areas by the black vertical line into *WT | h* and *WT | m* samples. As we can see, we have annotated the plot with the two cells/experiments (69 and 70 in Figure 58), where we do not include these in our comparison measurements since we have the case of two cells (one on top of each other and thus not reliable data).

In plot B, we have a histogram with the two distributions in comparison. If we perform a statistical significance test, we see that the hypothesis that they come from distribution with equal medians is rejected with a p-value< 0.001. The median values are:

$$median_{WT|h} = 2.95 \times 10^5 \ \& \ median_{WT|m} = 1.06 \times 10^5$$

7.3.1.1.2. Comparison between mutant hyphae (Mt | h) and mutant mother cell (Mt | m)

In the following figure, in A we have the comparison between *Mt | h* and *Mt | m*. In plot B, we have a histogram with the two distributions in comparison. If we perform a statistical significance test, we see that the hypothesis that they come from distribution with equal medians is rejected, but with a p-value of 0.012. The median values are:

$$median_{Mt|h} = 1.48 \times 10^6 \ \& \ median_{Mt|m} = 1.74 \times 10^6$$

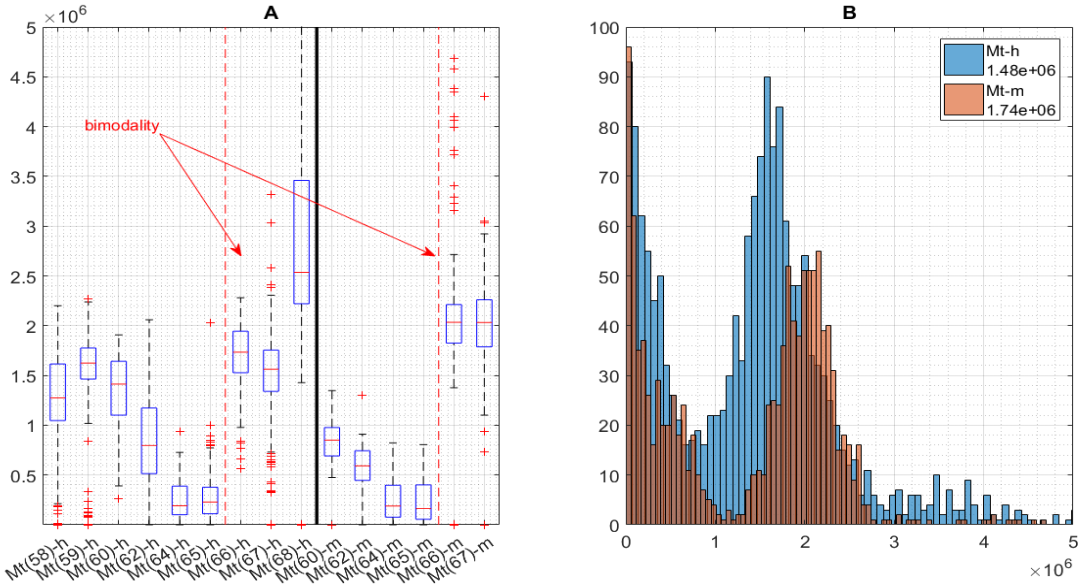

Figure 65: A; Modulus comparison between Mt | *h* and Mt | *m* with boxplots. The black line separates the plot into the two different areas. B: Histogram of the two distributions in A.

We can also observe a bimodality in both distributions, but we are not sure how to explain this finding.

7.3.1.1.3. Comparison between wild-type mother cell (WT | m) and mutant mother cell (Mt | m)

In the following plot, in A we have the comparison between $WT \mid m$ and $Mt \mid m$. We can observe that the experiments on the right of the black vertical line have a higher modulus than the relevant ones to the left. In plot B, we have a histogram with the two distributions in comparison. If we perform a statistical significance test, we see that the hypothesis that they come from distribution with equal medians is rejected, with a p-value< 0.001. The median values are:

$$median_{WT|m} = 1.06 \times 10^5 \;\&\; median_{Mt|m} = 1.74 \times 10^6$$

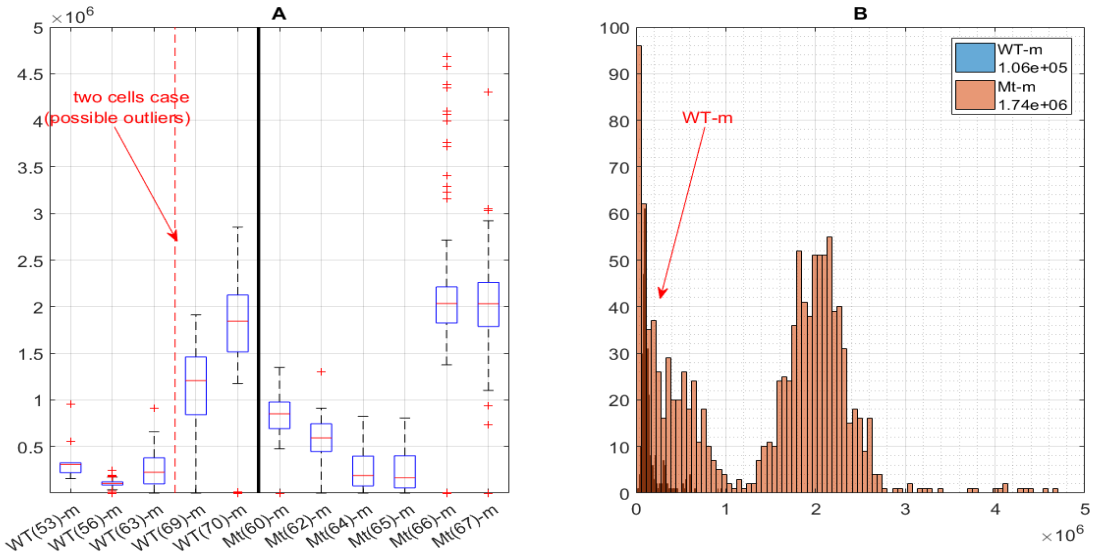

Figure 66: A: Modulus comparison between WT | *m* and Mt | *m* with boxplots. The black line separates the plot into the two different areas. The red dotted lines indicate the two experiments (69 and 70), which we choose not to include in the comparison. B: Histogram of the two distributions in A.

We see that modulus values in mutant are significantly higher, and this is an important finding that we will discuss later, after the comparison of *hyphae* between wild type and mutant cells.

7.3.1.1.4. Comparison between wild-type hyphae (WT | h) and mutant hyphae (Mt | h)

In the following plot, in A we have the comparison between $WT \mid h$ and $Mt \mid h$. Again, we can observe that the experiments on the right of the black vertical line have a higher modulus than the relevant ones to the left. In plot B, we have a histogram with the two distributions in comparison. If we perform a statistical significance test, we see that the hypothesis that they come from distribution with equal medians is rejected, with a p-value< 0.001. The median values are:

$$median_{WT|h} = 2.95 \times 10^5 \ \& \ median_{Mt|h} = 1.40 \times 10^6$$

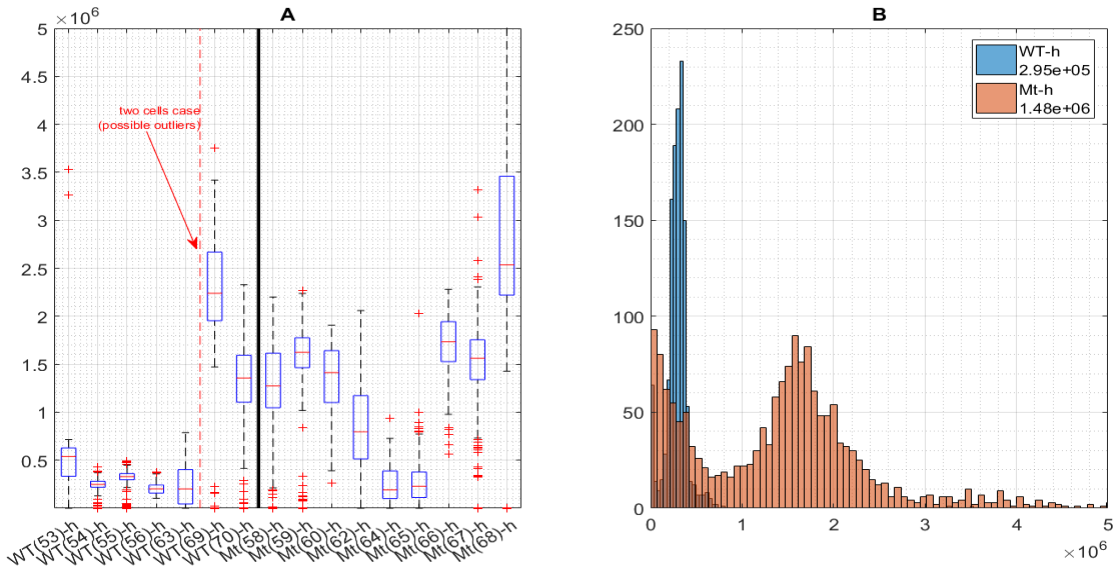

Figure 67: A: Modulus comparison between WT | *h* and Mt | *h* with boxplots. The black line separates the plot into the two different areas. The red dotted lines indicate the two experiments (69 and 70), which we choose not to include in the comparison. B: Histogram of the two distributions in A.

As we can see there is a big difference between the wild type and the mutant, both for the case of *mother cell* (previous comparison) and for the case of the *hyphae*. In the next section, we will collect all the experiments in a single analysis.

7.3.1.2. Comparison of modulus between Wild-type and mutants

Here, we compare modulus between wild-type and mutant cells overall, whether it is a *mother cell* or a *hyphae*. In order to compare modulus between wild-type and mutant cells, we extracted the values from all 16 experiments (9 mutant and 7 wild-type), and this resulted into the following collective chart, where in A we have all the boxplots of all the experiments, and in B we have the two histograms for the two distributions (wild type and mutant). We performed a statistical significance test, and the hypothesis that they come from distribution with equal medians is rejected, with a p-value of< 0.001. The median values are:

$$median_{WT} = 2.70 \times 10^5 \;\&\; median_{Mt} = 1.56 \times 10^6$$

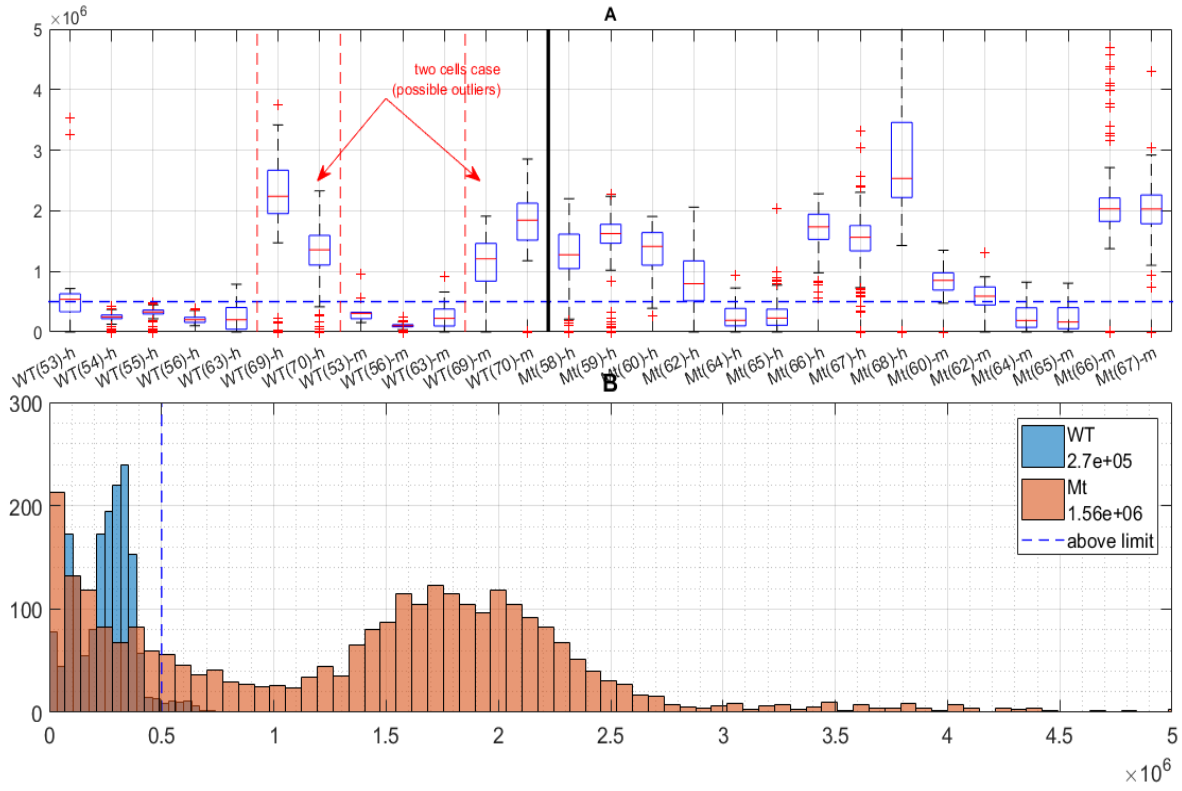

Figure 68: A: Modulus comparison between WT and Mt with boxplots. The black line separates the plot into the two different areas. The red dotted lines indicate the two experiments (69 and 70), which we choose not to include in the comparison. B: Histogram of the two distributions in A. The blue-dotted line in A is the same with the one in B.

We can see that modulus in mutant cells is higher than the wild type cells, even though the mutant distribution seems to be bimodal (due to experiments Mt (64) and Mt (65)), and this translates into the following plot where we present the mean of the means of the experiments, as grouped by cell type, excluding the data from the wild type double cells (indicated with the red arrows and the red-dotted vertical lines in the previous figure).

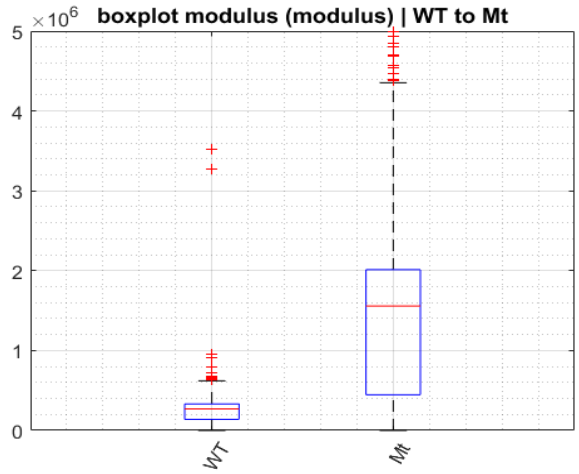

Figure 69: Boxplots representing the wild type and mutant populations for modulus. Mutant experiments have a higher median value. The vertical axis is in Pa and shows the modulus value.

7.3.2. Comparison of adhesion

Here, we are looking for differences in adhesion for the four cases of the four comparisons, as described before. We will compare the different populations of data by comparing the mean of adhesion value of the different experiments between the two groups of each comparison.

In order to do that, we firstly need to check into each single experiment's distribution of values in order to put confidence on our results, and for that, we conducted a separate test (Matlab's *lillietest*, as described earlier in the methods chapter) for each one of the aforementioned distributions with the aim to show that they can be represented by a normal distribution, and the result was positive for all the experiments.

In the following figures (Figure 70,Figure 71) we see that not all the distributions follow a normal-like distribution. For this reason, that we cannot assume normality for all the samples (there are also some outliers in the data that cannot be ignored), and since the sample size is relatively small (we compare modulus values from a specified RoI on top of the stomata and not all the values of the force map), the selection of hypothesis testing between the different groups of data (wild type and mutant) is the Matlab's *Wilcoxon ranksum test.*

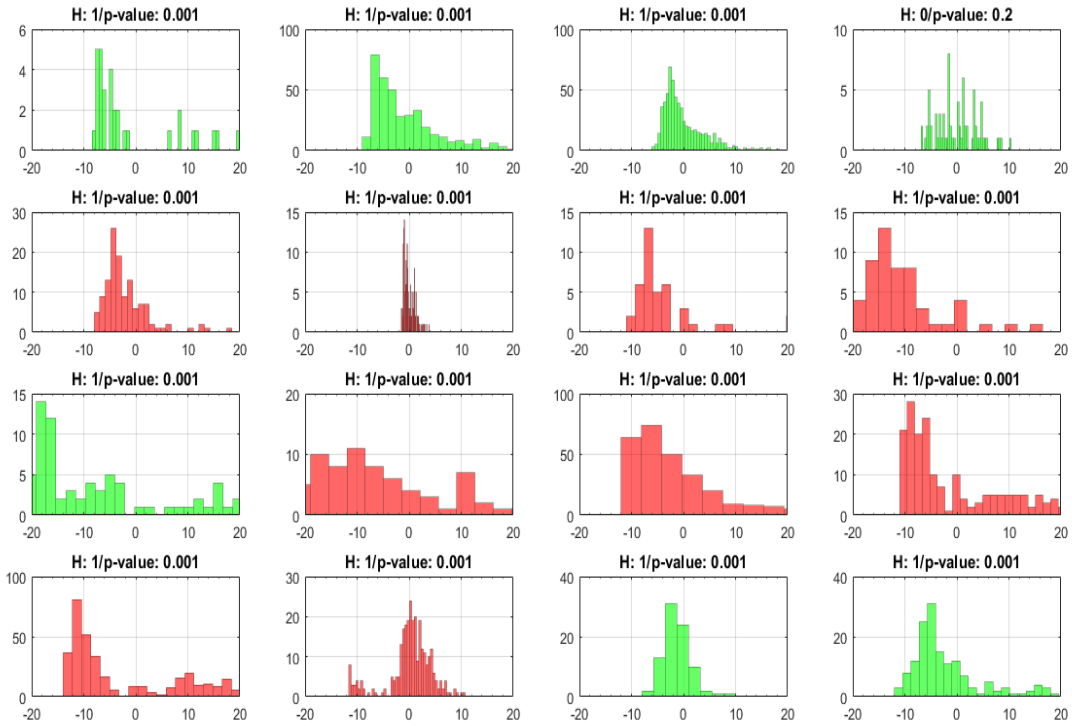

Figure 70: Distribution of adhesion values (for RoI) for every *mother cell* experiment of this work; as it seems, not all of the experiments have a normal distribution. In each title, we have the result for the null hypothesis test for normality of the distribution (H:1 -> rejection, H:0 -> failure of rejection). The x-axis limits are [-20 20].

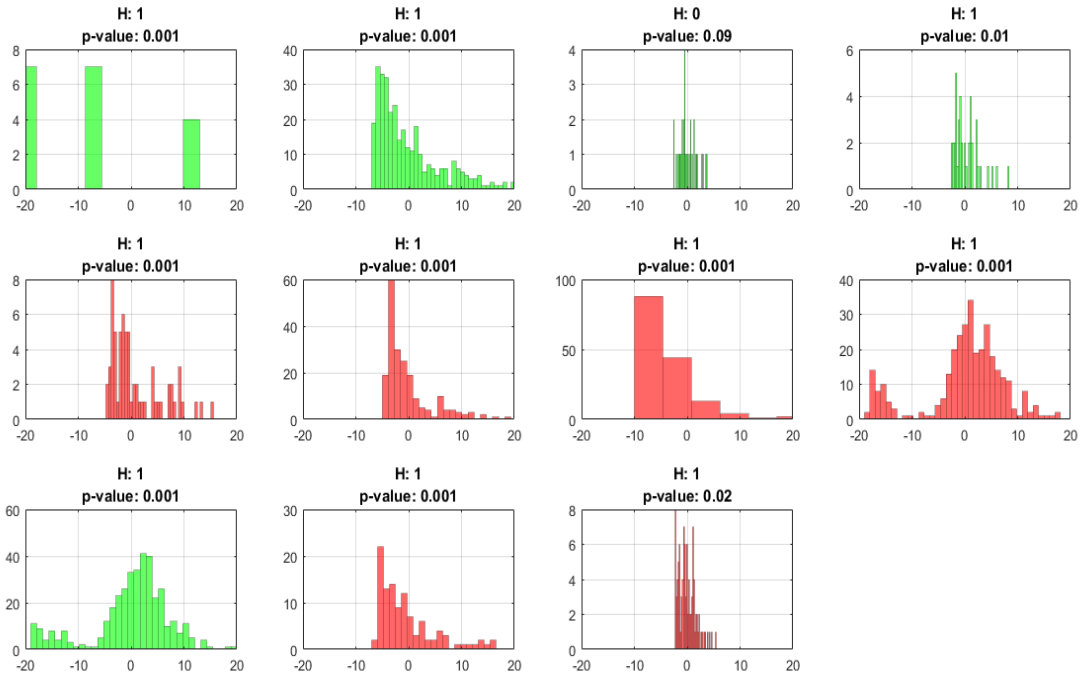

Figure 71: Distribution of adhesion values (for RoI) for every *hyphae* experiment of this work; as it seems, not all of the experiments have a normal distribution. In each title, we have the result for the null hypothesis test for normality of the distribution (H:1 -> rejection, H:0 -> failure of rejection). The x-axis limits are [-20 20].

Following, we will separate the analysis in the four comparison tests (as described before):

7.3.2.1. Comparison between wild-type hyphae (WT | h) and wild-type mother cell (WT | m)

In the following plot, in A we have the adhesion comparison between $WT \mid h$ and $WT \mid m$. If we perform a statistical significance test, we see that the hypothesis that they come from distribution with equal medians is rejected, with a p-value< 0.001. The median values are:

$$median_{WT|h} = 5.97 \;\&\; median_{WT|m} = 3.86$$

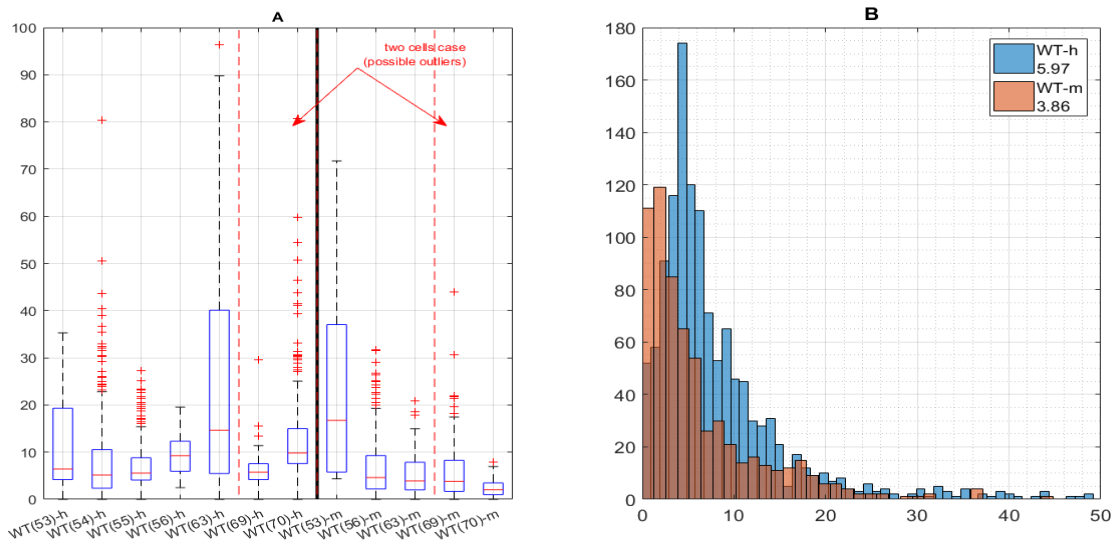

Figure 72: A: Adhesion comparison between WT | *h* and WT | *m*. The blue line separates wild type *mother cell* and wild type *hyphae* experiments. B: Histogram of the two distributions in A.

We can see that the *hyphae* in wild type *C. albicans* has a higher adhesion than the *mother cell.*

7.3.2.2. Comparison between mutant mother cell (Mt | m) and mutant hyphae (Mt | h)

In the following plot, in A we have the adhesion comparison between *Mt* | *m* and *Mt* | *h*. In plot B, we have a histogram with the two distributions in comparison. If we perform a statistical significance test, we see that the hypothesis that they come from distribution with equal medians is rejected, but with a p-value< 0.001. The median values are:

$$median_{MT|h} = 8.69 \;\&\; median_{Mt|m} = 15.4$$

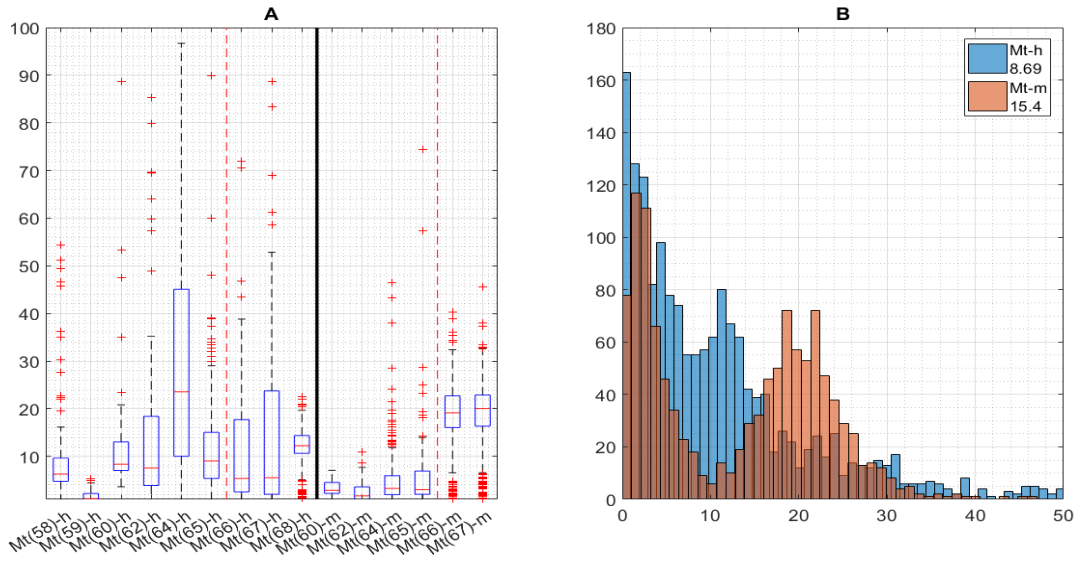

Figure 73: A: Adhesion comparison between Mt | *h* and Mt | *m*. The blue line separates mutant *hyphae* and mutant *mother cell* experiments. B: Histogram of the two distributions in A.

We can see that the *hyphae* in mutant *C. albicans* has a lower adhesion than the *mother cell*.

7.3.2.3. Comparison between wild-type mother cell (WT | m) and mutant mother cell (Mt | m)

In the following plot we have the comparison between *WT* | *m* and *Mt* | *m*. In plot B, we have a histogram with the two distributions in comparison. If we perform a statistical significance test, we see that the hypothesis that they come from distribution with equal medians is rejected, but with a p-value< 0.001. The median values are:

$$median_{WT|m} = 4.64 \;\&\; median_{Mt|m} = 15.4$$

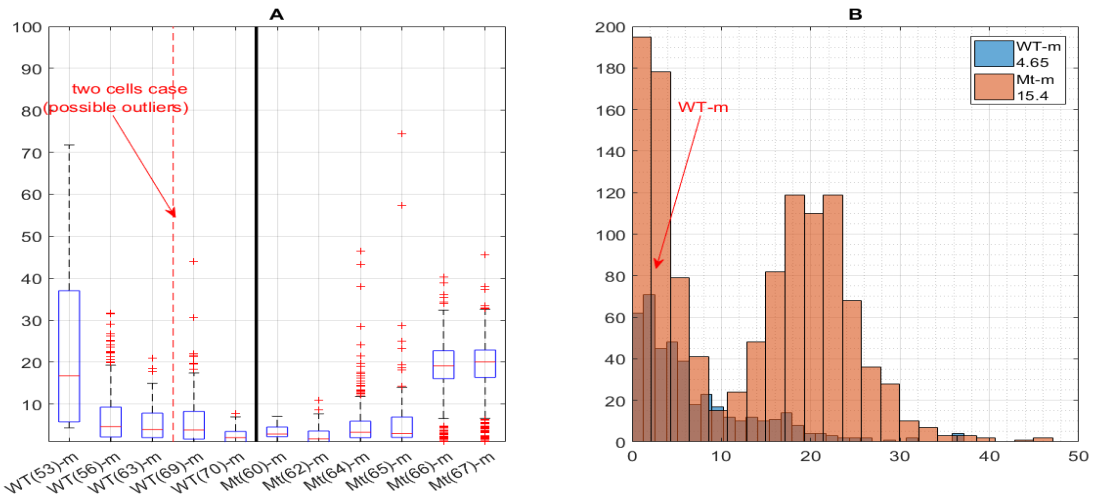

Figure 74: A: Adhesion comparison between WT | *m* and Mt | *m*. The blue line separates wild type *mother cell* and mutant *mother cell* experiments. B: Histogram of the two distributions in A.

We can see that the mutant in *mother cell C. albicans* has a higher adhesion than the *mother cell.*

7.3.2.4. Comparison between wild-type hyphae (WT | h) and mutant hyphae (Mt | h)

In the following plot we have the comparison between *WT* | *h* and *Mt* | *h*. In plot B, we have a histogram with the two distributions in comparison. If we perform a statistical significance test, we see that the hypothesis that they come from distribution with equal medians is rejected, but with a p-value< 0.001. The median values are:

$$median_{WT|h} = 5.97 \;\&\; median_{Mt|h} = 8.69$$

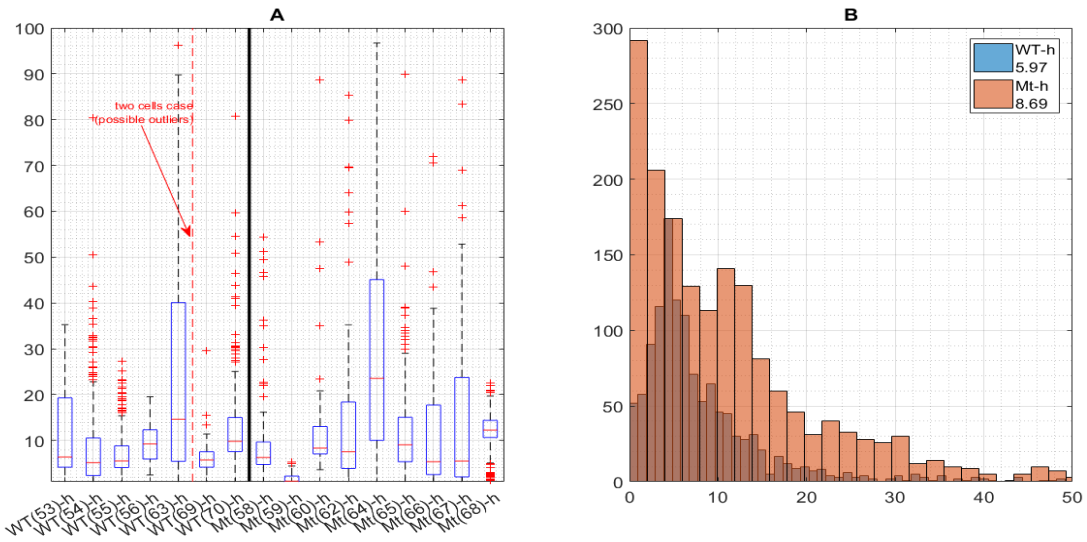

Figure 75: A: Adhesion comparison between WT | *h* and Mt | *h*. The blue line separates wild type *hyphae* and mutant *hyphae* experiments. B: Histogram of the two distributions in A.

We can see that the mutant in *hyphae C. albicans* has a higher adhesion than the *mother cell*.

7.3.2.5. Comparison between Wild-type (WT) and mutant (Mt) cells

Here, we compare adhesion between wild-type and mutant cells overall, whether it is a *mother cell* or a *hyphae*. In order to compare modulus between wild-type and mutant cells, we extracted the values from all 16 experiments (9 mutant and 7 wild-type), and this resulted into the following collective chart, where in A we have all the boxplots of all the experiments, and in B we have the two histograms for the two distributions (wild type and mutant). We performed a statistical significance test, and the hypothesis that they come from distribution with equal medians is rejected, with a p-value of < 0.001. The median values are:

$$median_{WT} = 5.69 \;\&\; median_{Mt} = 10.1$$

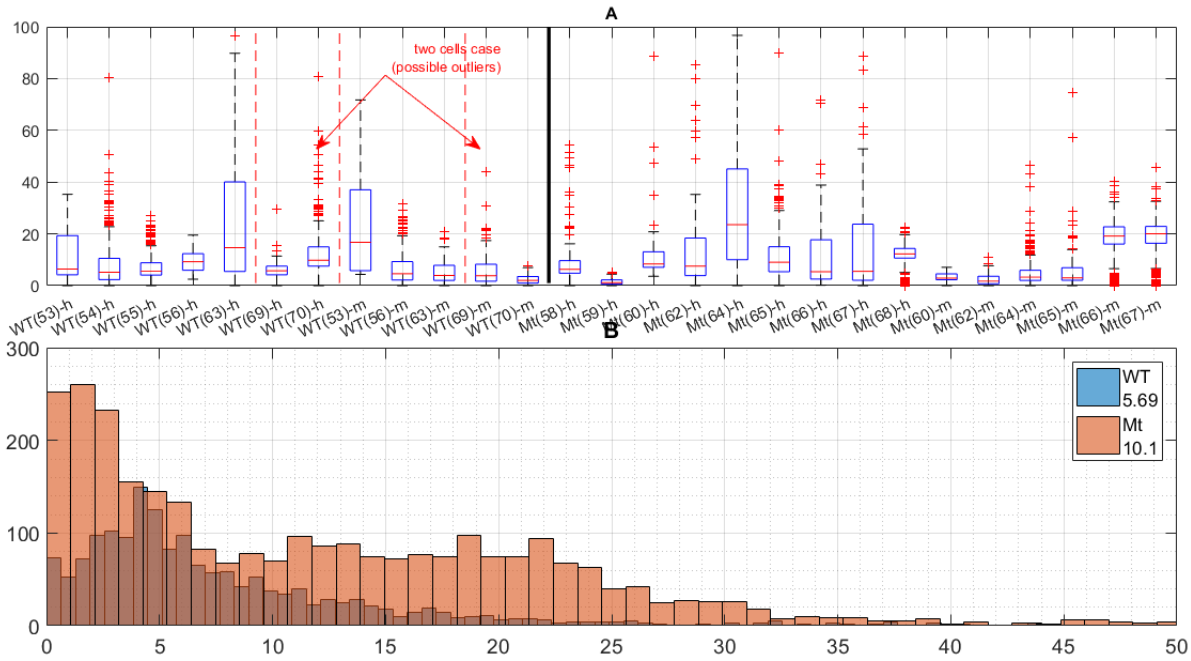

Figure 76: A: Adhesion comparison between wild type (WT) and mutant (Mt) cells. The blue line separates wild type and mutant experiments. B: Histogram of the two distributions in A.

7.4. Conclusions

The role of *C. albicans*' cell wall is to both structurally maintain the integrity of the cell via the load-bearing network of biopolymers which it consists of, and to provide an interface with the cell's environment for the exchange of important cargo (127). At the same time, we elaborated previously on the connection of the organization of the cell wall to the cell's pathogenicity in *C. albicans* (125) (72). The role of mechanics and composition in the cell's biological function and growth is the one put under examination in this project, and the findings are interesting since they manage to infer a clear relationship between cell wall composition and elasticity of the wall, while it is apparent from the AFM images the initial expectation for cell growth (shorter and wider mutant cells, compared to the wild-type ones).

Initially, we demonstrated the implementation of our technique into three individual *Candida albicans* experiment with the aim to both calculate the modulus values and the *beta* modulus

value according to the specialized curve fitting analysis routine, and secondly to show how we can analyze each experiment in order to get more mechanical insight in the data.

We showed that with our technique the cell's modulus exhibited variation across its surface (higher E in the middle of the cell), compared to the *Hertz* modulus calculation output ('flatter' modulus map). We did a profile analysis to show this finding in more detail, and also to show how this coincides to the cell's topography. Also, we demonstrated the relation of cell's morphology to its mechanical properties (higher adhesion and hysteresis at the edges of the cell), and we presented the reasoning behind our analysis method (lower RMSE | *beta* values due to specialized fitting) for the calculation of modulus. Finally, we showed through the 'tomography' analysis of features like modulus, *beta* values, and RMSE values that there is a -possible- contact differentiation taking place at ~50 nm from the free surface of the cell wall, and this can affect modulus measurements. One other reason for this finding is that, since the cell wall has an approximate thickness of 100 to 150 nm (128) (129) (130), and considering as well that one of the assumptions behind the use of Hertz-like contact mechanics models is the "half-space" assumption of the surface under investigation, the indentation depth was approaching the theoretical limit for modulus calculation of the underlying surface.

Later, we proceeded to the comparison of modulus and adhesion ratio between the two different groups of wild type and mutant cells, and between the two different parts of the same *C. albicans* cell, the *hyphae* and the *mother cell.* At the beginning of the chapter, when introducing the *C. albicans* cells and the specific mutants, we speculated on the altered mechanics and on what can this reveal for the cell's biological function.

Here, we did a normality check on the individual samples and we conducted statistical significance tests in order to place confidence in the comparison results. We did a hypothesis testing that the two groups of data (wild type and mutant) come from different distributions

with unequal medians and we got values of $p < 0.001$. We observed higher modulus values in the mutant experiments versus the wild type ones overall:

$$median_{WT} = 0.27 \times 10^6 \ \& \ median_{Mt} = 1.56 \times 10^6$$

This is an important finding, and it was initially expected for the mutants to have altered mechanics due to different cell wall composition and structure. This higher modulus in mutants is linked to the additional chitin substance in the cell wall matrix. Maybe a higher modulus could explain some changes in growth and morphology of the cell. And as for the differences between the different parts of the cell, in wild type, modulus in *hyphae* is higher whereas in mutant, modulus in *mother cell* is higher.

Finally, we compared the adhesion results between the different populations, we performed statistical analysis as well, and we found that the mutant cells have a higher adhesion overall:

$$median_{WT} = 5.69 \ \& \ median_{Mt} = 10.1$$

We are not in the position to reason on this finding since we do not know the full nature of the surface and the surface energy of the outer part of the cell wall.

Chapter 8: Conclusions & future work

8.1. Conclusion

8.1.1. Developed analysis technique

Specialized analysis of force-indentation curves from the surface of cells allowed us to observe local variation in the mechanical properties over the wall surface and helped us understand better the cell's biological function. It helped us distinguish the mechanical behavioral patterns of stomatal cells between different types of cell and between different parts of the same stomata cell. It also helped us investigate the altered mechanics between the wild type and mutant cells.

At the same time, the abundance of collected/processed data, and the belief that not a single model is able to characterize a whole force map, motivated us to examine further the indenter-surface mechanical interaction, and led us to some interesting findings.

8.1.1.1. Mapping of the fitting residuals

We mapped for the first time the fitting residuals of all the force curves of the same force map in a heat map manner. What we observed was that the variation in the fitting *RMSE | p* (fitting residuals under a power law of 1.5, as for the *Hertz* model) and *RMSE | c* (fitting residuals under a power law of 2, as for the *Sneddon* model) values correlated to the variation in topography, and thus, a specialized analysis was needed. Following this, we extracted the "optimal" fitting parameter *beta* from every curve of the map, and we mapped the fitting *RMSE | beta* (fitting residuals under the prevailing optimal power law *beta* of each curve)**.** What we found was that the topography effect had now almost vanished (Figure 30, Figure 54, Figure 55), indicating that the approached of specializing curve fitting in topographical cell surfaces is the optimal way of nano-indentation mechanical characterization.

Secondly, in order to test this in more detail, we designed a series of experiments where we would compare the variation in modulus values between a stomata cell (with high topography and variation in modulus values) and a replica of the stomata cell surface (with -still- high topography but no variation in modulus values, since the replica material was homogeneous). What we found from those experiments was not very helpful towards our assumption for the cancellation of the topography effect on the cell mechanics. Although the lower standard deviation and mean of modulus of the imprint experiments (compared to the stomata experiments) was a good indicator of our expectation, we found was that the coefficient of variation of the imprint experiments was similar to the stomata experiments.

$$stomata: CV_{stom} = 0.93 \quad imprint: CV_{impr} = 0.97$$

Because the standard deviation may had been lower, but 'relatively' lower. And this is a sign of similar behavior, just shifted in a lower range.

8.1.1.2. Specialized modulus calculation

Following the observation for the mapping of the fitting residuals, we observed a variation- inside the same force map- in the fitting constant *beta* values (varying between 1.1 and 2), for the different force curves of the map. This observation triggered a review in the literature of contact mechanics, and subsequently an examination the relations between the different models.

Subsequently, we applied different mathematical equations-according to the specialized fitting- for the calculation of elastic modulus, in the same force map, presenting a novel approach on the calculation of Young's modulus via AFM force map experiments. We did so, by combining the experimentally acquired curve fitting parameters *alpha* and *beta* from equation$P = a * h^{\beta}$, with a new approach for simulating the indenter's tip profile with a polynomial function, and

with equation $P = \frac{2E_{eff}}{\sqrt{\pi}c^{1/n}} * \left(\frac{n}{n+1}\right) \times \left[\frac{\Gamma\left(\frac{n}{2}+\frac{1}{2}\right)}{\Gamma\left(\frac{n}{2}+1\right)}\right]^{1/n} * D^{1+1/n}$ of *Pharr* and *Bolshakov* based on *Sneddon*'s work.

The developed automated indentation analysis technique generated for this work helped us understand in a good level the nature of nano-indentation, mechanically interpret our experimental results, and hopefully, can stand as a model analysis for future relevant work in the field.

8.1.2. Stomata experiments

Initially, we demonstrated the implementation of our novel technique into a single AFM force mapping stomata experiment with the aim to both calculate the modulus value according to the specialized curve fitting analysis routine, and secondly to show how we can analyze each experiment in order to get more mechanical insight in the data.

We showed that with our technique the cell's modulus (*Pharr-Bolshakov* model) exhibited variation across the surface of its cell wall (especially in the highest points of the surface, mid-wall), compared to *Hertz*. We did a profile analysis to show this finding in more detail, and we found an interesting profile across the middle of the cell wall, compared to the relevant *Hertz* profile analysis. Also, we demonstrated the relation of the cell's morphology to other mechanical properties (higher curve hysteresis at the edges of the cell and the surrounding pavement cells), and we presented the reasoning behind our analysis method (lower RMSE | *beta* values due to specialized fitting) for the calculation of modulus.

Finally, we showed through the 'tomography' analysis of features like modulus, *beta* values, and RMSE fitting values that there is a *beta* (power law exponent) decrease overall in the cell, and thus a lower indentation depth was preferred for the analysis of the curves.

Then, we conducted comparison tests between the different groups in modulus and adhesion data. At the beginning of the chapter, when introducing the *stomata* cells and the *pme6* mutants, we speculated on the altered mechanics and on what can this reveal for the cell's biological function. We performed normality checks (Matlab's *lillietest*) on the individual samples, and we did statistical significance analysis tests (Matlab's *Wilcoxon ranksum test*[47]) in order to compare the values that we acquired from the separate experiments, and we observed higher modulus values in the mutant experiments versus the wild type ones:

$$median_{WT} = 0.99 \times 10^7 \ \& \ median_{WT} = 1.79 \times 10^7.$$

This is an important finding since it shows a clear link between the cell wall composition and the mechanics (elasticity) of the wall, as obtained from AFM experimentation. The mutation taking place in the *pme6* mutant causes an excess of pectin concentration in the cell wall matrix, thus enhancing the wall biopolymer matrix, possibly resulting in stiffer cell wall as shown here. This finding is also important both for an enhanced understanding of the stomatal biological function, and for the control and regulation of it for optimal growth under stress conditions.

Looking more into the results, we observed a bimodality in the histogram of the two populations of data, and we split each one in two categories, depending on the buffer used for experimentation.

$$median_{WT_M} = 0.81 \times 10^7 \ [Pa]^{48} \& \ median_{WT_{n-M}} = 1.10 \times 10^7 \ [Pa]$$

$$median_{Mt_M} = 1.20 \times 10^7 \ [Pa] \& \ median_{Mt_{n-M}} = 3.40 \times 10^7 \ [Pa]$$

[47] This test was chosen due to the non-normality of all the distributions, observed through the normality check.
[48] WT: wild-type, Mt: mutant, M: use of Mannitol, n-M: not use of Mannitol

If we break the two groups and analyze their distribution, we see that whenever we used *Mannitol* as a liquid buffer, modulus values between the two groups were similar, but in the absence of it, differences arose. We did a hypothesis testing that the two groups of data (wild type and mutant) come from different distributions with unequal medians and we got values of $p < 0.001$ for both the cases of *Mannitol* and no-*Mannitol.* The reason for the difference in the modulus values is believed to be due to cell wall compositional differences.

Following, the reason behind the different values in wild type with the use of a different cantilever may be because the tip-sample contact area in *Mannitol* treated cells is different compared to the one with no use of *Mannitol*, and this can only be seen through our method where it takes in account the elaborate fitting of the curve for the calculation of modulus, and as such, the calculation is expected to vary under different contact.

Another thing to note is that when the indentation is higher (technically, we analyze a bigger part of the FI curve), in the case of mutant samples with no use of Mannitol, the modulus as calculated by the 'Pharr-Bolshakov' model is smaller. This is a finding which would not otherwise be visible, but with our technique we were able to observe. The fact that it is not observable with the use of Mannitol makes it even clearer that the optimal experimental conditions to investigate the mechanics of the wall are with no removal of the cell's turgor pressure.

As for the adhesion results between the different populations, we performed statistical analysis tests as well, but we did not observe clear differences between the two different populations of data (wild-type and mutant).

Finally, we conducted some experiments with a replica of the cell's surface in order to check the effect of the surface's topography in our results and whether our method accounted for it, but it was difficult to find a straightforward answer to this. This is because, we observed that

by comparing the two different groups' data, the distributions' standard deviation on the imprint experiments was significant lower, but the 'relative standard deviation' was similar for both stomata and imprint experiments: $CV_{stom} = 0.93$ & $CV_{impr} = 0.97$.

8.1.3. *C. Albicans* experiments

We demonstrated the implementation of our technique into three individual *Candida. Albicans* experiment. We showed that with our technique the cell's modulus exhibited variation across its surface (higher modulus in the middle of the cell), compared to the *Hertz* modulus calculation output ('flatter' modulus map). We did a profile analysis to present this finding in more detail, and also to show how this coincides to the cell's high topography. Also, we demonstrated the relation of cell's morphology to its mechanical properties (higher adhesion and hysteresis at the edges of the cell), and we presented the reasoning behind our analysis method (lower RMSE | *beta* values due to specialized fitting) for the calculation of modulus. Finally, we showed through the 'tomography' analysis of features like modulus, *beta* values, and RMSE values that there is a -possible- contact differentiation taking place at ~50 nm from the free surface of the cell wall, and this can affect modulus measurements.

Later, we proceeded to the comparison of modulus and adhesion ratio between the two different groups of wild type and mutant cells, and between the two different parts of the same *C. albicans* cell, the *hyphae* and the *mother cell.* To do that, we did a normality check on the individual samples and we conducted statistical significance tests between the groups of samples in order to place confidence in the comparison results. We did a hypothesis testing that the two groups of data (wild type and mutant) come from different distributions with unequal medians and we got values of $p < 0.001$. We observed higher modulus values in the mutant experiments versus the wild type ones overall:

$$median_{WT} = 0.27 \times 10^6 \;\&\; median_{Mt} = 1.56 \times 10^6$$

And as for the differences between the different parts of the cell, in wild type, modulus in *hyphae* is higher whereas in mutant, modulus in *mother cell* is higher. This is an important finding, since it was expected for the mutants to have altered mechanics due to different cell wall composition (induced by the absence of AP-2 in the mutant which is responsible for the increase of Chs3 in the cell wall). Maybe a higher modulus could explain some changes in growth and morphology of the cell. Finally, we compared the adhesion results between the different populations, we performed statistical analysis as well, and we found that the mutant cells have a higher adhesion overall:

$$median_{WT} = 5.69 \;\&\; median_{Mt} = 10.1$$

8.2. Further improvements & developments

The areas which may need improvement can be divided in five clear groups: 1. Sample preparation, 2. Experiment design, 3. Data analysis, 4. Altered mechanics analysis, and 5. Biological data interpretation.

8.2.1. Sample preparation and mounting optimization

Since the beginning of this project, one of the goals was to establish a protocol for the preparation of the sample, the right choice of buffers and the correct mounting of it inside the petri dish. As of the first, the procedure followed didn't need improve, but as new findings may be of interest in the future, new ways of sample preparation may be preferred (e.g. different choice of control environment for the cultivation of plants, different strain selection for investigation of their relevant properties, etc.). As of the buffer selection, this plays a centre role in the experimentation, thus in the future it may be decided that there is needed a different one for the sample to be immersed into -higher PH, or a more acidic environment for the plant cell, different concentration of MES since its effect on plant's physiology is not totally clear-

and also a different immersion technique in conjunction with the selection of the petri dish. Speaking of the latter, there was not enough time (and resources) in this project to check all the alternative options to the standard petri dish for the mounting of the sample. The choice of green glue and the 8mm petri dish worked good in our case, but there are other useful resources to work with, like the "closed fluid cell" offered by the Asylum's MFP3D kit. This can offer a controlled and sealed environment during the scanning of the sample, with the control of gases and liquids and the subsequent control of temperature.

8.2.2. Experiment design optimization

The combination of a dynamic sample, such as a living cell, and the many options for parameterization offered by most of the commercially available AFMs, make it very difficult for the scientist on the field to check all the options when it comes to designing an experiment. Initially, the cantilever choice is the most important of all, it is chosen by the type of experiment, it is considered in the calculation of modulus -by defining the contact area between the indenter and the sample's surface-, and most importantly one needs to choose the optimal shape and material characteristics for the prevailing experiment. In the case of this project, different cantilevers were tested. Optimally, a spherical indenter of around 0.1 to 3 N/m is suitable for this experiment, but other types may be preferred as well.

Later, as discussed in the previous section, there are commercially available resources for the establishment of a controlled temperature environment during scanning. This plays an important role in the investigation of dynamic properties of biological samples, and during this project it was not possible to take this parameter into account. But in the future, it is a significant leap towards the understanding of the material's properties.

Continuing, the MFP3D-BIO was the instrument for all the experiments conducted in this PhD project. It is very good for nano-mechanical analysis, but there are other ones as well that work

well with nano-indentation data, like the JPK's QI mode, or Bruker's PeakForce mode for nano-mechanical characterization of cells.

The scanning map resolution is also important, and it depends on the size of the RoI. It is crucial to know what surface resolution one needs for the investigation of the mechanics, in order to choose area size and subsequently resolution to be divided by the area. In our case, the stomatal cell is relatively big in size, thus the size area should be around 15 μm. So, a scan map of 64-by-64 points offers resolution of around 235 nm, whereas a scan map of 128-by-128 offers resolution of around 120 nm. The same resolution limits for the case of *candida* cells experiments, with size areas of around 5 μm are respectively 78 and 39 nm. It is obvious that the smaller the area, the better the resolution of the mechanics, but that relies mostly on the cell topography. Finally, it is good to know that since the scanning of the area is a 2-D grid, as the resolution increases, the time of the experiment increases geometrically, and so does the analysis time.

There is also a difficulty when scanning relatively large regions in AFM force mapping experiments, and this is called surface heterogeneity. Commonly, a cell has relatively big differences in height from area to area, and that makes it difficult for dissimilar areas to be investigated simultaneously at the same experiment. When the tip of the AFM scans the surface, and when it performs an indentation at different surface points which have big relative height difference, the tip must abruptly adjust its height position and this abrupt adjustment will either result in 'bad' data, "out of range" warnings, or no data at all. There are commercially available high z-range scanners to be attached on the instruments, but it is not always preferred. In this work, the "out of range" problem came up many times, and the way to face this was either with the use of specialized buffers to reduce cell turgor pressure (and

subsequently surface height), or with the selection of smaller areas onto the cell, avoiding cell edges (in the case of candida cells) that would fail the indentation.

Finally, experimental parameters like tip z-velocity, scan rate, indentation total points affect the quality of the experiment and need to be adjusted every time to facilitate the acquisition of "good" data. Tip velocity in biological adhesive samples needs to be set relatively higher than non-adhesive materials, but not too high as it will damage and blunt the tip. Scan rate needs to be set not too high, as it will affect the surface of soft materials, and finally there need to be collected a lot of data points -since in some extreme cases not enough data are collected and a contact mechanics model cannot be applied to fit the indentation data- but not too much since it will increase significantly the analysis time.

8.2.3. Data analysis

Research software like this can commonly break down in three clear parts: import data, analyze data, and present data. As for the first, this technique can automatically read and extract most of the information from an .ARDF file (Asylum's format for storing force maps, i.e. collections of FD curves), and all the information from the file coming out of the relevant force map file from the JPK Nano wizard instrument. One improvement would be the integration of all the commercially available commercial formats to the technique, so it makes it easier for the user to run the analysis of an experiment with minimum effort. Regarding data analysis, there are things to add, starting from the non-elastic, adhesive analysis part, which this project didn't include much. Although the algorithm can analyze the retract part of the FD curve easily, it has not been used extensively, and thus, there is room for supplementary analysis. Moreover, the optimization algorithm used for the fitting of the curves is based on Matlab's implementation of the *Nelder-Mead* (119) simplex algorithm, which possibly could be changed to another one for faster analysis (depending on the parameters). Finally, the cp calculation will always be a

problem on its own, since it is more of a problem of definition, especially in the case of soft biological material. Finally, the presentation of data conveys a similarly crucial role, as it must deliver the output of the analysis. There are many ways to do this, depending on the scientific audience (important for interdisciplinary research), the standard plots commonly used in similar research, etc. The technique delivers the results in a manner considered optimal by the authors, but still the output data can be extracted and manipulated in a different way, with different plots, in a different programming language (e.g. Python or even Excel).

8.2.4. Altered mechanics analysis

Furthermore, with the options that the developed technique is providing us with, there are a series of analytics that can be conducted in order to understand different aspects of the sample's mechanics. Here, in the result chapters, are presented statistical measurements between different mutants, between stomatal cell walls and their imprint, etc. Modulus maps, adhesion maps and power-law (*beta*) maps are presented together with some histograms and statistical quantities to complement the analysis with comparable numbers. In the future, other maps resulting from the analysis technique can be used for the mechanical analysis, like hysteresis maps, "yield-point" maps, and, other analyses can be implemented to present the altered mechanics via the help of the analysis set of metadata.

Finally, we can make a comment on the way our technique collects mechanical data from the different experiment maps in order to make the relevant comparisons between different cell populations. The RoI on top of the cell is designed manually and chosen visually from the experimenter, according to his expertise. In order to validate -statistically- this approach of collecting data for group comparative analysis, we performed a statistical test on each sample with the aim to prove the normality of each sample's distribution (so we can use its sample statistics to perform comparative analysis). We think that there are more rigorous ways of

selecting RoI's for this purpose, but their implementation could not fit the time limit of this work. One of them is to let the algorithm select -inside the limits of a specified region- all these map points for which the degree of curvature wouldn't exceed a threshold value (since we have as well data on the surface topography of the scanned surface and thus we can calculate surface normal vectors), and discard the rest. Another one would be to perform -instantly, during RoI selection- a normality test on the selected data, and discard outliers.

8.2.5. Biological interpretation optimization

The actual interpretation of biological data, in general, and of mechanical nature, especially, is by definition a very challenging task. One must hold simultaneously many weapons in his arsenal. These include a very clear image of the research objective, a good background of the biology of the problem, a good understanding of the contact mechanics theory, and a good understanding of the underlying physical principles of the indenter-surface contact. Compared to FI analysis of relevant non-biological material, the dynamic nature and the surface complexity of them gives rise to research complexity, and this complexity can be faced with the proper strategy. There are too many independent variables to consider (from the experimental parameters to some analysis parameters like the choice of the appropriate contact mechanics model, the RoI to investigate, etc.). As such, the focus of the analysis may deviate slightly during the research.

8.3. Future work

8.3.1. AFM bio-mechanical experiments

In the time limit of this work, a big set of bio-mechanical experiments were conducted. Many challenges had to be dealt with, ranging from the sample preparation protocol establishment, to the challenging experimentation design, to the development of a suitable analysis technique

for the more accurate processing of the experimental results, to the complex by nature interpretation of these. As a result, a structured workflow was designed, and hopefully, this will work as guidance to future researchers on the field. But more importantly, there is abundant room for more experiments in the future of mechanical investigation of biological samples. Mechanics plays a key role in the biological function of cells. It is connected to biochemical processes, to cell morphology and growth, and to cell wall constituents. Finally, a not so obvious investigation of plant (and of other biological) cells is the characterization of cells' electromechanical properties with the AFM, which –as discussed in chapter 2.2.2.3- is a long-pursued research goal but with not much recent applications.

8.3.2. Data analysis

The developed technique creates a big set of metadata from its analysis output, which can be further analysed for the mechanical and surface properties of the sample. This set of structured and labelled data can prove to be extremely useful in the sample analysis, especially when this is backed up by more advanced techniques like Machine Learning (ML). In such case, the plethora of "good/labelled" data is well appreciated and needed, and the analysis of them can stand as an important research project on its own. Moreover, there exist a numerous -and easily implementable- ML models available through the common numerical computing languages like Python and Matlab. Furthermore, it has been shown in recent papers (110) (131) (132) how ML can have a great impact in research, and especially in the fields of AFM, materials science and biomedical sciences. In the review paper of (132) it is shown how neural networks can help in experimental optimization, AFM image analysis, and classification of material properties at the nanoscale. In the review paper of (131), the authors focus on the applications that big data and deep data analysis have on the materials' physical and chemical characterization, resulting from multidimensional structural and functional imaging and spectroscopic data. Thus, it goes without saying that this advantage must be exploited, and future research should be focused on

the advanced statistical analysis of experimental data (both imaging and mechanical) under ML.

Bibliography

1. *Atomic Force Microscope.* **Binnig, G, Quate, CF and Gerber, C.** 1986, Physical Review Letters, Vol. 56.

2. *Stomatal openings involve polar not radials stiffenning.* **Carter, Ross, et al.** 2018, JOurnal of biochemistry, pp. 95-99.

3. *Bacterial turgor pressure can be measured by atomic force microscopy.* **Arnoldi, M, et al.** 1, July 2000, Phys Rev E Stat PhysPlasmas Fluids Relat InterdiscipTopics, Vol. 62, pp. 1034-44.

4. *The interplay between cell wall mechanical properties and the cell cycle in Staphylococcus aureus.* **Bailey, R, et al.** 11, 2014, Biophysical Journal, Vol. 107.

5. *Bacterial cell enlargement requires control of cell wall stiffness mediated by peptidoglykan hydrolases.* **Wheeler, R, et al.** 2015, mBio.

6. *AFM indentation study of breast cancer cells.* **Li, Q.S., et al.** 4, 2008, Biochemical and biophysical research communications, Vol. 374, pp. 609-613.

7. *Mechanics, malignancy, and metastasis: The force journey of a tumor cell.* **Kumar, S and Weaver, VM.** 1-2, 2009, Cancer and metastasis review, Vol. 28.

8. *Brown algal morphogenesis: atomic force microscopy as a tool to study the role of mechanical forces.* **Tesson, B and B, Charrier.** 471, 2014, Frontiers in Plant Science, Vol. 5.

9. *Measuring the microelastic propertiesof Biological Material.* **Tao, NJ, Lindsay, SM and Lees, S.** 1992, Biophysics Journal, Vol. 63.

10. *Tissue section AFM: In situ ultrastructural imaging of native biomolecules.* **Graham, HK, et al.** s.l. : Matrix Biology, 2010.

11. *Measuring the micromechanical properties of embryonic tissues.* **Chevalier, NR, et al.** s.l. : Methods, 2016, Vol. 94.

12. *Mechanics of Brain Tissues studied by Atomic Force Microscopy: A Perspective.* **Viji Babu, PM and Radmacher, M.** s.l. : Frontiers in Neuroscience, 2019.

13. *Multifrequency AFM reveals lipid membrane mechanical properties and the effect of cholesterol in modulating viscoelasticity.* **Al-Rekabi, Z and Contera, S.** 11, 2018, PNAS, Vol. 115.

14. *Measuring the mechanical properties of Living cells using Atomic Force Microscopy.* **Thomas, G, et al.** 2013, J. Vis. Exp., Vol. 76.

15. *Electromechanical imaging of biomaterials by Scanning probe microscope.* **Rodriguez, BJ, et al.** 2, 2006, Journal of Structural Biology, Vol. 153, pp. 151-159.

16. *Mechanics and modeling of plant cell growth.* **Geitmann, A and Ortega, KE.** 9, 2010, Trends in Plant Science, Vol. 14.
17. *Cell wall mechanics and growth control in plants: the role of pectins revisited.* **Peaucelle, A, Braybrook, S and Hofte, H.** 2012, Frontiers in Plant Science.
18. *Relating the mechanics of the primary plant cell wall to morphogenesis.* **Bidhendi, AJ and Geitmann, A.** 2, 2015, Journal of Experimental Botany, Vol. 67.
19. *Measuring the mechanics of morphogenesis.* **Routier-Kierzkowska, AL and Smith, RS.** 1, 2013, Current Opinion in Plant Biology, Vol. 16, pp. 25-32.
20. *Cellular Force Microscopy for in vivo Measurements of Plant Tissue Mechanics.* **Routier-Kierzkowska, AL, et al.** 4, 2012, Plant Physiology, Vol. 158, pp. 1514-1522.
21. *Models and Mechanisms of Stomatal Mechanics.* **Woolfenden, Hugh, et al.** 9, 2018, Trends in Plant Science, Vol. 23.
22. *Measuring the Mechanical Properties of Plant Cells by Combining Micro-indentation with Osmotic Treatments.* **Weber, A, et al.** 11, 2015, Journal of Experimental Botany, Vol. 66, pp. 3229-41.
23. *Stiffness Tomography by Atomic Force Microscopy.* **Roduit, C, et al.** 2, 2009, Biophysical Journal, Vol. 97, pp. 674-677.
24. **Commons, Wikipedia.** Plant cell wall diagram. [Online] https://commons.wikimedia.org/wiki/File:Plant_cell_wall_diagram-en.svg.
25. **Epidermis (botany).** ***Wikipedia.*** **[Online] https://en.wikipedia.org/wiki/Epidermis_(botany).**
26. Transport in plants. [Online] http://cronodon.com/BioTech/Plant_Transport.html.
27. ***Open or Close the Gate - Stomata Action Under the Control of Phytohormones in Drought Stress Conditions.*** **Daszkowska-Golec, A and Szarejko, I. 138, s.l. : Frontiers in Plant Science, 2013, Vol. 4.**
28. ***Closing gaps: linking elements that control stomatal movement.*** **Kollist, H, Nuhkat, M and MR, Roelfsema. 1, 2014, New Phytologist, Vol. 203, pp. 44-62.**
29. ***Cellular Force Microscopy for in Vivo Measurements of Plant Tissue MEchanics.*** **Routier-Kierzkowska, AL, et al. 2012, Plant Physiology.**
30. ***Functional Analysis of Cellulose and Xyloglycan in the Walls of Stomatal Guard Cells of Arabidopsis.*** **Rui, Y and Anderson, CT. 2016, Plant Physiology.**
31. ***Stomatal Mechanics.*** **Aylor, DE, Parlange, JY and Krikorian, AD. 2, 1973, American Journal of Botany, Vol. 60, pp. 163-171.**
32. ***Automated AFM force curve analysis for determining elastic modulus of biomaterials and biological samples.*** **Chang, YR, et al. 2014, Journal of the mechanical behavior of biomedical materials, pp. 209-18.**

33. ***Plant cell wall extensibility: connecting plant cell growth with cell wall structure, mechanics, and the action of wall-modifying enzymes.*** **Cosgrove, DJ. 2, 2015, Journal of Experimental Botany, Vol. 67, pp. 463-476.**

34. ***A study of stomatal mechanics using the cell pressure probe.*** **Franks, PJ, Cowan, IR and Farquhar, GD. 2002, Plant, Cell and Environment.**

35. ***Viscoelastic properties of cell walls of single living plant cells determined by dynamic nanoindentation.*** **Hayot, CM, et al. 7, s.l. : Journal of Experimental Botany, 2011, Vol. 63.**

36. ***The anisotropic elasticity of the plant cell wall.*** **Cave, ID. 4, 1968, Wood Science and Technology, Vol. 2, pp. 268-278.**

37. ***Stomatal Opening: The role of cell-wall mechanical anisotropy and its analytical relations to the bio-composite characteristics.*** **Marom, Z, Shtein, I and Bar-On, B. 2007, Frontiers in Plant Science.**

38. Atwell, BJ. Stomatal structure and Function. ***Plants in Action: Adaptation in Nature, Performance in Cultivation.*** **Melbourne : MacMillan Education Australia, 1999.**

39. ***Bioelectrochemical signalling in green plants induced by photosensory systems.*** **Volkov, AG, et al. 2004, Bioelectrochemistry, Vol. 63.**

40. ***The dielectric properties of Cellulose.*** **Stoops, WN. 7, 1934, Journal of the American Chemical Society, Vol. 56, pp. 1480-1483.**

41. Schwendener, S. Über Bau und Mechanik der Spaltöffnungen. s.l. : Monatsberichte der Königlichen preussischen Akademie der Wissenschaften zu Berlin, Physikalischmathematische Klasse, 1881.

42. ***Cell wall arabinan is essential for guard cell function.*** **Jones, L, et al. Washington : Proceedings of the National Academy of Sciences of the United States of America, 2003.**

43. ***Toward a systems approach to understanding plant cell walls.*** **Somerville, C, et al. 2004.**

44. ***Cellulose orientation determines mechanical anisotropy in onion epidermis cell walls.*** **Suslov, D and Verbelen, JP. 2006, Journal of Experimental Botany, pp. 2183-92.**

45. ***Mechanical Anisotropy in Crystalline Saccharin: Nanoindentation studies.*** **Kiran, MSRN, et al. 2010, Crystal Growth & Design, pp. 4650-4655.**

46. ***Anisotropic Expansion of the plant cell wall.*** **Baskin, TI. 2005, Annual Review of Cell and Developmental Biology, pp. 203-222.**

47. ***A computational approach for inferring the cell wall properties that govern guard cell dynamics.*** **Woolfenden, HC, et al. s.l. : The Plant Journal, 2017.**

48. ***Viscoelastic Cell mechanics and actin remodelling are dependent on the rate of applied pressure.*** **Pravincumar, P, Bader, DL and Knight, MM. s.l. : PLOS ONE, 2012.**

49. ***Mapping nanomechanical properties of live cells using multi-harmonic atomic force microscopy.*** **Raman, A, et al. s.l. : Nature Nanotechnology, 2011.**
50. ***Mechanosensitivity of cell membranes. Ion channels, lipid matrix nad cytoskeleton.*** **Petrov, AG and Usherwood, PN. 1, 1994, European Biophysics Journal, Vol. 23, pp. 1-19.**
51. ***Investigating cell mechanics with Atomic force microscopy.*** **Haase, K and Pelling, AE. 2015, Journal of the royal society interface.**
52. ***Rapid hydropassive opening and subsequent active stomatal closure follow heat-induced electrical signals in Mimosa pudica.*** **Kaiser, H and Grams, TE. 9, 2006, Journal of Experimental Botanology, Vol. 57, pp. 2087-92.**
53. ***Loss of Stability: A new look at the physics of cell wall behavior during plant cell growth.*** **Wei, C and Lintilhac, PM. s.l. : Plant Physiology, 2007.**
54. ***Ion channels in plants.*** **Hedrich, R. 2012, Physiological reviews.**
55. ***Plant ion channels: Gene families, Physiology, and Functional Genomics Analyses.*** **Ward, JM, Maser, P and Schroeder, JI. 2009, Annual Review of Physiology.**
56. ***Calcium and plant action potentials.*** **Beilby, MJ. 1984, Plant, Cell & Environment.**
57. ***Simulation of action potential propagation in plants.*** **Sukhov, V, et al. 2011, Journal of Theoretical Biology.**
58. ***Electrical signals and their physiological significance in plants.*** **Fromm, J and Lautner, S. 3, 2007, Plant, cell & Environment, Vol. 30, pp. 249-257.**
59. ***Simulation of action potential propagation in plants.*** **Sukhov, V, et al. 2011, Journal of Theoretical Biology, Vol. 291, pp. 47-55.**
60. ***Stomatla movementsand long-distance signaling in plants.*** **Wensuo, J and Jianhua, Z. 10, 2008, Plant Signaling & Behaviour, Vol. 3, pp. 772-777.**
61. ***The role of the mesophyll in stomatal responses to light and CO2.*** **Mott, KA, ED, Sibbernsen and Shope, JC. 9, 2008, Plant cell Environment, Vol. 31, pp. 1299-1306.**
62. ***Apoplastic mesophyll signals induce rapid stomatal responses to CO2 in Commelina communis.*** **Fujita, T, Noguchi, K and Terashima, I. 2013, New Phytologist, Vol. 2, pp. 395-406.**
63. ***On the piezoelectric effect of bone.*** **Fukada, E and Yasuda, I. 1957, Journal of the Physical Society of Japan, Vol. 12, pp. 1158-62.**
64. ***Piezoelectricity as a fundamental property of wood.*** **Fukada, E. 4, 1968, Wood Science and Technology, Vol. 2, pp. 299-307.**
65. ***Piezoelectric effects in biological materials.*** **Williams, WS. 1982, Ferroelectrics.**
66. ***Piezoelectricity as a fundamental property of biological tissues.*** **Shamos, MH and Lavine, LS. 1967, Nature.**

67. ***Flexoelectricity in soft materials and biological membranes.*** **Deng, Q, Liu, L and Sharma, P. 2014, Journal of the Mechancics and Physics of Solids, Vol. 62, pp. 209-227.**
68. ***Electricity and mechanics of biomembrane systems: flexoelectricity in living membranes.*** **Petrov, AG. 1, 2006, Analutica chimica acta, Vol. 568, pp. 70-83.**
69. ***First Observation of the Converse Flexoelectric Effect in Bilayer Lipid Membranes.*** **Todorov, AT, Petrov, AG and Fendler, JH. 12, 1994, The Journal of Physical Chemistry, Vol. 98, pp. 3076-3079.**
70. ***Flexoelectric effects in model and native membranes containing ion channels.*** **Petrov, AG, et al. 4, 1993, European Biophysics Journal, Vol. 22, pp. 289-300.**
71. ***Surface ultrastructure and elasticity in growing tips and mature regions of Aspergillus hyphae describe wall maturation.*** **Ma, H, et al. 151, 2005, Microbiology, pp. 3679-3688.**
72. ***AFM combined to ATR-FTIR reveals Candida cell wall changes under caspofungin treatment.*** **Quiles, F, et al. 36, 2017, Nanoscale.**
73. ***Force-induced formation and propagation of adhesion nanodomains in living fungal cells.*** **Alsteens, D, et al. 2010, PNAS.**
74. ***AP-2-Dependent Endocytic Recycling of the Chitin Synthase Chs3 Regulates Polarized Growth in Candida Albicans.*** **Knafler, HC, et al. s.l. : mBio, 2019.**
75. ***Visualization of plant cell walls by AFM.*** **Kirby, AR, et al. 1996, Biophysical Journal, pp. 1138-1143.**
76. ***Measuring the Mechanical Properties of Plant Cell Walls.*** **Vogler, H, et al. 2, 2015, Plants, Vol. 4, pp. 167-182.**
77. ***Cell mechanics using Atomic Force Microscopy-based single cell compression.*** **Lulevich, V, et al. 2006, Langmuir, pp. 8151-5.**
78. ***Ball tonometry: a rapid, nondestructive method for measuring cell turgor pressure in thin-walled plant cells.*** **Lintilhac, PM. 2000, Journal of plant growth regulation.**
79. ***Hydration Forces.*** **Leikin, S, et al. 1993, Annual Reviews of Physical Chemistry, Vol. 44.**
80. ***Force Measurements with the Atomic Force Microscope: Technique, interpretation and applications.*** **Butt, HJ, Cappella, B and Kappl, M. 1-6, 2005, Surface Science Reports, pp. 1-152.**
81. ***Theory of the stability of strongly charged lyophobic sols and of the adhesion of strongly charged particles in solutions of electrolytes.*** **Derjaguin, B and Landau, L. 1-4, s.l. : Elsevier, 1993, Progress in Surface Science, Vol. 43.**
82. ***Theory of the Stability of Lyophobic Colloids.*** **Verwey, EJW. 3, s.l. : ACS Publications, 1947, Journal of Physical Chemistry, Vol. 51.**

83. Domain, Public. [Online] https://commons.wikimedia.org/w/index.php?curid=3592868.

84. ***Single Cell Wall Nonlinear Mechanics Revealed by a Multiscale Analysis of AFM Force-Indentation Curves.*** **Digiuni, S, et al. 9, 2015, Biophysical Journal, Vol. 108, pp. 2235-2248.**

85. ***In vivo analysis of local wall stiffness at the shoot apical meristem in Arabidopsis using atomic force microscopy.*** **Milani, P, et al. 6, 2011, The Plant Journal, Vol. 67, pp. 1116-23.**

86. ***Atomic Force Microscopy stiffness tomography on living Arabidopsis thaliana cells reveals the mechanical properties of surface and deep cell-wall layers during growth.*** **Radotic, K, et al. 3, 2012, Biophysical Journal, Vol. 103, pp. 386-94.**

87. ***Atomic Force Microscopy based nanoindentation study of onion abaxial epidermis walls in aqueous environment.*** **Xi, X, Kim, SH and Tittmann, B. 2015, Journal of Applied Physics, Vol. 117.**

88. ***The stiffening of the cell walls observed during physiological softening of pears.*** **Zdunek, A, et al. 2, 2016, Planta, Vol. 243, pp. 519-529.**

89. ***Measuring the elastic properties of living cells with Atomic force microscopy indentation.*** **MacKay, JL and Kumar, S. 2012, Cell Imaging Techniques, pp. 313-329.**

90. ***Measuring elasticity of biological materials by atomic force microscopy.*** **Vinckier, A and Semenza, G. 1-2, 1998, FEBS Letters, Vol. 430, pp. 12-16.**

91. ***Nanoindentation of biological materials.*** **Ebenstein, DM and Pruitt, LA. 3, 2006, nanotoday, Vol. 1, pp. 26-33.**

92. ***Dynamic atomic force microscopy methods.*** **Garcia, R and Perez, R. 6, s.l. : Surface Science reports, 2002, Vol. 47, pp. 197-301.**

93. Asylum Research. Closed fluid cell for MFP-3D Atomic Force Microscopes. ***Asylum Research.*** **[Online] https://afm.oxinst.com/products/mfp-3d-liquid-environmental-control/mfp-3d-closed-fluid-cell.**

94. ***Toward the realization of reproducible Atomic force microscopy measurements of elastic modulus in biological samples.*** **Demichelis, A, et al. 6, 13 04 2015, Journal of Biomechanics, Vol. 48, pp. 1099-1104.**

95. ***Study of the AFM Force Spectroscopy method for elastic modulus measurement of living cells.*** **Demichelis, A, et al. s.l. : Journal of Physics Conference series, 2013.**

96. ***Mutants of Arabidopsis Thaliana defective in the acquisition of tolerance to high temperature stress.*** **Hong, SW and Vierling, E. 2000, PNAS.**

97. Hertz, H. ***Miscellaneous Papers by H. Hertz.*** **London : Macmillan, 1896.**

98. ***Surface energy and the contact of elastic bodies.*** **Johnson, KL, Kendall, K and Roberts, AD. 1971, Proceedings of the Royal Society A.**

99. ***Effect of contact deformations on the adhesion of particles.*** **Derjaguin, BV, Muller, VM and Toporov, YP. 2, 1975, Journal of Colloid and Interface Science, Vol. 53, pp. 314-326.**

100. ***An improved technique for determining hardness and elastic modulus using load and displacement sensing indentation experiments.*** **Oliver, WC and Pharr, GM. 6, 1992, Journal of Materials Research, Vol. 7, pp. 1564-1583.**

101. ***Measurement of hardness and elastic modulus by instrumented indentation - Advances in understanding and refinements to methodology.*** **Oliver, WC and Pharr, GM. 1, 2004, Journal of Materials Research, Vol. 19, pp. 3-20.**

102. ***The relation between load and penetration in the axisymmetric boussinesq problem for a punch of arbitrary profile.*** **Sneddon, IN. 1, May 1965, International Journal of Engineering Science, Vol. 3, pp. 47-57.**

103. ***Atomic force microscopy probing of cell elasticity.*** **Kuznetsova, TG, et al. 8, February 2007, Micron, Vol. 38, pp. 824-33.**

104. Borodich, FM. Hertz type contact problems for power law shaped bodies. [book auth.] GLM Gladwell and LA Galin. ***Contact problmes: the legacy of L.A. Galin.*** **2008.**

105. ***Understanding nanoindentation unloading curves.*** **Pharr, GM and Bolshakov, A. 10, October 2002, Journal of Materias Science, Vol. 17, pp. 2660-2671.**

106. ***Adhesion of spheres: The JKR-DMT transition using a dugdale model.*** **Maugis, D. 1, April 1992, Journal of Colloid and Interface Science, Vol. 150, pp. 243-269.**

107. ***The temperature dependence of cell mechanics measured by atomic force microscopy.*** **Sunyer, R, et al. s.l. : Physical Biology, 2009, Vol. 6.**

108. ***Robust strategies for automated AFM force curve analysis; Non-adhesive indentation of soft, inhomogeneous materials.*** **Lin, DC, Dimitriadis, EK and Horkay, F. 2007, Journal of Biomechanical Engineering, pp. 430-40.**

109. ***Automated Force Volume Image Processing for Biological Samples.*** **Polyakov, P, et al. 29 April 2011, PLOS ONE.**

110. ***A fully-automated neural network analysis of AFM force-distance curves for cancer tissue diagnosis.*** **Minelli, E, et al. 2017, Applied Physical Letters.**

111. O'Connor, S,. ***A high throughput matlab program for automated force-curve processing using the AdG polymer model.*** **2014. MSc Thesis.**

112. Kolambkar, Yash M. ***Extracting mechanical properties of cells/biomaterials using the Atomic Force Microscope.*** **2004. MS Thesis.**

113. ***Measuring the elastic properties of biological samples with the AFM.*** **Radmacher, M. 2, 1997, IEEE Eng Med Biol Mag, Vol. 16.**

114. ***Measurement and characterization of whole-cell mechanical behavior.*** **Yaasma MJ, Jackson WM, Keaveny TM. 2006, Annals of Biomedical Engineering.**

115. ***Determination of elastic moduli of thin layers of soft material using the atomic force microscope.*** **Dimitriades EK, Horkay F, Maresca J, Kachar B, Chadwick RS. 2002, Biophysical Journal, pp. 2798-2810.**

116. ***Morphology and Transverse Stiffness of Drosophila Myofibrils Measured by Atomic Force Microscopy.*** **Nyland LR, Maughan DW. 2000, Biophysical Journal.**

117. Geron, Aurelien. ***Hands-On Machine Learning with Scikit-Learn and TensorFlow: Concepts, Tools, nad Techniques to Build Intelligent Systems.*** **s.l. : O'Reilly Media, 2017.**

118. ***Scikit-learn: Machine Learning in {P}ython .*** **Pedregosa, F, et al. 2011, Journal of Machine Learning Research, Vol. 12, pp. 2825-2830.**

119. ***Convergence properties of the Nelder-Mead Simplex method in low Dimensions.*** **Lagarias, JC, et al. 1998, SIAM Journal of Optimization.**

120. ***Nanoscale tomographic reconstruction of the subsurface mechanical properties of low-k high-aspect ratio patterns.*** **Stan, G, et al. 48, 2016, Nanotechnology, Vol. 27.**

121. ***Atomic Force Microscopy Stiffness Tomography on Living Arabidopsis Thaliana Cells Reveals the Mechanical Properties of Surface and Deep Cell-Wall Layers during Growth.*** **Radotic, K, et al. 3, 2012, Biophysical Journal, Vol. 103, pp. 386-394.**

122. ***Growth of the plant cell wall.*** **Cosgrove, DJ. s.l. : Nature Reviews Molecular Cell Biology, 2005, Vol. 6, pp. 850-861.**

123. ***Plant Cell Walls.*** **Srivastava, V, McKee, LS and Bulone, V. s.l. : Wiley Online Library, 2017.**

124. ***Stomatal function requires pectin de-methyl-esterification of the guard cell wall.*** **Amsbury, S, et al. 21, 2016, Vol. 26.**

125. ***Molecular organization of the cell wall of Candida albicans and its relation to pathogenicity.*** **Ruiz-Herrera, J, et al. 1, s.l. : OXFORD ACADEMIC, 2006, FEMS Yeast Research, Vol. 6.**

126. MATLAB Box Plot. [Online] https://uk.mathworks.com/help/stats/boxplot.html.

127. ***Candida albicans Cell wal properties.*** **LaJean Chaffin, W. s.l. : American Society for Microbiology, 2008, Microbiology and Molecular biology Reviews.**

128. ***Measuring cell wall thickness in living yeast cells using single molecular rulers.*** **Dupres, V, Dufrene, YF and Heinisch, JJ. 2010, ACS Nano.**

129. ***Determination of yeast cell wall thickness and cell diameter using new methods.*** **Srinorakutara, T. 3, 1998, Journal of fermentation and bioengineering, Vol. 86.**

130. ***Cell Wall Architecture in Yeast: New Structure and New Challenges.*** **Lipke, PN and Ovalle, R. 1998, Journal of Bacteriology.**

131. ***Big data and deep data in Scanning and Electron Microscopies: deriving functionality from multidimensional data sets.*** **Belianinov, A, et al. 2015, Advanced Structural and Chemical Imaging.**

132. ***Artificial intelligence in Nanotechnology.*** **Sacha, GM and Varona, P. 45, 2013, Nanotechnology, Vol. 24.**

133. ***Guard cell pressures an wall properties during Stomatal opening.*** **Meidner, H. 1982, Journal of Experimental Botany, Vol. 33, pp. 355-359.**

134. ***Guard cells elongate: Relationship of Volume and Surface Area during Stomatal Movement.*** **Meckel, Tobias, et al. 3, 2007, Biophysics Journal, Vol. 92, pp. 1072-1080.**

135. ***Plant Biomechanics.*** **Vincent, JFV. 2011, Wiley Online Library.**

136. ***Unraveling the effects of Plant Hydraulics on Stomatal Closure during Water Stress in Walnut.*** **Cochard, H, et al. 2002, Plant Physiology.**

137. ***The role of Microtubules in Guard Cell Function.*** **Marcus, Al, Moore, RC and Cyr, RJ. 2001, Plant Physiology.**

138. ***The mechanical diversity of stomata and its significance in gas-exchange control.*** **Franks, PJ and Farquhar, GD. 1, 2006, Plant Physiology, Vol. 143, pp. 78-87.**

139. ***Stomatal mechanics: volume changes during opening.*** **Sharpe, PJ and Wu, HI. 1978, Plant, Cell & the Environment.**

140. JPK, Instruments. JPK Application note - Investigation of living cells using JPK's QI mode. ***https://www.jpk.com/app-technotes-img/AFM/pdf/jpk-app-living-cells-qi.14-1.pdf.*** **[Online]**

141. team, Nanowizard scientific. ***JPK Application note - Investigation of living cells using JPK's QI mode.***

142. ***Measurement of hardness and elastic modulus by instrumented indentation - Advances in understanding and refinements to methodology.*** **Oliver, WC and Pharr, GM. 1, 2004, Journal of Materials Research, Vol. 19, pp. 3-20.**

143. ***Combined strategies for optimal detection of the contact point in AFM force-indentation curves obtained on thin samples and adherent cells.*** **Gavara, N. 2016, Nature Scientific Reports, Vol. 6.**

144. Pedregosa, F. and Varoquaux, G. and Gramfort, A. and Michel, V.

145. ***Pedregosa, F. Varoquaux, G. and Gramfort, A. and Michel, V.***

146. Pedregosa F, Varoquaux G.

147. Pedregosa, Varoquaux.

148. A fully-automated neural network analysis of AFM force-distance curves for cancer tissue diagnosis. Minelli E, Ciasca G, Sassun TE, Antonelli M, Palmieri V, Papi M, Maulucci G, Santoro A, Giangaspero F, Delfini R, Campi G, De Spirito M. 2017, Applied Physics Letters, Vol. 111.

149. sodfjks. Z Marom, I Shtein.

150. High spatial resolution surface imaging and analysis of fungal cells using SEM and AFM. Kaminskyj, SGW and Dahms, TES. 2008, Micron.

151. Atomic Force Microscopy of fungal cells; An update. Dufrene, YF. 27, 2010, Yeast, pp. 465-471.

152. A study of stomatal mechanics using the cell pressure probe. Franks, PJ, Cowan, IR and Farquhar, GD. 1, 2002, Plant, Cell & Environment, Vol. 21.

153. MATLAB. https://www.mathworks.com/help/matlab/ref/fminsearch.html. [Online]

154. Plant physiology. [Online] http://plantphys.info/plant_physiology/bluelight.shtml.

155. Stomatal Action. Raschke, K. 1975, Annual review of plant physiology.

Appendix

The codes developed in this project, needed for the completion of the different side projects, are posted here. We start with the *python* code for the training of the logistic regression model for the calculation of the cp, and we end with the algorithm/code for the analysis of an individual force map. The last one is described (not documented) in 5.1.

Contact point calculation method (logistic regression) [*python code*]

```
% import libraries
import pandas
import numpy as np
from sklearn import preprocessing,metrics
import matplotlib.pyplot as plt
from sklearn.linear_model import LogisticRegression
from sklearn.svm import SVC
from sklearn.model_selection import train_test_split
import seaborn as sns
from sklearn.utils import shuffle
 % import scores here
scores = scores[pandas.notnull(scores['c1'])]
X=scores.loc[:,'c1':'c5']\
y=scores.loc[:,'result']
 from pandas import read_csv
from sklearn.decomposition import PCA
pca = PCA(n_components=4)
mod = pca.fit(X)
 X_new=mod.transform(X)
X_new
mod.components_
% train algorithm
X_train, X_test, y_train, y_test = train_test_split(X, y, test_size=0.3,
random_state=0)
logreg = LogisticRegression(C=100)
logreg.fit(X_train, y_train)
 % calculate predictions
y_pred = logreg.predict(X_test)
print('Accuracy of logistic regression binary classifier:
{:.2f}'.format(logreg.score(X_test, y_test)))
from sklearn.metrics import confusion_matrix
print(confusion_matrix(y_test, y_pred))
from sklearn.metrics import classification_report
print(classification_report(y_test, y_pred))
```

Developed technique algorithm [*Matlab code*]

```
% Nano-indentation Analysis - Calculation of mechanical properties from imported AFM "Force
Maps"
% Spyridon Sovatzoglou / 19-September-2019
% Version 8.1
%% s1 clear evrything, start counter & begin
close all;clc;tic;
%% s2 - insert raw data & read initial parameter values for E calculation and for error
analysis
EXD=table2array(readtable([pwd '\FMAPS\AFM_exp_details.xlsx']));
Height_data_file=EXD{3,expt}; AFM_instrum=(EXD{4,expt});
FI_data_folder=EXD{2,expt}; if ismember('MFP',AFM_instrum)==1
```

```
fid=fopen([pwd '\FMAPS\In\' FI_data_folder '\' Height_data_file(1:end-7) '.ARDF'],'r','n','US-
ASCII');
C2=fread(fid,20000,'int8=>char');MFP=transpose(C2);
MFP2=cell(1000,1); MFP3=cell(1000,2); g1=1; g5=1; g2=1;
while g1<20000
    if MFP(1,g1)==':'; MFP2{g5,1}=(MFP(1,g2+1:g1)); g5=g5+1; g2=g1; end; g1=g1+1;
end
gg1=1;
while gg1<g5
    mfp34=char(MFP2{gg1,1});  mfp44=textscan(mfp34,'%s');   MFP3{gg1,1}=mfp44{1,1}{1};
    if size(mfp44{1,1},1)==2; MFP3{gg1,2}=mfp44{1,1}{2}; end;    gg1=gg1+1;
end
T_x=15; X=cell(1,T_x); X{1,1}='ForceScanRate'; X{1,2}='ForceDist'; X{1,3}='Velocity';
X{1,4}='NumPtsPerSec'; X{1,5}='TriggerPoint';
X{1,6}='ForceMode'; X{1,7}='FMapScanPoints'; X{1,8}='FMapScanPoints';
X{1,9}='ForceFilterBW'; X{1,10}='FMapXYVelocity'; X{1,11}='ScanSize';
X{1,12}='DriveFrequency'; X{1,13}='InvOLS'; X{1,14}='SpringConstant'; X{1,15}='ThermalQ';
ass=zeros(1,T_x); for t=1:T_x; ass(t)=size(char(X(t)),2); end
Intxt=char([T_x,max(ass)]); Outtxt=cell(1,T_x);
for l=1:T_x; Intxt(l,1:ass(l))=char(X(l)); end
for i=1:T_x
    a=Intxt(i,1:ass(i));  jk=1;
    while jk<=size(MFP3,1)
        sds=char(MFP3{jk,2});
        if isempty(sds)==0
            if ismember([a ':'],sds(1,:))==1
                if size([a ':'],2)==size(sds,2)
                    if ischar(char(MFP3(jk,2)))==1
                        Outtxt(i)=cellstr(char(MFP3(jk+1,1)));
                    else
                        Outtxt(i)=num2cell(char(MFP3(jk+1,1)));
                    end
                    break
                end
            end
        end; jk=jk+1;
    end
end
elseif ismember('JPK',AFM_instrum)==1
FMap_name=FI_data_folder;
JPK=table2cell(readtable([pwd '\FMAPS\In\' FI_data_folder '.txt'],'Delimiter','#'));
T_x=9; X=cell(1,T_x); X{1,1}='springConstant'; X{1,2}='extend-k-length'; X{1,3}='velocity';
X{1,4}='iLength'; X{1,5}='jLength';
X{1,6}='fastSize'; X{1,7}='feedbackMode'; X{1,8}='date'; X{1,9}='scan-time';
ass=zeros(1,T_x); for t=1:T_x; ass(t)=size(char(X(t)),2); end
Intxt=char([T_x,max(ass)]); Outtxt2=cell(1,T_x);
for l=1:T_x; Intxt(l,1:ass(l))=char(X(l)); end
for i=1:T_x
    a=Intxt(i,1:ass(i)); Lia=false(1,size(a,2)); Lia2=false(1,size(a,2));
Locb=zeros(1,size(a,2));
    Locb2=zeros(1,size(a,2)); j12=1;
    while j12<=200
        jpk=char(JPK(j12,2));
                [Lia,Locb]=ismember(a,jpk);
                if sum(Lia)==size(a,2)
                    for k=1:size(jpk,2)-1
                        for j=1:size(a,2)
                            [Lia2(j),Locb2(j)]=ismember(a(1,j),jpk(k-1+j:end));
                            if sum(Lia2)==size(a,2) && sum(Locb2)==size(a,2); break; end
                        end
                        if sum(Lia2)==size(a,2) && sum(Locb2)==size(a,2); break; end
                    end
                end
                if Lia2==ones(size(a,2))
                    if issorted(Locb2)==1
                        jpkk24=strsplit(jpk,' ');
                        if ischar(char(jpkk24(1,2)))==1
                            Outtxt2(i)=cellstr(char(jpkk24(1,2)));
                        else
                            Outtxt2(i)=num2cell(str2double(char(jpkk24(1,2))));
                        end
                        break
                    end
                end;   j12=j12+1;
    end
end
```

```
K_t=str2double(cell2mat(Outttxt2(1))); Samplerate=str2double(cell2mat(Outttxt2(2)));
Z_velocity=str2double(cell2mat(Outttxt2(3)));
PandL=str2double(cell2mat(Outttxt2(4))); PandL2=str2double(cell2mat(Outttxt2(5)));
Scan_size=str2double(cell2mat(Outttxt2(6))); AFM_mode=cell2mat(Outttxt2(7));
for j11=1:100
    if isempty(JPK{j11,2})==1 && isempty(JPK{j11+1,2})==1
        JPK2=JPK(j11+2:end,1:end);    garJ=j11-1;
    end
end
clear JPK;
j21=0;j_em=zeros(1000,1);
for j2=1:size(JPK2,1)
    if isempty(JPK2{j2,2})==1
        j21=j21+1; j_em(j21)=j2;
        if mod(j21,2)==0;  end
    end
end
end
PandL = str2double(Outtxt(7)); PandL2 = str2double(Outtxt(8));
Scan_size=str2double(Outtxt(11));AFM_mode=EXD{7,expt};
K_t =str2double(Outtxt(14));Z_velocity=str2double(Outtxt(3));
Samplerate=str2double(Outtxt(4));Forcemode=cell2mat(Outtxt(6));
XYVelocity=str2double(Outtxt(10));FMap_name=EXD{1,expt};
Sample=EXD{5,expt}; Sample_age=str2double(EXD(6,expt)); if isnan(Sample_age)==1; Sample_age=0;
end
Buffer=EXD{8,expt};Sample_mount=EXD{9,expt}; Cantilever_name=EXD{10,expt};
Cantilever_geometry=EXD{11,expt};Ltip = str2double(EXD(12,expt)); if isnan(Ltip)==1; Ltip=0;
end
deltaLtip =str2double(EXD(13,expt)); if isnan(deltaLtip)==1; deltaLtip=0; end
Wtip = str2double(EXD(14,expt)); if isnan(Wtip)==1; Wtip=0; end
deltaWtip = str2double(EXD(15,expt));  if isnan(deltaWtip)==1; deltaWtip=0; end
Rtip = str2double(EXD(16,expt)); if isnan(Rtip)==1; Rtip=1E-8; end;  Rtip=2e-8;
deltaRtip = str2double(EXD(17,expt)); if isnan(deltaRtip)==1; deltaRtip=0; end
phi = str2double(EXD(18,expt))/360*2*pi; if isnan(phi)==1; phi=0; end
deltaphi = str2double(EXD(19,expt)); if isnan(deltaphi)==1; deltaphi=0; end
Etip=str2double(EXD(21,expt)); if isnan(Etip)==1; Etip=1.72E+11; end
deltaEtip=str2double(EXD(22,expt)); if isnan(deltaEtip)==1; deltaEtip=0; end
Pratiotip=str2double(EXD(23,expt)); if isnan(Pratiotip)==1; Pratiotip=0; end
deltaPratiotip=str2double(EXD(24,expt)); if isnan(deltaPratiotip)==1; deltaPratiotip=0; end
Freqtip = str2double(Outtxt(12)); if isnan(Freqtip)==1; Freqtip=0; end
deltaFreqtip = str2double(EXD(26,expt)); if isnan(deltaFreqtip)==1; deltaFreqtip=0; end
QFactor = str2double(Outtxt(15)); if isnan(QFactor)==1; QFactor=0; end
deltaQFactor = str2double(EXD(28,expt)); if isnan(deltaQFactor)==1; deltaQFactor=0; end
Pratiosample=str2double(EXD(29,expt)); if isnan(Pratiosample)==1; Pratiosample=0.5; end
deltaPratiosample=str2double(EXD(30,expt)); if isnan(deltaPratiosample)==1;
deltaPratiosample=0; end
deltaKtip = K_t*((4*(deltaWtip^2)*(Wtip^(-2))+(deltaLtip^2)*(Ltip^(-2))+(deltaQFactor^2)*...
(QFactor^(-2))+4*(deltaFreqtip^2)*((2*(3.14)*Freqtip)^(-2)))^(0.5)); if isnan(deltaKtip)==1;
deltaKtip=0; end% as calculated from propagation of error
SampleRate2=ceil(Samplerate/1);
Low_pass_filter=str2double(Outtxt(9)); if isnan(Low_pass_filter)==1; Low_pass_filter=0; end
Temperature=str2double(EXD(45,expt)); if isnan(Temperature)==1; Temperature=20; end
DelfInvOLS=str2double(Outtxt(13));
Trigger_point_V=str2double(Outtxt(5));
Trigger_point_nN=Trigger_point_V*DelfInvOLS*K_t;
Force_distance=str2double(Outtxt(2));
Scan_rate=str2double(Outtxt(1)); if isnan(Scan_rate)==1; Scan_rate=1; end
smooth=0; if smooth==1; SampleRate=ceil(nthroot(SampleRate2/2000,4))*1000;
smooth_factor=ceil(SampleRate2/SampleRate); else; SampleRate=SampleRate2/Scan_rate;
smooth_factor=1; end
Note=[AFM_instrum,'v = ' Z_velocity,'SS= ' Scan_size,'k= ' K_t];
CM_model='Hertz - parabolic'; % choice of CM model
%%% CM_model='Hertz - conic'; CM_model='Hertz - both'; %%% CM_model='JKR';
%%%CM_model='DMT'; %% CM_model='Oliver-Pharr';
DMT=1; O_PHARR=1; epsil=0.75; beta=1.05; OP_Ac=1; C_0=0; C_1=0; C_2=0;
cp_perc1=60; cp_perc2=60;cp_perc3=66;
cp_perc_deltadefl=5; % *?(defl) for CP trigger
cp_perc_deltagraddefl=90; % *d(defl)/d(indent) for CP trigger
step_CP=(1)*ceil((ceil(1*(nthroot(SampleRate/1500,2))))*ceil(SampleRate/2500)); % around 5-10
if step_CP==0;step_CP=1;end
cp_numpoints2=ceil((1)*ceil((ceil(SampleRate2/250)+ceil(12*...
nthroot(((Z_velocity*(10^6))/10),1.25))*nthroot(SampleRate2/1000,2))*...
(ceil(1100/SampleRate2)*1)*(smooth+1)*(.75))*(ceil(SampleRate2/2500)));
step_cp_numpoints=1;
fit_perc_start=0;
cut=1; cutp=cutp_out(ooo);
```

```
if cut==1; fit_perc_end='absolute'; cut_ind_Fmax='indentation'; else;
fit_perc_end=fit_perc_end1(ooo); cut_ind_Fmax='Fmax'; end
cpddf=cpddf1(ooo);
chinincl_3=10;
chinincl_4=30;
fixCP=4;
Figs.Main=1;     Figs.Main_no=1001;    Figs.Main_Analytics=1;    Figs.Main_Analytics_no=1101;
Figs.FI=1;     Figs.FI_no='1-10';
Figs.FI_gpf=4;
Figs.NonElastic=1;     Figs.NonElastic_no=1003;     Figs.Misc=1;     Figs.Misc_no=1002;
Figs.Tomography=0;     Figs.Tomography_NoWay=0;
Figs.Tomography_no=1004;    Figs.beta=0;     Figs.beta_1=1;    Figs.beta_NoWay=0;
Figs.beta_no=1013;     Figs.paper=0;     Figs.paper_NoWay=0;
Figs.paper_no=548;    Figs.pleIndent=0;    Figs.pleIndent_NoWay=0;    Figs.pleIndent_no=1012;
Figs.pleIndent2=0;    Figs.pleIndent2_NoWay=0;
Figs.pleIndent2_no=1011;    Figs.effIndShape=0;     Figs.effIndShape_NoWay=0;
Figs.effIndShape_no=1048;     Figs.effIndShape2=0;     Figs.effIndShape2_NoWay=0;
Figs.effIndShape2_no=547;    modtomo=1; modtomo_plus=1;
if modtomo==1 && modtomo_plus==1; msp_ple_values=[1 2 3 4 5 6 7 8 9 10]; else;
msp_ple_values=[1 2 3 4 5 6 7 8 9 10]; end
if modtomo==1 && modtomo_plus==1 && Figs.beta_NoWay==0; Figs.beta=1; end
if modtomo==1 && modtomo_plus==1 && Figs.paper_NoWay==0; Figs.paper=1; end
if modtomo==1 && Figs.Tomography_NoWay==0; Figs.Tomography=1; end
if modtomo==1 && modtomo_plus==1 && Figs.pleIndent_NoWay==0; Figs.pleIndent=1; end
if modtomo==1 && modtomo_plus==1 && Figs.pleIndent2_NoWay==0; Figs.pleIndent2=1; end
if modtomo==1 && modtomo_plus==1 && Figs.effIndShape_NoWay==0; Figs.effIndShape=1; end
if modtomo==1 && modtomo_plus==1 && Figs.effIndShape_NoWay==0; Figs.effIndShape2=1; end
stposa=10;    modtomo_Hertz_or_Sned=1;    SPaIDYoN=1;    tip_shape=1;    CP_adjustm=0;
select_CP_manually=2;    MinLStofindCP=0;    printpdf=0;
Figs.Points=0; Figs.justpoints=0;    Figs.line=0; Figs.polygon=1;    FlatLim=0; FlatlimDeg=3;
if FlatLim==0; FlatlimDeg=0; end
% Automatically_find_optimum_ple_and_CP_section=0; % stopped in version 4.23
%% s3 - import raw data (Ascii) and input waves (vectors) in a multiDimensional cell array
M_ZSnsr=cell(PandL,PandL2);M_Defl=cell(PandL,PandL2);M_height=zeros(PandL,PandL2);
if AFM_instrum(1,1:3)=='MFP'
try
    M_height = csvread([pwd '\FMAPS\In\' FI_data_folder '\' Height_data_file '.csv'],2,1);
catch
    M_height = table2array(readtable([pwd '\FMAPS\In\' FI_data_folder...
        '\' Height_data_file '.txt'],'Delimiter','tab'));
end
if size(M_height,1)>PandL; M_height(PandL+1:end,:)=[]; end;
if size(M_height,2)>PandL; M_height(:,PandL+1:end)=[]; end
if size(M_height,1)<PandL; M_height(PandL,:)=0; end; if size(M_height,2)<PandL;
    M_height(:,PandL)=0; end
files = dir(['FMAPS\In\' FI_data_folder '\*.txt']);
num_files = length(files);
for k=1:num_files
    D1=[files(k).folder '\' files(k).name];    D11=strsplit(D1,'Lin');
    if size(D11,2)==1; continue; end;    D12=D11(1,2);
    D2=strsplit(char(D12),'e');
    D21=strsplit(char(D2(1,2)),'t'); if D21{2}(5)=='D'; D22=D2(1,2); end
    D3=sscanf(cell2mat(D21(1,1)),'%f');    D4=sscanf(cell2mat(D21(1,2)),'%f');
    D41=cell2mat(D21(1,2));    D42=D41(5);
    if     D42=='D' && D22{1}(end)=='D';       D5=1;    elseif D42=='R';
        D5=2;    elseif D42=='Z';       D5=3; else; D5=0;    end
    fid=fopen([files(k).folder '\' files(k).name]);
    if     D5==1;    M_ZSnsr(D3+1,D4+1,:) = textscan(fid,'%f64');    elseif D5==3;
    M_Defl(D3+1,D4+1,:) = textscan(fid,'%f64');
    elseif D5==2;    end
    fclose(fid);
end
elseif AFM_instrum(1,1:3)=='JPK'
for jfk=1:(size(j_em)-1)/2
    cursp=JPK2(j_em(2*(jfk-1)+abs((abs(ceil(2/jfk)-2))-1))*...
        (abs(ceil(2/jfk)-2))+1:j_em(2*jfk)-1,2);
    c12=1; c121=0;
    while c12<=size(cursp,1)
        jpkc=char(cursp(c12,1));
        if size(jpkc,2)>=5 && isempty(jpkc)==0
            if jpkc(1:6)=='iIndex'
                jpkc2=strsplit(jpkc,' ');
                iIndex=str2double(char(jpkc2(1,2)));
                c121=c121+1;
            elseif jpkc(1:6)=='jIndex'
                jpkc2=strsplit(jpkc,' ');
```

```
                jIndex=str2double(char(jpkc2(1,2)));
                c121=c121+1;
            end
        end
        if c121==2; break; end
        c12=c12+1;
    end
    cursp2=JPK2(j_em(1+2*(jfk-1))+1:j_em(2*jfk)-1,2);
    cursp3=zeros(size(cursp2,1),8);
    for curs1=1:size(cursp2,1)
        curs_temp=strsplit(char(cursp2(curs1,1)),' ');
        for curs2=1:size(curs_temp,2)
            cursp3(curs1,curs2)=str2double(char(curs_temp(1,curs2)));
        end
    end
    cursp4=cursp3(:,2); cursp4c=(cursp4);    cursp5=cursp3(:,7); cursp5c=(cursp5);
    AllC1 = {cat(1, cursp4c)};    AllC2 = {cat(1, cursp5c)};
    M_ZSnsr(iIndex+1,jIndex+1,:)=AllC2;    M_Defl(iIndex+1,jIndex+1,:)=AllC1;
end
end
if expt==52
M_ZSnsr(1:120,1:120)=M_ZSnsr(1:120,21:140); M_ZSnsr(121:200,:)=[]; M_ZSnsr(:,121:200)=[];
M_Defl(1:120,1:120)=M_Defl(1:120,21:140); M_Defl(121:200,:)=[]; M_Defl(:,121:200)=[];
M_height(:,200)=0; M_height(1:120,1:120)=M_height(1:120,21:140); M_height(121:200,:)=[];
M_height(:,121:200)=[];
end
if expt==52; PandL=120; PandL2=120; end
%% s4 - Force-Indentation analysis for each pair of Deflection vs ZSnsr of imported FMap
noRcol_1=15;noRcol_2=15;noRcol=noRcol_1+noRcol_2;noMAPSsize=144;
MAPS=zeros(PandL,PandL2,noMAPSsize);MAPS(:,:,91)=M_height(:,:);
am=zeros(1,10); a4m=4e-9;
a2=[1 10/9 10/8 10/7 10/6 10/5 10/4 10/3 10/2 10];
for uk=1:10;am(uk)=((10*a4m)-((uk-1)*(a4m)))/((Rtip)^a2(uk));    end
evi=0;noCP_prev=0;Fmax=0; Fmax_CP=0;miss_data=0;noR_test=randi(PandL*PandL2);
grpie_parab=0;grpie_conic=0;FI_num=0;gr_numRows=1;cp_start=1;Rsize12=ceil(SampleRate*1);
R1=single(zeros(Rsize12,noRcol_1,PandL,PandL2));
R2=single(zeros(Rsize12,noRcol_2,PandL,PandL2));
M_ZSnsr_empty=cellfun('isempty',(M_ZSnsr));
M_Defl_empty=cellfun('isempty',(M_Defl)); % boolean cell array to check for lost data
a2_1=zeros(PandL,PandL2); goodCP_1=zeros(PandL,PandL2); cp_numpoints211=zeros(PandL,PandL2);
cp_numpoints_1=zeros(PandL,PandL2);cnt1=0;
parfor i1=1:1:PandL
[num2str(ceil(i1/PandL*100),'%10.4g') ' %']
if mod(i1+10,2)==1; i2iod=[1,1,PandL2]; elseif mod(i1+10,2)==0; i2iod=[PandL2,-1,1]; end
MAPS2=zeros(PandL2,noMAPSsize);if tip_shape==1; iou=am; else;
iou=[3.33333333333333,22.2046763895516,240.960534295959,...

5261.14815043852,328828.276577397,111111111.111111,725774738602.423,1.80213392461435e+18,1.316
87242798354e+31,8.67076495791631e+69]; end
iou3=[1,10/9,10/8,10/7,10/6,10/5,10/4,10/3,10/2,10/1]; iou4=[1,2,3,4,5,6,7,8,9,10];
abest_all_10_CP=zeros(5,2); fval_all_10_CP=zeros(5,2);
a2=zeros(1,PandL2); f_n=zeros(1,PandL2); p3=zeros(1,PandL2); psi_p2=zeros(1,PandL);
goodCP=zeros(1,PandL2); Fmax_CP=zeros(1,PandL2); cp_numpoints21=zeros(1,PandL2);
ci1=zeros(1,PandL2); abest_all1=zeros(PandL2,10,10); fval_all_101=zeros(PandL2,10,10);
if modtomo==1 && modtomo_plus==1; MAPStomo3=zeros(PandL2,100,1); end
ci2=zeros(1,PandL2); ci3=zeros(1,PandL2);
fval_min=zeros(1,PandL2);
cp_numpoints=zeros(1,PandL2);
R13=zeros(Rsize12,noRcol_1,PandL2);
R23=zeros(Rsize12,noRcol_2,PandL2);
for i2=1:1:PandL2
    cp_numpoints21(i2)=cp_numpoints2;
    R1_2(:,:)=zeros(Rsize12,noRcol_1);     R2_2(:,:)=zeros(Rsize12,noRcol_2);
    ci78=0;    st456=0; st09=1;    abest=0; % loop-vars
    evi=0;
    bh37=zeros(1,10);
    if i2==1; cp_start=1; else; cp_start=ceil((80/100)*MAPS2(i2-1,13))+1; end
    if M_ZSnsr_empty(i1,i2)==1 || M_Defl_empty(i1,i2)==1 % skipping lost waves
    MAPS2(i2,:)=0; R1_2(:,:)=zeros(Rsize12,noRcol_1); R2_2(:,:)=zeros(Rsize12,noRcol_2);
    miss_data=miss_data+1;
    continue
    end
    % raw data in R, and initial R formation
    MDefl1=size(cell2mat(M_Defl(i1,i2,:)),1); MZSnsr1=size(cell2mat(M_ZSnsr(i1,i2,:)),1);
    if MDefl1==MZSnsr1; dz=MDefl1; else; dz=min(MZSnsr1,MDefl1); end
    MDM1=cell2mat(M_Defl(i1,i2)); MDM2=cell2mat(M_ZSnsr(i1,i2));
```

```
    if smooth==1
        array1(:,1,1,1)=MDM1(1:dz); we23=size(array1,1);
        array2(:,1,1,1)=MDM2(1:dz); smooth_factor=ceil(we23/SampleRate);
        for sm1=1:smooth_factor:we23
             array1(sm1+1:sm1+smooth_factor-1,1,1,1)=0; array2(sm1+1:sm1+smooth_factor-
1,1,1,1)=0;
        end
      R(:,1,1,1)=array1(array1~=0);      R(:,2,1,1)=array2(array2~=0);
    else
      R(:,1,1,1)=MDM1(1:dz);      R(:,2,1,1)=MDM2(1:dz);
    end
    FI_size=int16(size(R,1));
    [a1,a2(i2)]=max(R(1:ceil(FI_size*(.95)),2,1,1));
    if a2(i2)<=ceil(cp_numpoints21(i2)*1.5)
    MAPS2(i2,:)=0; R1_2(:,:)=zeros(Rsize12,noRcol_1); R2_2(:,:)=zeros(Rsize12,noRcol_2);
    miss_data=miss_data+1; R=[];
    continue
    end
    ghq1=0; ghq3=0; ghq4=0;
    for ghq2=1:10
        if abs(R(a2(i2),1,1,1)-R(1,1,1,1)) < abs(R(a2(i2)-ghq2,1,1,1)-R(1,1,1,1));
            ghq1=ghq1+1; end
        if abs(R(a2(i2)-1,1,1,1)-R(1,1,1,1)) < abs(R(a2(i2)-1-ghq2,1,1,1)-R(1,1,1,1));
            ghq3=ghq3+1; end
    end
    if abs(R(a2(i2)-1,1,1,1)-R(1,1,1,1)) < abs(R(a2(i2)-1,1,1,1)-R(1,1,1,1));
        ghq3=ghq3+1; end
    if ghq1>1 || (ghq3>1 && ghq4==1) % skipping lost waves
    MAPS2(i2,:)=0; R1_2(:,:)=zeros(Rsize12,noRcol_1); R2_2(:,:)=zeros(Rsize12,noRcol_2);
    miss_data=miss_data+1; R=[];
    continue
    end
    if a2(i2)<=FI_size/4 || FI_size<=noCP_prev; cp_start=1; st09=2; end
    R(:,9:10,1,1)=R(:,1:2,1,1); R(:,26:27,1,1)=R(:,9:10,1,1); %
    [a3,a4]=min(R(:,10,1,1));
    R(a2(i2):end,1:2,1,1)=0; R(1:a2(i2),26:27,1,1)=0;
    R(2:a2(i2)-1,5,1,1)=abs((R(2:a2(i2)-1,2,1,1)-R(1:a2(i2)-2,2,1,1))./(R(2:a2(i2)-1,1,1,1)...
        -R(1:a2(i2)-2,1,1,1))); % vectorised version
    evrosdefl = abs(R(a2(i2)-1,2,1,1)-R(1,2,1,1)); % CP calc. vars
    evrosraw = abs(R(a2(i2)-1,1,1,1)-R(1,1,1,1)); % CP calc. vars
    deflgradtot = (R(a2(i2)-1,2,1,1)-R(1,2,1,1))/(R(a2(i2)-1,1,1,1)-R(1,1,1,1)); % CP calc.
vars
    if select_CP_manually==2
        goodCP(i2)=fixCP; cp151=1; cp152=1; cp153=1; cp154=1; cp155=1; cp156=1; cp99=1;
        while goodCP(i2)<5
            cp_numpoints21(i2)=ceil(cp_numpoints21(i2)/cp156);
            for n=ceil(cp_start*(a2(i2)/(SampleRate/2))):1:a2(i2)-1*cp_numpoints21(i2)*(.13)
                gr_Avn6=abs((R(a2(i2),2,1,1)-R(a2(i2)-3,2,1,1))/(R(a2(i2),1,1,1)-R(a2(i2)-
3,1,1,1)))/abs((R(a2(i2)-3,2,1,1)-R(cp_start,2,1,1))/(R(a2(i2)-3,1,1,1)-R(cp_start,1,1,1)));
                cp_numpoints(i2)=ceil(abs(ceil((cp_numpoints21(i2))-
2*(nthroot(((a2(i2))/(a2(i2)-n)),1.2))+ceil(gr_Avn6)^(0)))/st09);
                if  cp_numpoints(i2)>=cp_numpoints21(i2); cp_numpoints(i2)=cp_numpoints21(i2);
end
                if  cp_numpoints(i2)<=3 || isnan(cp_numpoints(i2))==1; cp_numpoints(i2)=3; end

cp_num=1;cp_1stcon_defl=0;cp_2ndcon_unwantincl=0;cp_3rdcon_graddefl=0;cp15=1;cp16=0;cp17=0;cp_
4thcon_diffincl=0;cp_5thcon_signum=0; % initial declaration of cp variables
                gr_Avn=abs((R(n+ceil((a2(i2)-n)*(3/6)),2,1,1)-R(n+ceil((a2(i2)-
n)*(0/6)),2,1,1))/(R(n+ceil((a2(i2)-n)*(3/6)),1,1,1)-R(n+ceil((a2(i2)-
n)*(0/6)),1,1,1)))/abs((R(n+ceil((a2(i2)-n)*(1/6)),2,1,1)-R(n,2,1,1))/(R(n+ceil((a2(i2)-
n)*(1/6)),1,1,1)-R(n,1,1,1))); % gr_Avn: ration of gradient between puI and the 1/6 of puI
                if  gr_Avn>1e+5; gr_Avn=1e+5; end
                if  gr_Avn<1; gr_Avn=1; end
                gr_Avn2=abs((R(a2(i2),2,1,1)-R(n,2,1,1))/(R(a2(i2),1,1,1)-
R(n,1,1,1)))/abs((R(n+ceil(2*cp_numpoints(i2)/2),2,1,1)-
R(n,2,1,1))/(R(n+ceil(2*cp_numpoints(i2)/2),1,1,1)-R(n,1,1,1))); % gr_Avn: ratio of gradient
between puI and the 1/6 of puI
                gr_Avn3=abs((R(a2(i2),2,1,1)-R(n,2,1,1))/(R(a2(i2),1,1,1)-
R(n,1,1,1)))/abs((R(a2(i2),2,1,1)-R(1,2,1,1))/(R(a2(i2),1,1,1)-R(1,1,1,1))); % gr_Avn: ratio
of gradient between (n-1) and the puI
                gr_Avn4=abs((R(n+ceil((a2(i2)-n)/1.33),2,1,1)-R(n,2,1,1))/(R(n+ceil((a2(i2)-
n)/1.33),1,1,1)-R(n,1,1,1)))/abs((R(n+ceil((a2(i2)-n)/1),2,1,1)-R(1,2,1,1))/(R(n+ceil((a2(i2)-
n)/1),1,1,1)-R(1,1,1,1))); % gr_Avn: ration of gradient between puI and the 1/6 of puI
                gr_Avn41=abs((R(n+ceil((a2(i2)-n)/1.33),2,1,1)-R(n,2,1,1))/(R(n+ceil((a2(i2)-
n)/1.33),1,1,1)-R(n,1,1,1)))/abs((R(n+ceil((a2(i2)-n)/1),2,1,1)-R(n,2,1,1))/(R(n+ceil((a2(i2)-
n)/1),1,1,1)-R(n,1,1,1))); % gr_Avn: ration of gradient between puI and the 1/6 of puI
```

```
                gr_Avn5=abs((R(a2(i2),2,1,1)-R(a2(i2)-5,2,1,1))/(R(a2(i2),1,1,1)-R(a2(i2)-
5,1,1,1)))/abs((R(a2(i2)-5,2,1,1)-R(1,2,1,1))/(R(a2(i2)-5,1,1,1)-R(1,1,1,1))); % gr_Avn: ratio
of gradient between puI and the 1/6 of puI
                MAPS2(i2,[14 34 38 50 56 77])=[gr_Avn gr_Avn2 gr_Avn3 gr_Avn4 gr_Avn5
gr_Avn6]; % Mapping of gr_Avn values
                cp_num2=ceil(((nthroot((100-5),2))/100)*cp_numpoints(i2)*(2/3));
                cp_perc_graddefl_relpos=cp152*((n/a2(i2))/nthroot(gr_Avn,5)+(((1-
(n/a2(i2)))^2)/nthroot(gr_Avn,5))^(1))*(1); % instead of cp_perc_deltagraddefl

cp_perc_deltadefl_relpos=cp151*((Z_velocity*(10^6))*(1*cpddf))*(((50+((5)*(nthroot(ceil(Sample
Rate2/250),4)))))/(((ceil(5000/SampleRate2))^(5/3))*nthroot(SampleRate2,2)));
                MAPS2(i2,87)=cp_perc_graddefl_relpos; MAPS2(i2,86)=cp_perc_deltadefl_relpos;
                MAPS2(i2,35:36)=[cp_perc_deltadefl_relpos,cp_perc_graddefl_relpos];
                deflgradtot2 = (R(a2(i2)-1,2,1,1)-R(n,2,1,1))/(R(a2(i2)-1,1,1,1)-R(n,1,1,1));
                ratio_deflgradtot=deflgradtot2/deflgradtot;
                MAPS2(i2,37)=ratio_deflgradtot;
                evrosdefl2=R(a2(i2)-1,2,1,1)-R(n,2,1,1);
                cp_perc0_relpos=(30*nthroot(gr_Avn,3)+1)/cp153;

cp_perc1_relpos=50/cp154+((ceil(nthroot(SampleRate/1000,1.4)+1))^(2))*((ratio_deflgradtot)^(1/
4));

cp_perc2_relpos=50/cp155+(ceil(SampleRate/1000))^(2.15)+(nthroot(gr_Avn5,2))^(0);
                if  cp_perc2_relpos>=95; cp_perc2_relpos=95; end
                cp_num_end=ceil(step_cp_numpoints)*cp_numpoints(i2);
                cp_num_end_2=ceil((cp_num_end)); MAPS2(i2,85)=cp_num_end_2;
                if a2(i2)<=n+cp_num_end_2+cp_num2; cp_num_end_2=a2(i2)-1-cp_num2-n; end
                cpkalo1=(R(n+1*cp_num_end_2,2,1,1)-R(n,2,1,1));
cpkalo2=abs(R(n+ceil(cp_num_end_2/2),2,1,1)-R(n,2,1,1));
                for cp_num=1:step_cp_numpoints:ceil(cp_num_end_2)
                    % 1ST CONDITION - check (for each cp_num) how the DEVIATION IN DEFLECTION
                    % (y-axis) between n and cp_num compares to the whole puI (part under
Investigation)
                    if     abs(R(n+cp_num,2,1,1)-
R(n,2,1,1))>=(cp_perc_deltadefl_relpos/100)*abs(evrosdefl) ...
                        && (R(n+1*cp_num,2,1,1)-
R(n,2,1,1))>=((cp_perc_deltadefl_relpos/100/2))*abs(evrosdefl2)...
                        && (R(n+cp_num,2,1,1)-R(n,2,1,1))<=cpkalo1
                           cp_1stcon_defl=cp_1stcon_defl+1;
                    else
                    end
                    % 2ND CONDITION - check for UNWANTED INCLINATION inside the puI / huge
(relatively) inclinations that would decrease
                    % the possibilities of a possible (& plausible) contact point
                    cp_puI_divs=1; % split puI in equal parts [puI/cp_numpoints]
                    cp132=(abs(R(n+ceil(cp_numpoints(i2)/2*ceil(SampleRate/2000)),2,1,1)-
R(n,2,1,1)))/(abs(R(n+ceil(cp_numpoints(i2)/2*ceil(SampleRate/2000)),1,1,1)-R(n,1,1,1)));
                    if cp_num<ceil(cp_numpoints(i2)/10)
                    else
                        if  (abs(R(n+cp_puI_divs*cp_num+2,2,1,1)-
R(n+cp_num,2,1,1)))/(abs(R(n+cp_puI_divs*cp_num+2,1,1,1)-R(n+cp_num,1,1,1)))...
                         >= (nthroot(gr_Avn2,3)+2)*(cp132)
                            cp_2ndcon_unwantincl=cp_2ndcon_unwantincl+1;
                        end
                    end
                    % 3RD CONDITION - check how the DEVIATION IN GRADIENT OF THE DEFLECTION
WITH RESPECT TO ZSNSR (inclination)
                    % between n and cp_num compares to the whole puI (part under
Investigation) with respect to ZSnsr
                    if (n-cp_num)<1
                        if     abs((R(n+cp_num,2,1,1)-R(n,2,1,1))/(R(n+cp_num,1,1,1)-
R(n,1,1,1))) >= (cp_perc_graddefl_relpos)*abs(deflgradtot)...
                               && abs((R(n+ceil(cp_num/2),2,1,1)-
R(n,2,1,1))/(R(n+ceil(cp_num/2),1,1,1)-R(n,1,1,1))) >=
(cp_perc_graddefl_relpos)*abs(deflgradtot)...
                               cp_3rdcon_graddefl=cp_3rdcon_graddefl+1;
                        else
                        %      cp14=cp14-0.5;
                        end
                    else
                        if     abs((R(n+cp_num,2,1,1)-R(n,2,1,1))/(R(n+cp_num,1,1,1)-
R(n,1,1,1))) >= (cp_perc_graddefl_relpos)*abs(deflgradtot)...
                               && abs((R(n+ceil(cp_num/2),2,1,1)-
R(n,2,1,1))/(R(n+ceil(cp_num/2),1,1,1)-R(n,1,1,1))) >=
(cp_perc_graddefl_relpos)*abs(deflgradtot)...
```

```
                            && ((R(n+cp_num,2,1,1)-R(n,2,1,1))/(R(n+cp_num,1,1,1)-R(n,1,1,1)))
>= 1.5*((R(n-cp_num,2,1,1)-R(n,2,1,1))/(R(n-cp_num,1,1,1)-R(n,1,1,1)))...
                                cp_3rdcon_graddefl=cp_3rdcon_graddefl+1;
                        end
                    end
                    % 4TH CONDITION - check if there is DIFFERENT INCLINATION
                    if      (((R(n+cp_num,2,1,1)-R(n,2,1,1))/(R(n+cp_num,1,1,1)-R(n,1,1,1)))>=0
&& deflgradtot>=0)...
                        || (((R(n+cp_num,2,1,1)-R(n,2,1,1))/(R(n+cp_num,1,1,1)-R(n,1,1,1)))<=0
&& deflgradtot<=0)
                            cp_4thcon_diffincl=cp_4thcon_diffincl+1;
                    end
                    % 5TH CONDITION - check (for each cp_num) if the SIGNUM of
                    % the whole puI (part under Investigation) is the same with each
(cp_num+1)-(cp_num)
                    if sign(evrosdefl)==sign(R(n+cp_num+5,2,1,1)-R(n,2,1,1))
                       cp_5thcon_signum=cp_5thcon_signum+1;
                    end
                    % 6TH CONDITION - check (for each cp_num) if the SIGNUM of
                    % the whole puI (part under Investigation) is the same with each
(cp_num+1)-(cp_num)
                    cp_6thcon_signum=n/a2(i2);
                end
                % CP MEET CONDITIONS START
                coefs1=[cp_1stcon_defl/cp_num_end_2 cp_2ndcon_unwantincl/cp_num_end_2
cp_3rdcon_graddefl/cp_num_end_2...
                                        cp_4thcon_diffincl/cp_num_end_2
cp_5thcon_signum/cp_num_end_2 cp_6thcon_signum];
                cp_score=1/(1+exp(-(coefs1*...
                [3.80905338,  0.75496138,  4.44411382, -1.45598453,  2.10051403, -
0.50757607]'-3.80602123)));
                MAPS2(i2,113)=cp_score;
                if cp_score>.5
                            evi=n+ceil((1-cp_1stcon_defl/cp_num_end_2)*cp_num_end_2)+1; evi=n;
                            MAPS2(i2,28:32)=[cp_1stcon_defl cp_2ndcon_unwantincl
cp_3rdcon_graddefl cp_4thcon_diffincl cp_5thcon_signum];
                            MAPS2(i2,[13,84])=evi;
                            break
                else
                end
            end
            if goodCP(i2)==4
                goodCP(i2)=goodCP(i2)+1;
            else
                Fmax_CP(i2)=abs(R(a2(i2)-1,2,1,1));
                msp_all_valuesCP=30;
                msp_ple_valuesCP=[5 10];
                optionsCP=optimset('MaxFunEvals',1000,'MaxIter',200,'TolFun',1e-8,'TolX',1e-
4);
                for msp_pleCP=msp_ple_valuesCP
                    for msp_allCP=msp_all_valuesCP
                        msp_parcon2CP=(R(evi+ceil((a2(i2)-evi)*((msp_allCP/5-
(sqrt(msp_allCP/5))*.5)/10)),2,1,1)-0.05*Fmax_CP(i2))...
                                        /(R(evi+ceil((a2(i2)-evi)*((msp_allCP/5-
(sqrt(msp_allCP/5))*.5)/10)),1,1,1)^(2));
                        %
                        [abest_all_10_CP(ceil(msp_allCP/5)-
5,msp_pleCP/5),fval_all_10_CP(ceil(msp_allCP/5)-5,msp_pleCP/5)] = ...
                        fminsearch(@(a) nthroot((sum((abs(abs(R(ceil(evi+(a2(i2)-
evi)*(msp_allCP/5-1)/10):a2(i2),2,1,1))-...
                                        a.*abs(R(ceil(evi+(a2(i2)-evi)*(msp_allCP/5-
1)/10):a2(i2),1,1,1)).^((msp_pleCP/5)-.5*ceil(msp_pleCP/5)+(ceil(5/msp_pleCP))^1))).^(2)))/...
                                        (((abs(a2(i2)-ceil(evi+(a2(i2)-evi)*(msp_allCP/5-
1)/10)))/1)^(1)),2),msp_parcon2CP,optionsCP);
                    end
                end
                %
                if fval_all_10_CP(1,1) > Fmax_CP(i2)/100 || fval_all_10_CP(1,2) >
Fmax_CP(i2)/100 ...
                    cp151=cp151*2/cp99;  cp152=cp152*2/cp99;    cp153=cp153*1.01357/cp99;
                    cp154=cp154*1.2/cp99;    cp155=cp155*1.2/cp99;    cp156=cp156*1.05;
                    goodCP(i2)=goodCP(i2)+1;
                else
                    goodCP(i2)=goodCP(i2)+5; MAPS2(i2,13)=evi;
                end
            end
```

```
        end
    elseif select_CP_manually==0
        goodCP(i2)=fixCP; cp151=1; cp152=1; cp153=1; cp154=1; cp155=1; cp156=1; cp99=1;
        while goodCP(i2)<5
            cp_numpoints21(i2)=ceil(cp_numpoints21(i2)/cp156);
            for n=ceil(cp_start*(a2(i2)/(SampleRate/2))):step_CP:a2(i2)-
1*cp_numpoints21(i2)*(.13)
                gr_Avn6=abs((R(a2(i2),2,1,1)-R(a2(i2)-3,2,1,1))/(R(a2(i2),1,1,1)-R(a2(i2)-
3,1,1,1)))/abs((R(a2(i2)-3,2,1,1)-R(cp_start,2,1,1))/(R(a2(i2)-3,1,1,1)-R(cp_start,1,1,1)));
                cp_numpoints(i2)=ceil(abs(ceil((cp_numpoints21(i2))-
2*(nthroot(((a2(i2))/(a2(i2)-n)),1.2))+ceil(gr_Avn6)^(0)))/st09);
                if  cp_numpoints(i2)>=cp_numpoints21(i2); cp_numpoints(i2)=cp_numpoints21(i2);
end
                if  cp_numpoints(i2)<=3 || isnan(cp_numpoints(i2))==1; cp_numpoints(i2)=3; end

cp_num=1;cp_1stcon_defl=0;cp_2ndcon_unwantincl=0;cp_3rdcon_graddefl=0;cp15=1;cp16=0;cp17=0;cp_
4thcon_diffincl=0;cp_5thcon_signum=0; % initial declaration of cp variables
                gr_Avn=abs((R(n+ceil((a2(i2)-n)*(3/6)),2,1,1)-R(n+ceil((a2(i2)-
n)*(0/6)),2,1,1))/(R(n+ceil((a2(i2)-n)*(3/6)),1,1,1)-R(n+ceil((a2(i2)-
n)*(0/6)),1,1,1)))/abs((R(n+ceil((a2(i2)-n)*(1/6)),2,1,1)-R(n,2,1,1))/(R(n+ceil((a2(i2)-
n)*(1/6)),1,1,1)-R(n,1,1,1))); % gr_Avn: ration of gradient between puI and the 1/6 of puI
                if  gr_Avn>1e+5; gr_Avn=1e+5; end
                if  gr_Avn<1; gr_Avn=1; end
                gr_Avn2=abs((R(a2(i2),2,1,1)-R(n,2,1,1))/(R(a2(i2),1,1,1)-
R(n,1,1,1)))/abs((R(n+ceil(2*cp_numpoints(i2)/2),2,1,1)-
R(n,2,1,1))/(R(n+ceil(2*cp_numpoints(i2)/2),1,1,1)-R(n,1,1,1))); % gr_Avn: ratio of gradient
between puI and the 1/6 of puI
                gr_Avn3=abs((R(a2(i2),2,1,1)-R(n,2,1,1))/(R(a2(i2),1,1,1)-
R(n,1,1,1)))/abs((R(a2(i2),2,1,1)-R(1,2,1,1))/(R(a2(i2),1,1,1)-R(1,1,1,1))); % gr_Avn: ratio
of gradient between (n-1) and the puI
                gr_Avn4=abs((R(n+ceil((a2(i2)-n)/1.33),2,1,1)-R(n,2,1,1))/(R(n+ceil((a2(i2)-
n)/1.33),1,1,1)-R(n,1,1,1)))/abs((R(n+ceil((a2(i2)-n)/1),2,1,1)-R(1,2,1,1))/(R(n+ceil((a2(i2)-
n)/1),1,1,1)-R(1,1,1,1))); % gr_Avn: ration of gradient between puI and the 1/6 of puI
                gr_Avn41=abs((R(n+ceil((a2(i2)-n)/1.33),2,1,1)-R(n,2,1,1))/(R(n+ceil((a2(i2)-
n)/1.33),1,1,1)-R(n,1,1,1)))/abs((R(n+ceil((a2(i2)-n)/1),2,1,1)-R(n,2,1,1))/(R(n+ceil((a2(i2)-
n)/1),1,1,1)-R(n,1,1,1))); % gr_Avn: ration of gradient between puI and the 1/6 of puI
                gr_Avn5=abs((R(a2(i2),2,1,1)-R(a2(i2)-5,2,1,1))/(R(a2(i2),1,1,1)-R(a2(i2)-
5,1,1,1)))/abs((R(a2(i2)-5,2,1,1)-R(1,2,1,1))/(R(a2(i2)-5,1,1,1)-R(1,1,1,1))); % gr_Avn: ratio
of gradient between puI and the 1/6 of puI
                MAPS2(i2,[14 34 38 50 56 77])=[gr_Avn gr_Avn2 gr_Avn3 gr_Avn4 gr_Avn5
gr_Avn6]; % Mapping of gr_Avn values
                cp_num2=ceil(((nthroot((100-5),2))/100)*cp_numpoints(i2)*(2/3));
                cp_perc_graddefl_relpos=cp152*((n/a2(i2))/nthroot(gr_Avn,3)+(((1-
(n/a2(i2)))^2)/nthroot(gr_Avn,3))^(1))*(1); % instead of cp_perc_deltagraddefl

cp_perc_deltadefl_relpos=cp151*((Z_velocity*(10^6))*(cpddf))*(((50+((5)*(nthroot(ceil(SampleRa
te2/250),4)))))/(((ceil(5000/SampleRate2))^(5/3))*nthroot(SampleRate2,2)));
                MAPS2(i2,87)=cp_perc_graddefl_relpos; MAPS2(i2,86)=cp_perc_deltadefl_relpos;
                MAPS2(i2,35:36)=[cp_perc_deltadefl_relpos,cp_perc_graddefl_relpos];
                deflgradtot2 = (R(a2(i2)-1,2,1,1)-R(n,2,1,1))/(R(a2(i2)-1,1,1,1)-R(n,1,1,1));
                ratio_deflgradtot=deflgradtot2/deflgradtot;
                MAPS2(i2,37)=ratio_deflgradtot;
                evrosdefl2=R(a2(i2)-1,2,1,1)-R(n,2,1,1);
                cp_perc0_relpos=(30*nthroot(gr_Avn,3)+1)/cp153;

cp_perc1_relpos=50/cp154+((ceil(nthroot(SampleRate/1000,1.4)+1))^(2))*((ratio_deflgradtot)^(1/
4));

cp_perc2_relpos=50/cp155+(ceil(SampleRate/1000))^(2.15)+(nthroot(gr_Avn5,2))^(0);
                if  cp_perc2_relpos>=95; cp_perc2_relpos=95; end
                cp_num_end=ceil(step_cp_numpoints)*cp_numpoints(i2);
                cp_num_end_2=ceil((cp_num_end)); MAPS2(i2,85)=cp_num_end_2;
                if a2(i2)<=n+cp_num_end_2+cp_num2; cp_num_end_2=a2(i2)-1-cp_num2-n; end
                cpkalo1=(R(n+1*cp_num_end_2,2,1,1)-R(n,2,1,1));
cpkalo2=abs(R(n+ceil(cp_num_end_2/2),2,1,1)-R(n,2,1,1));
                for cp_num=1:step_cp_numpoints:ceil(cp_num_end_2)
                    % 1ST CONDITION - check (for each cp_num) how the DEVIATION IN DEFLECTION
                    % (y-axis) between n and cp_num compares to the whole puI (part under
Investigation)
                    if     abs(R(n+cp_num,2,1,1)-
R(n,2,1,1))>=(cp_perc_deltadefl_relpos/100)*abs(evrosdefl) ...
                        && abs(R(n+1*cp_num,2,1,1)-
R(n,2,1,1))>=((cp_perc_deltadefl_relpos/100/2))*abs(evrosdefl2)...
                            cp_1stcon_defl=cp_1stcon_defl+1;
                    else
                    end
```

```
                    % 2ND CONDITION - check for UNWANTED INCLINATION inside the puI / huge
(relatively) inclinations that would decrease
                    % the possibilities of a possible (& plausible) contact point
                    cp_puI_divs=1; % split puI in equal parts [puI/cp_numpoints]
                    cp132=(abs(R(n+ceil(cp_numpoints(i2)/2*ceil(SampleRate/2000)),2,1,1)-
R(n,2,1,1)))/(abs(R(n+ceil(cp_numpoints(i2)/2*ceil(SampleRate/2000)),1,1,1)-R(n,1,1,1)));
                    if cp_num<ceil(cp_numpoints(i2)/10)
                    else
                        if  (abs(R(n+cp_puI_divs*cp_num+2,2,1,1)-
R(n+cp_num,2,1,1)))/(abs(R(n+cp_puI_divs*cp_num+2,1,1,1)-R(n+cp_num,1,1,1)))...
                         >= (nthroot(gr_Avn2,3)+2)*(cp132)
                            cp_2ndcon_unwantincl=cp_2ndcon_unwantincl+1;
                        end
                    end
                    % 3RD CONDITION - check how the DEVIATION IN GRADIENT OF THE DEFLECTION
WITH RESPECT TO ZSNSR (inclination)
                    % between n and cp_num compares to the whole puI (part under
Investigation) with respect to ZSnsr
                    if     abs((R(n+cp_num,2,1,1)-R(n,2,1,1))/(R(n+cp_num,1,1,1)-R(n,1,1,1)))
>= (cp_perc_graddefl_relpos)*abs(deflgradtot)...
                        && abs((R(n+ceil(cp_num/2),2,1,1)-
R(n,2,1,1))/(R(n+ceil(cp_num/2),1,1,1)-R(n,1,1,1))) >=
(cp_perc_graddefl_relpos)*abs(deflgradtot)...
                            cp_3rdcon_graddefl=cp_3rdcon_graddefl+1;
                    else
                    %      cp14=cp14-0.5;
                    end
                    % 4TH CONDITION - check if there is DIFFERENT INCLINATION
                    if     (((R(n+cp_num,2,1,1)-R(n,2,1,1))/(R(n+cp_num,1,1,1)-R(n,1,1,1)))>=0
&& deflgradtot>=0)...
                       || (((R(n+cp_num,2,1,1)-R(n,2,1,1))/(R(n+cp_num,1,1,1)-R(n,1,1,1)))<=0
&& deflgradtot<=0)
                            cp_4thcon_diffincl=cp_4thcon_diffincl+1;
                    end
                    % 5TH CONDITION - check (for each cp_num) if the SIGNUM of
                    % the whole puI (part under Investigation) is the same with each
(cp_num+1)-(cp_num)
                    if sign(evrosdefl)==sign(R(n+cp_num+5,2,1,1)-R(n,2,1,1))
                       cp_5thcon_signum=cp_5thcon_signum+1;
                    end
                    % 6TH CONDITION - check (for each cp_num) if the SIGNUM of
                    % the whole puI (part under Investigation) is the same with each
(cp_num+1)-(cp_num)
                    cp_6thcon_signum=n/a2(i2);
                end
                % CP CONDITIONS END
                % CP MEET CONDITIONS START
                if     cp_1stcon_defl       >=   (cp_perc1_relpos/100)*ceil((cp_num_end_2))
&& ...
                       cp_2ndcon_unwantincl <=   (cp_perc0_relpos/100)*ceil((cp_num_end_2))
&& ...
                       cp_3rdcon_graddefl   >=   (cp_perc2_relpos/100)*ceil((cp_num_end_2))
&& ...
                       cp_4thcon_diffincl   >=   (cp_perc3/100)*ceil((cp_num_end_2))
&& ...
                       cp_5thcon_signum     >=   (cp_perc3/100)*ceil((cp_num_end_2))
&& ...
                       evi==0
                            evi=n+ceil((1-cp_1stcon_defl/cp_num_end_2)*cp_num_end_2); %noCP=n;
                            MAPS2(i2,28:32)=[cp_1stcon_defl cp_2ndcon_unwantincl
cp_3rdcon_graddefl cp_4thcon_diffincl cp_5thcon_signum];
                            MAPS2(i2,[13,84])=evi;
                            break
                else
                end
            end
            % under test CP evaluation section [test_CP_22.31]
            if goodCP(i2)==4
                goodCP(i2)=goodCP(i2)+1;
            else
                Fmax_CP(i2)=abs(R(a2(i2)-1,2,1,1));
                msp_all_valuesCP=30;
                msp_ple_valuesCP=[5 10];
                optionsCP=optimset('MaxFunEvals',1000,'MaxIter',200,'TolFun',1e-8,'TolX',1e-
4);
                for msp_pleCP=msp_ple_valuesCP
```

```
                    for msp_allCP=msp_all_valuesCP
                        msp_parcon2CP=(R(evi+ceil((a2(i2)-evi)*((msp_allCP/5-
(sqrt(msp_allCP/5))*.5)/10)),2,1,1)-0.05*Fmax_CP(i2))...
                                      /(R(evi+ceil((a2(i2)-evi)*((msp_allCP/5-
(sqrt(msp_allCP/5))*.5)/10)),1,1,1)^(2));
                        [abest_all_10_CP(ceil(msp_allCP/5)-
5,msp_pleCP/5),fval_all_10_CP(ceil(msp_allCP/5)-5,msp_pleCP/5)] = ...
                        fminsearch(@(a) nthroot((sum((abs(abs(R(ceil(evi+(a2(i2)-
evi)*(msp_allCP/5-1)/10):a2(i2),2,1,1))-...
                                        a.*abs(R(ceil(evi+(a2(i2)-evi)*(msp_allCP/5-
1)/10):a2(i2),1,1,1)).^((msp_pleCP/5)-.5*ceil(msp_pleCP/5)+(ceil(5/msp_pleCP))^1))).^(2)))/...
                                        (((abs(a2(i2)-ceil(evi+(a2(i2)-evi)*(msp_allCP/5-
1)/10)))/1)^(1)),2),msp_parcon2CP,optionsCP);
                    end
                end
                if fval_all_10_CP(1,1) > Fmax_CP(i2)/100 || fval_all_10_CP(1,2) >
Fmax_CP(i2)/100
                    cp151=cp151*2/cp99;
                    cp152=cp152*2/cp99;   % under test CP evaluation section [test_CP_23.5.31]
                    cp153=cp153*1.01357/cp99;
                    cp154=cp154*1.2/cp99;
                    cp155=cp155*1.2/cp99;
                    cp156=cp156*1.05;
                    goodCP(i2)=goodCP(i2)+1;
                else
                    goodCP(i2)=goodCP(i2)+5;
                    MAPS2(i2,13)=evi;
                end
            end
        end
    end
    if evi==0; MAPS2(i2,88)=1; end
    if i2>1
        if (evi==0 || isnan(evi)==1) && FI_size>=MAPS2(i2-1,13)
                evi=ceil(.95*a2(i2));
                MAPS2(i2,13)=evi;
        elseif (evi==0 || isnan(evi)==1) && FI_size<MAPS2(i2-1,13)
                evi=ceil(.95*a2(i2));
                MAPS2(i2,13)=evi;
        end
    else
        if (evi==0 || isnan(evi)==1)
            evi=ceil(.95*a2(i2));
            MAPS2(i2,13)=evi;
        end
    end
    cistart100 = ceil(((100-cp_perc_deltagraddefl)/100)*cp_numpoints(i2)); cincl=0;
    for ci100=MAPS2(i2,13)+cistart100+5:ceil(SampleRate/2000):a2(i2)-5
        ci1(i2)=0; ci2(i2)=0; ci3(i2)=0;
        if    abs((R(ci100+5,2,1,1)-R(ci100,2,1,1))/(R(ci100+5,1,1,1)-R(ci100,1,1,1))) <= ...
              abs((R(ci100,2,1,1)-R(MAPS2(i2,13)+cistart100,2,1,1))/(R(ci100,1,1,1)-
R(MAPS2(i2,13)+cistart100,1,1,1)))
              ci1(i2)=ci1(i2)+1;
              ci78=ci100+1*ceil((ceil(a2(i2)*2))*20/1000); if ci78>a2(i2); ci78=a2(i2); end
              for cp1121=ci100:ceil(SampleRate*5/1000):ci78
                  if   abs((R(cp1121+5,2,1,1)-R(cp1121,2,1,1))/(R(cp1121+5,1,1,1)-
R(cp1121,1,1,1))) <= ...
                       abs((R(ci100+5,2,1,1)-R(ci100,2,1,1))/(R(ci100+5,1,1,1)-
R(ci100,1,1,1)))
                       ci3(i2)=ci3(i2)+1;
                  end
              end
              if  ci3(i2)>=(SampleRate*20/1000)*(8/10)/7
                  ci2(i2)=ci2(i2)+1;
              end
        end
        if  ci1(i2)>=1 && ci3(i2)>=1
            cincl=cincl+1;
            MAPS2(i2,11)=.5;
            MAPS2(i2,10)=ci100+(SampleRate*20/1000)*(4/10); MAPS2(i2,10)=ci100+2;
            MAPS2(i2,53)=100-((MAPS2(i2,10)-MAPS2(i2,13))/(a2(i2)-MAPS2(i2,13)))*100;
            break
        end
    end
    if CP_adjustm==1
        Fmax_CP(i2)=abs(R(a2(i2)-1,2,1,1));
```

```
        k32=find(R(:,1,1,1),1,'last');
        k_adj=ceil((a2(i2)-evi)/10);
        k91=evi-ceil(1.5*k_adj); if k91<=0; k91=1; end
        a91=find(R(:,1,1,1),1); a92=find(R(:,1,1,1),1,'last');
        k93=evi+ceil(.5*k_adj); k94=ceil((k93-k91)/10);
        k92=find(R(:,1,1,1),1,'last')+1;
        k_abest_all(:)=0; k_fval_all(:)=0;
        options=optimset('MaxFunEvals',200,'MaxIter',200,'TolFun',1e-7);
        for k_msp_ple=1:10
            for k_msp_all=1:10
                k_msp_parcon2=(abs(R(k91+ceil((k93-k91)*((k_msp_all-
(nthroot(k_msp_all,2))*.5)/10)),2,1,1))-0.1*...
                    Fmax_CP(i2))/abs((R(k91+ceil((k93-k91)*((k_msp_all-
(sqrt(k_msp_all))*.5)/10)),1,1,1))^(1+7.5/10));
                [k_abest_all(k_msp_all,k_msp_ple),k_fval_all(k_msp_all,k_msp_ple)] = ...
                    fminsearch(@(k_a) nthroot((sum((abs(abs(R(ceil(k91+(k_msp_all/10)*(k93-
k91)):ceil(SampleRate/4000):a2(i2),2,1,1))-...
                    k_a.*abs(R(ceil(k91+(k_msp_all/10)*(k93-
k91)):ceil(SampleRate/4000):a2(i2),1,1,1)).^((k_msp_ple/10)+1))).^(2)))/...
                    (((a2(i2)-ceil(k91+(k_msp_all/10)*(k93-
k91)))/ceil(SampleRate/4000))^(1)),2),k_msp_parcon2,options); % ,optimset('MaxFunEvals',200)
            end
        end
        [k_fval_min,k_fval_pos] = min(nonzeros(k_fval_all(:)));
        [k_fval_pos_row, k_fval_pos_col] = ind2sub(size(k_fval_all),k_fval_pos);
        MAPS2(i2,33)=k_fval_pos_row;
        MAPS2(i2,4)=1+k_fval_pos_col/10;
        evi=k91+k_fval_pos_row*k94;
        MAPS2(i2,13)=evi;
    end
    R(:,3:4,1,1)=[(R(:,1,1,1)-R(:,2,1,1))-(R(evi,1,1,1)-R(evi,2,1,1)),(K_t).*(R(:,2,1,1)-
R(evi,2,1,1))];
    defl_for_error_analysis = R(evi,2,1,1);
    R(1:evi-1,1:8,1,1)=0; % leave only CP data
    R(:,11:12,1,1)=[(R(:,9,1,1)-R(:,10,1,1))-(R(evi,9,1,1)-R(evi,10,1,1)),(K_t).*(R(:,10,1,1)-
R(evi,10,1,1))]; %
    a31=find(R(:,1,1,1),1);
    a32=find(R(:,1,1,1),1,'last');
    if isempty(a31)==1 && isempty(a32)==1 % skipping distorted waves
    MAPS2(i2,:)=0; R=[];
    continue
    end
    R(:,[13:14 28:29],1,1)=R(:,[11:12 11:12],1,1); %
    R(1:a2(i2),28:29,1,1)=0;
    R(1:a2(i2),13:14,1,1)=0;
    f_n2= find(R(:,14,1,1)<0,1);
    if isempty(f_n2)==0
        f_n(i2) = f_n2;
    else
    end
    p=0;
    Fad=0;
    a6=0;
    MAPS2(i2,40)=a2(i2);
    if f_n(i2)>0
    MAPS2(i2,39)=1;
    MAPS2(i2,41)=f_n(i2);
    p=(R(f_n(i2)-1,28,1,1)+R(f_n(i2),28,1,1))/2;
    p3(i2)=R(f_n(i2)-1,28,1,1);
    p1=R(f_n(i2)-1,28,1,1);
    R(f_n(i2):end,13:14,1,1)=0;
    end
    R(:,13,1,1)=fliplr(R(:,13,1,1))-p;
    R(:,14,1,1)=fliplr(R(:,14,1,1)); %
    if isempty(f_n(i2))==0
            R_del=zeros(FI_size,1);
            R_del(:)=R(:,28,1,1);
            R_del(R_del<0)=0;
            R(:,28,1,1)=R_del(:);
            a_del=find(R(:,28,1,1),1,'last');
            R(a_del:end,29,1,1)=0;
            [a5,a6]=min(R(:,29,1,1));
            MAPS2(i2,45)=a6;
            R(a6+1:end,28:29,1,1)=0;
            Fad=abs(R(a6,12,1,1));
            Fad_d=abs(R(a6,11,1,1));
```

```
    else
    for i09=a2(i2)+(FI_size-a2(i2))/4:2:FI_size-(FI_size-a2(i2))/4
        if abs(R(i09,28,1,1)-R(evi,28,1,1))<=(R(a2(i2),28,1,1)-R(1,28,1,1))/200
            a6=i09;
        end
    end
    MAPS2(i2,45)=SampleRate-evi;
    R((evi+2*(a2(i2)-evi))+1:end,28:29,1,1)=0; % leave only CP data
    end
    Fmax=abs(R(a2(i2),12,1,1));
    delta_max=abs(R(a2(i2),11,1,1));
    Adhes_work=-2/3*(Fad/pi*Rtip);
    Fratio=Fad/Fmax*100;
    MAPS2(i2,44)=Fad;
    MAPS2(i2,42)=Fmax; % map of Fmax
    MAPS2(i2,15)=Fratio;
    MAPS2(i2,16)=Adhes_work;
    R(:,28,1,1)=fliplr(R(:,28,1,1)); %
    R(:,28,1,1)=R(:,28,1,1); %
    R(:,29,1,1)=fliplr(R(:,29,1,1)); %
    R(:,29,1,1)=R(:,29,1,1)+Fad; %
    f_r=f_n(i2)-1;
    if isempty(f_r)==1
        f_r=FI_size-evi-abs(a2(i2)-evi)/4;
        p5=0;
    else
        p5=Fad_d;
    end
    if DMT==1
    msp_ple_DMT=5;
    msp_parcon_DMT2=abs((R(a2(i2)+ceil((f_r-a2(i2))/2),29,1,1)-
0.05*Fmax)/((R(a2(i2)+ceil((f_r-a2(i2))/2),28,1,1)-p5)^(3/2)));
    options=optimset('MaxFunEvals',200,'MaxIter',200,'TolFun',1e-7,'TolX',1e-4);
    msp_all_DMT=10;
    [abest_DMT,fval_DMT] = fminsearch(@(w)
sqrt(double(sum((abs(R(a2(i2):10:ceil(a2(i2)+(msp_all_DMT/10)*(a6-a2(i2))),29,1,1))-...
                            w.*abs(R(a2(i2):10:ceil(a2(i2)+(msp_all_DMT/10)*(a6-
a2(i2))),28,1,1)-p5).^((msp_ple_DMT/10)+1)).^2)/...
                            ((ceil(a2(i2)+(msp_all_DMT/10)*(a6-a2(i2)))-
a2(i2))^(1)))),msp_parcon_DMT2,options);
    E_DMT=(3*abest_DMT)/(4*((Rtip)^(0.5)));
    MAPS2(i2,43)=(1-(Pratiosample)^2)/abs((1/(E_DMT))-((1-(Pratiotip)^2)/(Etip))); % modulus
map
    R(:,30,1,1) = abest_DMT.*(R(:,28,1,1).^(1.5));
    MAPS2(i2,55)=abest_DMT;
    else
    R(:,30,1,1)=0;
    end
    if O_PHARR==1
    S=(R(a2(i2)+ceil(SampleRate/500),12,1,1)-R(a2(i2)+5*ceil(SampleRate/500),12,1,1))/...
      (R(a2(i2)+ceil(SampleRate/500),11,1,1)-R(a2(i2)+5*ceil(SampleRate/500),11,1,1));
    delta_c=abs(R(a2(i2),11,1,1))-(epsil*(Fmax/S));
    if     OP_Ac==1
        A_c=24.5*(delta_c)^2;
    elseif OP_Ac==2
        A_c=C_0*(delta_c)^2+C_1*(delta_c)+C_2*sqrt(delta_c);
    end
    E_OPHARR=(S*sqrt(pi))/(2*beta*sqrt(A_c));
    MAPS2(i2,46)=(1-(Pratiosample)^2)/abs((1/(E_OPHARR))-((1-(Pratiotip)^2)/(Etip))); %
modulus map
    end
    if DMT==1
        f_r=f_n(i2)-1;
        if isempty(f_r)==1
            f_r=FI_size-evi-abs(a2(i2)-evi)/4;
            p2=0;
            p4=0;
            p5=0;
        else
            p2=p3(i2);
            p4=Fad;
            p5=Fad_d;
        end
        msp_ple_retract=5;
        options=optimset('MaxFunEvals',200,'MaxIter',200,'TolFun',1e-7,'TolX',1e-1);
        msp_all_retract=10;
```

```
        [abest_retract,fval_retract] = ...
                                fminsearch(@(w_r)
sqrt(double(sum((abs(R(a2(i2):5:ceil(a2(i2)+(msp_all_retract/10)*(f_r-a2(i2))),29,1,1))-...
                                ((w_r.*abs(R(a2(i2):5:ceil(a2(i2)+(10/10)*(f_r-
a2(i2))),28,1,1)-p5)).^((msp_ple_retract/10)+1))).^2)/...
                                ((ceil(a2(i2)+(msp_all_retract/10)*(f_r-a2(i2)))-
a2(i2))^(1)))),msp_parcon_DMT2,options);
        [fval_min_r,fval_pos_r] = min(fval_retract(:));
        rb1=1+fval_pos_r/10;
        if      isempty(f_n(i2))==0
                fun2 = @(x2) abest_DMT*((x2-p5)^(1.5))-p4;
                psi_p2(i2) = abs(integral(fun2,p2,delta_max,'ArrayValued',true));
        elseif  isempty(f_n(i2))==1
                psi_p2(i2)=1;
        end
    end
    R(:,21:22,1,1)=R(:,3:4,1,1);
if modtomo==1
 st2=10;
else
 st2=1;
end
for st1=10/stposa:10/stposa:st2
stkk=1;
    if st1==stkk
        if cut==1
            a3101=0;
            a3102=0;
            c_01=.005;
            while a3101==0
                c_01=c_01*2;
                for i=a31+1:a32
                    if abs(R(a31,3)-R(i,3))>(1-c_01)*cutp && abs(R(a31,3)-
R(i,3))<(1+c_01)*cutp
                        a3101=i;
                        break;
                    end
                end
                if a3101>0
                    R(a3101:end,[1:8 15:20],1,1)=0; % delete last 8% of CP data
                end
                if c_01>.8; break; end
            end
        else
            R(a32-ceil((fit_perc_end/100)*(a32-1-a31)):end,[1:8 15:20],1,1)=0; % delete last
8% of CP data
        end
        a91=find(R(:,4,1,1),1)+1;
        a92=find(R(:,4,1,1),1,'last');
        R(a31:a91,21:22,1,1)=0; %
        R(a92+(a92-a91):end,21:22,1,1)=0; %
        R(a32:end,3:6,1,1)=0;
    end
    if st1==stkk
        if isempty(a91)==1 % skipping lost waves
            MAPS2(i2,:)=0; R1_2(:,:)=zeros(Rsize12,noRcol_1);
R2_2(:,:)=zeros(Rsize12,noRcol_2); miss_data=miss_data+1; R=[]; st456=1;
        break
        end
    end
    if st1==stkk
        if modtomo==1
            msp_all_values=ceil(10/stposa):ceil(10/stposa):10;
        else
            msp_all_values=[5 10];
        end
        options=optimset('MaxFunEvals',1000,'MaxIter',1000,'TolFun',1e-12,'TolX',1e-4);
        abest_all_10=zeros(size(msp_all_values,2),size(msp_ple_values,2));
fval_all_10=zeros(size(msp_all_values,2),size(msp_ple_values,2));
        for msp_ple=msp_ple_values
            for msp_all=msp_all_values
                msp_parcon2=(R(a91+ceil((a92-a91)*((msp_all-(sqrt(msp_all))*.5)/15)),4,1,1)-
0.05*Fmax)/(R(a91+ceil((a92-a91)*((msp_all-(sqrt(msp_all))*.5)/15)),3,1,1)^(msp_ple));
                [abest_all_10(msp_all,msp_ple),fval_all_10(msp_all,msp_ple)] = ...
```

```
                fminsearch(@(a)
nthroot((sum((abs(abs(R(ceil(a91):ceil(SampleRate/3000):ceil(a91+(msp_all/10)*(a92-
a91)),4,1,1))-...
                a.*abs(R(ceil(a91):ceil(SampleRate/3000):ceil(a91+(msp_all/10)*(a92-
a91)),3,1,1)).^((msp_ple/10)+1))).^(2)))/...
                (((abs(ceil(a91+(msp_all/10)*(a92-a91))-
a91+1))/ceil(SampleRate/3000))^(1)),2),msp_parcon2,options);
            end
        end
        if abest_all_10(3,5)==0; abest_all_10(3,5)=abest_all_10(4,5); end
        if abest_all_10(2,5)==0; abest_all_10(2,5)=abest_all_10(3,5); end
        if abest_all_10(1,5)==0; abest_all_10(1,5)=abest_all_10(2,5); end
        if abest_all_10(3,10)==0; abest_all_10(3,10)=abest_all_10(4,10); end
        if abest_all_10(2,10)==0; abest_all_10(2,10)=abest_all_10(3,10); end
        if abest_all_10(1,10)==0; abest_all_10(1,10)=abest_all_10(2,10); end
        [bh71, bh72]=min(fval_all_10,[],2);
        [fval_min(i2),fval_pos] = min(abs(fval_all_10(10,:)));
        [fval_pos_row, fval_pos_col] = ind2sub(size(fval_all_10(10,:)),fval_pos);
        MAPS2(i2,78)=1+fval_pos_col/10;
        if modtomo==1 && modtomo_plus==1
            for klkl1=1:9
                [fval_min1,fval_pos(klkl1)] = min(fval_all_10(klkl1,:));
                [fval_pos_row, fval_pos_col(klkl1)] =
ind2sub(size(fval_all_10(klkl1,:)),fval_pos(klkl1));
                MAPS2(i2,91+klkl1)=1+fval_pos_col(klkl1)/10;
                MAPS2(i2,114+klkl1)=fval_min1;
                MAPS2(i2,124+klkl1)=fval_all_10(klkl1,5);
                MAPS2(i2,134+klkl1)=fval_all_10(klkl1,10);
            end
            [fval_min2,fval_pos2] = min(fval_all_10(10,:));
            [fval_pos_row2, fval_pos_col2] = ind2sub(size(fval_all_10(10,:)),fval_pos2);
            MAPS2(i2,78)=1+fval_pos_col2/10;
            MAPS2(i2,124)=fval_min2;
            MAPS2(i2,134)=fval_all_10(10,5);
            MAPS2(i2,144)=fval_all_10(10,10);
        end
        MAPS2(i2,83)=fval_min(i2);
        abest2=0;
            if fval_all_10(10,5)<=fval_all_10(10,10)
                abest=abest_all_10(10,5);
                MAPS2(i2,51)=abest;
                abest2=abest_all_10(10,10);
                % ple=1.5;
            elseif fval_all_10(10,5)>fval_all_10(10,10)
                abest=abest_all_10(10,5);
                abest2=abest_all_10(10,10);
                % ple=2;
            end
            deltaabest=options.TolX;
    end
    if st1==stkk
            R(:,6,1,1) = abest.*(R(:,3,1,1).^(1.5));
        R(:,23,1,1) = abest.*(R(:,21,1,1).^(1.5));
            R(:,15,1,1) = abs(abest2).*(R(:,3,1,1).^(2));
        R(:,24,1,1) = abs(abest2).*(R(:,21,1,1).^(2));
        R(:,7,1,1) = (R(:,15,1,1) - R(:,4,1,1)).^2;
        R(:,8,1,1) = (R(:,6,1,1) - R(:,4,1,1)).^2;
        R(a91+1:3:a92,19,1,1)=abs((R(a91+1:3:a92,4,1,1)-R(a91:3:a92-
1,4,1,1))./(R(a91+1:3:a92,3,1,1)-R(a91:3:a92-1,3,1,1)));
        R(a91+1:3:a92,25,1,1)=abs((R(a91+1:3:a92,4,1,1)-R(a91:3:a92-
1,4,1,1))./((R(a91+1:3:a92,3,1,1)-R(a91:3:a92-1,3,1,1)).^2));
            R(:,17,1,1)=R(:,22,1,1);
        R(a91:1:a91+(a92-a91),17,1,1)=R(a91,17,1,1)+((R(a92,17,1,1)-R(a91,17,1,1))/((a92)-
a91))*(0:1:(a92-a91));
        R(:,18,1,1) = (R(:,6,1,1) - R(:,17,1,1)).^2;
        R(:,16,1,1) = (R(:,15,1,1) - R(:,17,1,1)).^2;
        R(:,20,1,1) = (R(:,17,1,1) - R(:,4,1,1)).^2;
    end
    % fit error analysis
    SumOfResids_p = sum(R(a91:ceil(a91+((stposa+1-st1)*(100/stposa)/100)*(a92-a91)),8)); %
    SumOfResids_c = sum(R(a91:ceil(a91+((stposa+1-st1)*(100/stposa)/100)*(a92-a91)),7)); %
    SumOfResids_l = sum(R(a91:ceil(a91+((stposa+1-st1)*(100/stposa)/100)*(a92-a91)),20)); %
    SumOfResids_p_l = sum(R(a91:ceil(a91+((stposa+1-st1)*(100/stposa)/100)*(a92-a91)),18));
    SumOfResids_c_l = sum(R(a91:ceil(a91+((stposa+1-st1)*(100/stposa)/100)*(a92-a91)),16));
    rms_p = sqrt(SumOfResids_p/abs(ceil(a91+((stposa+1-st1)*(100/stposa)/100)*(a92-a91))-1-
a91)); %
```

```
    rms_c = sqrt(SumOfResids_c/abs(ceil(a91+((stposa+1-st1)*(100/stposa)/100)*(a92-a91))-1-
a91)); %
    rms_l = sqrt(SumOfResids_l/abs(ceil(a91+((stposa+1-st1)*(100/stposa)/100)*(a92-a91))-1-
a91)); %
    if st1==stkk
        MAPS2(i2,7:9)=[rms_p rms_c rms_l];
    end
    rms_ple1=sqrt(SumOfResids_p_l/(ceil(a91+((stposa+1-st1)*(100/stposa)/100)*(a92-a91))-1-
a91));
    rms_ple2=sqrt(SumOfResids_c_l/(ceil(a91+((stposa+1-st1)*(100/stposa)/100)*(a92-a91))-1-
a91));
    if st1==stkk
        MAPS2(i2,5)=abs((SumOfResids_p_l-SumOfResids_p)/SumOfResids_p_l);
        MAPS2(i2,6)=abs((SumOfResids_c_l-SumOfResids_c)/SumOfResids_c_l);
        if          MAPS2(i2,6)>=0.5 && MAPS2(i2,6)<=1 && MAPS2(i2,8)<MAPS2(i2,7)
                    MAPS2(i2,3)=2;
        elseif      MAPS2(i2,5)>=0.5 && MAPS2(i2,5)<=1 && rms_p<rms_c
                    MAPS2(i2,3)=1.5;
        elseif      MAPS2(i2,5)<=0.5 && MAPS2(i2,5)>=-0.5 ...
                && MAPS2(i2,6)<=0.5 && MAPS2(i2,6)>=-0.5
                    MAPS2(i2,3)=1;
        else
                    MAPS2(i2,3)=0.5;
        end
    else
        sto_1=abs((SumOfResids_p_l-SumOfResids_p)/SumOfResids_p_l);
        sto_2=abs((SumOfResids_c_l-SumOfResids_c)/SumOfResids_c_l);
        if          sto_2>=0.4 && sto_2<=1 && MAPS2(i2,8)<MAPS2(i2,7)
                    MAPS2(i2,77-st1)=2;
        elseif      sto_1>=0.4 && sto_1<=1 && rms_p<rms_c
                    MAPS2(i2,77-st1)=1.5;
        elseif      sto_1<=0.4 && sto_1>=-0.4 ...
                && sto_2<=0.4 && sto_2>=-0.4
                    MAPS2(i2,77-st1)=1;
        else
                    MAPS2(i2,77-st1)=0.5;
        end
    end
    if st1==stkk
        if      strcmp(CM_model,'Hertz - parabolic')==1
                E=(3*abest)/(4*((Rtip)^(0.5)));
                grpie_parab=1;
        elseif strcmp(CM_model,'Hertz - conic')==1
                E=(abest2*pi)/(2*tan(phi));
                grpie_conic=1;
        elseif strcmp(CM_model,'Hertz - both')==1
                if      MAPS2(i2,3)==1.5
                        E=(3*abest)/(4*((Rtip)^(0.5)));
                elseif MAPS2(i2,3)==2
                        E=(abest2*pi)/(2*tan(phi));
                elseif MAPS2(i2,3)==1
                        E=(3*abest)/(4*((Rtip)^(0.5)));
                else
                        E=(3*abest)/(4*((Rtip)^(0.5)));
                end
                grpie_parab=1;
                grpie_conic=1;
        end
    end
    if st1==stkk
        fun1 = @(x1) abest*(x1^(1.5));
        psi_p1 = integral(fun1,0,delta_max,'ArrayValued',true);
        if   psi_p2(i2)==1
             psi_p2(i2)=psi_p1;
        else
        end
        psi_p=abs(psi_p1-psi_p2(i2))/psi_p1;
        MAPS2(i2,48)=psi_p*100;
        if MAPS2(i2,48)<=50
            if MAPS2(i2,15)<=15
                if      MAPS2(i2,3)==2
                        MAPS2(i2,49)=0.5; % Sneddon
                else
                        MAPS2(i2,49)=1; % Hertz
                end
            else
```

```
                MAPS2(i2,49)=1.65; % DMT
            end
        elseif MAPS2(i2,48)>50 && isempty(f_n(i2))==0
                MAPS2(i2,49)=2.9; % O-P
        elseif MAPS2(i2,48)>50 && isempty(f_n(i2))==1
                MAPS2(i2,49)=2.3; % Viscocity
        end
    end
end
if st456==1
continue
end
    % Young's modulus of sample (E1 +- DE1) is then calculated from E
    MAPS2(i2,1)=(1-(Pratiosample)^2)/abs((1/(E))-((1-(Pratiotip)^2)/(Etip))); % modulus map
    Eerr(1:9,1)=[4*(Pratiosample^2)*(deltaPratiosample^2)*((1-(Pratiosample^2))^2),...
                 4/3*sqrt(Rtip)*((1-(Pratiosample^2))^(-1))*(abest^(-1))-(Etip^(-1))*(1-
Pratiotip^2),...
                 4/3*sqrt(Rtip)*((1-(Pratiosample^2))^(-1))*(abest^(-1)),...
                 (.5)*deltaRtip*(Rtip^(-1)),...
                 2*deltaPratiosample*Pratiosample*((1-(Pratiosample^2))^(-1)),...
                 deltaabest*(abest^(-1)),...
                 (Etip^(-1))*(1-Pratiotip^2),...
                 2*deltaPratiotip*Pratiotip*(1-Pratiotip^2),...
                 deltaEtip*(Etip^(-1))];

    MAPS2(i2,2)=MAPS2(i2,1)*sqrt((Eerr(1,1)+((Eerr(2,1)^(-
1))*sqrt((abs(Eerr(3,1))*sqrt(Eerr(4,1)^2+Eerr(5,1)^2+Eerr(6,1)^2))^2+(abs(Eerr(7,1))*sqrt(Eer
r(8,1)^2+Eerr(9,1)^2))^2))^2)); % modulus error map
    Eerr=[];
    MAPS2(i2,17:18)=[max(R(:,4,1,1)),abs(R(a92,3,1,1)-R(a91,3,1,1))];

MAPS2(i2,19:26)=[(min(R(:,9,1,1))),(max(R(:,9,1,1))),(min(R(:,10,1,1))),(max(R(:,10,1,1))),...
    (min(R(:,11,1,1))),(max(R(:,11,1,1))),(min(R(:,12,1,1))),(max(R(:,12,1,1)))];
    R(size(R,1):Rsize12,:)=0;
    szR=size(R,1); if size(R,1)>Rsize12; R(Rsize12+1:end,:)=[]; end
    R1_2(:,:)=real(R(:,1:noRcol_1));
    R2_2(:,:)=real(R(:,noRcol_1+1:noRcol));
    R=[];
    array1=[]; array2=[];
    if modtomo==1
        for ster1=ceil(10/stposa):ceil(10/stposa):10
            try
                MAPS2(i2,56+ster1)=(1-
(Pratiosample)^2)/abs((1/((3*vpa(abest_all_10(ster1,5*modtomo_Hertz_or_Sned),10))/(4*((Rtip)^(
0.5)))))-((1-(Pratiotip)^2)/(Etip)));
            catch
                MAPS2(i2,56+ster1)=0;
            end
        end
        MAPS2(:,76)=MAPS2(:,3);
    end
    if modtomo==1 && modtomo_plus==1
            MAPStomo_2=zeros(100,1);
            for ster2=1:1:10
                for ster3=1:1:10
                MAPStomo_2((ster2-1)*10+ster3)=vpa(abest_all_10(ster3,ster2),10);
                end
            end
            MAPS2(:,76)=MAPS2(:,3);
        plnf1=[1.07850713095751e-14,5.00024998750062e-08];
        plnf2=[937453134.373828,-6.57830211739396e-15,1.87509372187641e-08];
        plnf3=[-288.925205773263,937453134.373831,1.01217597472848e-16,1.87509372187640e-08];
        plnf4=[-8.20189504383761e+24,-293.839938853527,1640543005.65893,1.80176862384832e-
14,1.17193354980688e-08];
        plnf5=[-7.88663413350908e+17,-8.20189504383765e+24,-
315.038508044421,1640543005.65894,1.52593314116600e-14,1.17193354980689e-08];
        plnf6=[1.46594227312860e+41,7.97454601303156e+18,-2.81940154958915e+25,-
1100.33341411788,2307013643.35813,2.04609064530311e-14,8.54534852297913e-09];
        plnf7=[-5.16848789072914e+35,1.46594227312860e+41,6.61237482460087e+19,-
2.81940154958915e+25,-2026.13353514102,2307013643.35813,7.68724016110062e-
15,8.54534852297912e-09];
        plnf8=[-3.33730322072998e+57,-
5.78393271372560e+35,7.69619763475903e+41,7.64966850206845e+19,-6.41413890691851e+25,-
2772.89460750707,2960667578.87395,2.57530005664057e-14,6.72946167587244e-09];
        plnf9=[-1.70149274466309e+52,-
3.33730322072998e+57,2.93579553687227e+36,7.69619763475899e+41,-1.41154104260417e+20,-
```

```
6.41413890691848e+25,1888.60786129952,2960667578.87394,-1.12597265681062e-
14,6.72946167587248e-09];
        plnf10=[8.62977609853574e+73,2.93201230010437e+52,-2.37782890074824e+58,-
5.85601744875808e+36,2.45316327203264e+42,3.93788420737930e+20,-1.20265113343323e+26,-
9986.51782841312,3608313716.98458,7.50757141213487e-14,5.55180559115409e-09];
        bh=MAPS2(i2,78);
        bh2=single((bh-1)*10);
        Beta2=iou(11-bh2); % Beta2=4.34*10^(-8)
        Beta3=(iou(11-bh2))*2^(iou3(11-bh2)-1)*((iou3(11-bh2)^2)/(iou3(11-
bh2)+1))*((gamma(iou3(11-bh2)/2)^2)/gamma(iou3(11-bh2)));
        Beta4=(iou(11-bh2))*2^(iou4(11-bh2)-1)*((iou4(11-bh2)^2)/(iou4(11-
bh2)+1))*((gamma(iou4(11-bh2)/2)^2)/gamma(iou4(11-bh2)));
        bh4=abs(single(ceil((100-MAPS2(i2,53))/10))); if bh4>10; bh4=10; end
        bh69=bh72(bh4);
        bh3=(abest_all_10(10,bh2)*((sqrt(3.14)*((Beta2)))^(bh-1))*(1/(bh-1)+1))/...
                        (2*(1/(bh-1))*(((gamma(1/(2*(bh-1))+1/2))/(gamma(1/(2*(bh-
1))+1)))^(bh-1)));
        bh31=(abest_all_10(10,bh2)*((sqrt(3.14)*((Beta4)))^(bh-1))*(1/(bh-1)+1))/...
                        (2*(1/(bh-1))*(((gamma(1/(2*(bh-1))+1/2))/(gamma(1/(2*(bh-
1))+1)))^(bh-1)));
        bh391=(abest_all_10(bh4,bh69)*((sqrt(3.14)*((Beta2)))^(bh-1))*(1/(bh-1)+1))/...
                        (2*(1/(bh-1))*(((gamma(1/(2*(bh-1))+1/2))/(gamma(1/(2*(bh-
1))+1)))^(bh-1)));
        for tyui56=1:bh
                bh37(tyui56)=(abest_all_10(10,tyui56)*((sqrt(3.14).*((iou(11-
(tyui56))))).^(((tyui56)/10+1)-1))*(1./(((tyui56)/10+1)-1)+1))/...
                        (2*(1./(((tyui56)/10+1)-1))*(((gamma(1/(2.*(((tyui56)/10+1)-
1))+1/2))/(gamma(1/(2.*(((tyui56)/10+1)-1))+1))).^(((tyui56)/10+1)-1)));
        end
        if     bh2==1
                        bh32=bh37(1);
        elseif bh2==2
                        bh32=plnf2(1)/sum(plnf2)*bh37(1)+ plnf2(2)/sum(plnf2)*bh37(2);
        elseif bh2==3
                        bh32=plnf3(1)/sum(plnf3)*bh37(1)+ plnf3(2)/sum(plnf3)*bh37(2)+
plnf3(3)/sum(plnf3)*bh37(3);
        elseif bh2==4
                        bh32=plnf4(1)/sum(plnf4)*bh37(1)+ plnf4(2)/sum(plnf4)*bh37(2)+
plnf4(3)/sum(plnf4)*bh37(3)+ plnf4(4)/sum(plnf4)*bh37(4);
        elseif bh2==5
                        bh32=plnf5(1)/sum(plnf5)*bh37(1)+ plnf5(2)/sum(plnf5)*bh37(2)+
plnf5(3)/sum(plnf5)*bh37(3)+ plnf5(4)/sum(plnf5)*bh37(4)+ plnf5(5)/sum(plnf5)*bh37(5);
        elseif bh2==6
                        bh32=plnf6(1)/sum(plnf6)*bh37(1)+ plnf6(2)/sum(plnf6)*bh37(2)+
plnf6(3)/sum(plnf6)*bh37(3)+ plnf6(4)/sum(plnf6)*bh37(4)+ plnf6(5)/sum(plnf6)*bh37(5)+
plnf6(6)/sum(plnf6)*bh37(6);
        elseif bh2==7
                        bh32=plnf7(1)/sum(plnf7)*bh37(1)+ plnf7(2)/sum(plnf7)*bh37(2)+
plnf7(3)/sum(plnf7)*bh37(3)+ plnf7(4)/sum(plnf7)*bh37(4)+ plnf7(5)/sum(plnf7)*bh37(5)+
plnf7(6)/sum(plnf7)*bh37(6)+ plnf7(7)/sum(plnf7)*bh37(7);
        elseif bh2==8
                        bh32=plnf8(1)/sum(plnf8)*bh37(1)+ plnf8(2)/sum(plnf8)*bh37(2)+
plnf8(3)/sum(plnf8)*bh37(3)+ plnf8(4)/sum(plnf8)*bh37(4)+ plnf8(5)/sum(plnf8)*bh37(5)+
plnf8(6)/sum(plnf8)*bh37(6)+ plnf8(7)/sum(plnf8)*bh37(7)+ plnf8(8)/sum(plnf8)*bh37(8);
        elseif bh2==9
                        bh32=plnf9(1)/sum(plnf9)*bh37(1)+ plnf9(2)/sum(plnf9)*bh37(2)+
plnf9(3)/sum(plnf9)*bh37(3)+ plnf9(4)/sum(plnf9)*bh37(4)+ plnf9(5)/sum(plnf9)*bh37(5)+
plnf9(6)/sum(plnf9)*bh37(6)+ plnf9(7)/sum(plnf9)*bh37(7)+ plnf9(8)/sum(plnf9)*bh37(8)+
plnf9(9)/sum(plnf9)*bh37(9);
        elseif bh2==10
                        bh32=plnf10(1)/sum(plnf10)*bh37(1)+ plnf10(2)/sum(plnf10)*bh37(2)+
plnf10(3)/sum(plnf10)*bh37(3)+ plnf10(4)/sum(plnf10)*bh37(4)+ plnf10(5)/sum(plnf10)*bh37(5)+
plnf10(6)/sum(plnf10)*bh37(6)+ plnf10(7)/sum(plnf10)*bh37(7)+ plnf10(8)/sum(plnf10)*bh37(8)+
plnf10(9)/sum(plnf10)*bh37(9)+ plnf10(10)/sum(plnf10)*bh37(10);
        end
        MAPS2(i2,79)=(1-(Pratiosample)^2)/abs((1/(bh3))-((1-(Pratiotip)^2)/(Etip))); %
        MAPS2(i2,80)=(1-(Pratiosample)^2)/abs((1/(bh391))-((1-(Pratiotip)^2)/(Etip)));
        MAPS2(i2,81)=(1-(Pratiosample)^2)/abs((1/(bh31))-((1-(Pratiotip)^2)/(Etip))); % Pharr-
Bolshakov
        MAPS2(i2,82)=(1-(Pratiosample)^2)/abs((1/(bh32))-((1-(Pratiotip)^2)/(Etip))); %
superposition according to beta
    end
    abest=0;
    deltaabest=0;
    abest_all1(i2,:,:)=abest_all_10(:,:);
    abest_all_10=[];
```

```
    k_abest_all=[]; k_fval_all=[];
    abest_all_10_CP=[];
    fval_all_101(i2,:,:)=fval_all_10(:,:);
    fval_all_10=[];
    abest_retract=[]; fval_retract=[];
    fval_all_10_CP=[];
    if modtomo==1 && modtomo_plus==1
    MAPStomo3(i2,:,:)=MAPStomo_2(:,:);
    MAPStomo_2=[];
    end
    R13(:,:,i2)=R1_2(:,:);
    R1_2=[];
    R23(:,:,i2)=R2_2(:,:);
    R2_2=[];
    ci78=[]; evi=[];
end
goodCP_1(i1,:)=goodCP(1,:);
a2_1(i1,:)=a2(1,:);
cp_numpoints211(i1,:)=cp_numpoints21(1,:);
a2=[]; f_n(i2)=[]; p3=[]; goodCP=[]; Fmax_CP=[]; cp_numpoints21=[];
abest_all_10_CP=[]; fval_all_10_CP=[];
ci1=[]; ci2=[]; ci3=[];
fval_min=[];
cp_numpoints_1(i1,:)=cp_numpoints(1,:);
cp_numpoints=[];
MAPS(i1,:,:)=MAPS2(:,:);
MAPS2=[];
if modtomo==1 && modtomo_plus==1
    abest_all1_2(i1,:,:,:)=abest_all1(:,:,:);    fval_all(i1,:,:,:)=fval_all_101(:,:,:);
    MAPStomo(i1,:,:,:)=MAPStomo3(:,:,:);    MAPStomo3=[];
end
abest_all1=[];fval_all_101=[];R1(:,:,i1,:)=R13(:,:,:);R13=[];R2(:,:,i1,:)=R23(:,:,:);R23=[];xa
b=[];
end
MAPS(:,:,90)=double(cp_numpoints211);MAPS(:,:,89)=double(M_ZSnsr_empty);
hold off
MAPS=real(MAPS);run_time=ceil(toc);
%%
num_randomspots=5*ceil((ceil((sqrt(PandL*PandL2))/10))^(2/2)); if num_randomspots<=8;
num_randomspots=9; end % how many random spots are picked for display
if PandL*PandL2<=50; num_randomspots=PandL*PandL2; end
listofgraphs=zeros(num_randomspots,2);
for nrs=1:num_randomspots;listofgraphs(nrs,1:2)=[randi(PandL),randi(PandL2)];end
for nrs2=1:num_randomspots
if nrs2>num_randomspots;    break;end
if MAPS(listofgraphs(nrs2,1),listofgraphs(nrs2,2),89)==1
    listofgraphs(nrs2,:)=[];    num_randomspots=num_randomspots-1;
end
end
shlog=0;shlog2=0;
%% s5 - create randomly selected FI curves and colormaps
cop89=strsplit(datestr(datetime)); cop92=strsplit(string(cop89(1)),'-');
cop93=strsplit(string(cop89(2)),':');
edo=['FMaps\Out\' FMap_name ' [' num2str(expt) '] ' char(cop92(3)) '_' char(cop92(2)) '_'
char(cop92(1)) '_' char(cop93(1)) '_' char(cop93(2)) '_' char(cop93(3))]; mkdir(edo);
eikon=[];close all
if shlog==1
SH1=MAPS(:,:,1); SH2=MAPS(:,:,1); for shh=1:PandL; for shj=1:PandL2; if SH(shh,shj)==1;
SH1(shh,shj)=max(SH2(:)); end; end; end
figure(512); imagesc(rot90(transpose(SH1))); colormap hot; caxis auto;
listofgraphs=LOG21;
end
if shlog2==1
if size(LOG,1)<21
    listofgraphs=LOG;
elseif size(LOG,1)>=21
    for jkjk=1:20
        listofgraphs(jkjk,1:2)=LOG(ceil((size(LOG,1))/20*jkjk),1:2);
    end
end
end
R_graphs=zeros(Rsize12,noRcol,1,1);spots_CHinIncl_ple=zeros(15,4);
i98=min(MAPS(:,:,79));i99=min(i98);
for i79=1:PandL
for i792=1:PandL2
    i97=MAPS(i79,i792);
```

```
    if isnan(i97)==1
        MAPS(i79,i792)=i98(1,1);
    end
end
end
ImAn1=MAPS(:,:,1);ImAn2=MAPS(:,:,49);ImAn3=sort(ImAn1(:));ImAn4=sort(ImAn2(:));
sk=zeros(1,1536);gr=zeros(1,17);for isuar=1:1536; sk(isuar)=isuar; end
SR=reshape(sk,[48,32]); SR=SR';fghrt1=1; rtyt=5;
if modtomo==1
PSpM11=MAPS(:,:,1); PSpM31=MAPS(:,:,57); PSpM21=reshape(PSpM11,[PandL*PandL2,1]);
[PSpM1,PSpI1]=sort(PSpM21); PSpM41=PSpM31(PSpI1);
PSpM12=MAPS(:,:,1); PSpM32=MAPS(:,:,58); PSpM22=reshape(PSpM12,[PandL*PandL2,1]);
[PSpM2,PSpI2]=sort(PSpM22); PSpM42=PSpM32(PSpI2);
PSpM13=MAPS(:,:,1); PSpM33=MAPS(:,:,59); PSpM23=reshape(PSpM13,[PandL*PandL2,1]);
[PSpM3,PSpI3]=sort(PSpM23); PSpM43=PSpM33(PSpI3);
PSpM14=MAPS(:,:,1); PSpM34=MAPS(:,:,60); PSpM24=reshape(PSpM14,[PandL*PandL2,1]);
[PSpM4,PSpI4]=sort(PSpM24); PSpM44=PSpM34(PSpI4);
PSpM15=MAPS(:,:,1); PSpM35=MAPS(:,:,61); PSpM25=reshape(PSpM15,[PandL*PandL2,1]);
[PSpM5,PSpI5]=sort(PSpM25); PSpM45=PSpM35(PSpI5);
PSpM16=MAPS(:,:,1); PSpM36=MAPS(:,:,62); PSpM26=reshape(PSpM16,[PandL*PandL2,1]);
[PSpM6,PSpI6]=sort(PSpM26); PSpM46=PSpM36(PSpI6);
PSpM17=MAPS(:,:,1); PSpM37=MAPS(:,:,63); PSpM27=reshape(PSpM17,[PandL*PandL2,1]);
[PSpM7,PSpI7]=sort(PSpM27); PSpM47=PSpM37(PSpI7);
PSpM18=MAPS(:,:,1); PSpM38=MAPS(:,:,64); PSpM28=reshape(PSpM18,[PandL*PandL2,1]);
[PSpM8,PSpI8]=sort(PSpM28); PSpM48=PSpM38(PSpI8);
PSpM19=MAPS(:,:,1); PSpM39=MAPS(:,:,65); PSpM29=reshape(PSpM18,[PandL*PandL2,1]);
[PSpM9,PSpI9]=sort(PSpM29); PSpM49=PSpM39(PSpI9);
PSpM110=MAPS(:,:,1); PSpM310=MAPS(:,:,66); PSpM210=reshape(PSpM110,[PandL*PandL2,1]);
[PSpM10,PSpI10]=sort(PSpM210); PSpM410=PSpM310(PSpI10);
PSpM411=cat(1,PSpM41,PSpM42,PSpM43,PSpM44,PSpM45,PSpM46,PSpM47,PSpM48,PSpM49,PSpM410);
PSpM412=sort(PSpM411);
th = (2*pi)/(PandL*PandL2):(2*pi)/(PandL*PandL2):2*pi;
if Figs.pleIndent==1
    figure(1012)

ps1=scatter(fghrt1:fghrt1:PandL*PandL2,PSpM41(fghrt1:fghrt1:PandL*PandL2),'Marker','o','SizeDa
ta',rtyt);
    hold on

ps2=scatter(fghrt1:fghrt1:PandL*PandL2,PSpM42(fghrt1:fghrt1:PandL*PandL2),'Marker','o','SizeDa
ta',rtyt);

ps3=scatter(fghrt1:fghrt1:PandL*PandL2,PSpM43(fghrt1:fghrt1:PandL*PandL2),'Marker','o','SizeDa
ta',rtyt);

ps4=scatter(fghrt1:fghrt1:PandL*PandL2,PSpM44(fghrt1:fghrt1:PandL*PandL2),'Marker','o','SizeDa
ta',rtyt);

ps5=scatter(fghrt1:fghrt1:PandL*PandL2,PSpM45(fghrt1:fghrt1:PandL*PandL2),'Marker','o','SizeDa
ta',rtyt);

ps6=scatter(fghrt1:fghrt1:PandL*PandL2,PSpM46(fghrt1:fghrt1:PandL*PandL2),'Marker','o','SizeDa
ta',rtyt);

ps7=scatter(fghrt1:fghrt1:PandL*PandL2,PSpM47(fghrt1:fghrt1:PandL*PandL2),'Marker','o','SizeDa
ta',rtyt);

ps8=scatter(fghrt1:fghrt1:PandL*PandL2,PSpM48(fghrt1:fghrt1:PandL*PandL2),'Marker','o','SizeDa
ta',rtyt);

ps9=scatter(fghrt1:fghrt1:PandL*PandL2,PSpM49(fghrt1:fghrt1:PandL*PandL2),'Marker','o','SizeDa
ta',rtyt);

ps10=scatter(fghrt1:fghrt1:PandL*PandL2,PSpM410(fghrt1:fghrt1:PandL*PandL2),'Marker','o','Size
Data',rtyt);
    axis([1 PandL*PandL2 .5*PSpM412(ceil(.1*PandL*PandL2*10))
2*PSpM412(ceil(.9*PandL*PandL2*10))])
    lgd1=legend('10%','20%','30%','40%','50%','60%','70%','80%','90%','100%');
    lgd1.FontSize=8;
    lgd1.Location='northwest';
end
end
MAPS_sorted=sort(reshape(MAPS,size(MAPS,1)*size(MAPS,2),size(MAPS,3)));
MAPS_sorted_max=(max(real(MAPS_sorted)));MAPS_sorted_min=(min(real(MAPS_sorted)));
Msmax_rms=max([MAPS_sorted_max(7),MAPS_sorted_max(8),MAPS_sorted_max(9)]);
MAPS_1_Temp=MAPS(:,:,1);
```

```
MAPS_1_Temp(~MAPS_1_Temp)=MAPS_sorted(find(MAPS_sorted(:,1),1)+1,1);
MAPS(:,:,18)=abs(MAPS(:,:,18));tpoio=0; klax=1;
while klax<2
klaxon=0;
for log1=1:size(listofgraphs,1)
    log2=listofgraphs(log1,1); log3=listofgraphs(log1,2);

listofgraphs(log1,[3,4,5,6])=[MAPS(log2,log3,1),MAPS(log2,log3,15),log1,MAPS(log2,log3,48)];
    if isnan(listofgraphs(log1,4))==1 || isnan(listofgraphs(log1,6))==1 ||
listofgraphs(log1,6)==0 || listofgraphs(log1,4)==0 || isnan(listofgraphs(log1,3))==1 ||
listofgraphs(log1,3)==0
        break
    else
        klaxon=klaxon+1;
    end
    if Figs.beta==1; listofgraphs(log1,7)=MAPS(log2,log3,79);   end
end
if klaxon==size(listofgraphs,1) ;    klax=klax+1;else
    if log1==1; listofgraphs(1,2)=randi(PandL2); else;
listofgraphs(log1,1:2)=listofgraphs(log1-1,1:2); end
end
end
if shlog==1
for log1=1:size(listofgraphs2,1)
    log2=listofgraphs2(log1,1); log3=listofgraphs2(log1,2);

listofgraphs2(log1,[3,4,5,6])=[MAPS(log2,log3,1),MAPS(log2,log3,15),log1,MAPS(log2,log3,48)];
    listofgraphs2(1:20,8:9)=LOG21;
    if Figs.beta==1
        listofgraphs2(log1,7)=MAPS(log2,log3,79);

listofgraphs2(log1,[10,11,12,13,14,15,16,17,18,19])=[MAPS(log2,log3,57),MAPS(log2,log3,58),MAP
S(log2,log3,59),MAPS(log2,log3,60),MAPS(log2,log3,61)...

MAPS(log2,log3,62),MAPS(log2,log3,63),MAPS(log2,log3,64),MAPS(log2,log3,65),MAPS(log2,log3,66)
];

listofgraphs2(log1,[20,21,22,23,24,25,26,27,28,29])=[MAPS(log2,log3,101),MAPS(log2,log3,102),M
APS(log2,log3,103),MAPS(log2,log3,104),MAPS(log2,log3,105)...

MAPS(log2,log3,106),MAPS(log2,log3,107),MAPS(log2,log3,108),MAPS(log2,log3,109),MAPS(log2,log3
,110)];
    end
end
else
listofgraphs2=listofgraphs;
end
if shlog2==1
listofgraphs2=LOG;
for log1=1:size(listofgraphs2,1)
    log2=listofgraphs2(log1,1); log3=listofgraphs2(log1,2);

listofgraphs2(log1,[3,4,5,6])=[MAPS(log2,log3,1),MAPS(log2,log3,15),log1,MAPS(log2,log3,48)];
    if Figs.beta==1
        listofgraphs2(log1,7)=MAPS(log2,log3,79);
    end
end
elseif shlog2==0
end
grls=find(listofgraphs(:,1),1,'last'); gr_list2=zeros(grls,2);
gr_list2(:,:)=listofgraphs(1:grls,1:2);if sqrt(PandL*PandL2)<=3; a10=1; end
% create figures of random FI data for evaluation of FI
% analysis and CP calculation
if Figs.FI==1
gpf=Figs.FI_gpf;gr1=1;
for gr2=1:ceil(grls/gpf)
    figure(gr2)
    hold on
    for gr3=1:gpf-(ceil(gr2/(ceil(grls/gpf)-1))-1)*(gpf-(grls-gpf*(ceil(grls/gpf)-1)))
        gr4=(gr1-1)*gpf+gr3;
        gr(6:10)=find(R1(:,[3,4,6,11,12],gr_list2(gr4,1),gr_list2(gr4,2)),1);
        gr(11)=find(R2(:,24-noRcol_2,gr_list2(gr4,1),gr_list2(gr4,2)),1);
        gr(12)=find(R1(:,3,gr_list2(gr4,1),gr_list2(gr4,2)),1,'last');
        gr(13)=find(R1(:,4,gr_list2(gr4,1),gr_list2(gr4,2)),1,'last');
        gr(14)=find(R1(:,6,gr_list2(gr4,1),gr_list2(gr4,2)),1,'last');
        gr(15)=find(R1(:,11,gr_list2(gr4,1),gr_list2(gr4,2)),1,'last');
```

```
        gr(16)=find(R1(:,12,gr_list2(gr4,1),gr_list2(gr4,2)),1,'last');
        gr(17)=find(R2(:,24-noRcol_2,gr_list2(gr4,1),gr_list2(gr4,2)),1,'last');

R_graphs(1:Rsize12,1:noRcol_1,1,1)=R1(1:Rsize12,1:noRcol_1,gr_list2(gr4,1),gr_list2(gr4,2));

R_graphs(1:Rsize12,noRcol_1+1:noRcol,1,1)=R2(1:Rsize12,1:noRcol_2,gr_list2(gr4,1),gr_list2(gr4
,2));
        subplot(gpf*2,gpf*2,[2*gr3-1 2*gr3 2*gr3-1+gpf*2 2*gr3+gpf*2])

plot(R_graphs(gr(6):gr(12),3),R_graphs(gr(6):gr(13),4),'o','MarkerSize',4,'MarkerEdgeColor','b
') %plot curve
        hold on

plot(R_graphs(gr(6):gr(12),3),R_graphs(gr(6):gr(14),6),'o','MarkerSize',4,'MarkerEdgeColor','r
') %plot fit

plot(R_graphs(gr(6):gr(12),3),R_graphs(gr(6):gr(14),15),'o','MarkerSize',4,'MarkerEdgeColor','
y') %plot fit

plot(R_graphs(gr(6):gr(12),3),R_graphs(gr(6):gr(14),17),'o','MarkerSize',4,'MarkerEdgeColor','
g') %plot fit
        title1 = sprintf([num2str(MAPS(gr_list2(gr4,1),gr_list2(gr4,2),3))]);
        title(title1,'FontSize',12);
        legend('raw data','fit-parab','fit-conic','fit-line','Location','NorthWest')
        set(legend,'FontSize',8);
        dim = [0.15 0.60 0.3 0.3]; %annotation tool
        annot1 = {['Indentation = ' num2str(MAPS(gr_list2(gr4,1),gr_list2(gr4,2),18),'%10.4e')
' (m)'],...
                  ['Max Force = ' num2str(MAPS(gr_list2(gr4,1),gr_list2(gr4,2),17),'%10.4e') '
(N)'],...
                  ['E = (' num2str(MAPS(gr_list2(gr4,1),gr_list2(gr4,2),1),'%10.4e') ' +- '
num2str(MAPS(gr_list2(gr4,1),gr_list2(gr4,2),2),'%10.4e') ') Pa'],...
                  ['Line/Point: ' num2str(gr_list2(gr4,1), '%i') ' / '
num2str(gr_list2(gr4,2), '%i')],...
                  ['Fit limits start - start/end: ' num2str(fit_perc_start, '%i') ' / '
num2str(fit_perc_end, '%i') '%'],...
                  ['CM model: Hertz ' num2str(MAPS(gr_list2(gr4,1),gr_list2(gr4,2),3))]};
%annotation tool
        grid on; grid minor;   xt1 = get(gca, 'XTick'); set(gca, 'FontSize', 5,'TickDir','in')
        yt1 = get(gca, 'YTick');    set(gca, 'FontSize', 3+(ceil(3.5/gpf)-1)*3)
        set(gca,'TickDir','in','FontSize',8)
        gr2limx1=-1*abs(R_graphs(gr(12),3,1,1));
        gr2limx2=2*abs(R_graphs(gr(12),3,1,1));
        gr2limy1=-1*abs(R_graphs(gr(13),4,1,1));
        gr2limy2=2*abs(R_graphs(gr(13),4,1,1));
        subplot(gpf*2,gpf*2,[2*gr3-1+gpf*4 2*gr3+gpf*4 2*gr3-1+gpf*2+gpf*4 2*gr3+gpf*2+gpf*4])
        hold on

plot(R_graphs(1:gr(15),11),R_graphs(1:gr(16),12),'o','MarkerSize',1.2,'MarkerEdgeColor','k','M
arkerFaceColor','k')

plot(R_graphs(gr(6):gr(12),3),R_graphs(gr(6):gr(13),4),'o','MarkerSize',4,'MarkerEdgeColor','b
')

plot(R_graphs(gr(6):gr(12),3),R_graphs(gr(6):gr(14),6),'o','MarkerSize',4,'MarkerEdgeColor','r
') %plot fit for ple = 1.5

plot(R_graphs(gr(6):gr(12),3),R_graphs(gr(6):gr(14),15),'o','MarkerSize',4,'MarkerEdgeColor','
y') %plot fit for ple = 2

plot(R_graphs(gr(6):gr(12),21),R_graphs(gr(6):gr(12),17),'o','MarkerSize',4,'MarkerEdgeColor',
'g') %plot linear fit
        annot2 = {['CM model: Hertz ' num2str(MAPS(gr_list2(gr4,1),gr_list2(gr4,2),3))]};
%annotation tool
        axis([gr2limx1 gr2limx2 gr2limy1 gr2limy2])
        xt2 = get(gca, 'XTick');
        set(gca, 'FontSize', 5)
        set(gca,'TickDir','in')
        yt2 = get(gca, 'YTick');
        set(gca, 'FontSize', 5+(ceil(3.5/gpf)-1)*3)
        set(gca,'TickDir','in','FontSize',8)
        grid on; grid minor
        subplot(gpf*2,gpf*2,[2*gr3-1+gpf*8 2*gr3+gpf*8 2*gr3-1+gpf*2+gpf*8 2*gr3+gpf*2+gpf*8])

plot(R_graphs(1:gr(15),11),R_graphs(1:gr(16),12),'o','MarkerSize',1,'MarkerEdgeColor','k')
        hold on
```

```
        const_graph3=max(R_graphs(:,12));

plot(R_graphs(gr(6):gr(12),3),R_graphs(gr(6):gr(13),4),'o','MarkerSize',3,'MarkerEdgeColor','b
')
        if MAPS(gr_list2(gr4,1),gr_list2(gr4,2),39)==1

plot(R_graphs(MAPS(gr_list2(gr4,1),gr_list2(gr4,2),40):20:MAPS(gr_list2(gr4,1),gr_list2(gr4,2)
,45),28)+...
                MAPS(gr_list2(gr4,1),gr_list2(gr4,2),47)...

,R_graphs(MAPS(gr_list2(gr4,1),gr_list2(gr4,2),40):20:MAPS(gr_list2(gr4,1),gr_list2(gr4,2),45)
,29)-...

MAPS(gr_list2(gr4,1),gr_list2(gr4,2),44),'+','MarkerSize',3,'MarkerEdgeColor','r')
        end
        v=R_graphs(:,11);
        v1=find(v==max(v));
        axis([MAPS_sorted_min(23) MAPS_sorted_max(24) MAPS_sorted_min(25)
MAPS_sorted_max(26)])
        annot3 = {
                  ['Trig. point (N): ' num2str(Trigger_point_nN,'%10.4e')]...
                  ['Tot. cant. defl. (m): ' num2str(Trigger_point_nN/K_t,'%10.4g')]...
                  ['Tot. Indent. (m): ' num2str(R_graphs(v1,11),'%10.4g')]}; %annotation tool
        annotation('textbox',[.131+(gr3-1)*(.198+(ceil(3.5/gpf)-1)*.075) .40-(ceil(3.5/gpf)-
1)*0.077*2 .1
.1],'String',annot3,'FitBoxToText','on','EdgeColor','none','FontSize',5,'FontWeight','bold');
        xt3 = get(gca, 'XTick');
        set(gca, 'FontSize', 5)
        set(gca,'TickDir','in')
        yt3 = get(gca, 'YTick');
        set(gca, 'FontSize', 5+(ceil(3.5/gpf)-1)*3)
        set(gca,'TickDir','in','FontSize',8)
        grid on
        if Figs.FI_gpf==4
            subplot(8,8,[2*gr3-1+48 2*gr3+48 2*gr3-1+8+48 2*gr3+8+48])
            plot(R_graphs(:,9),R_graphs(:,10),'o','MarkerSize',1.5,'MarkerEdgeColor','k')
            xlabel('ZSnsr (m)')
            ylabel('Deflection (m)')
            hold on

plot(0,linspace(MAPS_sorted_min(21),MAPS_sorted_max(22),SampleRate/5),'o','MarkerSize',1,'Mark
erFaceColor','k')
            str_gr4 = {['CM model: Hertz '
num2str(MAPS(listofgraphs(gr4,1),listofgraphs(gr4,2),3))]}; %annotation tool
            annotation('textbox',[.131+(gr3-1)*(.198) .19 .1
.1],'String',str_gr4,'FitBoxToText','on','EdgeColor','none','FontSize',5,'FontWeight','bold');
            axis([MAPS_sorted_min(19) MAPS_sorted_max(20) MAPS_sorted_min(21)
MAPS_sorted_max(22)])
            xt4 = get(gca, 'XTick');
            set(gca, 'FontSize', 5)
            set(gca,'TickDir','in')
            yt4 = get(gca, 'YTick');
            set(gca, 'FontSize', 5)
            set(gca,'TickDir','in')
            grid on
        end
        spots_CHinIncl_ple(gr4,1)=MAPS(gr_list2(gr4,1),gr_list2(gr4,2),1);
        spots_CHinIncl_ple(gr4,2)=MAPS(gr_list2(gr4,1),gr_list2(gr4,2),2);
        spots_CHinIncl_ple(gr4,3)=MAPS(gr_list2(gr4,1),gr_list2(gr4,2),11);
        spots_CHinIncl_ple(gr4,4)=MAPS(gr_list2(gr4,1),gr_list2(gr4,2),49);
    end
    gr1=gr1+1;
    hold off;
end
else
end
O_PHARRmod=MAPS(:,:,46);
O_PHARRmod_sorted=sort(O_PHARRmod(:));
if Figs.NonElastic==1
figure(1003)
hold on
if O_PHARR==1
subplot(4,6,[5 6 11 12])
imagesc(rot90(transpose(MAPS(:,:,46)))); %# Create a colored map of the matrix values
colormap hot
colorbar('eastoutside','Box','on')
```

```
caxis([O_PHARRmod_sorted(1*PandL) MAPS_sorted(end-1*PandL,1)])
title({'Modulus (Pa) map';'Oliver-Pharr model'},'FontSize',10)
axis off
end
if DMT==1
subplot(4,6,[3 4 9 10])
imagesc(rot90(transpose(MAPS(:,:,43)))); %# Create a colored map of the matrix values
colormap hot
colorbar('eastoutside','Box','on')
caxis([O_PHARRmod_sorted(10*PandL) MAPS_sorted(end-1*PandL,1)])
title({'Modulus (Pa) map';'DMT model'},'FontSize',10)
axis off
end
subplot(4,6,[1 2 7 8])
imagesc(rot90(transpose(MAPS(:,:,1)))); %# Create a colored map of the matrix values
colormap hot
colorbar('eastoutside','Box','on')
caxis([MAPS_sorted(ceil(PandL*PandL*(.05)),1) MAPS_sorted(ceil(PandL*PandL*(.98)),1)])
title({'Modulus (Pa) map';'Hertz model'},'FontSize',10)
axis off
subplot(4,6,[13 14 19 20])
imagesc(rot90(transpose(MAPS(:,:,15))))
colormap hot
colorbar('eastoutside','Box','on')
title({'Adhesion ratio';'F_{ad}/F_{max}'},'FontSize',10)
caxis([0 100])
axis off
subplot(4,6,[15 16 21 22])
imagesc(rot90(transpose(MAPS(:,:,48))))
colormap hot
title({'Plasticity index';'psi_{p}'},'FontSize',10)
colorbar('eastoutside','Box','on')
caxis([0 100])
axis off
subplot(4,6,[17 18 23 24])
imagesc(rot90(transpose(MAPS(:,:,49))))
colormap hot
title({'CM Model selection / r: Hertz';'y: DMT / w: Oliver-Pharr'},'FontSize',10)
colorbar('eastoutside','Box','on','Ticks',[0 1 2 3],'TickLabels',{'Sneddon','Hertz','DMT','O-
P'})
caxis([0 3]);
axis off
hold off
end
qwertyui=zeros(PandL,PandL2);
for hf1=1:PandL
for hf2=1:PandL2
    brcu=MAPS(hf1,hf2,13);
    if brcu==0; brcu=1; end
    qwertyui(hf1,hf2)=R1(brcu,9,hf1,hf2);
end
end
if Figs.beta==1 && Figs.beta_1==1
figure(1013)
hold on
subplot(2,3,1)
imagesc(rot90(transpose(MAPS(:,:,78))))
colormap hot
title('beta values','FontSize',8.5)
caxis([1.1 2])
colorbar('eastoutside','Box','on')
subplot(2,3,2)
imagesc(rot90(transpose(MAPS(:,:,1))));
colormap hot
colorbar('eastoutside','Box','on')
caxis([MAPS_sorted(ceil(PandL*PandL*(.05)),79) MAPS_sorted(ceil(PandL*PandL*(.98)),79)])
title('Modulus (Pa) map','FontSize',8.5)
subplot(2,3,4)
imagesc(rot90(transpose(MAPS(:,:,49))))
colormap hot
title({'CM Model selection'},'FontSize',8.5)
colorbar('eastoutside','Box','on','Ticks',[0.5 1 1.5 1.65 2.3 2.75
2.9],'TickLabels',{'Sneddon','Hertz','"big" adhesion','DMT','"Viscocity"','"big"
hysteresis','O-P'},'FontSize',7)
caxis([0 3]);
axis off
```

```
subplot(2,3,5)
imagesc(rot90(transpose(MAPS(:,:,53))))
colormap hot
title('"Yield-like" point map','FontSize',8.5)
colorbar('eastoutside','Box','on','Ticks',[0 5 10 15 20 25 30 35 40 45 50 55 60 65 70 75
100],'TickLabels',{'max indent.','   |','   |','   |','   |','75% of','   |','   |','   |','
|','50% of','   |','   |','   |','   |','25% of','free surf.'},'FontSize',7)
caxis([0 100])
axis off
subplot(2,3,3)
ipr=imresize(qwertyui(:,:),1);
if FlatLim==1
e=1:PandL*1;
for ipr1=1:PandL*1
    e1=ipr(ipr1,:);
    p14=polyfit(e,e1,FlatlimDeg);
    e2=e1-polyval(p14,e);
    ipr(ipr1,:)=e2;
end
end
imagesc(imresize(medfilt3(rot90(transpose(-ipr(:,:))),[3 3 3]),5))
colormap hot
colorbar('eastoutside','Box','on')
title({'Contact point / flat ' FlatlimDeg},'FontSize',8.5)
axis off
caxis auto
subplot(2,3,6)
imagesc(rot90(transpose(MAPS(:,:,79))));
colormap hot
colorbar('eastoutside','Box','on')
caxis([MAPS_sorted(ceil(PandL*PandL*(.05)),79) MAPS_sorted(ceil(PandL*PandL*(.98)),79)])
title('Modulus (Pa) map - Sneddon/O-P','FontSize',8.5)
hold off
if SPaIDYoN==1
    qwertyui90=zeros(PandL,PandL2);
    for iDr11=1:PandL
        for iDr21=1:PandL2
            if iDr11==31 && iDr21==5 || iDr11==32 && iDr21==5
            else
                gri3=zeros(1,17);
                R_IDe(1:Rsize12,1:noRcol_1,1,1)=R1(1:Rsize12,1:noRcol_1,iDr11,iDr21);
                R_IDe(1:Rsize12,noRcol_1+1:noRcol,1,1)=R2(1:Rsize12,1:noRcol_2,iDr11,iDr21);
                nnm=nnz(R_IDe);
                if nnm==0
                else
                    gri3(6:10)=find(R1(:,[3,4,6,11,12],iDr11,iDr21),1);
                end
            end
            if gri3(12)==0 && gri3(6)==0
                gri3(6)=1; gri3(12)=1;
            end
        end
    end
    xm1=((40*(120/200))*1e-6)/PandL:((40*(120/200))*1e-6)/PandL2:(40*(120/200))*1e-6;
    xm2=((40*(120/200))*1e-6)/PandL:((40*(120/200))*1e-6)/PandL2:(40*(120/200))*1e-6;
    qwert23=zeros(PandL,PandL2,3);
    for gt1=1:PandL
        qwert23(gt1,:,1)=xm1(gt1);
    end
    for gt2=1:PandL2
        qwert23(:,gt2,2)=xm2(gt2);
    end
    qwert23(:,:,3)=qwertyui;
    [Nx,Ny,Nz]=surfnorm(qwert23(:,:,1),qwert23(:,:,2),qwert23(:,:,3));
    we1=zeros(PandL,PandL2);
    for rt12=1:PandL
        for rt13=1:PandL2
           we1(rt12,rt13)=-
Nz(rt12,rt13)/(sqrt((Nx(rt12,rt13))^2+(Ny(rt12,rt13))^2+(Nz(rt12,rt13))^2));
        end
    end
    IDe=zeros(PandL,PandL2);
    for iDr1=1:PandL
        for iDr2=1:PandL2
            if iDr1==31 && iDr2==5 || iDr1==32 && iDr2==5 || iDr1==48 && iDr2==10
            else
```

```
                gri3=zeros(1,17);
                R_IDe(1:Rsize12,1:noRcol_1,1,1)=R1(1:Rsize12,1:noRcol_1,iDr1,iDr2);
                R_IDe(1:Rsize12,noRcol_1+1:noRcol,1,1)=R2(1:Rsize12,1:noRcol_2,iDr1,iDr2);
                nnm=nnz(R_IDe);
                if nnm==0 || any(R1(:,3,iDr1,iDr2))==0 || any(R1(:,4,iDr1,iDr2))==0 ||
any(R1(:,6,iDr1,iDr2))==0 || any(R1(:,11,iDr1,iDr2))==0 || any(R1(:,12,iDr1,iDr2))==0
                else
                    gri3(6:10)=find(R1(:,[3,4,6,11,12],iDr1,iDr2),1);
                    gri3(12)=find(R1(:,3,iDr1,iDr2),1,'last');
                    gri3(13)=find(R1(:,4,iDr1,iDr2),1,'last');
                    gri3(14)=find(R1(:,6,iDr1,iDr2),1,'last');
                    gri3(15)=find(R1(:,11,iDr1,iDr2),1,'last');
                    gri3(16)=find(R1(:,12,iDr1,iDr2),1,'last');
                end
            end
            if gri3(12)==0 && gri3(6)==0
                gri3(6)=1; gri3(12)=1;
            end
            IDe(iDr1,iDr2)=R_IDe(gri3(12),3)-R_IDe(gri3(6),3);
        end
    end
    if tip_shape==1
        iou=am;
    else

iou=[3.33333333333333,22.2046763895516,240.960534295959,5261.14815043852,328828.276577397,1111
11111.111111,725774738602.423,1.80213392461435e+18,1.31687242798354e+31,8.67076495791631e+69];
    end
    DFD=MAPS(:,:,78); bh=round(mean(DFD(logical(DFD>0)))*10)/10; bh2=single((bh-1)*10);
Beta2=iou(11-bh2);
    for i1=1:PandL
        for i2=1:PandL2
            for ster1=ceil(10/stposa):ceil(10/stposa):10
                bh=MAPS(i1,i2,91+(ceil(ster1/9)-1)*(-13)+abs(ceil(ster1/9)-2)*ster1); if
bh==0; bh=1.1; end
                bh2=single((bh-1)*10); Beta2=iou(11-bh2);
                hhh21=(abest_all1_2(i1,i2,ster1,bh2)*((sqrt(3.14)*((Beta2)))^(bh-1))*(1/(bh-
1)+1))/...
                            (2*(1/(bh-1))*(((gamma(1/(2*(bh-1))+1/2))/(gamma(1/(2*(bh-
1))+1)))^(bh-1)));
                MAPS(i1,i2,100+ster1)=(1-(Pratiosample)^2)/abs((1/(hhh21))-((1-
(Pratiotip)^2)/(Etip)));
            end
        end
    end
    plnf1=[1.07850713095751e-14,5.00024998750062e-08];
    plnf2=[937453134.373828,-6.57830211739396e-15,1.87509372187641e-08];
    plnf3=[-288.925205773263,937453134.373831,1.01217597472848e-16,1.87509372187640e-08];
    plnf4=[-8.20189504383761e+24,-293.839938853527,1640543005.65893,1.80176862384832e-
14,1.17193354980688e-08];
    plnf5=[-7.88663413350908e+17,-8.20189504383765e+24,-
315.038508044421,1640543005.65894,1.52593314116600e-14,1.17193354980689e-08];
    plnf6=[1.46594227312860e+41,7.97454601303156e+18,-2.81940154958915e+25,-
1100.33341411788,2307013643.35813,2.04609064530311e-14,8.54534852297913e-09];
    plnf7=[-5.16848789072914e+35,1.46594227312860e+41,6.61237482460087e+19,-
2.81940154958915e+25,-2026.13353514102,2307013643.35813,7.68724016110062e-
15,8.54534852297912e-09];
    plnf8=[-3.33730322072998e+57,-
5.78393271372560e+35,7.69619763475903e+41,7.64966850206845e+19,-6.41413890691851e+25,-
2772.89460750707,2960667578.87395,2.57530005664057e-14,6.72946167587244e-09];
    plnf9=[-1.70149274466309e+52,-
3.33730322072998e+57,2.93579553687227e+36,7.69619763475899e+41,-1.41154104260417e+20,-
6.41413890691848e+25,1888.60786129952,2960667578.87394,-1.12597265681062e-
14,6.72946167587248e-09];
    plnf10=[8.62977609853574e+73,2.93201230010437e+52,-2.37782890074824e+58,-
5.85601744875808e+36,2.45316327203264e+42,3.93788420737930e+20,-1.20265113343323e+26,-
9986.51782841312,3608313716.98458,7.50757141213487e-14,5.55180559115409e-09];
    SPrmap=zeros(PandL,PandL2);
    SPaID=zeros(PandL,PandL2);
    SPAID2=zeros(PandL,PandL2);

iou45=[2.7027,19.4742,233.1204,5.7745e+3,4.2703e+5,1.8262e+8,1.6983e+12,7.5982e+18,1.8026e+32,
4.0617e+72];
for spa1=1:PandL
        for spa2=1:PandL2
            bh981=zeros(1,10);
```

```
            SPr=ceil(((IDe(spa1,spa2))*(we1(spa1,spa2)))/Rtip);
            if SPr>10
                SPr=10;
            end
            SPrmap(spa1,spa2)=SPr;
            for tyui56=1:SPr
                  bh981(tyui56)=(abest_all1_2(spa1,spa2,10,tyui56)*((sqrt(3.14).*((iou(11-
(tyui56))))).^(((tyui56)/10+1)-1))*(1./(((tyui56)/10+1)-1)+1))/...
                        (2*(1./(((tyui56)/10+1)-1))*(((gamma(1/(2.*(((tyui56)/10+1)-
1))+1/2))/(gamma(1/(2.*(((tyui56)/10+1)-1))+1))).^(((tyui56)/10+1)-1)));
            end
            bh9045=MAPS(spa1,spa2,78);
            if bh9045==0; bh9045=1.1; end
            bh29045=single((bh9045-1)*10);
            Beta24=iou(11-bh29045);
            bh9801=(abest_all1_2(spa1,spa2,10,bh29045)*((sqrt(3.14)*((Beta24)))^(bh9045-
1))*(1/(bh9045-1)+1))/...
                        (2*(1/(bh9045-1))*(((gamma(1/(2*(bh9045-1))+1/2))/(gamma(1/(2*(bh9045-
1))+1)))^(bh9045-1)));
            if     SPr==1;
                        bh980=bh981(1);
            elseif SPr==2
                        bh980=plnf2(1)/sum(plnf2)*bh981(1)+ plnf2(2)/sum(plnf2)*bh981(2);
            elseif SPr==3
                        bh980=plnf3(1)/sum(plnf3)*bh981(1)+ plnf3(2)/sum(plnf3)*bh981(2)+
plnf3(3)/sum(plnf3)*bh981(3);
            elseif SPr==4
                        bh980=plnf4(1)/sum(plnf4)*bh981(1)+ plnf4(2)/sum(plnf4)*bh981(2)+
plnf4(3)/sum(plnf4)*bh981(3)+ plnf4(4)/sum(plnf4)*bh981(4);
            elseif SPr==5
                        bh980=plnf5(1)/sum(plnf5)*bh981(1)+ plnf5(2)/sum(plnf5)*bh981(2)+
plnf5(3)/sum(plnf5)*bh981(3)+ plnf5(4)/sum(plnf5)*bh981(4)+ plnf5(5)/sum(plnf5)*bh981(5);
            elseif SPr==6
                        bh980=plnf6(1)/sum(plnf6)*bh981(1)+ plnf6(2)/sum(plnf6)*bh981(2)+
plnf6(3)/sum(plnf6)*bh981(3)+ plnf6(4)/sum(plnf6)*bh981(4)+ plnf6(5)/sum(plnf6)*bh981(5)+
plnf6(6)/sum(plnf6)*bh981(6);
            elseif SPr==7
                        bh980=plnf7(1)/sum(plnf7)*bh981(1)+ plnf7(2)/sum(plnf7)*bh981(2)+
plnf7(3)/sum(plnf7)*bh981(3)+ plnf7(4)/sum(plnf7)*bh981(4)+ plnf7(5)/sum(plnf7)*bh981(5)+
plnf7(6)/sum(plnf7)*bh981(6)+ plnf7(7)/sum(plnf7)*bh981(7);
            elseif SPr==8
                        bh980=plnf8(1)/sum(plnf8)*bh981(1)+ plnf8(2)/sum(plnf8)*bh981(2)+
plnf8(3)/sum(plnf8)*bh981(3)+ plnf8(4)/sum(plnf8)*bh981(4)+ plnf8(5)/sum(plnf8)*bh981(5)+
plnf8(6)/sum(plnf8)*bh981(6)+ plnf8(7)/sum(plnf8)*bh981(7)+ plnf8(8)/sum(plnf8)*bh981(8);
            elseif SPr==9
                        bh980=plnf9(1)/sum(plnf9)*bh981(1)+ plnf9(2)/sum(plnf9)*bh981(2)+
plnf9(3)/sum(plnf9)*bh981(3)+ plnf9(4)/sum(plnf9)*bh981(4)+ plnf9(5)/sum(plnf9)*bh981(5)+
plnf9(6)/sum(plnf9)*bh981(6)+ plnf9(7)/sum(plnf9)*bh981(7)+ plnf9(8)/sum(plnf9)*bh981(8)+
plnf9(9)/sum(plnf9)*bh981(9);
            elseif SPr==10
                        bh980=plnf10(1)/sum(plnf10)*bh981(1)+ plnf10(2)/sum(plnf10)*bh981(2)+
plnf10(3)/sum(plnf10)*bh981(3)+ plnf10(4)/sum(plnf10)*bh981(4)+
plnf10(5)/sum(plnf10)*bh981(5)+ plnf10(6)/sum(plnf10)*bh981(6)+
plnf10(7)/sum(plnf10)*bh981(7)+ plnf10(8)/sum(plnf10)*bh981(8)+
plnf10(9)/sum(plnf10)*bh981(9)+ plnf10(10)/sum(plnf10)*bh981(10);
            elseif SPr==0
                        bh980=0;
            end
            SPaID(spa1,spa2)=(1-(Pratiosample)^2)/abs((1/(bh980))-((1-(Pratiotip)^2)/(Etip)));
% superposition according to indent. & depth
            SPAID2(spa1,spa2)=(1-(Pratiosample)^2)/abs((1/(bh9801))-((1-
(Pratiotip)^2)/(Etip))); % superposition according to indent. & depth


        end
end
end
figure(1048)
hold on
subplot(2,3,1)
imagesc(rot90(transpose(MAPS(:,:,79)))); %# Create a colored map of the matrix values
M567=MAPS(:,:,79);
m568=max(M567(:));
m569=min(M567(:));
colormap hot
colorbar('eastoutside','Box','on')
caxis([5e+4 4e+6])
```

```
title('Modulus (Pa) map - Pharr-Bolshakov','FontSize',8.5)
subplot(2,3,2)
imagesc(rot90(transpose(MAPS(:,:,1)))); %# Create a colored map of the matrix values
colormap hot
colorbar('eastoutside','Box','on')
caxis([5e+4 4e+6])
title('Modulus (Pa) map - Hertz','FontSize',8.5)
subplot(2,3,3)
imagesc(rot90(transpose(MAPS(:,:,81)))); %# Create a colored map of the matrix values
colormap hot
colorbar('eastoutside','Box','on')
caxis([5e+4 4e+6])
title('Modulus (Pa) map - Borodichanalytical-???','FontSize',8.5)
subplot(2,3,4)
imagesc(rot90(transpose(SPAID2))); %# Create a colored map of the matrix values
colormap hot
colorbar('eastoutside','Box','on')
caxis([5e+4 4e+6])
title('Modulus (Pa) map - Varying beta','FontSize',8.5)
subplot(2,3,5)
imagesc(rot90(transpose(SPaID))); %# Create a colored map of the matrix values
colormap hot
colorbar('eastoutside','Box','on')
O_PHARRmod=MAPS(:,:,46);
O_PHARRmod_sorted=sort(O_PHARRmod(:));
caxis([5e+6 7e+7])
title({'Modulus (Pa) map - Superposition according to indent. & depth'},'FontSize',8.5)
subplot(2,3,6)
imagesc(rot90(transpose(MAPS(:,:,78))))
colormap hot
title('beta values','FontSize',8.5)
caxis([1.1 2])
colorbar('eastoutside','Box','on')
hold off
figure(1049); subplot(4,6,[5 6 11 12]); box on; kolp=7;
eqgrx=[0 0 0 0 0 0]; eqgry=[1 2 3 4 5 6]; plot(eqgrx,eqgry,'.','Color','k'); xlim([0 2]);
ylim([0 7]); axis off; laq=10;
text(0,6,['  Hertz:' ' ' '$$F = (\frac{4}{3} * E_{eff} * R_{t}^{1/2}) *
\delta^{3/2}$$'],'Color','b','FontSize',laq,'Interpreter','latex');
text(0,5,['  Varying beta:' ' ' '$$P = \frac{2E_{eff}}{\sqrt{\pi}c^{1/n}} * (\frac{n}{n+1}) *
[\frac{\Gamma(\frac{n}{2}+\frac{1}{2})}{\Gamma(\frac{n}{2}+1)}]^{\frac{1}{n}} *
D^{1+\frac{1}{n}}$$' newline '  where n is
uniform'],'Color','r','FontSize',laq,'Interpreter','latex');
text(0,4,['  Superposition:' ' ' '$$P = \frac{2E_{eff}}{\sqrt{\pi}c^{1/n}} * (\frac{n}{n+1}) *
[\frac{\Gamma(\frac{n}{2}+\frac{1}{2})}{\Gamma(\frac{n}{2}+1)}]^{\frac{1}{n}} *
D^{1+\frac{1}{n}}$$' newline '  where n is NOT uniform'],'Color','[.8 .8
0]','FontSize',laq,'Interpreter','latex');
text(0,3,['  uniform opt beta:' ' ' 'P_{\Sigma} = \Sigma(P_i)'],'Color','m','FontSize',laq);
text(0,2,['  O Pharr:' ' ' 'retract curve'],'Color','g','FontSize',laq);
text(0,1,['  DMT:' ' ' 'retract curve'],'Color',[0 .8 .8],'FontSize',laq);
subplot(4,6,[1 2 3 4 7 8 9 10]);
    PHMS=[fitdist(reshape(MAPS(:,:,1),PandL*PandL2,1),'Normal')
fitdist(reshape(SPAID2(:,:),PandL*PandL2,1),'Normal')...
        fitdist(reshape(SPaID(:,:),PandL*PandL2,1),'Normal')
fitdist(reshape(MAPS(:,:,110),PandL*PandL2,1),'Normal')...
        fitdist(reshape(MAPS(:,:,46),PandL*PandL2,1),'Normal')
fitdist(reshape(MAPS(:,:,43),PandL*PandL2,1),'Normal')];
    PHMS34=[(reshape(MAPS(:,:,1),PandL*PandL2,1)) (reshape(SPAID2(:,:),PandL*PandL2,1))...
        (reshape(SPaID(:,:),PandL*PandL2,1)) (reshape(MAPS(:,:,110),PandL*PandL2,1))...
        (reshape(MAPS(:,:,46),PandL*PandL2,1)) (reshape(MAPS(:,:,43),PandL*PandL2,1))];
    plok=[PHMS(1,1).mu PHMS(1,2).mu PHMS(1,3).mu PHMS(1,4).mu PHMS(1,5).mu PHMS(1,6).mu];
plok1=mean(plok); plok2=std(plok);
    PHJ=reshape(MAPS(:,:,1),PandL*PandL2,1); PKL=PHMS(1,1);
    for rt=1:6; PHMS2(:,rt)=pdf(PHMS(1,rt),PHMS34(:,rt)); end
    plot3(ones(size(PHMS2,1),6)*[1 0 0 0 0 0;0 2 0 0 0 0;0 0 3 0 0 0;0 0 0 4 0 0;0 0 0 0 5 0;0
0 0 0 0 6],PHMS34(:,:),PHMS2(:,:),...
        'o','MarkerSize',4);  view(-84,14); grid minor; ylim([plok1-kolp*plok2
plok1+kolp*plok2]); hold on;
    for uu1=1:6;
plot3(linspace(uu1,10,50),ones(50,1).*PHMS(1,uu1).mu,ones(50,1).*max(pdf(PHMS(1,uu1),PHMS34(:,
uu1)))); end
    ploks=max(pdf(PHMS(1,1),PHMS34(:,1))); for aql1=2:6 ploks=[ploks
max(pdf(PHMS(1,aql1),PHMS34(:,aql1)))]; end
    plot3(ones(6,1)*10,plok,ploks,'o','MarkerFaceColor','r');
    legend('Hertz','varying beta',['super acc to' newline 'beta & depth'],'uniform opt
beta','O_Pharr','DMT'); box on;
```

```
subplot(4,6,[15 16 21 22]); o09=100;
    histogram(MAPS(:,:,1),o09,'Normalization','pdf'); hold on;
histogram(SPAID2(:,:),o09,'Normalization','pdf');
histogram(SPaID(:,:),o09,'Normalization','pdf');
histogram(MAPS(:,:,110),o09,'Normalization','pdf');
    legend('Hertz','varying beta',['super acc to' newline 'beta & depth'],'uniform opt beta');
box on;  grid on; xlim([plok1-kolp*plok2 plok1+kolp*plok2]);
subplot(4,6,[17 18 23 24]); o09=100; nayt=MAPS(:,:,1); nayt2=MAPS(:,:,43);
    histogram(nayt(nayt>0),o09); hold on;  histogram(nayt(nayt>0),o09); legend('Hertz','DMT');
box on; grid on; xlim([plok1-kolp*plok2 plok1+kolp*plok2]); %ylim([0 700])
subplot(4,6,[13 14 19 20])
    plot(1:6,[PHMS(1,1).sigma PHMS(1,2).sigma PHMS(1,3).sigma PHMS(1,4).sigma PHMS(1,5).sigma
PHMS(1,6).sigma],'o','MarkerFaceColor','b','MarkerSize',10); hold on;
    plot(1:6,[PHMS(1,1).mu PHMS(1,2).mu PHMS(1,3).mu PHMS(1,4).mu PHMS(1,5).mu
PHMS(1,6).mu],'o','MarkerFaceColor','r','MarkerSize',7);
    xticks([1 2 3 4 5 6]); xticklabels({'Hertz','varying beta',['super acc to beta &
depth'],'uniform opt beta','O Pharr','DMT'});
    xtickangle(20); ylabel('sigma'); fg59=get(gca,'XTickLabel');
set(gca,'XTickLabel',fg59,'fontsize',10);  grid on; %xlim([0 7]);
    ylim([plok1-2*plok2 plok1+10*plok2]);set(figure(1049), 'Position', get(0, 'Screensize'));
figure(547)
hold on
subplot(4,6,[1 2 7 8])
imagesc(rot90(transpose(SPAID2)));
colormap hot
axis off
colorbar('eastoutside','Box','on','FontSize',13)
caxis([1e+5 6e+7])
title({'Modulus (Pa) map';'Superposition according to beta'},'FontSize',13)
subplot(4,6,[3 4 9 10])
imagesc(rot90(transpose(MAPS(:,:,1))));
colormap hot
axis off
colorbar('eastoutside','Box','on','FontSize',13)
caxis([1e+5 6e+7])
title('Modulus (Pa) map - Hertz','FontSize',13)
subplot(4,6,[5 6 11 12])
imagesc(rot90(transpose(MAPS(:,:,78))))
colormap hot
title('beta values','FontSize',13)
caxis([1.1 2])
axis off
colorbar('eastoutside','Box','on','FontSize',13)
subplot(4,6,[13 14 19 20])
imagesc(rot90(transpose(real(MAPS(:,:,7)))))
colormap hot
caxis([1e-12 1e-10])
colorbar('eastoutside','Box','on','FontSize',13)
title('RMS|p map','FontSize',13)
axis off
subplot(4,6,[15 16 21 22])
imagesc(rot90(transpose(MAPS(:,:,8))))
caxis ([0 Msmax_rms])
caxis([1e-12 1e-10])
colorbar('eastoutside','Box','on','FontSize',13)
title('RMS|c map','FontSize',13)
axis off
subplot(4,6,[17 18 23 24])
imagesc(rot90(transpose(MAPS(:,:,83))));
colormap hot
colorbar('eastoutside','Box','on','FontSize',13)
O_PHARRmod=MAPS(:,:,46);
caxis([1e-12 1e-10])
title('RMS|beta map','FontSize',13)
axis off
hold off
end
if Figs.paper==1
figure(548)
set(gcf,'color','w');
title(FMap_name);
hold on
subplot(4,6,[1 2 7 8])
imagesc(rot90(transpose(MAPS(:,:,1))));
set(gca,'xtick',0:10:40);
set(gca,'ytick',0:10:40);
```

```
colormap hot
colorbar('eastoutside','FontSize',13,'LineWidth',.5)
caxis([MAPS_sorted(ceil(PandL*PandL*(.05)),1) MAPS_sorted(ceil(PandL*PandL*(.98)),1)])
title('Modulus (Pa) map','FontSize',13)
axis off
subplot(4,6,[3 4 9 10])
ipr=imresize(qwertyui(:,:),1);
if FlatLim==1
e=1:PandL*1;
for ipr1=1:PandL*1
    e1=ipr(ipr1,:);
    p13=polyfit(e,e1,FlatlimDeg);
    e2=e1-polyval(p13,e);
    ipr(ipr1,:)=e2;
end
end
imagesc(rot90(M_height))
colormap hot
colorbar('eastoutside','LineWidth',.3,'FontSize',13)
title({'Height map'},'FontSize',13)
axis off
caxis auto
CMmodel=zeros(PandL,PandL2);
for po01=1:PandL
for po02=1:PandL2
        if MAPS(po01,po02,48)<=50
            if MAPS(po01,po02,15)<=5
                if      MAPS(po01,po02,3)==2
                        CMmodel(po01,po02)=0.5; % Sneddon
                else
                        CMmodel(po01,po02)=1; % Hertz
                end
            else
                CMmodel(po01,po02)=1.65; % DMT
            end
        elseif MAPS(po01,po02,48)>=50
                CMmodel(po01,po02)=2.9; % O-P
        end
end
end
subplot(4,6,[5 6 11 12])
imagesc(rot90(transpose(CMmodel)))
colormap hot
title({'CM Model selection'},'FontSize',13)
colorbar('eastoutside','Box','on','Ticks',[0.5 1 1.5 1.65 2.3 2.75
2.9],'TickLabels',{'Sneddon','Hertz','"big" adhes.','DMT','"Viscocity"','"big" hyster.','O-
P'},'FontSize',12)
caxis([0 3]);
axis off
subplot(4,6,[13 14 19 20])
imagesc(rot90(transpose(MAPS(:,:,53))))
colormap hot
colorbar('eastoutside','LineWidth',.3,'FontSize',13)
title('"Yield-like" point map','FontSize',13)
caxis([0 100])
axis off
subplot(4,6,[17 18 23 24])
imagesc(rot90(transpose(MAPS(:,:,110))))
colormap hot
colorbar('eastoutside','LineWidth',.3,'FontSize',13)
title('Modulus map - optimal b','FontSize',10)
caxis([MAPS_sorted(ceil(PandL*PandL*(.05)),1) MAPS_sorted(ceil(PandL*PandL*(.98)),1)])
axis off
subplot(4,6,[15 16 21 22])
av11=mean2(MAPS(:,:,7)); av12=mean2(MAPS(:,:,8)); av13=mean2(MAPS(:,:,83));
AVB1=MAPS(:,:,7); AVB2=MAPS(:,:,8); AVB3=MAPS(:,:,83);
AVB11=reshape(AVB1,[],1); AVB12=reshape(AVB2,[],1); AVB13=reshape(AVB3,[],1); Conca = cat(1,
AVB13, AVB11,AVB12);
hhh1=histogram(AVB13,100); hold on; hhh2=histogram(AVB11,100); hhh3=histogram(AVB12,100);
xlim([0 3e-8])
legend('RMSE|beta','RMSE|p','RMSE|c','Location','northeast')
title('RMSE Histogram','FontSize',13)
subplot(4,6,[17 18 23 24])
boxplot([AVB13, AVB11,AVB12],'OutlierSize',.02,'Notch','on','Labels',{'? = optimal','? =
1.5','? = 2'},'Jitter',.45)
title('RMSE boxplots','FontSize',13)
```

```
hold off
end
if Figs.Main_Analytics==1 && Figs.beta_1==1
figure(1101)
set(gcf,'color','w');
title(FMap_name);
hold on
subplot(32,48,[1 2 3 4 5 6 7 8 9 10 11 12 13 14 15 16 49 50 51 52 53 54 55 56 57 58 59 60 61
62 63 64 97 98 99 100 101 102 103 104 105 106 107 108 109 110 111 112 145 146 147 148 149 150
151 152 153 154 155 156 157 158 159 160 ...
193 194 195 196 197 198 199 200 201 202 203 204 205 206 207 208 241 242 243 244 245 246 247
248 249 250 251 252 253 254 255 256 289 290 291 292 293 294 295 296 297 298 299 300 301 302
303 304 337 338 339 340 341 342 343 344 345 346 347 348 349 350 351 352 385 386 387 388 389
390 391 392 393 394 395 396 397 398 399 400 ...
433 434 435 436 437 438 439 440 441 442 443 444 445 446 447 448 481 482 483 484 485 486 487
488 489 490 491 492 493 494 495 496 529 530 531 532 533 534 535 536 537 538 539 540 541 542
543 544 577 578 579 580 581 582 583 584 585 586 587 588 589 590 591 592 625 626 627 628 629
630 631 632 633 634 635 636 637 638 639 640 ...
673 674 675 676 677 678 679 680 681 682 683 684 685 686 687 688 721 722 723 724 725 726 727
728 729 730 731 732 733 734 735 736])
imagesc(rot90(transpose(MAPS(:,:,1)))); %# Create a colored map of the matrix values
set(gca,'xtick',0:10:40);
set(gca,'ytick',0:10:40);
colormap hot
colorbar('eastoutside','Box','on')
caxis([MAPS_sorted(ceil(PandL*PandL2*(.25)),1) MAPS_sorted(ceil(PandL*PandL2*(.7)),1)])
title('Modulus (Pa) map w/ spots','FontSize',8.5)
Aspots2=zeros(PandL,PandL2);
for gr5=1:grls
Aspots2(gr_list2(gr5,1),gr_list2(gr5,2))=gr5;
end
textStrings = num2str(Aspots2(:),'%d');  %# Create strings from the matrix values
Aspots3 = cellfun(@(x)x(logical(x)),num2cell(rot90(transpose(Aspots2))),'uni',false);
[x,y] = meshgrid(1:PandL,1:PandL2);   %# Create x and y coordinates for the strings
FFF=find(~cellfun(@isempty,Aspots3));
hStrings = text(x(FFF),y(FFF),Aspots3(FFF),'HorizontalAlignment','center','FontSize',8,
'FontWeight','bold'); %# Plot the strings
set(hStrings,'Color',[0 .8 0]);  %# Change the text colors
axis off
subplot(32,48,[1153 1154 1155 1156 1157 1158 1159 1160 1161 1162 1163 1164 1165 1166 1167 1201
1202 1203 1204 1205 1206 1207 1208 1209 1210 1211 1212 1213 1214 1215 1249 1250 1251 1252 1253
1254 1255 1256 1257 1258 1259 1260 1261 1262 1263 1297 1298 1299 1300 1301 1302 1303 1304 1305
1306 1307 1308 1309 1310 1311])
bar2=bar(spots_CHinIncl_ple(:,3),0.7);
set(bar2,'EdgeColor','k','FaceColor','b')
yticks([0 1])
xlim([0 grls])
ylim([0 1])
yticks(.5)
yticklabels({'ChinIncl'})
set(gca,'FontSize',7)
set(gca,'xticklabel',{[]})
grid on
subplot(32,48,[1345 1346 1347 1348 1349 1350 1351 1352 1353 1354 1355 1356 1357 1358 1359 1393
1394 1395 1396 1397 1398 1399 1400 1401 1402 1403 1404 1405 1406 1407 1441 1442 1443 1444 1445
1446 1447 1448 1449 1450 1451 1452 1453 1454 1455 1489 1490 1491 1492 1493 1494 1495 1496 1497
1498 1499 1500 1501 1502 1503])
bar3=bar(spots_CHinIncl_ple(:,4),0.7);
set(bar3,'EdgeColor','k','FaceColor','m')
yticks([.5 1 2 3])
yticklabels({'Sneddon','Hertz','DMT','O-Pharr'})
set(gca,'FontSize',7)
xlim([0 grls])
grid on
subplot(32,48,[865  866 867 868 869 870 871 872 873 874 875 876 877 878 879 913 914 915 916
917 918 919 920 921 922 923 924 925 926 927 961 962 963 964 965 966 967 968 969 970 971 972
973 974 975 1009 1010 1011 1012 1013 1014 1015 1016 1017 1018 1019 1020 1021 1022 1023 1057
1058 1059 1060 1061 1062 1063 1064 1065 1066 1067 1068 1069 1070 1071 1105 1106 1107 1108 1109
1110 1111 1112 1113 1114 1115 1116 1117 1118 1119])
bar1=bar(spots_CHinIncl_ple(:,1:2),0.7);
set(bar1,'EdgeColor','r')
xlim([0 grls])
set(gca,'FontSize',7)
set(gca,'xticklabel',{[]})
grid on
title('[(E+-\Delta E)(Pa) - CHinIncl - CM model] @ FMap spots','FontSize',8.5)
```

```
grid on
subplot(32,48,[sk(834:848) sk(882:896) sk(930:944) sk(978:992) sk(1026:1040) sk(1074:1088)
sk(1122:1136)...
           sk(1170:1184) sk(1218:1232) sk(1266:1280) sk(1314: 1328) sk(1362:1376)
sk(1410:1424) sk(1458:1472) sk(1506:1520)])
plot(listofgraphs2(:,5),listofgraphs2(:,3),'r*');
title({'Selected points - analytics - Modulus'},'FontSize',8.5)
% create analytics for list of graphs
subplot(32,48,[sk(18:32) sk(66:80) sk(114:128) sk(162:176) sk(210:224) sk(258:272)
sk(306:320)...
           sk(354:368) sk(402:416) sk(450:464) sk(498: 512) sk(546:560) sk(594:608)
sk(642:656) sk(690:704)])
plot(listofgraphs2(:,5),listofgraphs2(:,4),'g+');
title({'Selected points - analytics - Adhesion'},'FontSize',8.5)
% create analytics for list of graphs
subplot(32,48,[sk(34:48) sk(82:96) sk(130:144) sk(178:192) sk(226:240) sk(274:288) sk(322:336)
sk(370:384)...
           sk(418:432) sk(466:480) sk(514:528) sk(562:576) sk(610:624) sk(658:672)
sk(706:720)])

plot(listofgraphs2(:,5),listofgraphs2(:,6),'b^');
title({'Selected points - analytics - Plasticity index'},'FontSize',8.5)
if Figs.beta==1
subplot(32,48,[sk(850:864) sk(898:912) sk(946:960) sk(994:1008) sk(1042:1056) sk(1090:1104)
sk(1138:1152)...
              sk(1186:1200) sk(1234:1248) sk(1282:1296) sk(1330:1344) sk(1378:1392)
sk(1426:1440) sk(1474:1488) sk(1522:1536)])
plot(listofgraphs2(:,5),listofgraphs2(:,7),'kp');
title({'Selected points - analytics - Modulus_Sneddon/O-P'},'FontSize',8.5)
end
hold off
% end of figure 'Main-analytics'
end
if Figs.Main==1
figure(1001)
set(gcf,'color','w');
title(FMap_name);
hold on
subplot(32,48,[1 2 3 4 5 6 7 8 9 10 11 12 13 14 15 16 49 50 51 52 53 54 55 56 57 58 59 60 61
62 63 64 97 98 99 100 101 102 103 104 105 106 107 108 109 110 111 112 145 146 147 148 149 150
151 152 153 154 155 156 157 158 159 160 ...
193 194 195 196 197 198 199 200 201 202 203 204 205 206 207 208 241 242 243 244 245 246 247
248 249 250 251 252 253 254 255 256 289 290 291 292 293 294 295 296 297 298 299 300 301 302
303 304 337 338 339 340 341 342 343 344 345 346 347 348 349 350 351 352 385 386 387 388 389
390 391 392 393 394 395 396 397 398 399 400 ...
433 434 435 436 437 438 439 440 441 442 443 444 445 446 447 448 481 482 483 484 485 486 487
488 489 490 491 492 493 494 495 496 529 530 531 532 533 534 535 536 537 538 539 540 541 542
543 544 577 578 579 580 581 582 583 584 585 586 587 588 589 590 591 592 625 626 627 628 629
630 631 632 633 634 635 636 637 638 639 640 ...
673 674 675 676 677 678 679 680 681 682 683 684 685 686 687 688 721 722 723 724 725 726 727
728 729 730 731 732 733 734 735 736])
imagesc(rot90(transpose(MAPS(:,:,1)))); %# Create a colored map of the matrix values
set(gca,'xtick',0:10:40);
set(gca,'ytick',0:10:40);
colormap hot
colorbar('eastoutside','Box','on')
caxis([MAPS_sorted(PandL*ceil(PandL/40),1) MAPS_sorted(end-PandL*ceil(PandL/40),1)])
title('Modulus (Pa) map w/ spots','FontSize',8.5)
Aspots2=zeros(PandL,PandL2);
for gr5=1:grls
Aspots2(gr_list2(gr5,1),gr_list2(gr5,2))=gr5;
end
textStrings = num2str(Aspots2(:),'%d');  %# Create strings from the matrix values
Aspots3 = cellfun(@(x)x(logical(x)),num2cell(rot90(transpose(Aspots2))),'uni',false);
[x,y] = meshgrid(1:PandL,1:PandL2);   %# Create x and y coordinates for the strings
FFF=find(~cellfun(@isempty,Aspots3));
hStrings = text(x(FFF),y(FFF),Aspots3(FFF),'HorizontalAlignment','center','FontSize',8,
'FontWeight','bold'); %# Plot the strings
set(hStrings,'Color',[0 .8 0]);  %# Change the text colors
axis off
subplot(32,48,[1153 1154 1155 1156 1157 1158 1159 1160 1161 1162 1163 1164 1165 1166 1167 1201
1202 1203 1204 1205 1206 1207 1208 1209 1210 1211 1212 1213 1214 1215 1249 1250 1251 1252 1253
1254 1255 1256 1257 1258 1259 1260 1261 1262 1263 1297 1298 1299 1300 1301 1302 1303 1304 1305
1306 1307 1308 1309 1310 1311])
bar2=bar(spots_CHinIncl_ple(:,3),0.7);
set(bar2,'EdgeColor','k','FaceColor','b')
```

```
yticks([0 1])
xlim([0 grls])
ylim([0 1])
yticks(.5)
yticklabels({'ChinIncl'})
set(gca,'FontSize',7)
set(gca,'xticklabel',{[]})
grid on
subplot(32,48,[1345 1346 1347 1348 1349 1350 1351 1352 1353 1354 1355 1356 1357 1358 1359 1393
1394 1395 1396 1397 1398 1399 1400 1401 1402 1403 1404 1405 1406 1407 1441 1442 1443 1444 1445
1446 1447 1448 1449 1450 1451 1452 1453 1454 1455 1489 1490 1491 1492 1493 1494 1495 1496 1497
1498 1499 1500 1501 1502 1503])
bar3=bar(spots_CHinIncl_ple(:,4),0.7);
set(bar3,'EdgeColor','k','FaceColor','m')
yticks([.5 1 2 3])
yticklabels({'Sneddon','Hertz','DMT','O-Pharr'})
set(gca,'FontSize',7)
xlim([0 grls])
grid on
subplot(32,48,[865  866 867 868 869 870 871 872 873 874 875 876 877 878 879 913 914 915 916
917 918 919 920 921 922 923 924 925 926 927 961 962 963 964 965 966 967 968 969 970 971 972
973 974 975 1009 1010 1011 1012 1013 1014 1015 1016 1017 1018 1019 1020 1021 1022 1023 1057
1058 1059 1060 1061 1062 1063 1064 1065 1066 1067 1068 1069 1070 1071 1105 1106 1107 1108 1109
1110 1111 1112 1113 1114 1115 1116 1117 1118 1119])
bar1=bar(spots_CHinIncl_ple(:,1:2),0.7);
set(bar1,'EdgeColor','r')
xlim([0 grls])
set(gca,'FontSize',7)
set(gca,'xticklabel',{[]})
grid on
title('[(E+-\Delta E)(Pa) - CHinIncl - CM model] @ FMap spots','FontSize',8.5)
grid on
% create colormap for error in RMS values
%figure
subplot(32,48,[450 451 452 453 454 455 456 498 499 500 501 502 503 504 546 547 548 549 550 551
552 594 595 596 597 598 599 600 642 643 644 645 646 647 648 690 691 692 693 694 695 696 738
739 740 741 742 743 744])
imagesc(rot90(transpose(MAPS(:,:,43)))); %# Create a colored map of the matrix values
colormap hot
caxis([O_PHARRmod_sorted(ceil(.1*PandL)) MAPS_sorted(end-1*PandL,1)])
title({'Modulus (Pa) map - DMT'},'FontSize',8.5)
axis off
% create colormap for error in RMS values
%figure
subplot(32,48,[850 851 852 853 854 855 856 898 899 900 901 902 903 904 946 947 948 949 950 951
952 994 995 996 997 998 999 1000 1042 1043 1044 1045 1046 1047 1048 1090 1091 1092 1093 1094
1095 1096 1138 1139 1140 1141 1142 1143 1144])
imagesc(rot90(transpose(MAPS(:,:,15))))
colormap hot
% colorbar('eastoutside','Box','off')
title({'Adhesion ratio - F_{ad}/F_{max}'},'FontSize',8.5)
% caxis([MAPS_sorted(10,15) MAPS_sorted(end-50,15)])
caxis([0 100])
% caxis auto
axis off
% create colormap for error in RMS values
%figure
subplot(32,48,[857  858 859 860 861 862 863 905 906 907 908 909 910 911 953 954 955 956 957
958 959 1001 1002 1003 1004 1005 1006 1007 1049 1050 1051 1052 1053 1054 1055 1097 1098 1099
1100 1101 1102 1103 1145 1146 1147 1148 1149 1150 1151])
imagesc(rot90(transpose(MAPS(:,:,48))))
colormap hot
title({'Plasticity index - psi_{p}'},'FontSize',8.5)
axis off
% colorbar('eastoutside','Box','off')
caxis([0 100])
% create colormap for error in RMS values
%figure
subplot(32,48,[457 458 459 460 461 462 463 505 506 507 508 509 510 511 553 554 555 556 557 558
559 601 602 603 604 605 606 607 649 650 651 652 653 654 655 697 698 699 700 701 702 703 745
746 747 748 749 750 751])
imagesc(rot90(transpose(MAPS(:,:,46)))); %# Create a colored map of the matrix values
colormap hot
% colorbar('eastoutside','','on')
O_PHARRmod=MAPS(:,:,46);
O_PHARRmod_sorted=sort(O_PHARRmod(:));
```

```
caxis ([O_PHARRmod_sorted(PandL) O_PHARRmod_sorted(end-2*PandL)])
title({'Modulus (Pa) map - O-Pharr'},'FontSize',8.5)
axis off
subplot(32,48,[66 67 68 69 70 71 72 114 115 116 117 118 119 120 162 163 164 165 166 167 168
210 211 212 213 214 215 216 258 259 260 261 262 263 264 306 307 308 309 310 311 312 354 355
356 357 358 359 360])
imagesc(rot90(transpose(MAPS(:,:,53))))
colormap gray
title('"Yield-like" point map','FontSize',8.5)
caxis([0 100])
axis off
subplot(32,48,[73 74 75 76 77 78 79 121 122 123 124 125 126 127 169 170 171 172 173 174 175
217 218 219 220 221 222 223 265 266 267 268 269 270 271 313 314 315 316 317 318 319 361 362
363 364 365 366 367])
ipr=imresize(qwertyui(:,:),1);
if FlatLim==1
e=1:PandL*1;
for ipr1=1:PandL*1
e1=ipr(ipr1,:);
p12=polyfit(e,e1,FlatlimDeg);
e2=e1-polyval(p12,e);
ipr(ipr1,:)=e2;
end
end
imagesc(imresize(medfilt3(rot90(transpose(-ipr(:,:))),[3 3 3]),5))
colormap hot
title({'Contact point / flat ' FlatlimDeg},'FontSize',8.5)
axis off
caxis auto
subplot(32,48,[sk(1241:1247) sk(1289:1295) sk(1337:1343) sk(1385:1391) sk(1433:1439)
sk(1481:1487) sk(1529:1535)])
imagesc(rot90(transpose(MAPS(:,:,8))))
colormap hot
caxis ([0 Msmax_rms])
title('RMS|c map','FontSize',8.5)
axis off
subplot(32,48,[sk(1234:1240) sk(1282:1288) sk(1330:1336) sk(1378:1384) sk(1426:1432)
sk(1474:1480) sk(1522:1528)])
imagesc(rot90(transpose(real(MAPS(:,:,7)))))
colormap hot
caxis ([0 Msmax_rms])
title('RMS|p map','FontSize',8.5)
axis off
subplot(32,48,[sk(834:848) sk(882:896) sk(930:944) sk(978:992) sk(1026:1040) sk(1074:1088)
sk(1122:1136)...
          sk(1170:1184) sk(1218:1232) sk(1266:1280) sk(1314: 1328) sk(1362:1376)
sk(1410:1424) sk(1458:1472) sk(1506:1520)])
imagesc(rot90(transpose(MAPS(:,:,49))))
colormap hot
title({'CM Model selection'},'FontSize',8.5)
colorbar('eastoutside','Box','on','Ticks',[0.5 1 1.5 1.65 2.3 2.75
2.9],'TickLabels',{'Sneddon','Hertz','"big" adhes.','DMT','"Viscocity"','"big" hyster.','O-
P'},'FontSize',7)
caxis([0 3]);
axis off
% insert experiment parms in figure
AA=zeros(PandL,PandL2);
AA(:,:)=MAPS(:,:,49);
[aa1,aa2] = mode(AA(:));
if     aa1==0.5
aa12='Sneddon';
elseif aa1==1
aa12='Hertz';
elseif aa1==1.65
aa12='DMT';
elseif aa1==2.9
aa12='Oliver-Pharr';
elseif aa1==0
aa12='none';
end
if aa2 > ceil((PandL*PandL2-miss_data)/2)
ple_adj='dominant';
else
ple_adj='leading';
end
```

```
str_ad=['AFM Force map "' FMap_name '" (' num2str(PandL,'%10.4g') '*' num2str(PandL2,'%10.4g')
', ' num2str(Scan_size,'%10.4g') ' (m)' ')'...
   ' experiemnt of ' Sample ...
   ' was conducted with the ' AFM_instrum ' in ' AFM_mode ' mode,' ' using ' Cantilever_name '
cantilevers ['...
   num2str(K_t,'%10.4g') ' +- ' num2str(deltaKtip,'%10.4g') ' (N/m), ' Cantilever_geometry
'geometry' ...
   '], and inside a liquid environment (' Buffer '). The trigger point is '
num2str(Trigger_point_V,'%10.4g')...
   ' (V)' ' / ' num2str(Trigger_point_nN,'%10.4g') ' (N), the force distance is '
num2str(Force_distance,'%10.4g') ' (m),' ...
   ' the tip z-velocity is ' num2str(Z_velocity,'%10.4g') ' (m/s),'...
   ' and the DeflInvOLS is ' num2str(DelfInvOLS,'%10.4g') '.' ' The mechanical analysis was
done with ' ...
   'the use of ' CM_model ' contact mechanics model after removing '
num2str(fit_perc_end,'%10.4g')...
   ' % of the FI data from each curve.' ' In this experiment ' num2str(miss_data,'%10.4g') ...
   ' out of ' num2str(PandL*PandL2,'%10.4g') ' force map points consist of distorted data, the
average'...
   ' modulus value is ' num2str(mean2(MAPS(:,:,1)),'%10.4g') ...
   ', the time of analysis is ' num2str(run_time,'%10.4g') ' (s)' ', and' ' the ' ple_adj ...
   ' power law is ' aa12 '.']; % algorithm note
subplot(32,48,[33 34 35 36 37 38 39 40 41 42 43 44 45 46 47 48 81 82 83 84 85 86 87 88 89 90
91 92 93 94 95 96 129 130 131 132 133 134 135 136 137 138 139 140 141 142 143 144 177 178 179
180 181 182 183 184 185 186 187 188 189 190 191 192 225 226 227 228 229 230 231 232 233 234
235 236 237 238 239 240 273 274 275 276 277 278 279 280 281 282 283 284 285 286 287 288 321
322 323 324 325 326 327 328 329 330 331 332 333 334 335 336 369 370 371 372 373 374 375 376
377 378 379 380 381 382 383 384 417 418 419 420 421 422 423 424 425 426 427 428 429 430 431
432 465 466 467 468 469 470 471 472 473 474 475 476 477 478 479 480 513 514 515 516 517 518
519 520 521 522 523 524 525 526 527 528 561 562  563 564 565 566 567 568 569 570 571 572 573
574 575 576 ...
609 610 611 612 613 614 615 616 617 618 619 620 621 622 623 624 657 658 659 660 661 662 663
664 665 666 667 668 669 670 671 672 705 706 707 708 709 710 711 712 713 714 715 716 717 718
719 720 753 754 755 756 757 758 759 760 761 762 763 764 765 766 767 768])
t45=19;
t46=50;
Text45=zeros(t45,t46);
Text45(:)=100;
imagesc(rot90(transpose(Text45(:,:)))); %# Create a colored map of the matrix values
colormap hot
caxis([0 100])
title('Experiment details','FontSize',8.5)
str_ad=[blanks(4),str_ad];
str45=size(str_ad);
str46=str45(2);
str47=blanks(t45*t46-str46);
istr2=0;
str_ad34=[str_ad,str47];
for istr1=51:50:ceil(t45*t46/1)
if str_ad34(1,istr1)==' '
   str_ad34=[str_ad34(1:istr1-1) str_ad34(istr1+1:end)];
   istr2=istr2+1;
end
end
str_ad34=[str_ad34(1,:) blanks(istr2)];
strad31=reshape(str_ad34,[t45,t46]);
textStrings2 = num2str(strad31(:),'%d');  %# Create strings from the matrix values
Aspots5 = cellfun(@(x)x(logical(x)),num2cell(strad31),'uni',false);
[x,y] = meshgrid(1:t45,1:t46);   %# Create x and y coordinates for the strings
hStrings2 = text(y(:),x(:),Aspots5(:),'HorizontalAlignment','center','FontSize',10,
'FontWeight','normal','FontName','Georgia'); %# Plot the strings
set(hStrings2,'Color','k');  %# Change the text colors
axis off;
hold off
% end of figure 'Main'
end
if Figs.Tomography==1
eikon=[eikon,1004];
qw1(:,:,1:stposa)=MAPS(:,:,100+10/stposa:100+10);
q1=sort(qw1(:));
qwe1=q1(ceil(.99*(stposa*PandL*PandL2)));
qwe2=q1(ceil(.3*(stposa*PandL*PandL2)));
h = figure(1004);
title('Modulus_tomography')
axis tight manual
filename = [edo '\' FMap_name ' [' num2str(expt,'%10.4g') '] effindshape2_ModTomo.gif'];
```

```
for nt1=10/stposa:10/stposa:10
    subplot(4,6,[3 4 9 10])
    imagesc(rot90(transpose(MAPS(:,:,56+nt1))))
    colormap hot
    colorbar('eastoutside','Box','on')
    title(['Modulus map ' num2str((100/stposa)*nt1,'%10.4g') '% of total ' cut_ind_Fmax ' -
Hertz'],'FontSize',12)
    axis off
    caxis([qwe2 qwe1])
    hold on
    subplot(4,6,[1 2 7 8])
    imagesc(rot90(transpose(MAPS(:,:,100+nt1))))
    colormap hot
    colorbar('eastoutside','Box','on')
    title(['Modulus map ' num2str((100/stposa)*nt1,'%10.4g') '% of total ' cut_ind_Fmax ' -
optimal b'],'FontSize',12)
    axis off
    caxis([qwe2 qwe1])
    subplot(4,6,[5 6 11 12])
    if modtomo==1 && modtomo_plus==1
        imagesc(rot90(transpose(MAPS(:,:,91+(ceil(nt1/9)-1)*(-13)+abs(ceil(nt1/9)-2)*nt1))))
        colormap hot
        colorbar('eastoutside','Box','on','Ticks',[1.1 1.2 1.3 1.4 1.5 1.6 1.7 1.8 1.9 2],...

'TickLabels',{'1.1','1.2','1.3','1.4','1.5','1.6','1.7','1.8','1.9','2'},'FontSize',7)
        title(['beta values ' num2str((100/stposa)*nt1,'%10.4g') '% of total
Fmax'],'FontSize',12)
        caxis([1.1 2])
        axis off
    else
        imagesc(rot90(transpose(MAPS(:,:,66+nt1))))
        colormap hot
        colorbar('eastoutside','Box','on','Ticks',[0.5 1 1.5
2],'TickLabels',{'none','Linear','Hertz','Sneddon'},'FontSize',7)
        title(['CM model ' num2str((100/stposa)*nt1,'%10.4g') '% of total '
cut_ind_Fmax],'FontSize',12)
        axis off
        caxis([0.5 2])
    end
    subplot(4,6,[17 18 23 24])
    if modtomo==1 && modtomo_plus==1
        imagesc(rot90(transpose(MAPS(:,:,114+nt1))))
        colormap hot
        colorbar;
        title(['RMSE|b values ' num2str((100/stposa)*nt1,'%10.4g') '% of total '
cut_ind_Fmax],'FontSize',12)
        caxis([1e-12 1e-8])
        axis off
    end
    subplot(4,6,[13 14 19 20])
    if modtomo==1 && modtomo_plus==1
        imagesc(rot90(transpose(MAPS(:,:,124+nt1))))
        colormap hot
        colorbar;
        title(['RMSE|p values ' num2str((100/stposa)*nt1,'%10.4g') '% of total '
cut_ind_Fmax],'FontSize',12)
        caxis([1e-12 1e-8])
        axis off
    end
    subplot(4,6,[15 16 21 22])
    if modtomo==1 && modtomo_plus==1
        imagesc(rot90(transpose(MAPS(:,:,134+nt1))))
        colormap hot
        colorbar;
        title(['RMSE|c values ' num2str((100/stposa)*nt1,'%10.4g') '% of total '
cut_ind_Fmax],'FontSize',12)
        caxis([1e-12 1e-8])
        axis off
    end
    hold off
    drawnow
    set(figure(1004), 'Position', get(0, 'Screensize'));
    frame=getframe(h);
    im=frame2im(frame);
    [imind,cm] = rgb2ind(im,256);
    if nt1 == 1
```

```
imwrite(imind,cm,filename,'gif','Loopcount',inf,'DelayTime',1,'Screensize',[size(imind,2)
size(imind,1)]);
      else
          imwrite(imind,cm,filename,'gif','WriteMode','append','DelayTime',2);
    end
end
end
if Figs.Misc==1
figure(1002)
title(FMap_name);
hold on
subplot(16,24,[1 2 3 4 5 6 7 8 25 26 27 28 29 30 31 32 49 50 51 52 53 54 55 56 73 74 75 76 77
78 79 80 ...
97 98 99 100 101 102 103 104 121 122 123 124 125 126 127 128 145 146 147 148 149 150 151 152
169 170 171 172 173 174 175 176])
imagesc(rot90(transpose(MAPS(:,:,1)))); %# Create a colored map of the matrix values
colormap hot
colorbar('eastoutside','Box','on')
caxis([MAPS_sorted(PandL*ceil(PandL/40),1) MAPS_sorted(end-PandL*ceil(PandL/40),1)])
title('Modulus (Pa) map w/ spots')
axis off
HJK=MAPS(:,:,90);
subplot(16,24,[10 11 12 34 35 36 58 59 60])
imagesc(rot90(transpose(MAPS(:,:,28))))
colormap hot
title({'Defl criteria';'1st'},'FontSize',10)
axis off
caxis ([0 max(HJK(:))])% create colormap for error in RMS values
subplot(16,24,[13 14 15 37 38 39 61 62 63])
imagesc(rot90(transpose(real(MAPS(:,:,29)))))
colormap hot
caxis ([0 max(HJK(:))])
title({'UnwntIncl criteria';'2nd'})
axis off
subplot(16,24,[106 107 108 130 131 132 154 155 156])
imagesc(rot90(transpose(MAPS(:,:,30))))
colormap hot
title({'GradDefl criteria';'3rd'})
axis off
caxis ([0 max(HJK(:))])
subplot(16,24,[109 110 111 133 134 135 157 158 159])
imagesc(rot90(transpose(MAPS(:,:,31))))
colormap gray
title({'DifferIncl';'4th'},'FontSize',10)
caxis ([0 max(HJK(:))])
axis off
LoImapnew=zeros(PandL,PandL2);
for lmn1=1:PandL
for lmn2=1:PandL2
    LoImapnew(lmn1,lmn2)=abs(R_graphs(MAPS(lmn1,lmn2,40)+1,11)-
R_graphs(MAPS(lmn1,lmn2,13)+1,11));
end
end
subplot(16,24,[306 307 308 330 331 332 354 355 356])
imagesc(rot90(transpose(LoImapnew)))
colormap hot
caxis([0 1e-7])
title({'Indentation depth'},'FontSize',10)
axis off
subplot(16,24,[309 310 311 333 334 335 357 358 359])
imagesc(rot90(transpose(MAPS(:,:,33))))
title({'CP adjustment';'+-'},'FontSize',10)
axis off
caxis ([0 10])
subplot(16,24,[201 202 203 204 205 206 207 208 225 226 227 228 229 230 231 232 249 250 251 252
253 254 255 256 ...
273 274 275 276 277 278 279 280 297 298 299 300 301 302 303 304 321 322 323 324 325 326 327
328 ...
345 346 347 348 349 350 351 352 369 370 371 372 373 374 375 376])
imagesc(rot90(transpose(MAPS(:,:,14))))
colormap hot
colorbar('eastoutside')
title({'Ratio of gradient, gr_Avn';'puI/(1/6)*puI'})
caxis ([0 10])
subplot(16,24,[218 219 220 242 243 244 266 267 268])
```

```
imagesc(rot90(transpose(MAPS(:,:,40))))
title({'max point'},'FontSize',10)
caxis auto
axis off
subplot(16,24,[221 222 223 245 246 247 269 270 271])
imagesc(rot90(transpose(MAPS(:,:,35))))
title({'cp deltadefl'},'FontSize',10)
caxis auto
axis off
subplot(16,24,[290 291 292 314 315 316 338 339 340])
imagesc(rot90(transpose(MAPS(:,:,36))))
title({'cp graddefl'},'FontSize',5)
caxis auto
axis off
subplot(16,24,[293 294 295 317 318 319 341 342 343])
imagesc(rot90(transpose(MAPS(:,:,32))))
title({'cp_5thcon_signum'},'FontSize',5)
caxis auto
axis off
subplot(16,24,[18 19 20 42 43 44 66 67 68])
imagesc(rot90(transpose(MAPS(:,:,13))))
title({'noCP_after'},'FontSize',10)
caxis auto
axis off
subplot(16,24,[21 22 23 45 46 47 69 70 71])
imagesc(rot90(transpose(MAPS(:,:,84))))
title({'noCP_before'},'FontSize',10)
caxis auto
axis off
subplot(16,24,[114 115 116 138 139 140 162 163 164])
imagesc(rot90(transpose(MAPS(:,:,83))))
title({'fval_min'},'FontSize',10)
caxis auto
axis off
subplot(16,24,[117 118 119 141 142 143 165 166 167])
imagesc(rot90(transpose(MAPS(:,:,51))))
title({'abest'},'FontSize',10)
caxis auto
axis off
subplot(16,24,[210 211 212 234 235 236 258 259 260])
imagesc(rot90(transpose(MAPS(:,:,37))))
title({'ratio_deflgradtot'},'FontSize',10)
caxis auto
axis off
subplot(16,24,[213 214 215 237 238 239 261 262 263])
imagesc(rot90(transpose(MAPS(:,:,14))))
title({'gr_Avn'},'FontSize',10)
caxis auto
axis off
hold off
end
if Figs.FI==1
for numofig=1:gr2
    set(figure(numofig), 'Position', get(0, 'Screensize'));
end
print(1, '-dpng', [edo '\' FMap_name ' [' num2str(expt,'%10.4g') '] FI.png'],'-r300')
print(2, '-dpng', [edo '\' FMap_name ' [' num2str(expt,'%10.4g') '] FI 2.png'],'-r300')
eikon=[eikon,1];
eikon=[eikon,2];
end
if Figs.Main==1
set(figure(1001), 'Position', get(0, 'Screensize'));
print(1001, '-dpng', [edo '\' FMap_name ' [' num2str(expt,'%10.4g') '] Main.png'],'-r300')
eikon=[eikon,1001];
end
if Figs.Main_Analytics==1 && Figs.beta_1==1
set(figure(1101), 'Position', get(0, 'Screensize'));
print(1101, '-dpng', [edo '\' FMap_name ' [' num2str(expt,'%10.4g') '] Main_Analytics.png'],'-
r300')
eikon=[eikon,1101];
end
if Figs.beta==1 && Figs.beta_1==1
set(figure(1013), 'Position', get(0, 'Screensize'));
print(1013, '-dpng', [edo '\' FMap_name ' [' num2str(expt,'%10.4g') '] beta.png'],'-r300')
eikon=[eikon,1013];
end
```

```
if Figs.Misc==1
set(figure(1002), 'Position', get(0, 'Screensize'));
print(1002, '-dpng', [edo '\' FMap_name ' [' num2str(expt,'%10.4g') '] Miscellaneous.png'],'-
r300')
eikon=[eikon,1002];
end
if Figs.NonElastic==1
set(figure(1003), 'Position', get(0, 'Screensize'));
print(1003, '-dpng', [edo '\' FMap_name ' [' num2str(expt,'%10.4g') '] NonElastic.png'],'-
r300')
eikon=[eikon,1003];
end
if Figs.Tomography==1
set(figure(1004), 'Position', get(0, 'Screensize'));
end


if Figs.pleIndent==1
    set(figure(1012), 'Position', get(0, 'Screensize'));
    print(1012, '-dpng', [edo '\' FMap_name ' [' num2str(expt,'%10.4g') '] pleIndent.png'],'-
r300')
    eikon=[eikon,1012];
end
if Figs.pleIndent2==1
    set(figure(1011), 'Position', get(0, 'Screensize'));
    print(1011, '-dpng', [edo '\' FMap_name ' [' num2str(expt,'%10.4g') '] pleIndent
2.png'],'-r300')
    eikon=[eikon,1011];
end
if Figs.paper==1
set(figure(548), 'Position', get(0, 'Screensize'));
print(548, '-dpng', [edo '\' FMap_name ' [' num2str(expt,'%10.4g') '] paper.png'],'-r300')
eikon=[eikon,548];
end
if Figs.effIndShape2==1
    set(figure(547), 'Position', get(0, 'Screensize'));
    print(547, '-dpng', [edo '\' FMap_name ' [' num2str(expt,'%10.4g') ']
effindshape2.png'],'-r300')
    eikon=[eikon,547];
end
if Figs.effIndShape==1
    set(figure(1048), 'Position', get(0, 'Screensize'));
    print(1048, '-dpng', [edo '\' FMap_name ' [' num2str(expt,'%10.4g') ']
effindshape.png'],'-r300')
    eikon=[eikon,1048];
    set(figure(1049), 'Position', get(0, 'Screensize'));
    print(1049, '-dpng', [edo '\' FMap_name ' [' num2str(expt,'%10.4g') ']
histovariousE.png'],'-r300')
    eikon=[eikon,1049];
end
if printpdf==1;print(1,'AFCA','-dpdf');end
if Figs.Points==1 && Figs.Main_Analytics==1
figure(1001)
if Figs.justpoints==1
    [x,y] = ginput(20);
    listofgraphs=[];
    for i65=1:20
        listofgraphs(i65,1)=abs(ceil(PandL-y(i65,1)));
        listofgraphs(i65,2)=abs(ceil(ceil(x(i65,1))));
    end
end
if Figs.polygon==1
    [x,y] = ginput(20);
    shlog=1;
    listofgraphs=[];
    for i65=1:20
        listofgraphs(i65,1)=abs(ceil(PandL-y(i65,1)));
        listofgraphs(i65,2)=abs(ceil(ceil(x(i65,1))));
    end
    LOG21=listofgraphs(:,1:2);
    sh1=0;
    SH=zeros(PandL,PandL2);
    for i=1:20
        SH(listofgraphs(i,1),listofgraphs(i,2))=1;
    end
    for k=1:20-1
       kk1=listofgraphs(k,1);
```

```
        kk2=listofgraphs(k,2);
        kk3=listofgraphs(k+1,1);
        kk4=listofgraphs(k+1,2);
        kkk1=abs(kk3-kk1);
        kkk2=abs(kk4-kk2);
        kkk3=kkk1/kkk2;
        kkk4=kkk2/kkk1;
        if kk1<kk3
            if kk2<kk4
                for j=kk1:kk3
                    for o=kk2+ceil((j-kk1)*kkk4):kk4
                        SH(j,o)=1;
                    end
                end
            elseif kk4<kk2
                for j=kk1:kk3
                    for o=kk4+ceil((j-kk1)*kkk4):kk2
                        SH(j,o)=1;
                    end
                end
            end
        elseif kk1>kk3
            if kk2<kk4
                for j=kk3:kk1
                    for o=kk2+ceil((j-kk3)*kkk3):kk4
                        SH(j,o)=1;
                    end
                end
            elseif kk2>kk4
                for j=kk3:kk1
                    for o=kk4+ceil((j-kk3)*kkk3):kk2
                        SH(j,o)=1;
                    end
                end
            end
        end
    end
    for i=1:PandL
        jk1=find(SH(i,:),1);
        jk2=find(SH(i,:),1,'last');
        SH(i,jk1:jk2)=1;
    end
    for j=1:PandL2
        jk1=find(SH(:,j),1);
        jk2=find(SH(:,j),1,'last');
        SH(jk1:jk2,j)=1;
    end
    lg=1;
    LOG=zeros(sum(SH(:)),2);
    for i=1:PandL
        for j=1:PandL2
            if SH(i,j)==1
               LOG(lg,1:2)=[i j];
               lg=lg+1;
            end
        end
    end
    listofgraphs2=LOG;
end
if Figs.line==1
    [x,y] = ginput(2);
    listofgraphs=[];
    shlog2=1;
    for i65=1:2
        listofgraphs(i65,1)=abs(ceil(PandL-y(i65,1)));
        listofgraphs(i65,2)=abs(ceil(ceil(x(i65,1))));
    end
    SH=zeros(PandL,PandL2);
    for i=1:2
        SH(listofgraphs(i,1),listofgraphs(i,2))=1;
    end
    for k=1:1
        kk1=listofgraphs(k,1);
        kk2=listofgraphs(k,2);
        kk3=listofgraphs(k+1,1);
        kk4=listofgraphs(k+1,2);
```

```
        kk5=(abs(kk2-kk1))/(abs(kk4-kk3));
        kk6=(abs(kk4-kk3))/(abs(kk2-kk1));
        if kk1<kk3
            if kk2<kk4
                j=kk1;
                for o=kk3:kk4
                    SH(j,o)=1;
                    j=ceil(j+kk5);
                end
            elseif kk4<kk2
                j=kk1;
                for o=kk4:ceil(kk6):kk2
                    SH(j,o)=1;
                    j=round(j+kk5);
                end
            end
        elseif kk1>kk3
            if kk2<kk4
                j=kk1;
                for o=kk2:ceil(kk6):kk4
                    SH(j,o)=1;
                    j=round(j-kk5);
                end
            elseif kk2>kk4
                j=kk1;
                for o=kk4:ceil(kk6):kk2
                    SH(j,o)=1;
                    j=round(j-kk5);
                end
            end
        end
    end
    lg=1;
    LOG=zeros(sum(SH(:)),2);
    for i=1:PandL
        for j=1:PandL2
            if SH(i,j)==1
               LOG(lg,1:2)=[i j];
               lg=lg+1;
            end
        end
    end
    listofgraphs2=LOG;
end
end
save([edo '\' FMap_name ' [' num2str(expt,'%10.4g') '] - meatadata - ' char(cop92(3)) '_'...
char(cop92(2)) '_' char(cop92(1))]);
savefig(eikon,[edo '\' FMap_name ' [' num2str(expt,'%10.4g') '] - meatadata - '
char(cop92(3))...
'_' char(cop92(2)) '_' char(cop92(1))]);
```